STATISTICAL ANALYSIS OF THE SIZE AND ELEMENTAL COMPOSITION OF AIRBORNE COAL MINE DUST

Jan M. Mutmansky and Changwoo Lee

Generic Technology Center for Respirable Dust
The Pennsylvania State University
Department of Mineral Engineering
104 Mineral Sciences Building
University Park, PA 16802

Published March, 1987

Interim Report Covering Fall 1984 to Fall 1986

Availability Unlimited

Prepared for
Bureau of Mines
U.S. Department of the Interior
Washington, DC 20241

The views and conclusions contained in this document are those of the authors and should not be interpreted as necessarily representing the official policies or recommendations of the Interior Department's Bureau of Mines or of the U.S. Government.

REPORT DOCUMENTATION PAGE

1. Report No.	2.	3. Recipient's Accession No.
	Bu Mines OFR 06-90	PB90 161647/AS

4. Title and Subtitle
Statistical Analysis of the Size and Elemental Composition of Airborne Coal Mine Dust

5. Report Date
March 1987

6.

7. Author(s)
Jan M. Mutmansky and Changwoo Lee

8. Performing Organization Report No.

9. Performing Organization Name and Address
Department of Mineral Engineering
104 Mineral Sciences Building
The Pennsylvania State University
University Park, PA 16802

10. Project/Task/Work Unit No.
Fund No. 8540

11. Contract or Grant No.
G1135142

12. Sponsoring Organization Name and Address
Bureau of Mines
U.S. Department of the Interior
Washington, DC 20241

13. Type of Report
Interim Report,
Fall 1984 to Fall 1986

14.

15. Supplementary Notes

16. Abstract

This research was part of an ongoing effort at The Pennsylvania State University to investigate the characteristics of airborne mine dusts and its relationship to coal worker's pneumoconiosis (CWP). The specific purpose of this project was to analyze the size and elemental composition of airborne coal mine dusts and the ramifications of these characteristics.

A dust sampling strategy using multi-stage cascade impactors was established for characterization purposes. Analysis of the size distributions of the collected samples was performed based upon the aerodynamic diameter of the dust. Patterns of lognormality and bimodality were found in the data. Elemental analysis was performed by the PIXE method for both major and trace elements. Size dependency and locational variation of the elemental composition of the airborne dust were significant in some cases. Relationships to the mining section activities were also investigated.

17. Originator's Key Words	18. Availability Statement
Coal mine dust Dust characteristics Dust control Elemental Analysis Dust size distribution	Unlimited

19. U. S. Security Classif. of the Report	20. U. S. Security Classif. of This Page	21. No. of Pages	22. Price
Unclassified	Unclassified		

FOREWARD

This research has been supported by the Department of the Interior's Mineral Institute's program administered by the Bureau of Mines through the Generic Mineral Technology Center for Respirable Dust under allotment grant number G1135142.

TABLE OF CONTENTS

TABLE OF CONTENTS (continued)

TABLE OF CONTENTS (continued)

TABLE OF CONTENTS (continued)

LIST OF TABLES

LIST OF TABLES (continued)

LIST OF TABLES (continued)

LIST OF TABLES (continued)

LIST OF FIGURES

1. INTRODUCTION: HEALTH HAZARDS AND IMPACTS OF COAL MINE DUST

1.1 Historical Perspective

Although the most common form of pulmonary disease in the coal mining industry, Coal Workers' Pneumoconiosis (CWP), is known to be caused by inhaled coal mine dust, its recognition had not been made until recently. Awareness of potential health hazards associated with mine dust can be traced far back into the fourth century B.C. when Hippocrates noticed symptoms similar to silicosis in a miner (Breslin and Niewiadomski, 1982). Similar dust-related occupational disease was also described by Agricola in the sixteenth century (Tokuhata et al., 1970). Meanwhile, several different names had been applied to this occupational pulmonary disease: asthma, silicosis, anthracosis and anthracosilicosis. These names reflect the complexities in the nature of CWP since the distinction between CWP and silicosis was not clearly made.

It was 1951 when a more generic term, Coal Workers' Pneumoconiosis, was coined after it was found that CWP can be developed with little or no presence of silica dust (Heppelston, 1951). Since then, CWP has been treated separately from silicosis, which is generally considered to be less common than CWP for coal workers. Recently, an autopsy study (Sutherland, 1986) showed that a significant number of coal workers who contract silicosis are mistakenly diagnosed as having CWP due to the same roentgenographic clues and breathing function test results. Whether this argument is true or not, health hazards associated with coal mine dust certainly exist as long as coal miners work in a dusty environment.

While CWP had been extensively studied in many of the European countries including Britain, West Germany, France, Belgium and Holland, its significance had not been widely perceived in the United States until the roentgenographic examination of coal workers in the Pennsylvania anthracite coalfields and Utah bituminous coalfields was performed along with mine environmental studies in the 1930s. Since then, similar studies have been carried out by the Bureau of Mines and the Public Health Service. However, when the issue of the need for legislation on coal mine dust levels was raised in the late 1960s, no suitable epidemiological data on U.S. miners concerning the dose-effect relationship was available (Attfield, 1984).

The basis for dust regulations in the Federal Coal Mine Health and Safety Act of 1969 was the most extensive data available at that time, i.e., results of the British epidemiological studies performed over a span of 10 years for more than 4000 coal miners. Data gathered from the three surveys coded as the Pneumoconiosis Field Research (PFR) results were used to extrapolate the effects up to 35 years by a stochastic statistical technique, the Markov process (Jacobsen et al., 1971). This dose-effect relationship showed that the possibility

of progression to the simple pneumoconiosis category 2/1 or greater (for the definition of classifications of CWP, see Jacobsen et al., 1971), is near zero at 35 years of cumulative exposure to 2 mg/m³. This figure of 2 mg/m³ was believed to be critical to the decision made by the U.S. government. Recently, it has been shown (Attfield, 1984) that results from the National Coal Study on U.S. miners do not indicate that application of the British data to U.S. mining conditions is inappropriate.

1.2 Research on Coal Mine Dust

The immediate impact of dust regulations on the coal mining industry occurred mainly in the area of productivity caused by modification of mining practice to meet the standards and in the area of production cost due to black lung taxes imposed on every ton of coal mined. The decline in productivity experienced in the early 1970s was largely attributed to difficulties in complying with the dust standards (Brezovec, 1981). However, most of the mining operations were able to meet the regulation quicker than at first predicted. This achievement was possible by applying appropriate engineering control measures developed by research on respirable dust initiated by the Bureau of Mines.

The control of pneumoconiosis has been dealt with using three different measures: dust suppression, dust measurement and medical supervision of the miners (Jacobsen et al., 1970; Breslin and Niewiadomski, 1982). Since the primary objective of the Bureau of Mines dust research program has been to solve the most pressing dust-related problems, the first measure, dust suppression, has received more attention than the two latter measures. The two main areas of research on dust suppression include control of dust generation at the source and control of airborne dust. The priority put on the first measure was due to the immediate need for practical, reliable and cost-effective dust control measures to meet dust regulations in underground coal mines. As a result, relatively few citations are now being issued to mining sections employing continuous miners.

Many of the longwall mining sections still encounter difficulties in meeting the standards due to the intrinsic potential of high dust generation and the inherent difficulty of sweeping the dust away from the working areas. Although compliance difficulties also exist in continuous mining sections with augers and borer-type mining machines, the coal mining industry in general has achieved remarkable dust reduction for the most risky face occupations. In addition, important developments have been made in the field of dust measurement since the gravimetric dust sampling replaced microscopic counting of particles in 1970 in Britain. Gravimetric dust samplers simulating the human lung efficiency curve with elutriators or cyclones, multi-stage cascade impactors, instantaneous dust monitoring instruments and various types of sizing instruments are outcomes of the research on dust measurement.

The medical efforts associated with CWP have been directed at identifying causal agents and establishing threshold doses (Hammad et al., 1981). Data gathered through epidemiological surveys show regional differences in the prevalence of CWP. Subsequently, efforts to correlate this discrepancy with the environmental data have been made. Although some of the studies, particularly on free silica, show conflicting and inconsistent results, numerous factors are hypothesized to account for the observed regional discrepancy. These include rank of coal mined, free-silica content, mass of dust, and the chemical and mineralogical composition of the dust. One reference (Mutmansky and Lee, 1984) with a comprehensive list of literature on these factors can be consulted for more information. However, comparisons with environmental data were limited by the insufficient amount of information on the characteristics of coal, coal mine dust and lung dust. Even though some studies have been done on dust characterization for both engineering and medical purposes, most of the research was designed mainly for the establishment of the procedures for characterization.

As discussed so far, the potential health hazards associated with coal mine dust have been drastically reduced through engineering as well as medical efforts. However, dust control problems still prevail in the mining industry and technical and/or theoretical limitations on dust characterization necessitate research to reduce the dust contamination in the mine environment and also to identify the causal agent or agents of CWP. One desirable direction of dust research in the future is the determination of dust characteristics, so that benefits in the areas of engineering and medical control of dust can be realized in the long term. This necessity was well addressed by the National Academy of Sciences (Anon., 1980) as follows:

> Research should be directed more toward obtaining fundamental understanding of the origin, transport, and characteristics of respirable coal mine dust. (p. 3)

1.3 Objectives and Orientation of the Study

This report, based upon the necessity of performing fundamental research on dust, has two main objectives. Characterization of two basic characteristics of airborne coal mine dust, the size and elemental composition, is the first objective. The second objective is to analyze the size and elemental characteristics of samples at various locations to gain an understanding of some of the aspects associated with the source of airborne coal mine dust inclusing the transfer of chemical elements from point to point. This also includes the analysis of the ramifications of the study to medical studies attempting to study the development of CWP.

Section 2 is allocated for discussion of the significance of the size and elemental characteristics of coal mine dust on

engineering dust control measures and medical concerns. Elemental data of Pennsylvanian coals are analyzed to explore a possible association of the elemental composition with the rank of coal, a property which many researchers showed to be correlated with the prevalence of CWP. To establish a sampling strategy for dust sampling, related topics such as selection and operation of samplers and other ancillary instruments and selection of sampling locations are discussed in Section 3.

In Section 4, size data on the airborne dust samples from eleven underground coal mine sections using continuous miners are analyzed. The mass-size data of dust samples are studied to test primarily two aspects of the conventional practice for size presentation: assumptions on the lognormal model for mass-size distribution and unimodality. In addition, locational variation of the size distribution and effects of the mining operations on the size consist of airborne coal mine dust are discussed.

Size dependence of the elemental composition in dust samples and its locational variability are studied in Section 5. Finally, the association of the elemental characteristics among the dust and channel samples is examined along with the relationship between the size and element composition. Applicability of these data to the source and transportability of coal mine dust and for the study of the relationship between the characteristics of airborne coal mine dust and those of the materials being cut are discussed in the same section.

Some of the ramifications of this thesis related to the engineering dust control measures and medical aspects of airborne coal mine dust are discussed in Section 6.

2. RESEARCH ON SIZE AND ELEMENTAL COMPOSITION OF COAL MINE DUST: ITS SIGNIFICANCE

To various degrees, the size of airborne particles influences the effectiveness of engineering dust control measures presently being used in underground coal mines. Therefore, such control measures subsequently influence the size consist of coal mine dust in the return airways. Most of the health-related concerns associated with coal mine dust are focused only on the respirable fraction of airborne dust, even though nonrespirable dust is also known to be hazardous in some diseases such as bronchitis. Whether mine dust particles are respirable or not is mainly dependent upon their sizes.

Particle size is a governing variable in determining the settling rate and transportability of coal mine dust. Therefore, the size also affects mine safety concerns such as the effects on mine fire and explosion hazards associated with the dust deposited along the mine entries. In the following sections, the size of coal mine dust particles and their relationship with these other topics are discussed further. Along with the significance of the particle size, implications of the elemental characteristics on understanding the regional discrepancies of the prevalence of CWP are studied by analyzing the association between the rank of coal and the elemental composition.

2.1 Significance of the Size of Coal Mine Dust on Health and Safety Concerns

Various mining operations such as coal extraction, roof bolting, loading and haulage inevitably generate a certain amount of dust. In continuous mining sections, the continuous miner and roof bolter operations are primary sources, while the secondary sources are mainly due to reentrainment. The amount of dust generated from each source is not readily quantifiable. Even when effects of coal extraction by a continuous miner are considered under controlled situations which exclude all suppression measures, the dust generating potential can hardly be measured on an absolute value basis (Roepke and Hanson, 1986). It is even more difficult due to the fact that the airborne mine dust which contaminates the mine environment is only a fraction of the dust being generated. It is also complicated by the fact that the airborne dust concentration in a mine atmosphere depends largely upon the effectiveness of dust control measures employed at the source and/or after the dust is airborne.

Effectiveness of dust suppression devices is generally governed by their design specifications and operating parameters unless the characteristics of coal mine dust vary significantly from one application to another. The effects of the variation in the characteristics of mine dust upon dust control measures are not easily studied. The complications are reflected in the fact that most of the data presently available on dust control effectiveness come from controlled laboratory experiments using

prepared coal dust. A recent study on the relationship between dust concentration at the face in several different mines and dust control parameters such as air velocity and quantity, water flow rate and pressure, and spray type concluded that a consistent relationship was not observed (Rankin et al., 1983). This conclusion is largely attributed to the lack of knowledge of the interacting mechanisms between coal dust and control measures and also to the varying characteristics of coal mine dust at different mines.

Among the various characteristics of coal mine dust, one which the effectiveness of dust control measures is dependent upon is the size of dust particles. Interactions between the size of particle and some common types of dust control measures employed at the face in underground coal mines are discussed in section 2.1.2.

2.1.1 Effects of the Size on Health Hazards of Coal Mine Dust

Dust particles that escape from the dust suppression devices are carried along the mine entries by the airstream. Usually, the coal workers are exposed only to this fraction of coal mine dust. Whether a dust particle can be inhaled and trapped in the respiratory tract to stay long enough to damage lung tissues depends upon many factors. The inhalability, which is defined as the probability of an airborne particle being inhaled from the ambient air, is influenced by particle size, density, inspiratory volumetric flow rate, and direction and velocity of the airstream (Mercer, 1975).

Inhaled particles will be transported to the surfaces of the respiratory tract by various mechanisms such as diffusion, gravitational sedimentation and inertial impaction. Therefore, the two physical characteristics of particles which are the major parameters for these mechanisms, size and density, along with the particle residence time and respiratory volumetric flow rate, govern the deposition of particles in the respiratory tract (Heyder et al., 1980). Deposition can take place in the extrathoracic and tracheobronchial airways as well as in the alveolar regions. However, particles deposited may also be removed from the respiratory tract and even translocated to other regions by various body defense mechanisms, most of which are still controversial (Brain, 1977).

The shape of the particle is also known to affect the aerodynamic behavior. However, the effects are significant only at a low Reynolds number and for fibrous dust (McNown and Malaika, 1950; Timbrell, 1965). Consequently, inhalability and deposition of particles are affected most significantly by their physical properties, mainly size and density. Particles with different densities can be described as a function of an equivalent size, the aerodynamic diameter. This hypothetical size is defined as the size of a spherical particle of unit density with the same settling velocity as a given particle of

arbitrary shape and density. Figure 1 shows size dependence of the total deposition and alveolar deposition of particles. Particles are the main carriers of the toxic elements in the mine atmosphere. Therefore, mass and size characteristics of the dust particles have to be identified to evaluate the health hazards of the potentially toxic elements.

2.1.2 Effects of the Size on Particle Deposition and Related Safety Concerns

Except for the extremely small fraction of particles inhaled by workers, particles that escape from control measures travel along the airways and a large fraction of them are deposited on the surfaces of the airways. Deposition of coal dust in the returns involves increased possibility of a disastrous mine fire or explosion. Transportability of coal mine dust which is of great concern in mine health and safety considerations depends upon the kinematic behavior of particles with respect to fluid motion (Hammad et al., 1981).

Particle transport and deposition in turbulent flow which can be observed in underground coal mines are not yet fully understood (Friedlander, 1977). In general, diffusional transport and inertial deposition are the major mechanisms for small particles (less than about 1 μm) and larger particles, respectively. They are also affected by the air velocity and other external force fields as in the case of charged particles. The transition zone between convective diffusion and inertial deposition is not fully understood either. The amount of coal mine dust in this boundary range, 0.9-2.0 μm, varies with locations as shown in Appendix 4. Sometimes, it exceeds 10 percent of the total airborne dust.

A parameter which is most critical in the major mechanisms of particle settling and transportation is the terminal settling velocity. This parameter, in turn, is governed by the size of the particle. An underground measurement (Kost et al., 1981) shows that the settling of dust particles in the mine atmosphere is directly related to their sizes.

Coal mine dust deposited along the mine entries may also constitute fire and explosion hazards to some extent, depending upon its flammability. Regardless of the type of coal, the current federal standards require no less than 65 percent rock dust in all working faces and no less than 80 percent rock dust in the return airways. Although the effects of particle size on flammability are not fully known, the effects of variation in dust particle size and strength of initiation are known to be more significant than the rank of coal (Anon., 1981). Also, the peak burning velocity is known to depend upon particle size (Smoot, 1977). At the lean-limit dust concentration, there is no particle size dependence, while at higher concentrations, the flammability behavior clearly shows particle size dependence (Hertzberg et al., 1979). Consequently, the size of dust

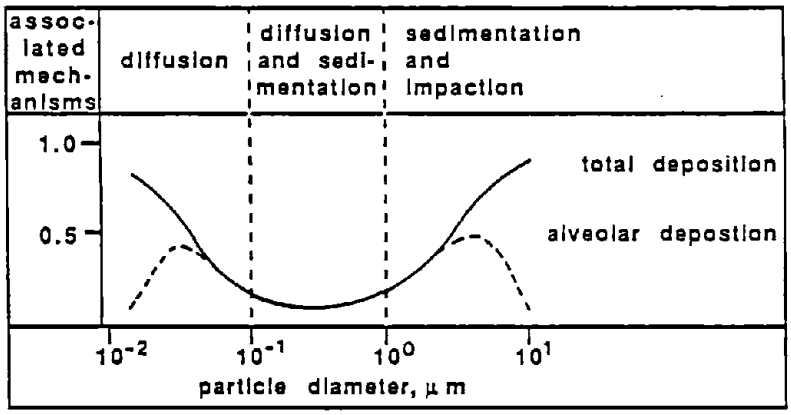

Figure 1. Deposition of Particles in the Human Respiratory Tract (after Heyder et al., 1980).

particles influences the potential of fire and explosion hazards in two different ways. First, particle size affects the transportability of coal mine dust and subsequently, the amount of dust deposited along the entries which is mainly combustible materials. Secondly, it directly affects the flammability of dust.

2.1.3 Effects of the Size on Dust Control Measures

The most common form of dust control measure presently in use at the face in underground coal mines is water sprays. Water sprays have been used to control the dust formation at the source, to prevent dust from becoming airborne, and to capture airborne dust. Another purpose recently developed is to control air currents in order to confine dusty air against the face and subsequently away from personnel. Among these diversified purposes, scrubbing of airborne dust from the air has been the major function of water sprays, even though their relative contributions to dust control are not yet fully known. The scrubbing effects of water sprays are widely studied, theoretically as well as experimentally. The way a spray works is that the water droplets enter the dust cloud, collide with dust particles to form water-dust agglomerates and then settle. Impaction is known to be the main mechanism for collection of dust particles greater than about 0.5 μm (Cheng, 1973).

Among the various design and operating parameters, the parameters extensively studied so far include water flow rate and pressure, the number, size and velocity of water droplets and the nozzle arrangement (Jayaraman et al., 1985). Because most of the experimental research is aimed at improvement of the collection efficiency of water sprays for dust particles in the respirable size range, the efficiency is described as the reduction of the overall dust concentration level. Consequently, although a size dependence of dust collection efficiency is known to exist, actual data on it are not readily available. An early report (Walton and Woolcock, 1960) indicates increasing efficiency with increasing particle size even though their experiment was done with droplets greater than 500 μm diameter. This observation on size dependence was confirmed by later research using theoretical modeling of the collection efficiency (Soo, 1967; Cheng, 1973) and using experimental measurement (Tomb et al., 1972).

In the theoretical equation developed by Cheng (1973), collection efficiency is described as a function of capture efficiency, characteristic length for the total capture process, mean drop size and flow rate of water and air. Further, particle size is a variable governing the capture efficiency (also called fraction impaction). The fraction impaction is defined as the ratio of the cross-sectional area of the original dust-laden airflow to the projected area of the water drop. According to the model, the size of particles significantly affects the overall collection efficiency. Information comparing the

predicted efficiency with experimental data collected in a horizontal duct using a solid-cone spray nozzle is reproduced in Figure 2. The overall respirable dust collection efficiency of water sprays currently in use ranges from 20 to 60 percent with a mean value of 35 percent (Emmerling and Seibel, 1975).

Another dust control device more recently introduced is the mechanical dust collector known as a scrubber. During the 1970s, about 150 scrubbers were installed to control dust in underground coal mines. Most of them are no longer operating due to various shortcomings in the design and operation. Disadvantages of the scrubber include high purchase and maintenance costs, low reliability and relatively low collection efficiency (Grigal et al., 1982). However, research on scrubbers has recently been resumed because the intrinsic characteristics of the scrubber have possible applications in a blowing brattice ventilation system for better methane and dust control and in deeper cuts up to 50 feet by increasing the brattice setback (Volkwein, et al., 1985). As a result, improved scrubbers such as the flooded fibrous-bed scrubber and water-powered scrubber were developed.

Scrubbers mounted on the mining machine or placed near the dust generating sources scrub dust-laden air using axial fans or water sprays. The collection-bed panel inside a scrubber is sprayed with water continuously and filters dust-laden air. Dust is impacted on the panel and settles on the bottom where it is pumped out. Finally, a mist eliminator removes water droplets from the air.

As for any type of dust collection device, the effectiveness or collection efficiency of scrubbers is the product of scrubbing efficiency times capture efficiency. The scrubbing efficiency, which is the probability of airborne dust particles being induced into the mechanical control devices, is not yet fully known, but lowering the turbulence of airflow at the tip of the line brattice by increasing the setback distance is inferred to lead to higher scrubbing efficiency for a machine-mounted scrubber (Volkwein et al., 1985). The scrubbing efficiency is comparable in nature to the inlet efficiency of dust sampling devices which is governed by the relative difference between the velocities of the main airstream and sampling inlet and also affected by the size of particles (Friedlander, 1977). Another similar situation can be observed at the inlet of the auxiliary tubing, which has been extensively studied. However, the dust capture efficiency has never been extensively studied. Figure 3 shows the collection efficiency for a flooded, fibrous-bed panel measured gravimetrically as well as on the particle number basis by Anderson impactors and the Donaldson Airborne Particle System, respectively.

Mainly due to poor maintenance of the dust collectors, roof bolter operations generate a certain amount of dust, usually with high content of silica (Anon., 1985). However, the amount of dust generated by a bolter also depends upon the collection

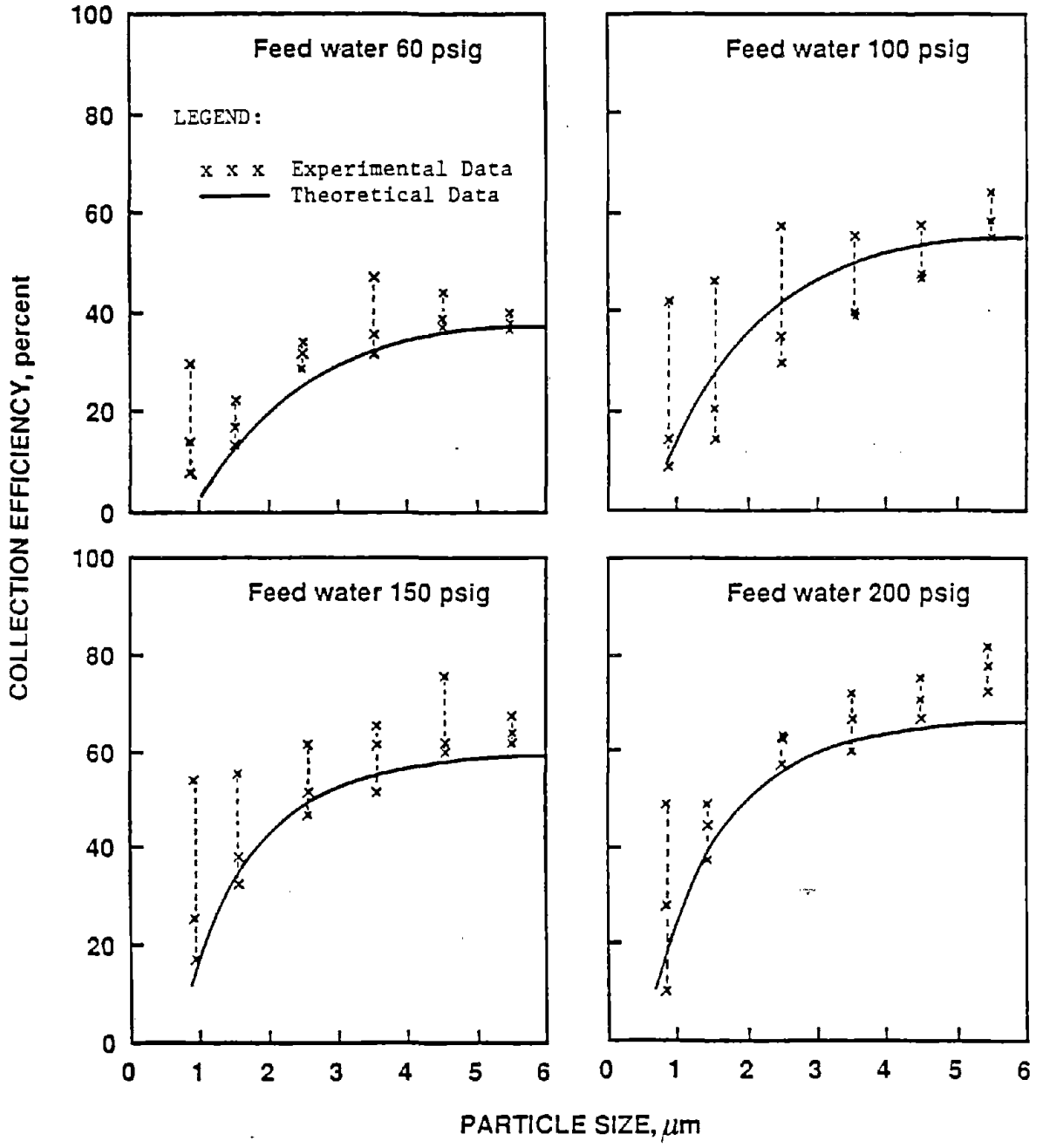

Figure 2. Effects of Particle Size on Water Spray Collection Efficiency (after Cheng, 1973).

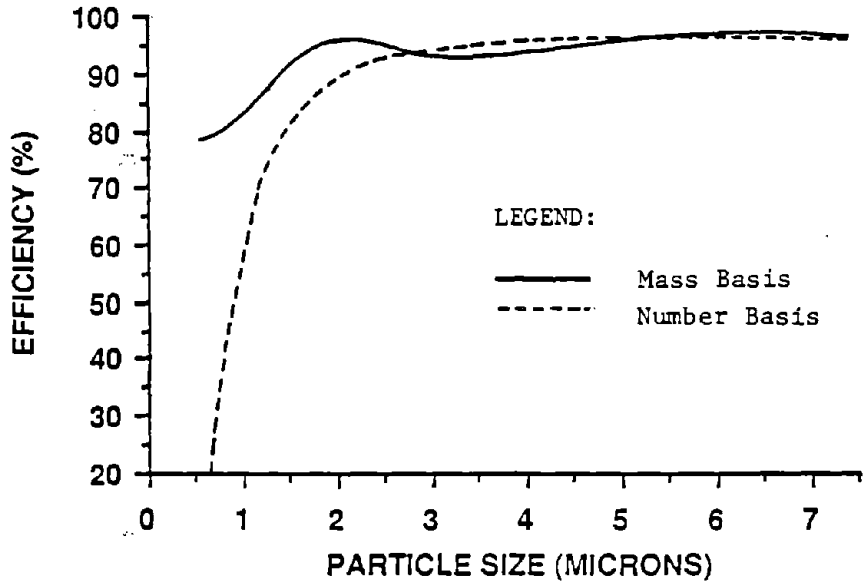

Figure 3. Collection Efficiency of a Scrubber Panel (after Grigal et al., 1982).

efficiency of the filter cartridge used in the dust collection system of the roof bolter. The most commonly used types of filters are cloth types and pleated paper types. The only information available concerning the collection efficiency of these filters for rock dust is the overall efficiency over the entire respirable size range. However, it is theoretically known that for large particles the interception mechanism controls the collection efficiency and the efficiency increases with particle size, while for the small particles, diffusion is the major mechanism and the efficiency increases as particle size decreases (Chen, 1955). Figure 4 shows the respirable dust generating potential using various types of filters measured in underground coal mines.

2.2 Relationship Between Elemental Variation and the Rank of Coal

Wide variation in the incidence of CWP among different coalfields has been reported in several countries including the U.S., Britain, West Germany and France. Even though the correlation is weak in some cases, the general trend shows a positive correlation with the rank of coal: i.e., the higher the rank of coal, the higher the incidence of CWP. Rank is the degree of metamorphism or the succession of changes in the properties and structures of coal due to the geochemical processes (Given, 1973). According to the American Society for Testing and Materials (ASTM) standards for coal classification, the rank of coal ranges from meta-anthracite and anthracite through various ranks of bituminous coal to lignite in decreasing order. The classification reflects the degree of coalification; the higher the rank, the higher the fixed carbon and the lower the volatile matter.

Although many epidemiological studies show a significant positive correlation between the incidence of CWP and the rank of coal being mined, the specific component or components which cause the regional discrepancy have not yet been identified. Furthermore, the suggestions related to the rank hypothesis have been subject to some criticism, mainly due to the questionable representativeness of the samples of coal workers studied. A critic (Naeye et al., 1971) says that some of the rank-related suggestions may be fortuitous.

Regardless of the constant criticism, the significance of the rank of coal on the progression of CWP has been a topic that many researchers have investigated. The efforts to find certain characteristics associated with the rank-related supposition of the incidence of CWP provided various hypotheses. In general, the physical and chemical changes in evolving coal are inferred to underlie the differences in the prevalence of CWP (Hicks et al., 1961).

More specifically, even though it is controversial (Naeye et al., 1971), the rank effect as measured by the amount of the

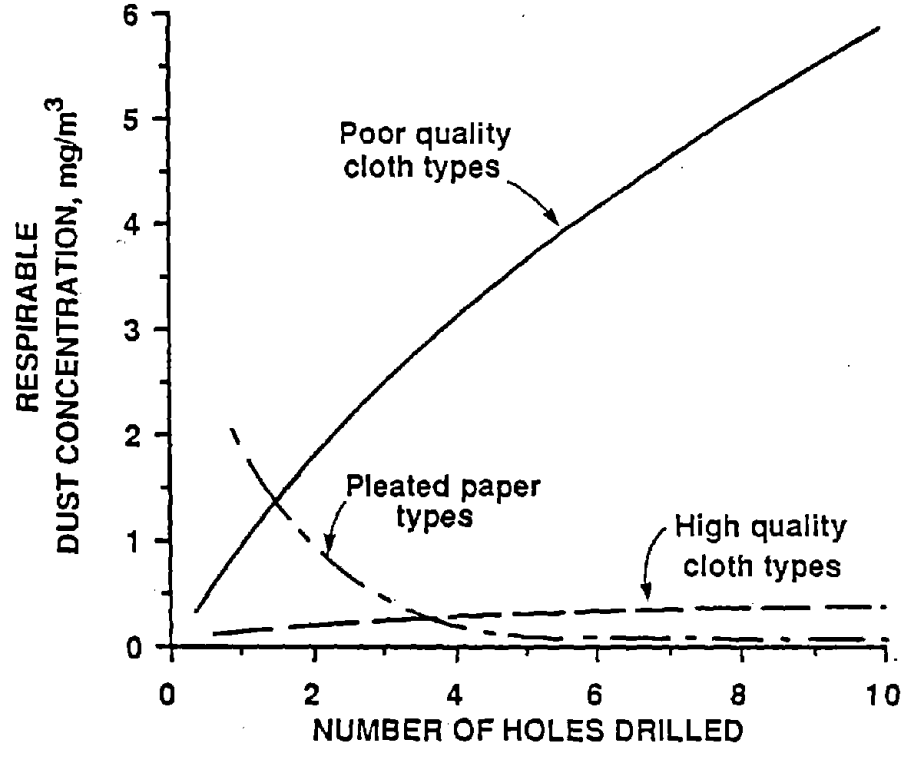

Figure 4. Respirable Dust Generation Using Various Filters on Roof Bolters (after Anon., 1985).

fixed carbon has been speculated as a possible causal agent leading to the regional differences in the incidence of CWP (McBride et al., 1963). Some of the components of coal mine dust such as the organic fraction of coal and free silica are found to be closely associated with the rank (Nagelschmidt, 1965). The size distribution of coal mine dust varies with the rank of coal being mined and consequently, the mass of respirable dust varies with the rank; higher mass concentration occurs in coal with higher rank (Leiteritz et al., 1967; Jacobson et al., 1971). On the contrary, a study by Reisner (1971) shows that coal with lower rank produces finer particle size. Recognizing the significance of the mass of respirable dust on the development of CWP, a more recent study (Bennett et al., 1979) suggested that the mining methods employed in the past at coal mines with high-rank coal generated higher concentrations of respirable dust and this might be a possible reason for the regional differences.

2.2.1 Studies on Elemental Characteristics

Possible linkage of elemental characteristics with the incidence of CWP has been supported by studies on elemental characterization of lung dust from deceased miners plus airborne coal mine dust as well as coal. A series of analyses of the concentrations of metals in the lung dust indicate that some of the trace metals such as Mg, Be and V positively correlate with the lung damage, while there are no significant correlations with Cr, Cu, Fe, Mn, Ni, Ti and Zn (Crable et al., 1967; Crable et al., 1968; Keenan et al., 1971; Carlberg et al., 1971; Sweet et al., 1974). Comparison of the levels of elements in miners' lungs with that in normal lungs shows that several elements such as Al, Ba, B, Ag and V have significantly higher concentrations in miners' lungs (Freedman and Sharkey, 1978).

Regional variation of the elemental composition in coal mine dust and coal being mined has been reported. Five major elements in respirable coal mine dust sampled by personal samplers are found to vary by region; samples from Pennsylvania and Ohio show higher concentrations of Si, Al, Fe and Mg, and little difference in Ca compared with those from Colorado and Utah (Wesson and Armstrong, 1975). Another study (Sorenson et al., 1974) compared some metals in coals from two different coalfields in Pennsylvania and Utah showing significantly different incidences of CWP. The results show that Fe, Ni, Cu, Pb and Zn have higher concentrations in Pennsylvania where higher incidence occurs; there is insignificant difference in the content of Cd. A more recent and comprehensive study on the inorganic components of U.S. coals (Glick, 1984) show regional variability of the elemental concentrations. The eastern province has high levels of Si, Al, Ti, K, Cr, Ga, La, Rb, Se, V, Y and Yb; low levels of Mg, Ca, Na, Mn and U. The interior province has high concentrations of Fe, Be, Mn, Ni, U, Zn and S, and low concentrations of Si, Al, Ti, P, Ba, Ga, La, Sr and Zr. The western province shows higher content of Mg, Ca, Na, P, Ba, Sr and Zr, and lower content of Fe, K, Be, Cr, Cu, Ni, Rb, Sa, V, Y,

Yb, Zn and S. In addition, significantly higher levels of Al and Si are found in the anthracite region compared to those in the Appalachian region. Variability of the oxides of major elements with the rank of coal show positive correlations with CaO, MgO, Na_2O, SO_2, SiO_2, Al_2O_3, TiO_2, while Fe_2O_3 does not appear to follow any definite pattern in relation to rank (O'Gorman, 1971).

Based upon these studies, it appears that concentrations of some of the elements vary among different coalfields and some of them may have correlations with the progression of CWP. However, as is the case in all the other suppositions explaining the regional discrepancy, the supposition that chemical characteristics are closely associated with the development of CWP, either directly or synergistically, has not been proven (Freedman, 1978). Although the observed correlation of element concentrations with the progression of lung damage might be caused synergistically in the presence of other causal agents, the relationships still need to be studied further until conclusive findings can be made.

Job-switching involving a change of mines and individual environment and susceptibility have not been accounted for in epidemiological studies to find the effects of elemental and other characteristics of coal mine dust. The presence of other pollutants makes the limitation worse. The difficulty of obtaining epidemiological and environmental data including coal mine dust characteristics is another obstacle. So far, based upon the limited data, various suppositions have been made. However, the wide variation in the incidence of CWP with rank is still one of the major questions yet to be answered along with the effects of free silica on the development of CWP (Hamilton, 1985).

2.2.2 Prevalence of CWP and the Rank of Coal in Pennsylvania

The state of Pennsylvania had been and still remains as one of the major coal producing regions in the U.S., even after the demand for anthracite coal plunged at the early part of this century. The rank of coal in Pennsylvania ranges from anthracite to high-volatile bituminous. Its anthracite coalfields and the Utah bituminous coalfields were the subjects of one of the first epidemiological studies on anthraco-silicosis performed by the U.S. Public Health Service in the 1930s.

Since then, similar epidemiological studies of coal workers have been carried out in different coalfields; in some cases, environmental studies have been done simultaneously. In 1963, the Pennsylvania Department of Health studied airborne coal mine dust at several anthracite coal mines mainly for identification of the dust generating sources. Between 1963 and 1966, 1,858 anthracite coal miners participated in roentgenographic examinations and 30 percent of the participants were found to have CWP (McBride et al., 1966). In a later study in Luzerne, Northumberland and Schuylkill counties (Tokuhata et al., 1970),

approximately 34 percent showed X-ray abnormalities. Another study by the Pennsylvania Department of Environmental Resources, which covered anthracite as well as bituminous coalfields, showed varying incidence rates of CWP; 19.3 percent in anthracite coal mines, 11.6 percent in low- and medium-volatile bituminous coal mines, and 6.4 percent in high-volatile coal mines.

A study done throughout the country by the U.S. Public Health Service and the Bureau of Mines found 60 percent of the Pennsylvania anthracite coal miners who participated had CWP, while 47 percent of the Pennsylvania bituminous coal miners who participated were found to have CWP (Morgan et al., 1972). The results of the first round of the National Coal Study (NCS), conducted from October 1969 through July 1971, indicated that 45 percent of the Pennsylvania anthracite coal miners had the simple form of CWP and 14 percent had Progressive Massive Fibrosis (PMF) (Morgan et al., 1973).

In the Central Pennsylvania bituminous coalfields covering low- and medium-volatile bituminous coals, the first extensive environmental study was performed in 1959 through 1961 (Baier and Diakun, 1961). A pneumoconiosis study on 5,072 coal miners in this region indicated that about 25 percent of the participants received positive roentgenographic classification. The first round of NCS showed 36.3 percent had simple CWP and 4.8 percent had PMF (Morgan et al., 1973). In the Western Pennsylvania coalfields with high-volatile bituminous coals, an early study, 1960 through 1961, reported that 11 percent of the participants in this region received positive roentgenographic classification (McBride et al., 1963). The first round of the NCS indicated that 48.3 percent of the participants from this region had simple CWP, while 1.3 percent had PMF (Morgan et al., 1973).

As shown in all the studies stated previously, the incidence of CWP varies among these coalfields with different ranks; diminishing incidence rate with decreasing rank of coal. In particular, the results of the first round of NCS confirm the association of the incidence of CWP with the rank of coal which had been observed previously in Britain and Germany (Attfield, 1985).

2.2.3 Analysis of the Elemental Composition of Pennsylvania Coals

In the previous section, the results of epidemiological studies indicate the significant differences in the incidence of CWP in the three Pennsylvania coalfields with different ranks. Therefore, in this section, possible association of the incidence of CWP with the elemental characteristics of each is statistically tested by studying the correlation between the ranks and elemental characteristics of coals from those fields.

2.2.3.1 Analysis of the Elemental Composition of Coal

The elemental characteristics of Pennsylvania coals used in this section were obtained from the Penn State Coal Data Base managed by the Penn State Coal Research Section. In this data base, coals from 25 states in the U.S. are analyzed and their physical, chemical, mineralogical and petrographical characteristics are stored along with descriptions of the origin of the samples. From this data file, only the elemental data of the whole-seam channel samples from Pennsylvania were searched and analyzed. The resulting data cover 99 whole-seam channel samples; more detailed information concerning the sampling location, coal seam and rank can be found in Appendix 1.

As stated previously, the purpose of this section is to find possible differences in the elemental characteristics of the coals from the three coalfields which have shown significantly different incidence rates of CWP. Therefore, for comparison with the previous epidemiological studies, the sorted 99 coal samples are categorized into three groups according to their sampling locations as shown in Figure 5: (1) the eastern anthracite coalfield, (2) the central low- and medium-volatile bituminous coalfield and (3) the western high-volatile bituminous coalfield. The number of data belonging to each group and the distribution by the county and coal seam are listed in Table 1. As shown in the table, coal samples are well diversified geographically and include a wide range of ranks and coal seams.

The elements analyzed for these samples include 17 trace and 10 major elements. The trace elements are Ba, Be, Cr, Cu, Ga, La, Mn, Ni, Rb, Sc, Sr, U, V, Y, Yb, Zn, and Zr, while Si, Al, Ti, Fe, Mg, Ca, Na, K, P and S are the major elements. However, not all the samples are analyzed for these 27 elements; many samples have missing values for some of the trace elements. This is mainly due to the fact that several different analytical

Table 1. Distribution of Elemental Data for Pennsylvania Coals.

Coalfield and Rank	Number of Samples	Number of Counties Sampled	Number of Coal Seams Sampled
Eastern Anthracite Coalfield			
Semi-anthracite	5	2	4
Anthracite	6	3	6
Central Bituminous Coalfield			
Low-volatile	21	3	11
Medium-volatile	29	6	9
Western Bituminous Coalfield			
High-volatile	37	9	10

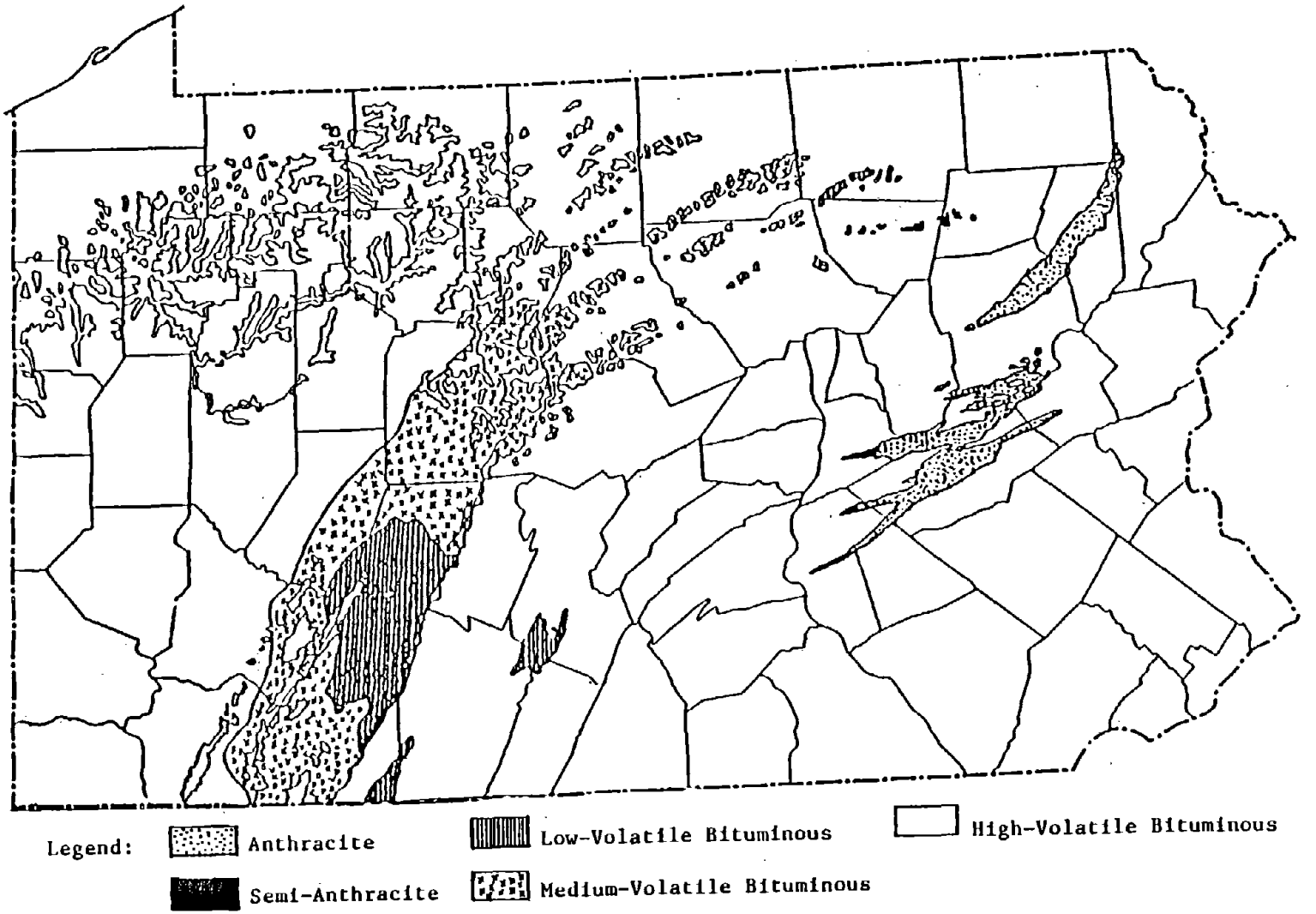

Figure 5. Distribution of Pennsylvania Coals.

methods have been employed for elemental analysis and some of the analytical tests are no longer routinely performed.

Application of several different methods for elemental analysis also resulted in a much wider range of lower detection limits; they are significantly wider than those expected from the application of a single multi-element analytical method. Even in the case where an element is undetected by an analytical method, its real concentration can be higher than those of some of the elements detected by another highly sensitive method. Therefore, all those elements with zero values in the data file cannot be treated as variables with true zero concentrations; instead, they have to be interpreted as either missing values, elements below the detection limits, or true zero concentrations. Consequently, this information is taken into consideration for the selection of the elements in this section.

The elements which have zero values in all the samples and those elements with zero values in some of the samples in a systematic manner are excluded from the analysis. In addition, the elements which had been analyzed by an analytical method that is no longer used are also excluded. This ends up with 11 trace and 10 major elements: Ba, Be, Cr, Cu, Mn, Ni, Rb, Sr, V, Zn and Zr for trace elements and all 10 major elements mentioned previously. The complete elemental data set for these samples can be found in another reference (Glick, 1984).

The 11 trace elements are analyzed separately from the major elements. This is intended to prevent some of the elements from being deleted in most of the multivariate statistical methods when the number of data is exceeded by the number of elements. Deletion of the extra number of variables occurs due to the singularity of the covariance matrices. Furthermore, as discussed previously, trace elements have been of more interest than major elements in the study of CWP.

2.2.3.1.1 Univariate Analysis

Table 2 shows the mean values of concentrations of each element and the spread of data in the three coalfields. The concentrations of the trace elements are in units of ppm (parts per million) by weight on a whole-coal basis, while the major element concentration is expressed by the weight percentage on a whole-coal basis. The sulfur content includes the total sulfur in the whole coal; pyritic sulfur, sulfur as sulfates and organic sulfur. The coefficient of variance, which is the ratio of the standard deviation to the mean values ranges from 37 percent to 295 percent for the trace elements and 34 percent to 170 percent for the major elements. Therefore, this wide range of data has to be considered to compare the differences in the mean values of the element concentrations among the three coalfields; in other words, to test the effects of the rank of coal.

Table 2. Univariate Analysis of Major and Trace Elements.

Elements	Eastern Coalfield		Central Coalfield		Western Coalfield	
	Mean	CV	Mean	CV	Mean	CV
Major Elements						
Si	4.33	44.5	3.24	64.8	2.57	41.9
Al	2.74	45.9	2.30	63.7	1.54	34.0
Ti	0.21	50.9	0.14	78.7	0.10	46.2
Fe	0.45	70.6	1.75	78.7	2.22	55.2
Mg	0.05	46.9	0.06	83.3	0.05	48.1
Ca	0.05	58.7	0.12	85.8	0.13	56.7
Na	0.04	69.9	0.03	65.0	0.02	62.6
K	0.34	50.7	0.27	100.3	0.16	56.0
P	0.01	107.5	0.03	169.8	0.04	116.0
S	0.85	55.8	2.06	66.6	2.93	49.2
Trace Elements						
Ba	113.53	42.3	117.33	97.7	165.33	220.9
Be	2.15	75.4	2.46	47.8	3.08	44.6
Cr	48.94	37.0	29.43	67.1	21.97	42.0
Cu	30.50	53.5	22.63	70.5	23.45	65.0
Mn	43.91	143.8	42.53	295.1	35.47	269.8
Ni	42.39	72.9	17.50	67.8	27.50	71.8
Rb	20.74	62.2	16.48	100.1	9.25	55.6
Sr	39.98	82.4	111.23	106.9	165.65	98.4
V	51.58	69.8	36.04	65.6	27.52	51.0
Zn	20.71	95.4	26.04	78.3	35.53	69.3
Zr	61.03	67.2	39.81	82.0	29.50	43.3

Notes: (1) The units for major and trace element concentrations are % and ppm by weight, respectively.
(2) CV denotes the coefficient of variation.

As an initial step for comparison, the analysis of variance (ANOVA) test is performed for each element. The ANOVA test compares the differences between the group (the rank of coal) means and the overall mean (among-group variances) and the differences between individual data and the overall mean (total variance). The test measures the significance of the ratio of these two variances; in other words, it measures the significance of the group effects. The results of the ANOVA tests are included in Table 3. It should be noted that all statistical tests performed in this thesis were executed using the well-known SAS statistical software package. Readers who are interested in obtaining more information on the statistical procedures used here are referred to the user's manual (Anon., 1985).

As shown, according to the univariate ANOVA, Be, Cr, Ni, Rb, Sr, V and Zr have significantly different concentrations in the three different coalfields at an alpha risk of 5 percent. All the major elements, except Mg and P, show significant differences at an alpha risk of 5 percent. Even among the elements showing significant rank effects, some elements such as Be, Rb, and Sr in the trace element group and Si, Ca, Na and K in the major element group show relatively weak effects.

Similar results are obtained from the Ryan-Einot-Gabriel-Welsch multiple F-test (REGW F-test) designed to control the type 1 error for comparison of more than two means simultaneously. Regional differences in the concentration of Be are insignificant according to this test, but all the other trace and major elements show identical inferences as in ANOVA tests at an alpha risk of 5 percent. Among the trace elements with significant statistical rank effects, all the elements except Sr have higher concentrations in the eastern anthracite coalfield than in the bituminous coalfields. Also, most of the major elements with significant differences among the three coalfields show higher concentrations in the anthracite coalfield, while the bituminous coalfields contain higher levels of Fe, Ca and S.

2.2.3.1.2 Multivariate Analysis

Effects of the rank of coal, if any, might have affected the characteristics of a part or all of the elements of coal at the same time in the three different coalfields. Therefore, if there exist strong associations among the elements, the correlation has to be taken into consideration for the test of the significance of the rank effects with respect to the element concentrations. So far, all the tests have been performed without consideration of the correlations of the elements. For treatment of the data with multiple attributes, multivariate statistical methods have usually been employed. The most common multivariate method for evaluation of the mean differences on two or more criteria variables simultaneously is multivariate analysis of variance (MANOVA) (Bray and Maxwell, 1985). An alternative to MANOVA is a separate ANOVA test for each criterion variable. However, because the possible associations are assumed to be zero in ANOVA

Table 3. ANOVA Tests of Major and Trace Elements.

Elements	F-Value	Prob>F	REGW Multiple F-test
Major Elements			
Si	4.73	0.0110*	1>2,3
Al	6.66	0.0020*	1,2>3
Ti	7.35	0.0011*	1>2,3
Fe	9.22	0.0002*	2,3>1
Mg	1.59	0.2096	no difference
Ca	4.45	0.0142*	2,3>1
Na	4.25	0.0170*	1,2>2,3
K	4.77	0.0106*	1,2>2,3
P	1.59	0.2091	no difference
S	12.01	0.0001*	3>2>1
Trace Elements			
Ba	0.48	0.6177	no difference
Be	3.38	0.0380*	no difference
Cr	12.31	0.0001*	1>2,3
Cu	1.24	0.2953	no difference
Mn	0.05	0.9485	no difference
Ni	10.17	0.0001*	1>2,3
Rb	5.00	0.0086	1,2>2,3
Sr	4.53	0.0131*	2,3>1,2
V	5.34	0.0063*	1>2,3
Zn	2.93	0.0580	no difference
Zr	5.75	0.0044*	1>2,3

Notes: (1) The asterisk indicates the significance of differences at an alpha risk of 5 percent.
(2) The numbers, 1, 2 and 3 in the column of REGW Multiple F-test denote the mean values of elemental concentrations in the eastern, central and western coalfields, respectively.
(3) Two numbers connected by a comma indicate no difference between them.

tests, the MANOVA test has an advantage when considering the correlations between the elements.

As in the univariate ANOVA test, MANOVA measures the significance of the ratio of the among-groups deviations to total sample deviations. However, in MANOVA, the deviations are in the form of sum of squares and cross product (SSCP) matrices including all the variables in question. MANOVA, which can replace many aspects of other multivariate analyses such as cannonical correlation, discriminant analysis and even principal component analysis, requires several assumptions such as random sampling of variables, statistical independence of data, normality of data and equality of the covariance matrices. The first two assumptions must apply strictly to almost all statistical methods, while departure from some of the other assumptions may not result in seriously biased inferences (Olson, 1974). Since the quality of resulting inferences is known to be dependent upon how close the sampled population is to the multivariate normal distribution (Johnson and Wichern, 1982), one of the assumptions that has drawn much attention is the normality requirement.

Robustness (the relative statistical insensitivity) of MANOVA to departure from normality is largely dependent upon the size of the data set as well as the characteristics of the data themselves. However, the degree of robustness has been questioned by many statisticians. Generally, this assumption is less crucial to large data sets, but for smaller data sets ($n < 25$), deviation of a sample from normality may significantly affect the interpretation of the data. Another difficulty in testing multivariate normality is complexities involved in the testing methods. In practice, multivariate normality has been tested by looking into the univariate normality of each variable, even though univariate normality is necessary but not sufficient for multivariate normality. The test statistics frequently used for the univariate normality include skewness, kurtosis, chi-square, Kolmogorov-Smirnov and Shapiro-Wilk procedures. All these statistics are not sensitive to all types of non-normality; some have advantages over the other procedures for certain types of distributions (Shapiro and Wilk, 1965). At the time of this writing, none of the major statistical computer packages such as BMDP, SPSS and SAS possesses multivariate normality test capability.

In some studies on the analysis of the organic and inorganic fractions of coal (Gerencher, 1983; Glick, 1984), the variables showing non-normality as the results of skewness and kurtosis tests are transformed for the multivariate analysis. Even when the scales of those variables are changed through transformation, the correlation structure remains unchanged. Transformation of the variables is done with various orders of power functions for different variables and as a result, careful interpretation of the results is required. In those studies, even after transformation using power functions, two different test

statistics often show significantly different results. This is mainly due to the intrinsic limitations in the test statistics; one test is more sensitive to certain types of data distributions than another test. Therefore, when multivariate normality by the chi-square test of the equal density contours (Green, 1978) is tested for a variable for which the two test statistics show different inferences, transformation does not always show significant improvement in the multivariate normality of the data distribution. This has been observed by the author during this thesis preparation.

Another assumption on equality of the covariance matrices has also been questioned and its robustness is more controversial than the normality assumption. In most practical applications, departure from this assumption has not been tested because MANOVA is considered to be fairly robust. However, if the group data size is unequal, MANOVA is generally found to be less robust (Ito, 1980).

In this report, the assumption on multivariate normality is not tested. This is partly due to the shortcomings associated with data transformation found in the related studies as stated previously. More importantly, in many cases the methods are more robust than the assumptions underlying them (Shapiro and Wilk, 1965) and fortunately, at least under many conditions, violating some of the assumptions does not necessarily result in invalidation of the results (Bray and Maxwell, 1985).

Table 4 contains the results of MANOVA tests for the equality of the centroids of the element concentrations in the three coalfields. All the statistics including Hotelling's T^2, Wilk's lambda, Hotelling-Lawley's trace, and Pillai's trace indicate significant differences in the trace and major element concentrations among the three different coalfields in Pennsylvania. The differences, which have been called the rank effects at several occasions in the previous sections, are significant even at an alpha risk of 1 percent.

Provided that significant differences exist in the overall concentrations of the 11 trace and 10 major elements among the three coalfields, discriminant analysis can be employed to test the significance of the classifying power of the discriminant function with respect to the elemental profiles of coal samples. A discriminant function is defined as a linear composite of the elemental variables to maximize the ratio of the between-groups variance to the within-group variance. As shown in the following table, because the covariance matrices in each coalfield for the trace as well as the major elements are not equal among the three coalfields, the discriminant functions take nonlinear forms. Based upon the quadratic discriminant functions, the posterior probability, which is defined as the ratio of the joint probability of a group being present and observing a profile of a sample to the total probability of the profile occurring, are calculated for each sample. As a result, a prediction is made

Table 4. MANOVA Tests of Major and Trace Elements.

Statistics	Measurement	F-Approximation	Prob>F
Major Elements			
Hotelling's T^2			
H_o: 1 = 2	43.6239	3.71	<0.01
H_o: 1 = 3	76.9008	6.22	<0.01
H_o: 2 = 3	42.1226	3.77	<0.01
Wilk's Lambda	0.4426	4.38	0.0001
Hotelling-Lawley's Trace	1.0666	4.59	0.0001
Pillai's Trace	0.6428	4.17	0.0001
Trace Elements			
Hotelling's T^2			
H_o: 1 = 2	47.1290	3.57	<0.01
H_o: 1 = 3	145.1318	10.39	<0.01
H_o: 2 = 3	57.3734	4.60	<0.01
Wilk's Lambda	0.4134	4.34	0.0001
Hotelling-Lawley's Trace	1.1863	4.58	0.0001
Pillai's Trace	0.6828	4.10	0.0001

Note: The numbers, 1, 2 and 3 in the column of Statistics denote the mean values of elemental concentrations in the eastern, central and western coalfields, respectively.

and the discriminant functions assign the sample to a group with the highest posterior probability.

Table 5 contains the identification numbers of samples and the posterior probabilities for misclassified samples. None of the samples from the eastern anthracite coalfield are misclassified. Two of the 50 samples from the central bituminous coalfield are misclassified to the anthracite coalfield using a discriminant based on the 10 major elements, while none of the bituminous coal samples is misclassified to the anthracite coalfield on the basis of the trace element discriminant. Some misclassifications occur between the central and western coalfields. However, the probability of misclassification is relatively low for every group of data; 27 percent misclassification is the maximum probability observed using the major element concentrations in the central low- and medium-volatile bituminous coalfield.

The results of the discriminant analyses show the same results as with the ANOVA and MANOVA tests, i.e., the presence of significant differences in the element concentrations of coals from the three Pennsylvania coalfields. In the next step, some variables which contribute significantly to the discrimination are identified by stepwise discriminant analysis. The statistic used for the selection of the entering and leaving variables at each iteration is Wilk's lambda which is defined as the ratio of the absolute values of the SSCP matrices associated with the error terms and the hypothesis.

Table 6 shows the results of the stepwise discriminant analysis. Among the 11 trace elements, Cr, Ni, Sr, Zn and Cu contribute most to the discriminant models in decreasing order. S, P, Al, Si and Mg are those major elements with higher discriminatory power. These results are somewhat contradictory to the previous results from ANOVA in Table 3. This is partly due to ignoring the correlation structure in ANOVA tests. ANOVA tests indicate that some of the elements which are identified as the variables contributing most to the discrimination of the three coalfields do not show significant differences in their concentrations; these include Cu, Zn, P, and Mg. As in the univariate stepwise regression analysis, the final model chosen by the stepwise discriminant analysis is not always the best model. Therefore, any final conclusion has to be made on the basis of all the available information.

The cannonical correlation analysis is not attempted in this section because it is designed to find linear composites of the criterion and predictor variables and to provide the relationships between the linear composites and each variable. In the case of unequal covariance matrices, discrimination by linear functions is known to be inappropriate (Green, 1978). As shown in the previous table, the hypothesis of the equality of group covariance matrices is rejected with the trace as well as the major elements.

Table 5. Analysis of Samples Misclassified Based upon the Major and Trace Element Concentrations.

Based upon Major Elements

Misclassified Sample ID (Penn State Sample No.)	Posterior Probability			
	From	To 1	To 2	To 3
620	2	0.00	0.22	0.78
631	2	0.00	0.10	0.90
632	2	0.00	0.30	0.70
879	2	0.95	0.03	0.02
324	2	0.00	0.05	0.95
635	2	0.00	0.08	0.92
1024	2	0.00	0.11	0.89
1026	2	0.00	0.06	0.94
1027	2	0.00	0.33	0.67
1028	2	0.77	0.04	0.19
1029	2	0.00	0.06	0.94
1195	2	0.00	0.27	0.73
1144	2	0.00	0.14	0.86
1261	2	0.00	0.11	0.89
102	3	0.00	0.62	0.38
328	3	0.00	0.94	0.06
1141	3	0.00	0.61	0.39

Test of equality of within-group covariance matrices:
chi-square = 363.22,
prob>chi-square = 0.0001,
significant differences.

Percentages of misclassifications:
4% from 2 to 1,
24% from 2 to 3,
8% from 3 to 2.

Table 5. (Continued).

Based upon Trace Elements

Misclassified Sample ID (Penn State Sample No.)	Posterior Probability			
	From	To 1	To 2	To 3
619	2	0.00	0.10	0.90
875	2	0.00	0.49	0.51
880	2	0.00	0.06	0.94
634	2	0.00	0.44	0.56
1027	2	0.00	0.42	0.58
1196	2	0.00	0.49	0.51
1261	2	0.00	0.32	0.68
102	3	0.00	0.71	0.29
328	3	0.00	0.96	0.04
331	3	0.00	0.57	0.43
614	3	0.00	0.88	0.12
1017	3	0.00	0.95	0.05
1018	3	0.00	0.75	0.25
1034	3	0.00	0.71	0.29
1035	3	0.00	0.73	0.27
1099	3	0.00	0.89	0.11
1171	3	0.00	0.66	0.34

Test of equality of within-group covariance matrices:
chi-square = 495.64,
prob>chi-square = 0.0001,
significant differences.

Percentages of misclassifications:
14% from 2 to 3,
28% from 3 to 2.

Note: The numbers, 1, 2 and 3 in the column of From, denote the eastern, central and western coalfields.

Table 6. Identification of Major and Trace Elements with Significant Discriminatory Power.

Order of Significance	Elements	Partial R^2	Wilk's Lambda	Prob>Lambda
Major Elements				
1	S	0.2001	0.8000	0.00
2	P	0.1266	0.6343	0.00
3	Al	0.0704	0.5897	0.00
4	Si	0.1081	0.5259	0.00
5	Mg	0.1473	0.4670	0.00
Trace Elements				
1	Cr	0.2042	0.6958	0.00
2	Ni	0.1754	0.6562	0.00
3	Sr	0.1786	0.5390	0.00
4	Zn	0.0906	0.4901	0.00
5	Cu	0.0686	0.4565	0.00

Note: This table is based upon the results of the stepwise discriminant analysis at an alpha risk of 15 percent.

2.2.3.2 Summary of the Analysis

The elemental data analysis was performed to test the significance of differences in the element concentrations of coals from the three different Pennsylvania coalfields with different ranks of coal and with different incidence rates of CWP. Differences in the overall composition of the major and trace elements in coals from those three Pennsylvania coalfields are shown to be significant. This indicates that differences in the elemental characteristics of coal may be associated with the regional differences in the incidence of CWP observed in those coalfields. As far as individual elements are concerned, most of the trace elements showing significant variation among the different coalfields show higher concentrations in the coalfields with higher rank. This includes Cr, Ni, Rb and Zr. However, Sr which is found to be highly concentrated in the western high-volatile bituminous coalfield, shows the lowest concentrations in the eastern anthracite coalfield. Among these trace elements, Cr and Ni contribute most to the discrimination of the three coalfields. Significantly higher levels of these two elements are observed in the eastern coalfield with the highest rank of coal.

Most of the major elements except Mg and P show some degree of association with the rank, while Al, Si, Ti, Fe, and S show significantly different concentrations among the three coalfields. Al, Si and Ti have the highest concentrations in the eastern anthracite coalfield. Among these major elements, S and Al show the most distinctive variation when the correlation among the elements is taken into account. Like Fe, the sulfur content decreases as the rank of coal increases; the western high-volatile bituminous coalfield shows the lowest levels of Al and Fe.

However, coal mine dust may not have the same elemental characteristics as the coal being mined. Mine dust can be contaminated by the noncoal materials from the face or external sources such as intake air, rock dust and utilization of mining equipment. Even though coal is the major component of the airborne coal mine dust in most cases, the information obtained in this section has to be carefully interpreted. Some of the differences between the elemental characteristics of in-place coal and coal mine dust are discussed in Section 5.

3. DESIGN OF A SAMPLING STRATEGY

Most of the coal mine dust sampling in the U.S. has been carried out for compliance purposes. Therefore, the results are evaluated for the assessment of risk involved in designated high-exposure occupations such as the miner and roof bolter operators in the continuous mining section. What is being sought in this type of occupational sampling is the probability of those occupations being overexposed to coal mine dust (Esmen, 1982). In most of these cases, the only parameter considered is the time-weighted average exposure on the basis of dust concentration data collected in the vicinity of workers at about the elevation of the breathing zone.

In measuring the risk of overexposure in occupational sampling, the major concern is when and how often the samples must be taken. Much research work has been performed on these topics at the institutions associated with enforcement of the related regulations including the Mine Safety and Health Administration (MSHA) and the National Institute for Occupational Safety and Health (NIOSH) (Bowman et al., 1983).

As stated previously in Section 1, the coal mine dust samples required for this study are primarily for characterization purposes. Also, the area of interest covers the entire working section to obtain information on the locational variability of the characteristics. In addition, sampling locations associated with the primary and secondary dust generating sources are included to study the effects of various sources on the dust characteristics. Therefore, the desirable sampling strategy for this study is different from that for occupational sampling.

In the following sections, the related topics such as selection of sampling locations for the sections in continuous miner development openings, choice of samplers and operation of samplers are discussed. Definition of the type and meaning of the dust samples collected for this study are other topics treated in this section.

3.1 Sampling Locations

Selection of the sampling locations is dependent primarily upon the layout of the mining operations and the ventilation scheme employed at the face. However, the following criteria have been applied to standardize the sampling plan at various mining sections employing different types of mining practices and face ventilation methods.

1. Characteristics of dust originating from different sources are to be studied separately. Therefore, if separate splits of air are used for the continuous miner and roof bolter operations, then the two splits will be sampled separately.

2. Secondary dust generating sources including reentrainment of dust by equipment movement will be studied.
3. Influence of the primary dust sources on return airway contamination will be studied.
4. Characteristics of coal mine dust will be compared with those of materials being mined by analyzing the channel samples taken from the face.

Figure 6 illustrates typical sampling locations based upon the above criteria. The sampling layout is shown with a continuous miner development section employing a double-split ventilation scheme with line brattices for the continuous miner and roof bolter. Sampling location 1 is for intake air sampling. Two locations are assigned to the vicinity of each of the primary dust generating sources, one in the immediate intake air and the other in the immediate return air. This is intended to make it possible to evaluate the effects of the source itself. Two additional sampling locations in the return airway of each operation are allocated to study the range of influence of the dust sources.

This sampling plan is basically a fixed-point method. However, all the sampling locations except one in the intake airways are not stationary. Since sampling duration required for most of the currently available samplers except the high-volume samplers is usually longer than the time to complete a cut, place changes of the continuous miner and/or roof bolter are expected during sampling. If a place change occurs, all the sampling locations allocated to each operation are moved in order to maintain relatively equal distances from the operations. This results in sampling locations designated as 2, 3, 4 and 5 moving with the continuous miner while sampling locations 6, 7, 8 and 9 move with the roof bolter.

The sampling plan is standardized in terms of distances from the face operations. This is for comparison of the data from the same sampling locations at different sections or mines. However, some modifications of the sampling plan are required at the faces utilizing a single-split of air for the continuous miner and roof bolter. In this case, one of the two units is to operate downstream of the other, depending upon their relative positions. Under this circumstance, it is difficult to separate the effects of the two operations on the return air contamination. Therefore, only two sampling locations are assigned in the return airway by keeping the same distance from the nearest unit; one at two crosscuts and the other at four crosscuts outby the unit in the return.

Another situation requiring modifications is where auxiliary fans and tubings are used instead of line brattices. This condition makes it difficult to choose a sampling location for the immediate return. However, a temporarily stagnant or slowly moving dust cloud can often be observed near the face and several

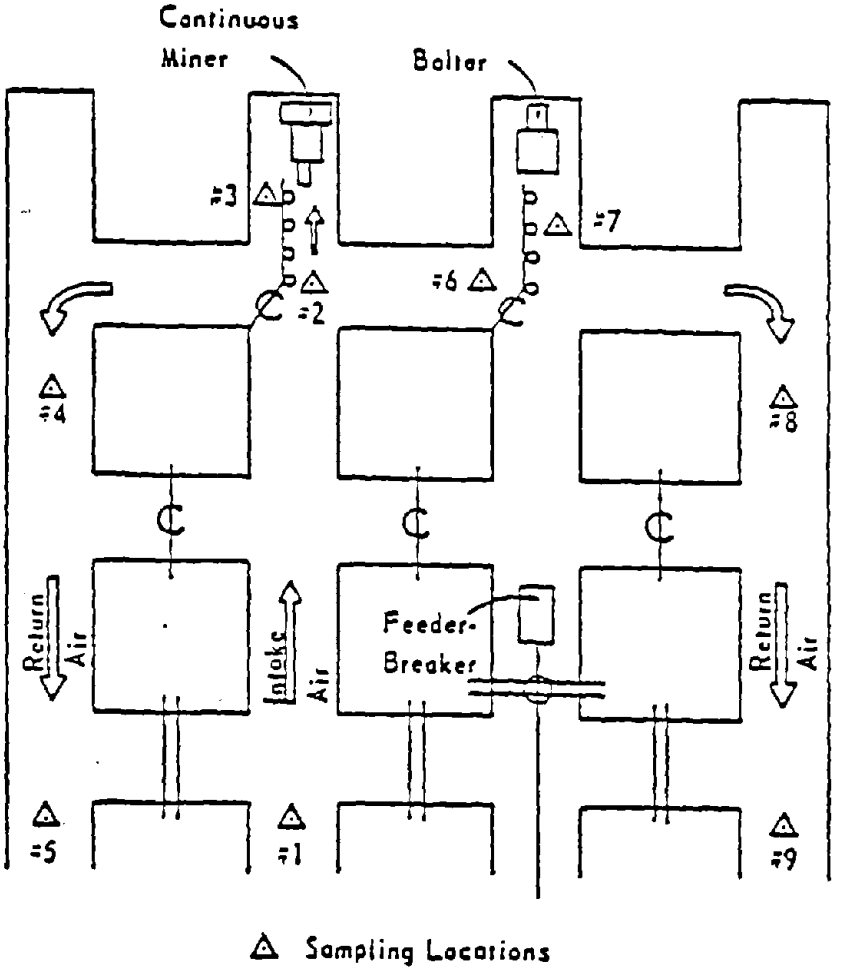

Figure 6. Sampling Locations for a Continuous Miner Development Section Using Line Brattices.

feet outby the inlet of tubing. Thus, an alternative sampling location can be chosen within this dust cloud. Depending upon the specific circumstances at each mine, choice of this location has to take into consideration the possibility of samplers being hit by the continuous miner's drum or water sprays.

Samples collected at any location should be representative of the total coal mine dust floating at that particular location during the assigned sampling time. This definition affects not only selection of the sampling point over the cross section of airway but also sampler selection.

Other than the physical characteristics of particles such as shape, size and density, velocity of the airstream is the most important parameter in governing particle transport and settling. Therefore, this implies that the air velocity is a critical factor in choosing a specific sampling point in the cross section of the airway. Air velocity varies over the cross section and also fluctuates with time. Errors in the measurement of velocity and dust concentration due to the time-dependent fluctuation of the velocity are difficult to control. Velocity measuring instruments can be traversed in order to minimize the cross-sectional variation of the air velocity. However, it appears almost impossible to traverse the sampling instruments in the same fashion due to the consequent changes in the inlet sampling efficiency and the large number of personnel required. In addition, those samplers assigned near the mining operation are likely to be in the shuttle car route. Therefore, sampling points near the rib and roof may be a necessity where shuttle cars must operate.

A typical cross-sectional variation of the air velocity is shown in Figure 7. As shown in this figure, the velocity contours were measured in the straight portion of a coal mine airway. The velocity near the rib is relatively low compared with that near the center, while the velocity gradient near the roof or bottom is much higher. Therefore, velocity at those points too close to the rib and roof is likely to be much lower than the average traversed velocity. This indicates that if there is no factor leading to perturbation of the airflow patterns, points close to the rib and roof are not desirable sampling locations (Rankin and Rodgers, 1980). Furthermore, velocity at the center is the highest and its magnitude of turbulence is the lowest (Thimons and Kohler, 1985). Therefore this point is also excluded for consideration.

The primary concern for selection of a fixed sampling point in the cross section of the airway is to find a point with near the average air velocity over the cross section. Therefore, based upon the typical velocity contour in Figure 7, samplers assigned to the intake and return airways such as samplers 4, 5, 8 and 9 in Figure 6, are placed midway between entry center and the roof. Samplers are hung from the roof bolt bearing plates. The samplers for the immediate returns of the miner and roof

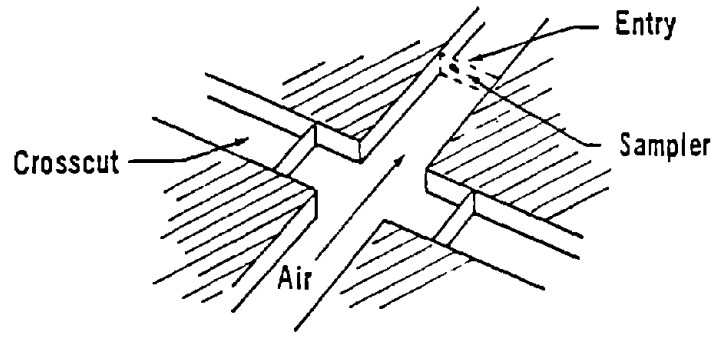

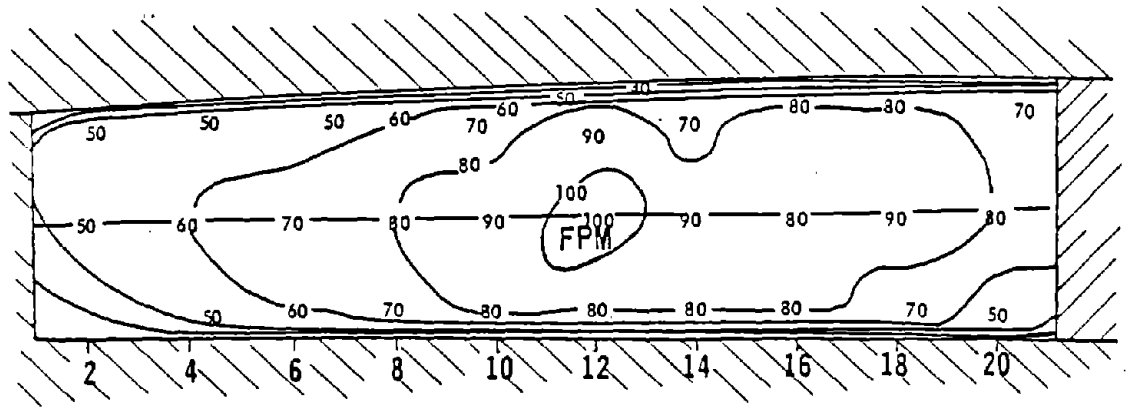

Figure 7. Cross-Sectional Variation of Air Velocity (after Rankin and Rodgers, 1980).

bolter operations can be placed at the same height midway between the line brattice and the rib. However, because the samplers for the immediate intake of the mine and bolter operations such as locations 2 and 6 are in the travel path of the equipment, the samplers are placed near the rib and the roof; usually, 1-3 feet from the roof and 4-6 feet from the rib, depending upon the entry dimension. Even though air velocities at these sampling points may be lower than the average velocity, high turbulence due to the frequent changes in the airflow pattern created by the equipment movement can reduce the possible errors resulting from the velocity differences. In addition, it is known that the cross-sectional variation of the dust concentration is less significant than that of the air velocity (Friedlander, 1977). Near the crosscuts, a change in air direction may result in high air velocity and dust concentration at one rib and low values at the other rib. In the corner of the entry possessing low velocity, air may be stagnant or recirculated. If this circumstance is observed, samplers are placed at the rib with the higher velocity.

3.2 Selection of Samplers

Most of the gravimetric dust samplers that have seen application in coal mines can be classified as either single- or multi-stage samplers. Open filters for total dust sampling belong in the single-stage class. Various size-selective samplers designed to simulate the efficiency curve of the human lung through the use of a preclassifier such as a cyclone or an elutriator also belong in the single-stage category. A typical example of a single-stage size-selective sampler is the personal sampler used for compliance dust sampling in underground coal mines. It is composed of a cyclone and a filter encapsulated inside a plastic cassette.

All these single-stage samplers collect samples on collection filters or in a liquid medium. For size analysis, dust samples from these samplers must be transferred and dispersed in a gaseous or liquid suspension medium. Subsequently, this process is likely to destroy the characteristics of agglomeration which are important in understanding the aerodynamic behavior of particles. As far as the size characteristics are concerned, use of a separate sizing instrument creates additional complexities. This is due to the fact that sizing instruments employing different principles are likely to provide different size data. The reported size may be dependent upon either volume, settling velocity, projected surface area or other characteristics of particles. Conversion of these sizes to the aerodynamic size which is of importance in this study is not always straightforward. Therefore, in order to reduce the possible problems associated with sample handling for the separate size analysis, the single-stage samplers which require sample transfer and separate sizing instruments were excluded from consideration.

One of the multi-stage samplers which is described as an ideal sampling instrument for the study of the association of dust characteristics with size is a multi-stage cascade impactor (Ahlberg et al., 1978). Even though there are disadvantages related to the small amount of sample in each size range, its usefulness is the ability to sample as well as classify the particles according to their aerodynamic diameters. However, in selecting a multi-stage cascade impactor for use in underground coal mines, several requirements must be met. First, its designed flow rate must be within the operating range of a commercially available permissible pump. If place changes occur during the sampling time, multi-stage impactors with pumps may have to be moved to other locations during sampling. Therefore, the second requirement is that the impactors and pumps must be compact and rugged enough for underground use. The high-volume impactors require relatively large pumps; permissible pumps for those impactors are not commercially available. Finally, since the samples required for this study are total airborne dust samples, any size-selective sampler was excluded.

Based upon these criteria, the Sierra Model 298 Marple cascade impactor now marketed by Anderson Samplers, Inc. was chosen. At the time of this writing, none of the multi-stage samples has been extensively tested with respect to the sampling efficiency in underground coal mines. In the last section, comparisons of the size and concentration data from the Sierra impactors with those from isokinetic sampling are made to study the sampling efficiency.

The disassembled form of a Sierra Model 298 equipped with the standard cowl and visor is shown in Figure 8 with a permissible Dupont Model P2500A pump. The Sierra Model 298 has eight collection stages and one backup stage. The principle of sampling is impaction of the particles with high inertia during the course of changes in the airflow direction. The dust-laden air is driven through the sampler by a pump and passes through a series of progressively smaller nozzles while the airflow changes direction on each stage. Larger particles are collected on the upper stages and smaller particles on the lower stages; collection is actually taking place on the surface of the collection substrates which are placed on all eight stages. Its classification size ranges from 0.5 to 21 μm. The common types of collection substrates are mylar and stainless steel. The finer particles which pass through all the eight stages are collected on the backup filter. A PVC filter with a 5-μm pore size is used for the backup filter with the collection efficiency shown in Table A.2.2 in Appendix 2.

3.3 Operation of Samplers

The accuracy of the size data provided from cascade impactors is governed by the sampling efficiency of the collection substrates as well as the amount of sample on each substrate. Particles impacting on a stage are to be collected on

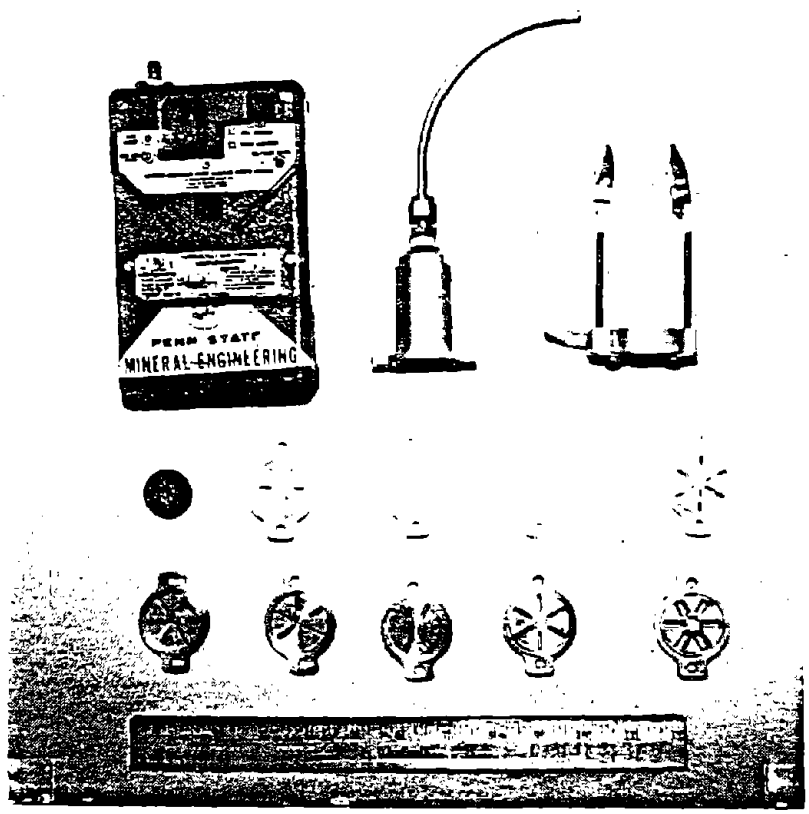

Figure 8. The Disassembled Form of a Sierra Model 298 Cascade Impactor with an Isokinetic Sampling Inlet.

the surface of the collection substrate. Therefore, bounce and blow-off of these particles are likely to lead to distortions of the size data (Esmen and Lee, 1980). To increase the collection efficiency of the substrates, a collection medium is usually applied to the surface. Several types of liquid or solid substances have been tested for various particles; the results show clear differences in the collection efficiency.

The amount of dust collected in various size ranges may be a significant factor in controlling the errors in size data. It must be at least larger than the sensitivity of the balance used for weighing and greater than the possible errors related to sample handling. However, in determining the amount of sample collected on each stage, the only controllable parameter is the sampling time; a longer sampling time always provides more samples if the concentration and the size distribution are assumed to be constant during sampling. Too much sample due to excessive sampling times may result in partial blocking of the nozzles and subsequently deviate the cut-off size of the stage (Burkhart et al., 1983). It may also increase the possibility of particle bounce and blow-off. In the following sections, these two main concerns, selection of a sticky substance for collection efficiency improvement and determination of the sampling time, are studied through experiments.

3.3.1 Selection of an Impaction Medium

Previously used impactor collection coatings include paraffin, high-vacuum greases and petroleum jelly. These are usually mixed with organic solutions and sprayed on the surface of the collection substrates. Therefore, in addition to the requirement for a high collection efficiency, a stable spraying mixture is needed to apply the mixture evenly over the collection area of the substrates.

To choose the most efficient collection medium, solutions of 20 percent by weight of paraffin, Apiezon L (a high-vacuum grease), and petroleum jelly were prepared using toluene as the organic base. All of the mixtures were found to be relatively stable and sprayable. The mixtures were sprayed using an artist's air brush operated at about 30 psi. Due to the evaporation of the solution, weight drift is often significant. Therefore, before weighing, all the greased substrates were put in desiccators for at least 12 hours for drying. The weighing balance used in this study is a Mettler Model M3 microbalance with a precision of 0.001 mg.

Six of the Sierra Model 298 cascade impactors were prepared for the experiments; two of the impactors were loaded with substrates using each grease. These impactors were placed in an aerosol chamber manufactured by Elpram Systems, Inc. and coal dust was dispersed by a TSI Model 3400 fluidized bed aerosol generator. Specifications of these pieces of laboratory

equipment can be found in the references by Marple et al. (1978) and Marple and Rubow (1983).

Coal dust used for this experiment was prepared in the laboratory by grinding channel samples. The ground coal dust was then classified using a cyclone to obtain a minus 21-μm size fraction for use in the chamber. The total dust concentration generated in the chamber was approximately 4 mg/m³, and the sampling duration was approximately 180 minutes. The dust-laden substrates were removed from the impactors and dried in the desiccators for more than 12 hours before weighing. None of the impactors were overloaded nor underloaded. The two mass size distributions from an identical type of grease were averaged and the final three size distributions are shown in Figure 9.

During the research for this study, the same dust was used for several other purposes. It was found that particles below 1 μm were usually less than 1 percent in mass. However, Figure 9 shows that the cumulative weight percentage of particles smaller than 1 μm is approximately 9 for Apiezon L and 10 for paraffin. Discrepancies of this type can be observed in the size ranges smaller than 6 μm. Overemphasis of the fine size fractions has also been observed by other researchers (Esmen and Lee, 1980). Particles bounced or blown off the upper stages end up on the lower stages and subsequently overemphasize the fine size fractions. To overcome these problems, it is desirable to choose the collection medium with the highest collection efficiency. However, it is also desirable to choose a medium that is organic to avoid interference with the subsequent analysis of the dust samples. Therefore, the mixture of petroleum jelly was chosen for all the sampling work in this study.

3.3.2 Sampling Time

As discussed previously, the sampling time determines the amount of sample collected and thus the accuracy of size data. In underground coal mines, dust concentration and size distribution vary at various locations. Therefore, application of an identical sampling time to all the samplers assigned to various sampling locations in Figure 6 may result in either underloading or overloading of certain samplers. The objective of the experiments was to find appropriate sampling times under various levels of dust concentration. In addition, the appropriate sampling time was defined as the shortest sampling time which leads to the statistically correct size distribution at a specific level of dust concentration.

To determine optimal sampling time, experiments were prepared using the aerosol chamber described in the previous section. The dust chamber was set to generate constant dust concentrations of about 1, 2, or 4 mg/m³. After a stable level was achieved, six impactors were placed in the chamber. Two impactors were removed after 90 minutes, two after 180 minutes, and the remaining two were left to run for the entire test time

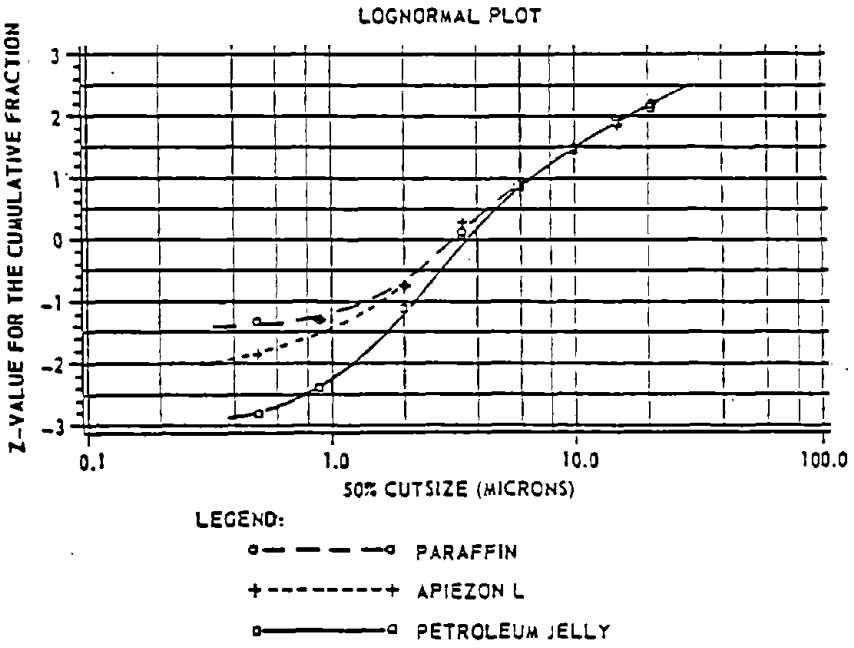

Figure 9. Lognormal Plot of the Mass Size Distribution of Coal Dust Using Three Different Impactor Substrate Coatings.

of 270 minutes. This experiment was run twice. To measure the dust concentration in the chamber during the tests, an instantaneous dust monitor (GCA Model PDM-1 Mini-RAM) was placed at the center of the chamber. Cross-sectional variation of the dust concentration inside the chamber was tested and found to be insignificant. Since the monitor has a preferential detection size range of minus 10 μm, the dust concentration reported in this section is that below 10 μm. The size data from the samplers with an equal sampling time and under the same concentration were averaged. Table 7 shows the size data from the experiments.

The average size distributions from different levels of dust concentration and different sampling times were compared to each other and to the known size distribution of the coal dust used in the experiments (Table 8). Statistical tests for this purpose assumed that all the size distributions can be approximated by the lognormal distribution with two parameters. Therefore, the test of the equality of a pair of size distributions can be accomplished by testing the equality of the two distribution parameters, the geometric mean and the geometric standard deviation. Table 9 illustrates the results of the modified Student t-test for the geometric mean comparison (Shen and Ring, 1984) and the F-test for the equality of the geometric standard deviation.

The experiments run at approximately 1 mg/m^3 indicate that the size distribution derived from a 180-minute sampling is close to the known distribution with a confidence level higher than 80 percent. The confidence level increases somewhat with the 270-minute sampling. However, even though the difference between the 180- and 270-minute sampling times is not statistically significant as shown in the table, the first two and the last two stages of the impactors from the 180-minute sampling were slightly underloaded. Underloading of a stage can be detected when the weight gain of the substrate is insignificant with respect to weight drift observed in the blank substrates. In the process of substrate preparation, several additional substrates which were not intended to collect samples were prepared only for weight calibration. After sampling was completed, the weight changes observed among these calibration substrates were averaged so that all the weight readings of the dust-loaded substrates could be adjusted. The weight change experienced through the experiments ranged from 5 to 10 μg. Considering that all the experiments were run in a well controlled situation, the errors associated with sampling handling are likely to increase in actual underground coal mine dust sampling. Therefore, it is concluded that for dust concentrations near 1 mg/m^3, sampling time for the impactors must be between 180 and 270 minutes.

At or about a level of 2 mg/m^3, the confidence level for a 180-minute sample is higher than 90 percent, while the 270-minute sampling also shows a relatively high confidence level of near 75 percent. However, the fifth, sixth and seventh stages of the

Table 7. Experimental Data for Optimal Sampling Time Determination.

Test Group	Sampling Time (minutes)	Dust Concentration (mg/m^3)	Geometric Mean (μm)	Geometric Standard Deviation
1	90	1.0	2.1	2.2
	180	0.9	3.0	2.0
	270	0.6	3.2	2.7
2	90	2.0	4.5	2.4
	180	2.5	3.1	2.6
	270	1.8	2.9	2.7
3	90	5.0	4.0	2.4
	180	3.5	4.9	2.0
	270	4.6	4.3	2.5

Table 8. Size Distribution of the Standard Dust Sample.

Impactor Stage	50% Cut Size (μm)	Cumulative Percentage (Finer Than %)
1	21.0	99.1
2	15.0	96.5
3	10.0	87.7
4	6.0	65.7
5	3.5	40.4
6	2.0	23.8
7	0.9	8.8
8	0.5	6.0

Note: The geometric mean and geometric standard deviation are 3.3 μm and 2.5, respectively.

Table 9. Comparisons of Size Data from Different Sampling Times.

Hypothesis	Test Value	Conclusion
GS(1,90) = GS(known) GM(1,90) = GM(known)	F = 0.77 t = 0.99	Equal Variance Confidence Level < 35%
GS(1,180) = GS(known) GM(1,180) = GM(known)	F = 0.64 t = 0.22	Equal Variance Confidence Level > 80%
GS(1,270) = GS(known) GM(1,270) = GM(known)	F = 1.17 t = 0.06	Equal Variance Confidence Level > 90%
GS(1,90) = GS(1,180) GM(1,90) = GS(1,180)	F = 1.21 t = 0.90	Equal Variance Confidence Level < 40%
GS(1,180) = GS(1,270) GM(1,180) = GM(1,270)	F = 0.55 t = 0.14	Equal Variance Confidence Level > 85%
GS(2,90) = GS(known) GM(2,90) = GM(known)	F = 0.92 t = 0.65	Equal Variance Confidence Level < 55%
GS(2,180) = GS(known) GM(2,180) = GM(known)	F = 1.08 t = 0.13	Equal Variance Confidence Level > 90%
GS(2,270) = GS(known) GM(2,270) = GM(known)	F = 0.77 t = 0.28	Equal Variance Confidence Level > 75%
GS(2,90) = GS(2,180) GM(2,90) = GM(2,180)	F = 0.36 t = 0.76	Equal Variance Confidence Level < 50%
GS(2,180) = GS(2,270) GM(2,180) = GM(2,270)	F = 1.40 t = 0.14	Equal Variance Confidence Level > 85%
GS(3,90) = GS(known) GM(3,90) = GM(known)	F = 0.92 t = 0.40	Equal Variance Confidence Level > 75%
GS(3,180) = GS(known) GM(3,180) = GM(known)	F = 0.64 t = 0.91	Equal Variance Confidence Level < 40%
GS(3,270) = GS(known) GM(3,270) = GM(known)	F = 1.00 t = 0.54	Equal Variance Confidence Level < 60%

Notes: (1) GS(known) and GM(known) denote the geometric standard deviation and geometric mean of the known standard sample size distribution, respectively.
(2) GS(a,b) and GM(a,b) denote the geometric standard deviation and geometric mean of the sample from test group 'a' that had a sampling time of 'b' minutes, respectively.

impactors run for 270 minutes often showed slight overloadings. Compared to underloading, overloading is much easier to detect by observing evidence of particle bounce or partial blocking of the nozzles. Therefore, 180 minutes was considered as an appropriate sampling time for a dust concentration near 2 mg/m^3. When the dust level was about 4 mg/m^3, sampling times longer than 90 minutes resulted in overloading and the size distributions were significantly deviated from the known. Even in the 90-minute sampling, slight overloadings were sometimes found. As results, it was concluded that the appropriate sampling time has to be shorter than 90 minutes.

In the subsequent field work, sampling time for each location was determined based upon the results of these experiments. The only sampling location which was assigned a sampling time less than 90 minutes was that behind the line brattice for a continuous miner. At this location, samplers were run only for one cut (usually less than an hour for a 20-foot advance) because most of the samplers operated for two cuts were seriously overloaded. Even though the amount of sample on each stage is determined by sampling time, dust concentration, and size distribution of dust, the experiments with a laboratory-fabricated sample having a size distribution different from the actual coal mine dust did not lead to significant errors based upon the sampling results.

3.4 Effects of Isokinetic Sampling Inlets

As mentioned previously, one of the objectives of this study is to study the possible size-dependency of the characteristics of the total airborne coal mine dust. The Sierra Model 298 impactor has a cowl and a visor which are designed to help prevent accidental contamination. Information concerning its sampling efficiency with this cowl and visor is available (Rubow et al., 1985), but the data were obtained with noncoal particles in calm air. Therefore, a different inlet sampling efficiency is expected in actual field sampling under different airflow patterns and velocities because along with the particle size, the ratio of the inlet sampling velocity and the ambient air velocity is the most important parameter in determining the sampling efficiency (Friedlander, 1977; Willeke and Tufto, 1983).

A series of experiments was performed in the Penn State simulated mine tunnel to compare the dust concentrations and the size distributions obtained from the impactors with and without isokinetic sampling inlets. Since isokinetic sampling inlets are not commercially available for the Sierra cascade impactors, special inlets were fabricated for this study (Figure 8). The isokinetic inlet was designed to be applicable to various velocities by exchanging only the nozzles of different diameters. A suite of six impactors was prepared; three with the isokinetic inlets and the others without them. Then the samplers were bound together with the inlets approximately 2 inches apart. The air velocity in the tunnel was controlled at 150 fpm by a centrifugal

fan, and a screw feeder was used to disperse fine sub-bituminous coal dust. The samplers were placed at the center of the tunnel and samples were taken for about 4 hours. An identical experiment was performed at an air velocity of 230 fpm. The experimental results are included in Table 10, while the size distributions are plotted in Figure 10.

During the field work performed for this study, effects of isokinetic sampling were studied on several occasions by placing multiple samplers at a given sampling location, some equipped with isokinetic sampling inlets. The averaged sample weights from these samplers with or without isokinetic inlets are included along with the air velocities and dust concentrations in Tables A.3.1 through A.3.7 in Appendix 3. Fitting of the mass size distributions plotted on lognormal paper by straight lines was not tried; this topic is discussed in more detail in Section 4.

The experimental results show that nonisokinetic sampling collected more dust than isokinetic sampling; the ratio of isokinetic sample weight to nonisokinetic sample weight was about 0.87. The maximum variation of the total sample weight among the data from the side-by-side samplers was 12 percent in terms of the coefficient of variation. This variation occurred for samples without the isokinetic inlets at a velocity of 150 fpm. In addition, the relative differences in the first three stages above 10 μm were apparently greater than those in the lower stages. However, these differences were neither consistent nor significant compared to the total sample weights. This is clearly shown in Figure 10 which indicates insignificant differences in the cumulative mass size distribution.

The ratio of the weights of the isokinetic to nonisokinetic samples in the field data ranges from 0.72 to 1.03, while that for the samples below 6 μm varies between 0.78 and 1.30. As shown, no definite correlation between the differences in the total sample weights and minus 6-μm sample weights was found. Therefore, as in the experimental data, differences in the sample weights were not correlated with the size.

The coefficient of variation of the total sample weight among the side-by-side samplers ranges from 9 to 26 percent. One study (Rankin and Rodgers, 1980) observed that the coefficient of variation among the side-by-side total dust samplers ranges from 13 percent in high dust concentration levels (> 1.5 mg/m^3) to 66 percent in low dust concentration levels (< 0.5 mg/m^3). Another study (Kost et al., 1981) shows a range from 3 to 11 percent. While contrary to the results of previous studies, the data by Kost et al. (1981) does not indicate any systematic variation with the level of dust concentration. Therefore, a considerable portion of the variation observed between the samplers with and without the isokinetic sampling inlets is believed to be associated with the intrinsic variation expected from the side-by-side samplers.

Table 10. Experimental Data for Isokinetic Sampling.

Sampler Stage	Cut size (μm)	Averaged Sample Weight (mg) Isokinetic Sampling (1)	Nonisokinetic Sampling (2)	Ratio (1)/(2)
		At an Air Velocity of 230 fpm		
1	21	0.224	0.248	0.90
2	15	0.226	0.359	0.63
3	10	0.486	0.748	0.65
4	6	0.936	0.932	1.00
5	3.5	0.635	0.662	0.96
6	2	0.544	0.539	1.01
7	0.9	0.049	0.044	1.11
8	0.5	0.015	0.021	0.71
F		0.009	0.008	1.31
Total Weight (mg)		3.122	3.561	0.88
		At an Air Velocity of 150 fpm		
1	21	0.055	0.081	0.68
2	15	0.081	0.124	0.65
3	10	0.181	0.244	0.74
4	6	0.326	0.320	1.02
5	3.5	0.236	0.254	0.93
6	2	0.209	0.235	0.89
7	0.9	0.027	0.024	1.13
8	0.5	0.016	0.014	1.14
F		0.004	0.007	0.57
Total Weight (mg)		1.135	1.303	0.87

Note: The total sample weight (mg) for each sampler is as follows:
at 230 fpm, isokinetic samplers: 3.228, 3.016,
nonisokinetic samplers: 3.622, 3.610, 3.450;
at 150 fpm, isokinetic samplers: 1.129, 1.220, 1.055,
nonisokinetic samplers: 1.127, 1.405, 1.375.

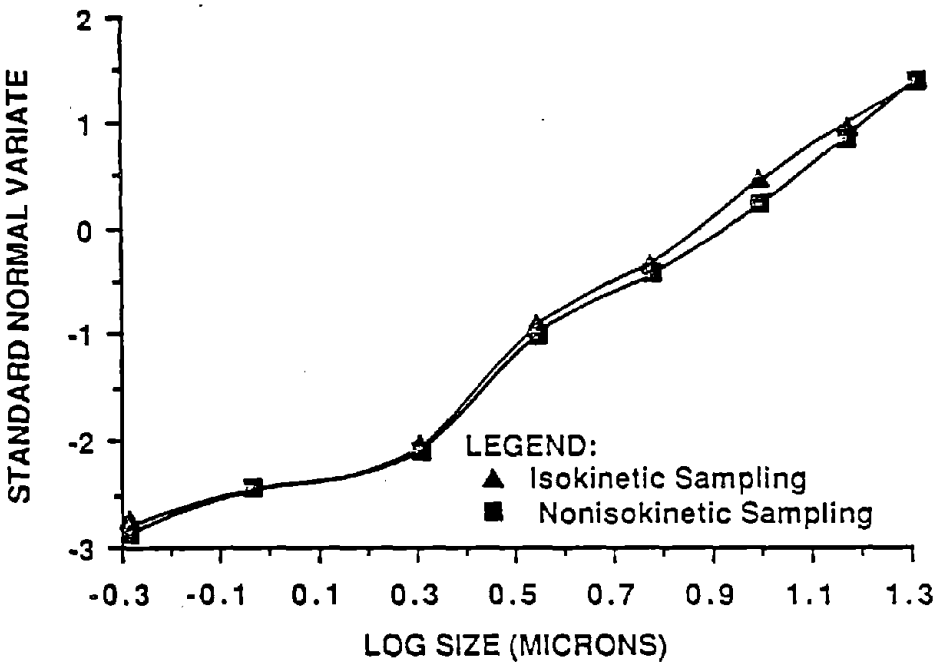

a. Lognormal Plot of the Data from 230 fpm.

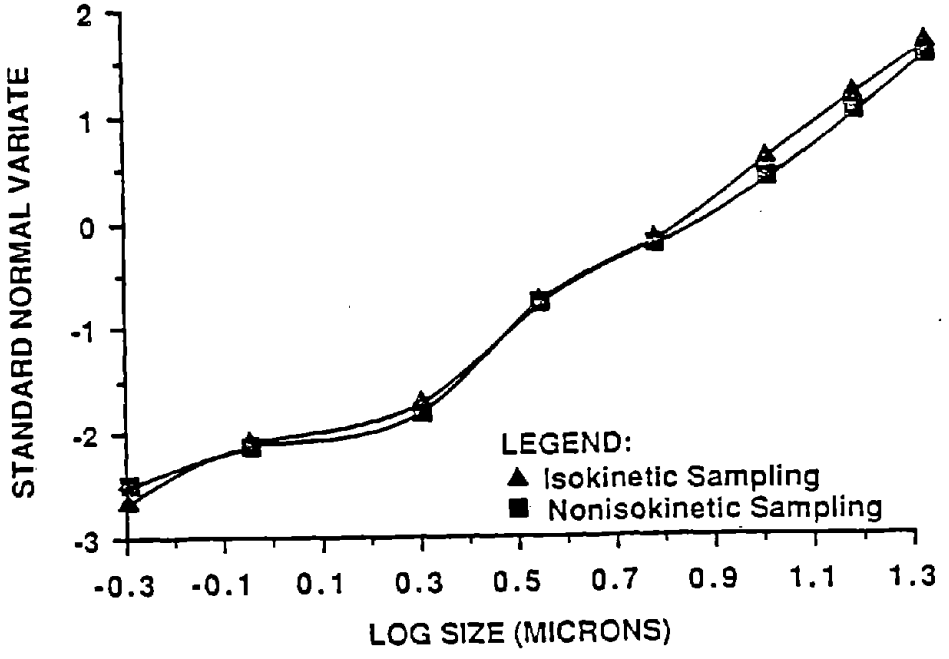

b. Lognormal Plot of the Data from 150 fpm.

Figure 10. Cumulative Lognormal Distributions of the Data in Table 10.

The mass size plots in Figures A.3.1 through A.3.7 indicate that in most of the cases the differences in sample weights in various size fractions between the isokinetic and nonisokinetic samples did not result in significantly different size distributions. Even among the size distributions showing some degree of discrepancy, no definite trends could be observed. Consequently, use of the Sierra Model 298 cascade impactors without isokinetic sampling inlets for total coal mine dust sampling is not likely to lead to significant errors with respect to dust concentration or mass size distribution.

4. ANALYSIS OF AIRBORNE COAL MINE DUST SIZE

The significance of airborne coal mine dust size in engineering control measures and dust-lung interactions is discussed in Section 2. Once coal mine dust size data are obtained either from the sizing instrument or directly from the samplers, representation of the size data may take various forms. Tabular representation is a common practice along with graphical representation which is often expressed as a histogram with either frequency or cumulative plottings being employed.

Another form of size data representation, the so-called analytical or statistical method, employs statistical distribution models to approximate the size data. Size data are often represented by statistical distributions using parameters usually associated with the mean value and spread of data. While not widely used on coal mine dust data, other statistical distributions utilizing more than two parameters are often employed. The analytical representation is aimed at finding the mathematical function whose behavior is known to be similar to the regularities observed in the size of particles in question (Deepak and Box, 1982). Therefore, for the purposes of size characterization and modeling of the behavior of atmospheric aerosols, the analytical method has been extensively studied.

An advantage of the analytical representation is that it is a compact way to describe the size distribution. The significance of the analytical representation of mine dust size can be readily appreciated because it can help gain insight into the dust formation mechanisms and transformations (Whitby, 1974) and can also help identify the source of dust (Perera, 1979). Therefore, the primary objective of this section is to examine the current practice for analytical representation of coal mine dust size. The two important assumptions implicitly made in the current practice, lognormality and unimodality, are tested. In addition, locational variation in the airborne coal mine dust size is discussed along with the effects of the mining operations on the size consists of coal mine dust.

4.1 Modeling of the Mass Size Distribution

Strictly speaking, whether the mean value and spread of data are simple, weighted or geometric, representation of size by distribution parameters does not necessarily require prior knowledge of the type of distribution model (Knutson and Lioy, 1983). These parameters can be calculated simply through mathematical manipulation. However, the resulting behavior (mathematical or statistical) of the parameters is governed by the distribution model itself. Thus, misapplication of the distribution parameters may lead to seriously biased inferences on the size data. Subsequently, size comparisons based upon the distributions may be incorrect in improper applications.

Distribution models with various numbers of parameters have been applied for size representation of mining and industrial workplace aerosols. Different distribution models have found application in different types of aerosols formed by various mechanisms. To list a few, they include the normal, lognormal, exponential, Weibull, Gaudin-Schumann, Gates-Meloy, power law, Rosin-Rammler, Rosin-Rammler-Bennet, Nukiyama-Tanasawa and Junge distributions.

As far as coal is concerned, the Gaudin-Schumann distribution is found to give remarkable agreement in the finer size range of crushed coal (Hogg, 1984), while the Rosin-Rammler distribution (which is identical to the two-parameter Weibull distribution) has been successfully applied to coal broken due to impaction (Allen, 1981). Meanwhile, the exponential distribution has been used to approximate the number size distribution of airborne coal mine dust (Wynn and Dawes, 1951). Power functions were also introduced for the same purpose (Hamilton and Knight, 1951). These applications of distribution models to coal mine dust were intended to acquire a knowledge of the size distribution to calibrate size data from instruments using different principles as well as to estimate the pneumoconiosis risk (Hodkinson, 1958). However, these two distributions are no longer used because gravimetric sampling has been employed in coal mines as a result of the recognition of the importance of the mass of coal mine dust in the development of CWP during the 1960s.

Among the various forms of distribution, the lognormal distribution has become the most widely applied model for a variety of materials and variables. Lognormality has been observed or assumed in many variables associated with coal mines; geologic variables such as grades and tonnage of deposits (Sinclair, 1976), variation in the coal mine dust concentrations at the face (Oldham, 1953), and coal workers' exposure to coal mine dust (Tuggle, 1981). One study (Coenen, 1966) listed four conditions as conducive to the occurrence of lognormality in environmental data:

1. a wide range of data, typically several decades wide;
2. asymmetric data close to a physical limit, e.g., a zero value;
3. increasing variability with increasing magnitude of data; and
4. finite probabilities of very large values occurring.

Based upon the central limit theorem, applicability of the lognormal distribution to environmental concentration data was theoretically studied in a paper by Esmen and Hammad (1977). The same theorem also shows that the distribution of a variable will be lognormal if the effects of its formation mechanisms are a function of the variable (Whitby, 1974). This applies to the nuclei and accumulation modes observed in the size distributions of atmospheric aerosols.

The mass-size relationship of coal mine dust seems to meet all four conditions listed above. However, these conditions are not sufficient to guarantee lognormality of coal mine airborne dust size. Questions can be raised whether it can be applied to all the dust samples taken at various locations when locational variability is significant. In addition, the central limit theorem predicts that in cases when dust samples are associated with multiple sources, the resulting size distribution is likely to be a normal distribution, whatever size distribution is generated from each source.

Critics of the method (Knutson and Lioy, 1983) list several factors that forge data into a lognormal mold:

1. ability and convenience of the graphical method to estimate the distribution parameters;
2. well-defined behavior of the distribution function; and
3. readily available probability paper.

This previous reference also reported significant departure from lognormality in many environmental data situations that seem to follow the lognormal distribution at first look. Among the factors listed above, the mathematical behavior of the lognormal distribution has played the major role in the assumption of lognormality in particle size distributions (Davies, 1974). Thus, this may lead to the preference for the lognormal distribution over other forms of distribution, even though the latter may give a better representation (Hogg, 1984).

The lognormality assumption for the mass size distribution of airborne coal mine dust has never been extensively tested before, even though its importance was often recognized. Therefore, the main objective in this section is to test the validity of the lognormality assumption in mass size distribution of coal mine dust by comparing the lognormal approximation with the empirical models. For this purpose, empirical models are derived without any assumption on the type of distribution, while derivation of the lognormal distribution is based upon the conventional practice which uses generalized histograms to obtain the continuous frequency distribution models.

4.1.1 Derivation of the Empirical Mass Size Distribution

On histograms representing the relationship between the size and mass of coal mine dust, the abscissa usually represents size and the mass in each size fraction is plotted on the ordinate. Because the height or area of each interval represents the mass of dust or its percentage, the overall shape of the histogram is closely associated with the selection of intervals. Even though some of the sizing instruments use equal linear or logarithmic increments (Knutson and Lioy, 1983), intervals are usually determined arbitrarily. Even the generalized histograms which adjust the height by the size intervals do not provide a unique

shape of histogram independent of the interval selection (Herdan, 1960).

The size interval for impactors is predetermined by the cut sizes of impactor stages which are defined as the sizes with collection efficiency of 50% on each stage. Therefore, the problem associated with the size interval is unavoidable in the graphical representation of the size data from impactors. Furthermore, as is the case for almost all sizing instruments including impactors, the relatively small number of intervals makes it even more difficult to conclude a specific size model from a histogram. Another complicated situation occurs when the dust samples are from a composite distribution, a mixture of more than one distribution. In many cases, presence of a composite distribution is not detectable in a histogram.

The conventional graphical methods to estimate the size parameters such as the mean and spread of data are based upon the cumulative plottings. Preference of a cumulative distribution in size representation seems to be due to the ease of data manipulation and relatively insignificant impacts of the arbitrary selection of intervals on the overall shape. Size data in each fraction are successively added and plotted on a type of probability paper which is assumed to be the best fit for the size data. Distribution parameters can be directly read from the plots or estimated through simple data manipulation. Therefore, validity of the final inferences on the estimates is largely dependent upon the goodness of fit of the size data plotted on probability paper.

Another limitation of the cumulative distribution is that it does often conceal detail in the mass-size relationship (Allen, 1981). Change in the slope may be an indication of the presence of a composite distribution in the dust samples. If the distribution can be partitioned into several component distributions generated from different sources, it is of importance in understanding the dust sources and aerodynamic behavior of particles. However, the most commonly used graphical techniques for partitioning of a composite distribution often require subjective judgment because slight changes in the slope of the cumulative plot are hardly detectable. For this reason, a frequency distribution which represents the rate of mass change in the cumulative plot with respect to the size is preferred (Whitby, 1983; Rubow, 1985). In order to minimize the limitations associated with the histogram and cumulative distribution, the first step taken for analytical modeling of coal mine dust size is to derive an empirical mass size frequency distribution.

The relationship between the frequency and cumulative distribution based upon the logarithmic scale of size is as follows:

$$y = \frac{1}{M} \left(\frac{d\ M_x}{d\ \log\ X}\right) \qquad (4.1.a)$$

$$= \frac{d\ Y}{d\ \log\ X} \qquad (4.1.b)$$

where,

M = total sample mass,
M_x = sample mass in the size range of x,
y = frequency density (percent/logarithmic size),
Y = cumulative percentage, and
X = size.

Therefore, if a cumulative distribution can be expressed as a differentiable continuous function, the corresponding frequency distribution can be derived from its first derivative.

In order to approximate the continuous cumulative distribution function which best fits the cumulative mass-size plot with a linear percentage scale as ordinate and a logarithmic scale of size as abscissa, two different approaches are employed in this study for comparison purposes. One is a nonlinear least-squares approximation procedure by the Chebychev approximation function, and the other is a piecewise-polynomial approximation method by cubic-spline interpolation (Otsu et al., 1983).

4.1.1.1 Chebychev Approximation

It is known that the Chebychev polynomial provides a good approximation to any continuous function by interpolating through the so-called Chebychev points (Conte and Boor, 1980). The Chebychev polynomial is:

$$Y_n(X) = \cos\ (n\ \cos^{-1} X) \qquad (4.2)$$

where,

$Y_n(X)$ = Chebychev polynomial of order n, and
X = size transformed as Chebychev points, $-1 < X < 1$.

Using this polynomial, the Chebychev approximation function is defined as:

$$Y = a_0\ Y_0(X) + a_1\ Y_1(X) + \ldots\ldots + a_n\ Y_n(X), \qquad (4.3)$$

where,

Y = the cumulative percentage,
$Y_i(X)$ = Chebyshev polynominal of order i, and
a_i = coefficient of the ith polynominal obtained by least-squares solution outlined below.

Application of this approximation function to filtering of geotechnical data to find anomalies can be found in a study by Ishii et al. (1978). This paper contains the least-squares solution of the coefficients, a_0, a_1, ... , and a_n in the above Chebychev approximation function. This procedure also has been applied to find mathematical equations for the cumulative distributions for geochemical data (Ostu et al., 1984).

The order of the polynomial in the Chebychev approximation function also affects the shape of the resulting frequency distribution. With the data from cascade impactors, it was found that polynomials with orders less than 4 are likely to generate a straight line, while no significant differences were observed among the orders 5 through 8. In this study, the order was set at 6.

4.1.1.2 Cubic-Spline Interpolation

As one of the simple forms of piecewise-polynomial interpolation, this method uses a polynomial of degree 3 for interpolation between all the adjacent data points using the following function:

$$Y_i(X) = a_{1,i} + a_{2,i}\,(X-X_i) + a_{3,i}\,(X-X_i)^2 + a_{4,1} \qquad (4.4)$$

where,

$Y_i(X)$ is the cubic-spline interpolation function in the interval of $a_{1,i}$, $a_{2,i}$, $a_{3,i}$, and $a_{4,i}$.

One constraint is that Y(X) must be twice differentiable in each size interval.

A solution algorithm for this method can be found in most references on numerical analysis. Recently, this method has become very popular (Conte and Boor, 1980) and most of the statistical computer packages include the facility of spline interpolation even though they do not usually provide mathematical expressions. Figure 11 shows the cumulative distributions approximated by the two methods and their empirical mass size frequency distributions for a coal mine dust sample.

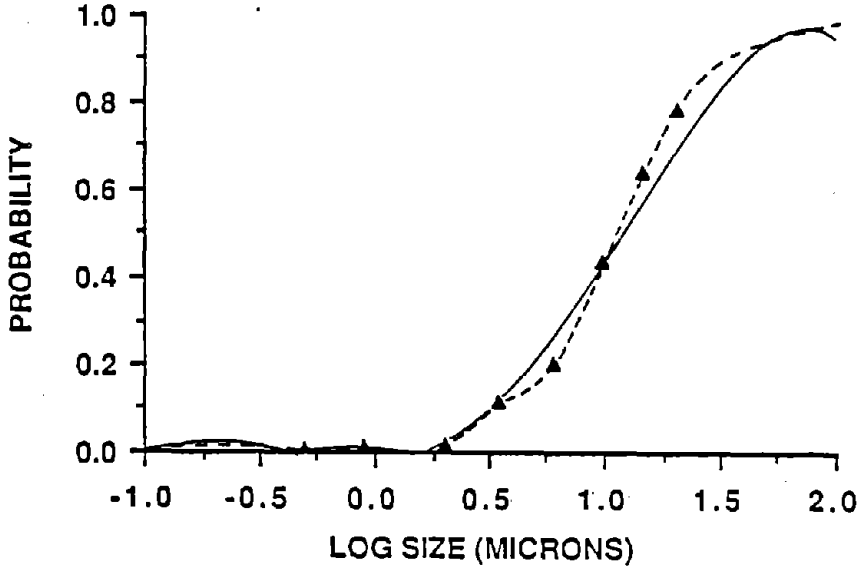

a. Cumulative Mass Size Distributions.

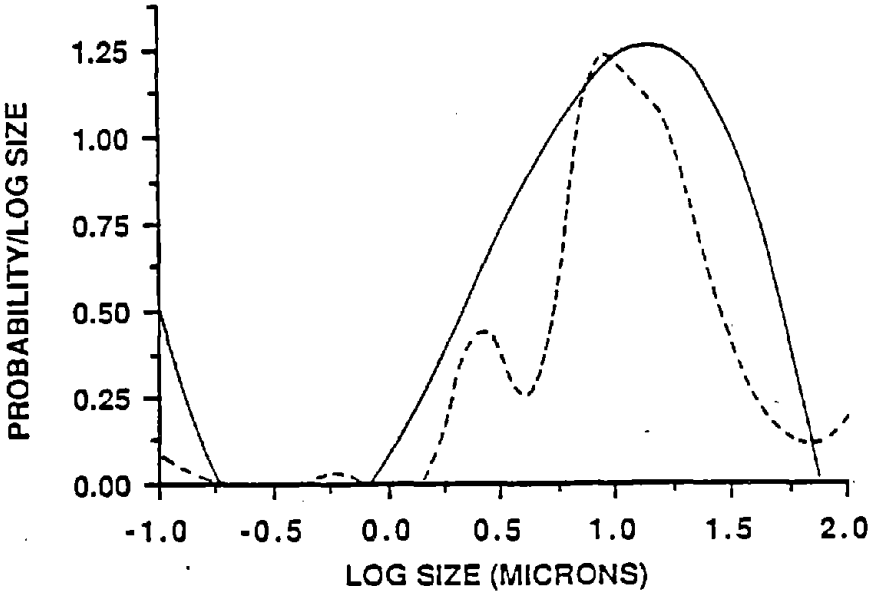

b. Mass Size Frequency Distributions.

Figure 11. Cumulative Mass Size Distributions Approximated by Chebychev Approximation Function (solid line) and Cubic-Spline Interpolation (dotted line) and their Corresponding Frequency Distributions.

4.1.2 Mass Size Distribution Under the Lognormality Assumption

The ordinate scale on lognormal probability paper is arranged such that a cumulative lognormal distribution will plot as a straight line. The cumulative probability is linearized with respect to the standard variate on probability paper using the following relationship:

$$Y = \frac{1}{\sqrt{2\pi}} \int_{-\infty}^{z} e^{-(z^2/2)} dz \qquad (4.5)$$

where

z = standard normal variate, and
Y = cumulative probability.

Using this property, logarithmic values of the size data are fit by a straight line and the distribution parameters, the geometric mean and the geometric standard deviation, can easily be obtained from it.

In this procedure to represent size by distribution parameters, the conventional way of measuring the goodness of fit by a lognormal model is to test the linearity of the straight line drawn over the data using the linear least-squares method (Shen and Ring, 1985). If significant deviation from a linear pattern is observed, it may be due to either improper assumption of lognormality, truncation of data, or presence of a composite distribution (Lepeltier, 1969; Sinclair, 1976).

Size distributions may be truncated from sizing instruments as a result of ignoring all particles smaller than their lower detection limits. In these cases, steepening of a cumulative distribution is observed at the truncated end. As shown in Table A.2.2 in Appendix 2, the collection efficiency of the final backup filter used for cascade impactors is relatively high even below 0.1 μm, and the mass of particles passing through the filter is extremely small compared to the total sample weight. Therefore, deviation from linearity on probability paper due to truncation is not likely to be significant in the mass size distributions of the total airborne coal mine dust samples from cascade impactors. In addition, in the case of an excess of large or fine particles in the sample, departure from linearity is likely. If this is the case, the resulting frequency distribution may show another distinctive mode in the large- or fine-size range. This situation can be described in the same way as that of the presence of a composite distribution.

The most complicated situation is the presence of a composite distribution which is a mixture of multiple distributions. In this case, the frequency distribution shows distinctive multiple modes unless all the component distributions

are completely overlapped by a distribution with the largest mass contribution to the sample. Therefore, in the following sections, apparent deviation of the size data from linearity is analyzed by testing the possibility of multi-modality and, in turn, presence of a composite distribution. A composite distribution can be partitioned into multiple component distributions, each of which represents an individual mode. The most accepted procedure for partitioning of a composite distribution employs an identical distribution model for all component distributions (Jaenicke and Davies, 1976; Whitby, 1983). In this study, each component distribution is approximated by a lognormal model.

4.1.2.1 Graphical Methods for Testing the Multi-Modality

Most of the graphical methods for partitioning of composite distributions (Lepeltier, 1969; Sinclair, 1976; Allen, 1981) require identification of the inflection points on cumulative distributions. Changes in the slope are a critical indication of the presence of a composite distribution. However, even if the slope changes, location of the inflection points is not always straightforward. Furthermore, with only a small number of data points, inflection points are not distinctive even if they exist. Subjective judgement is the most important criterion. Therefore, these procedures are designed primarily for manual analysis.

Another graphical procedure (Davies, 1974) uses templates specially prepared for the purpose of partitioning. Templates are made to have the shapes of lognormal frequency distributions with various values of the distribution parameters. Through a trial-and-error approach of overlapping, a set of templates which are considered to best fit the data is chosen. Subsequently, each template provides the distribution parameters and its contribution to the sample weight. However, the final set of templates may not be a unique solution. Since selection of the templates is arbitrary, there can be an infinite number of templates to reach an identical result unless there is enough prior knowledge on the size distribution.

In all the graphical methods using cumulative plots on lognormal probability paper, significant errors can occur due to the conventional practice for measuring the linearity of data plotted on lognormal probability paper. Linearity is measured by the coefficient of determination, R^2, using linear least-squares regression of the logarithmic values of size data on the nonlinear scale of cumulative percentage. On the ordinate of probability paper for cumulative percentage, values near the center are given more weight than those near the extremities. The conventional practice for measuring linearity using linear regression is to give equal weight to all the data regardless of their locations. Thus, unweighted least-squares regression is likely to result in overemphasis of the data near the extremities. Meanwhile, subjective weighting for the curve

fitting procedure can become a problem in interpreting the results (Sinclair, 1976).

The amount of coal mine dust sample collected on the lower stages of cascade impactors, particularly the seventh and eighth, is usually less than 0.1 mg and is seldom greater than 10 percent of the total sample weight. Therefore, relative errors of the size data from these stages associated with sampling and sample handling are likely to be much larger than those for the data from the upper stages. Giving an equal weight to these data points will eventually overemphasize those errors due to the intrinsic limitations of lognormal probability paper.

The limitations due to equal weighting may be handled by a useful rule; nonlinearity can be accepted if several consecutive points deviate from a linear trend in a systematic manner. This can be done by analyzing the trend in regression residuals. If the residuals fluctuate randomly, it is a better indication of linearity (Neter and Wasserman, 1974). Therefore, quantitative measurement of the linearity of data on lognormal probability paper is not tried in this study. Instead, residual analysis is performed to help test the lognormality.

4.1.2.2 Lognormal Frequency Distribution by Nonlinear Approximation

In the previous sections, empirical frequency distributions were approximated from cumulative distributions plotted on the percent-versus-logarthmic size scale. The conventional procedure to estimate the mass size frequency distribution is based upon the generalized histogram standardized by the total sample weight as well as the size interval. A continuous frequency distribution can be obtained by smoothing the histogram. The procedure for plotting generalized histograms for the size data from cascade impactors is well illustrated in a paper by Knutson and Lioy (1983).

Smoothing the histogram and approximating the resulting frequency distribution can be done by various methods. In a study for developing data reduction algorithms for sizing instruments by Kapadia (1980), simplex minimization and Twomey's nonlinear iterative method were compared to find a good agreement among the derived size frequency distributions. Another study for partitioning composite distributions of geochemical data by Ostu et al. (1984) used a nonlinear least-squares procedure known as the Marquardt method. The Marquardt technique is a compromise between the Gauss-Newton and gradient methods. Improvement in each iteration is based upon direction as well as distance. It is known to have a relatively good computation efficiency and selection of the starting values does not significantly affect the convergence time. Another method used in this study for purpose of comparison with the Marquardt method is called the DUD method (Ralston and Jennrich, 1978). This is the only method which does not need the derivatives of the nonlinear model as an

input. Figure 12 shows a generalized histogram and its corresponding frequency mass size distribution approximated by nonlinear least-squares methods.

Because all the nonlinear approximation algorithms require a user-provided functional form, the number of component distributions hidden in the size data has to be decided in advance. Usually the number is equal to the number of modes in a distribution if all the modes are significant. Therefore, it requires a priori knowledge on the size distribution. Presence of bimodel and trimodel distributions have been reported in the atmospheric aerosol size distributions (Willeke et al., 1974). However, some questions still prevail on the existence of the finest mode, the so-called Aitken nuclei mode found in the size range below 0.01 μm. Most of the critics point out the possible introduction of errors in sampling and sizing instruments (Jaenicke and Davies, 1976). In general, two modes in the size ranges of 0.1-1.0 μm and 10-100 μm have been observed in atmospheric aerosols.

Multi-modality was also studied for coal mine dust in papers by Whitby (1983) and Burkhart et al. (1983). The first paper introduced a possibility of bimodality in airborne coal mine dust. The latter paper reported bimodality in the mass size distributions of coal mine dust samples from cascade impactors at about 5 and 17 μm. The analytical procedure employed in this paper was spline interpolation. In mine workplace aerosols, it is not likely that a significant mass of particles below 2 μm will be found due to the energy limitations on the mining machinery (Welker et al., 1982). The only source for the Aitken nuclei mode found in underground mines was diesel exhaust particles at about 0.01 μm.

A mathematical constraint in assuming the number of modes is the number of data presented. As stated previously, cascade impactors provide only eight cumulative data points, even though this can be increased to nine through assumption of the hypothetical upper and lower size limits. Each partitioned component lognormal distribution has two unknowns, the geometric mean and geometric standard deviation. In addition, assumption of n modes requires (n-1) unknown variables on the mass percentage of each mode. Therefore, there are five unknowns in a bimodal distribution and eight in a trimodal distribution. Considering the mathematical constraint, the critics on trimodal distributions and the absence of internal combustion engines in the sections sampled in this study, only the possibility of bimodality is tested in this study.

4.1.3 Analysis Results

The size data from eleven continuous miner sections at seven different mines are analyzed in this section. The face layouts with sampling locations and some of the related information including ventilation measurements are included in Appendix 4.

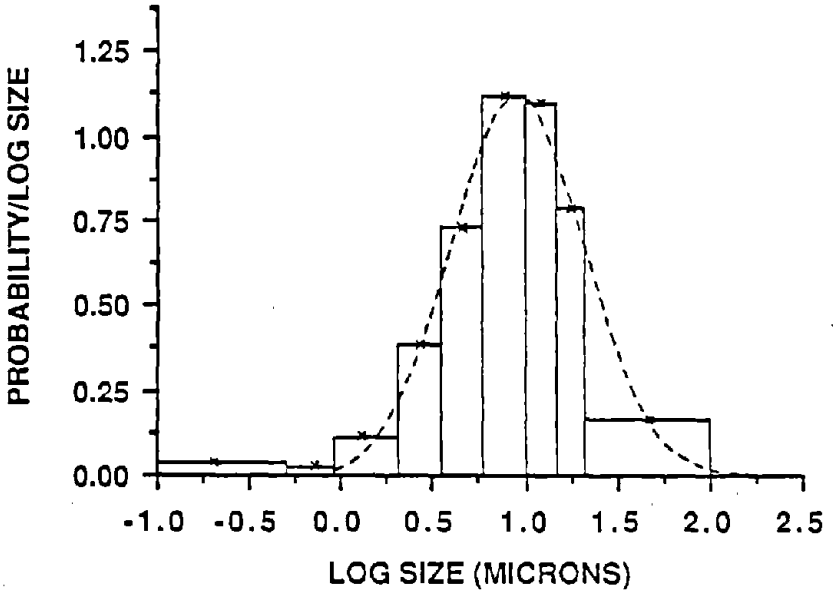

Figure 12. Generalized Histogram and its Corresponding Frequency Distribution Estimated by Nonlinear Least-Squares Method.

Size data on the 52 dust samples were obtained directly from the impactors; collection substrates were dried and weighed before and after sampling using a Mettler M3 microbalance with a least count of 0.001 mg. The resulting size distributions expressed in terms of cumulative percentages at the cut sizes of eight impactor stages are listed in Appendix 5 along with the dust concentration at each sampling location.

4.1.3.1 Residual Analysis

As an initial step to examine the current practice for analytical representation of coal mine dust size using the lognormal distribution, linearity of the cumulative size data plotted on lognormal probability paper is studied. Because of the intrinsic limitations in applying linear regression on the nonlinear scale of probability paper, it is not intended to measure the linearity quantitatively. Instead, the pattern of the residuals obtained from unweighted linear least-squares regression is analyzed. The results are included in the second column of the tables in Appendix 6. In the case of random fluctuation of the residuals, which is typical of a linear model, the data set is categorized as 'linear', while a data set showing some degree of systematic variation is labeled as 'curvilinear'. Figure 13 illustrates examples for the two categories.

The results of the residual analyses show that ten out of the twelve samples showing random variation of the regression residuals are either from the intake side of the face operations or from the return airways. This indicates that in the immediate returns of the miner and roof bolter operations, size distributions of the airborne dust may deviate from lognormality or they may be composed of a composite distribution which is likely to result in multiple modes. These aspects are further investigated in the subsequent analyses because it was found that the residual analysis alone provides inconclusive inferences on the validity of the lognormality assumption.

4.1.3.2 Empirical Distributions

In Appendix 6, the empirical mass size frequency distributions derived from the cumulative plottings using the Chebychev approximation function and spline interpolation are represented by their modal values. For comparison with the lognormal distribution derived from the generalized histograms, size data were extrapolated beyond the range of the cut size of the samplers to the hypothetical upper and lower limits at 0.1 and 100 μm. The modes estimated below 0.5 μm and above 21 μm are not considered in this study, since these modes are largely dependent upon the functional forms of the approximation polynomials.

For all the samples, the Chebychev approximation function of order six resulted in only one inflection point in the size range of interest. This led to the observation of one modal value in

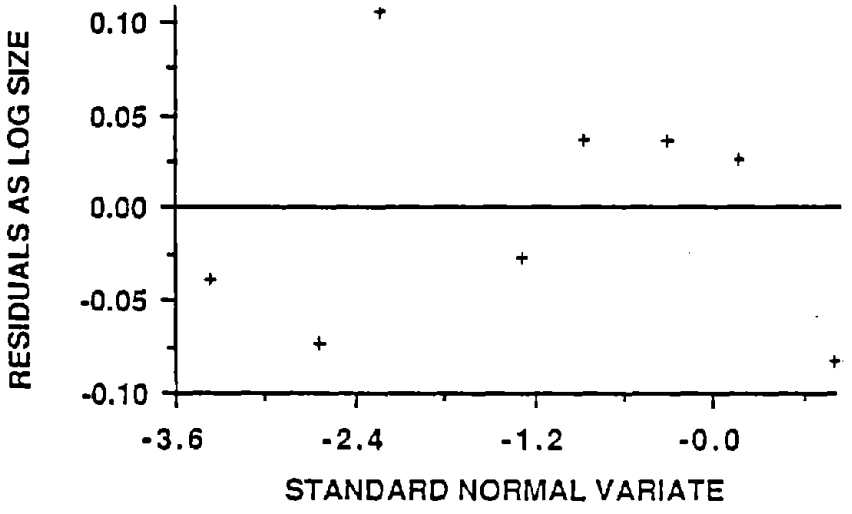

a. Random Variation of the Residuals.

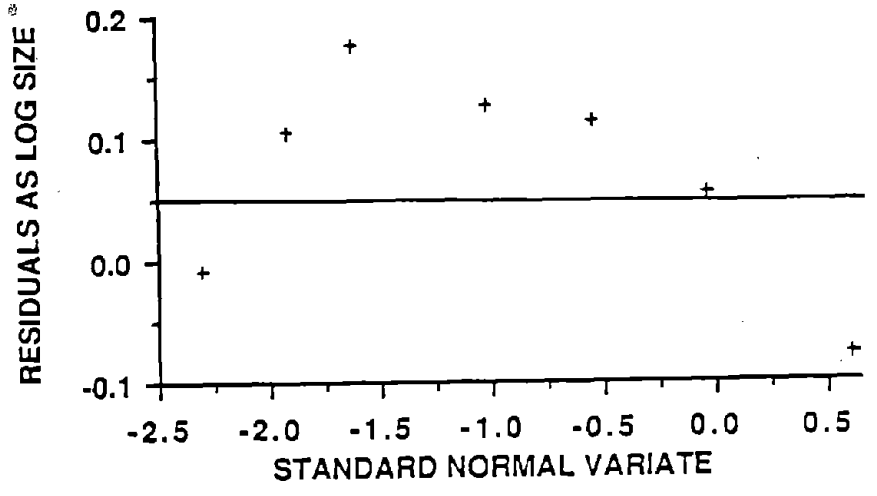

b. Curvilinear Variation of the Residuals.

Figure 13. Residual Analysis for the Lognormality Test.

the corresponding frequency distribution. Unlike the Chebychev approximation, spline interpolation is designed to go through all the data points presented. Therefore, any slight change in the slope of the cumulative plot due to the presence of outliers led to additional inflection points which were subsequently shown as extreme points or modes in the corresponding frequency distribution. As expected, the frequency distributions obtained through spline interpolation indicate multiple modes in most cases. The single mode observed by Chebychev approximation is similar to the prime mode with the largest percentage of mass contribution among the multiple modes estimated by spline interpolation. In the following section, the significance of these modes are discussed in association with multi-modality in the lognormal distribution.

4.1.3.3 Lognormal Distributions

As stated previously, rather than developing another creative distribution model, the objective of this section is to test the lognormality assumption currently being made in the analytical representation of airborne coal mine dust size distribution. Therefore, for the purpose of comparison with the empirical distributions, size data are fitted to the lognormal distribution on the basis of the generalized histogram. The presence of multi-modality is analyzed, while only bimodality is taken into consideration as discussed in the previous section.

The selection between unimodality and bimodality in the approximated lognormal distributions was primarily based upon a measure of the goodness of fit, the Chi-square statistic. The Chi-square statistic can be calculated by dividing the squared differences between the observed and expected (approximated) values by the expected value. Therefore, as is common in the fine size range (below 1 μm) of coal mine dust, if an expected value is extremely small, then the resulting Chi-square statistic becomes an extremely large value. To overcome this limitation, a modified Chi-square statistic (Whitby, 1983) uses the squared average of the observed and expected values as diviser. Even though the statistical test of significance of the modified Chi-square statistic is not yet known, a good judgement can be made by measuring the improvement in the statistic between the lognormal distributions with one and two modes. A large reduction of the measure of fit in the bimodal distribution is an indication of bimodality.

In addition to the Chi-square test, another indication of bimodality is the presence of multiple extreme points in an empirical distribution obtained by spline interpolation. As shown in Appendix 7, some modes seem to be distinctive compared to others. However, apparent distinctiveness of a mode in the frequency distribution does not imply the significance of those modes. Partitioning of a distribution can help measure the significance of modes in terms of the mass contribution to the dust samples. Even if a mode is indicated as a distinctive

extreme point by spline interpolation, sometimes partitioned lognormal distributions show that some extreme points in an empirical frequency distribution belong to a mode with an ignorably small percentage of mass contribution.

An even more important criterion in judging the significance of a mode is comparison with the size data of the other samples collected from the same split of air. Even though this method is subjective, it may have more significant physical meanings than the other criteria. If a majority of the samples from an identical split or some of the samples in the return airway of a mining operation indicate existence of a mode at about the same size, then it is a strong indication of the significance of that particular mode. This mode may exist even when there is no indication of multiple distinctive extreme points according to spline interpolation, and even when the regression residuals show relatively linear patterns. This condition is normally due to the fact that the mode is associated with a very small percent of the dust mass.

4.1.3.4 Comparisons

In the following sections, the results of the size analysis for each section (see Appendices 6 and 7) are discussed. For simplicity, all the mining sections are coded as shown in Appendix 4 and the sampling locations are coded as shown in Table 11.

4.1.3.4.1 Sample Set A (Mine Code 141-1-1)

All the samples except the 4X sample show relatively strong bimodality. However, a weak fine-size mode in the 4X sample can be detected at about 3.5 μm which is very similar to the first mode in the 2X sample in terms of the geometric mean and geometric standard deviation. A similar relationship is observed between the RI and RR samples.

Interestingly enough, the first modes in the CI, RI, RR and 2X samples estimated by spline interpolation are very similar in the range of 2.5 to 3.0 μm. The first modes observed in the size range of 2.1 to 4.2 μm by the lognormal models are also close to each other, and their mass percentages in the dust samples are greater than 13%. The highest contribution of this mode is made in the CI sample, while the lowest percentage can be found in the RI sample. It must be noticed that the roof bolter and continuous miner switched places in the same split of air during the sampling period and consequently the roof bolter was downstream of the miner about one-half of the sampling period. If these fine-size modes represent mine dust floating through the working section without being deposited, the contribution of the coarse particles generated from the miner operation to the RI sample appears to reduce the mass percentage of the fine-size mode. The significance of the existence of fine-size modes in this size range is discussed further in the subsequent sections.

Table 11. Codes for the Sampling Locations.

Codes	Sampling Locations
IN	In the intake airway
INOUT	At one crosscut outby the belt transfer point
ININ	At one crosscut inby the belt transfer point
CI	In the immediate intake airway of the continuous miner
CR	In the immediate return airway of the continuous miner
2XCR	At two crosscuts outby the miner operation
4XCR	At four crosscuts outby the miner operation
RI	In the immediate intake airway of roof bolter
RR	In the immediate return airway of roof bolter
2XRR	At two crosscuts outby the bolter operation
4XRR	At four crosscuts outby the bolter operation
2X	At two crosscuts outby the last unit in the return if a single split of air is used
4X	At four crosscuts outby the last unit in the return if a single split of air is used

Notes: (1) When two separate cuts were sampled, the CR sample for the first cut is coded as CR1; that for the second cut as CR2.

(2) When one sampling location was assigned in the intake airway to the miner and bolter operations at a face employing a double-split ventilation scheme, the sample is coded as CI/RI.

4.1.3.4.2 Sample Set B (Mine Code 142-1-1)

The samples from this set were taken in the same mining section as Sample Set A but from different cuts. Even though significant percentages of the coarse-size modes in the CI and CR samples made them undetected in the lognormal models, the first fine-size modes found in the previous set of samples can be seen in almost all samples. This is the case even for the CR sample where a coarse-size mode at about 12 μm is a dominant source. Even though the results from residual analysis and spline interpolation show bimodality in the RR and 2X samples, bimodality is very weak according to the mass percentage of dust in the first fine-size mode.

The result of residual analysis for the CI sample is somewhat misleading. Cubic-spline interpolation located three distinctive modes at about 3, 8 and 18 μm. The two coarse-size modes are also observed in the lognormal distribution, even though the significance of the first fine-size mode might be ignored due to its small percentage of mass. Furthermore, presence of similar modes in the CI sample from Sample Set A strongly indicates bimodality in the CI sample. The relatively large percentages of a coarse-size mode near 20 μm in the CI samples in Sample Sets A and B seem to be associated with reentrained dust because their sampling locations were on the shuttle car route.

4.1.3.4.3 Sample Set C (Mine Code 03-3-1)

As in the previous two sections, fine-size modes in the range of 2.6 to 2.9 μm can be found in almost all the samples. Its contribution is the highest in the IN sample which shows a distinctive bimodality. The source for the significant second mode near 6 μm in the intake airway sample is not clear. The first modes are relatively weak (mass percentages of less than 10%) in the CI/RI, CR, 2XCR and 4XCR samples. As dust travels in the return airways, the mass percentages of the fine-size modes seem to increase even though the differences are very small.

The CR sampling time was a portion of the time for the 2XCR sample. However, the overall size consists of these two samples are very similar. Also the CI/RI sample taken on the route of shuttle car shows a large contribution of the coarse-size mode near 9 μm. As shown in the RR sample, the roof bolter operation changed the size consist of the intake dust sample. On the contrary, in the previous two sections, dust size distributions inby and outby the roof bolter operation were not significantly different, even though the dust concentration in the outby sample was relatively higher than that in the inby sample.

4.1.3.4.4 Sample Set D (Mine Code 30-7-1)

The CR1 sample was taken during the cutting cycle, while the CR2 sample was obtained during the floor cleaning cycle of the

continuous miner. These two samples show totally different size distributions; a fine-size mode near 2.7 μm accounts for 13 percent in the CR2 sample, but it is not detected in the CR1 sample. Bimodality is distinctive in these two samples.

4.1.3.4.5 Sample Set E (Mine Code 200-2-1)

The CR1 and CR2 samples were taken from the two adjacent cuts at a face employing a single split of air and ventilation tubings with auxiliary fans. Their lognormal distributions show the presence of bimodality and similarity between the size consists of these two samples. It can be noticed that the RI and RR samples have similar fine-size modes at about 4 μm, while the large particles found in the coarse-size mode of the RI sample at about 30 μm appear to be due to reentrained dust from shuttle cars.

As in Sample Set D, the fine-size modes found in the CR samples in the size range of 3.5 to 6 μm have significant mass percentages. Considering their geometric standard deviation of about 1.7, the particles in these fine-size modes are predominantly respirable. All the samples show similar fine-size modes in the range of 3.4 to 4.7 μm. This mode is the major source in the RI sample.

4.1.3.4.6 Sample Set F (Mine Code 11-2-1)

These samples were collected from a three-entry development section utilizing line brattice for face ventilation. Based upon the measure of fit and shape of the lognormal distributions with unimodality, it is shown that the RI, RR, 2XRR and 4XRR samples have relatively weak bimodality. The modal values in the unimodal distributions for these samples illustrate a decreasing geometric mean from 11.1 to 4.7 μm as the dust travels from the intake side of the roof bolter operation to four crosscuts outby the operation.

The roof bolter was located downstream of the miner for about a half of the sampling time. Similar fine-size modes can be observed at near 3.0 μm in the intake air dust samples of the miner and roof bolter (the CI and RI samples). In the other samples, it is not detected apparently due to the relatively weak bimodality in their size distribution.

4.1.3.4.7 Sample Set G (Mine Code 63-7-1)

The ININ and INOUT samples were taken at one block inby and outby the feeder-breaker, respectively. The increase in the mass percentage of the fine-size mode at about 3 μm in the ININ sample probably indicates the introduction of fine particles due to breaker or shuttle car activity. At the same time, an increase in the amount of coarse particles with the geometric mean of 13 μm can be noticed.

A fine-size mode with a geometric mean of about 3.5 μm can be found in the intake air samples as well as in the CR1 and RI samples. Bimodality in the CR1, CR2 and RR samples is relatively weak because the miner and roof bolter operations generated size consists with geometric means of about 17.5 μm and 13.2 μm, respectively. The roof bolter operation significantly changed the level of dust concentration as well as the size distribution of the airborne dust.

4.1.3.4.8 Sample Set H (Mine Code 101-7-1)

The following four sample sets were collected from the same mine. Other than the 4X sample, all the samples show strong bimodality. A weak fine-size mode detected in the 4X sample at about 2.6 μm can also be observed in all the other samples. The 2X and 4X samples share similarity in the size distributions, even though unexpected movement of the vent tubing during the sampling time generated a higher dust concentration in the 4X sample. For a short period of time, the discharge point of the tubings was between the impactors for the 2X and 4X samples.

4.1.3.4.9 Sample Set I (Mine Code 102-7-1)

The fine-size modes observed in most of these samples have geometric means between 2.0 and 4.0 μm. The CR1 and CR2 samples were taken from different cuts. The fine-size modes at about 3 μm can be detected in these two samples even though in the CR1 sample, the coarse- size mode at 19 μm is the major mode in terms of the mass percentage. Bimodality in the CI sample is relatively weak with a predominant mode at about 11 μm.

4.1.3.4.10 Sample Set J (Mine Code 103-7-1)

As in the previous section, the CI sample with a major mode at about 4.5 μm shows relatively weak bimodality. The size distributions of the 2X and 4X samples are very similar except that the first fine-size mode in the 4X sample accounts for a higher percentage of the mass. The fine-size modal value at about 3.2 μm may be closely associated with the fine-size modes commonly found in most of the samples from the previous two sections.

4.1.3.4.11 Sample Set K (Mine Code 104-7-1)

Only the CR sample shows a distinctive bimodality. As shown, a fine-size mode at about 3 μm has a considerable mass percentage of 36%. Since its geometric standard deviation is 1.6, almost all particles are in the respirable size range. As observed often in the previous sections, the CI sample includes a relatively coarse mode which may originate from dust stirred up by shuttle cars. Bimodality in the 2X sample is very weak, while the 4X sample indicates bimodality with a high (46%) percentage of the dust in the fine-size mode at 2.8 μm.

4.2 Discussion

Chebychev approximation and cubic-spline interpolation techniques were applied to derive empirical mass size frequency distributions of the total airborne coal mine dust sampled by cascade impactors at various locations in the continuous miner sections. As stated previously, the discrepancies in the empirical models by these two methods are largely due to the differences in the methods. The apparent presence of multi-modality in most of the empirical models estimated by spline interpolation was created mainly due to the design of the method itself. However, it was shown that in many cases, the multiple modes observed in the empirical models are critical information to identify common size modes observed throughout the samples taken from the same section. However, the significance of these modes in the lognormal distributions is judged only by their mass contributions to the sample.

Residual analysis is an important criterion to test the lognormality of data. However, the results are acceptable if there exists only one mode in the size distribution. The analytical representation of coal mine size data obtained from cascade impactors by the lognormal distribution is significantly limited by the smaller number of data points obtained. The number of modes in the lognormal model was limited to two, even though in some samples, the possible presence of additional modes in the size range below 1.0 μm was observed.

Partitioning of composite distributions by nonlinear least-squares Marquardt and DUD methods do not require prior knowledge of the modal pattern in the size distribution because both methods are not significantly affected by the selection of the starting values. The importance of partitioning was well illustrated in the CR1 sample from Sample Set D where a composite distribution with two component distributions does not indicate any distinctive multi-modality in the empirical models estimated by approximation techniques.

The lognormal distribution is known to be a good fit for most types of size data (Davies, 1974). However, as shown in this section, it is correct only under the appropriate assumption on the number of modes being present in the dust samples. Assumption of only unimodality in the size distribution is likely to conceal the significance of smaller modes which may have significant physical meanings. In general, for the size of the total airborne coal mine dust, a bimodal lognormal distribution was a relatively good approximation. The bimodality assumption was shown to be capable of detecting most of the significant modes observed in the empirical models. However, the sources of bimodality cannot be easily identified because they can arise from one or a combination of the following possible causes:

1. due to the size- and time-dependent mechanisms associated with dust formation and transformation such as nucleation, coagulation and settlement;
2. the presence of multiple dust generating sources;
3. the possibility of liberation of relatively fine mineral particles from coal or surrounding strata in the process of mining operations; and
4. the possibility of preferential removal of the airborne dust in certain size fractions by dust control measures.

Some of the observations made at various sections can be summarized as follows:

1. Fine-size modes in the range of 2 to 4 μm were present in almost all samples from various locations in the continuous mining sections.
2. Almost all samples showed some degree of bimodality. However, no systematic variation in bimodality among the samples from various locations could be observed.
3. Most prominent modes in the samples from the immediate returns of the miner operation were found in the range of 12 to 18 μm regardless of the type of the face ventilation scheme. However, most of their fine-size modes found below 5 μm had mass percentages greater than 10%. With the geometric standard deviation of approximately 2, most of the particles in the fine-size modes are respirable.
4. The geometric standard deviations in individual modes were usually between 1.0 and 2.5.
5. Even though their mass percentages in the samples were not significant, the apparent presence of an additional mode below 1.0 μm was observed in some of the samples.
6. Most of the samples taken on the shuttle car route showed a considerable amount of coarse particles greater than 10 μm.
7. Even in the samples taken at two and four crosscuts outby the face operators, large particles with a geometric mean greater than 12 μm accounted for considerable weight percentages in the samples.
8. In several cases, the roof bolter operation was found to be an insignificant source in affecting the size consist of the airborne dust.

5. ANALYSIS OF THE ELEMENTAL COMPOSITION OF AIRBORNE COAL MINE DUST

In Section 2, some effects of the chemical elements on the development of CWP and possible association between the rank and elemental composition of coal were discussed along with the importance of the size of particles on the behavior of coal mine dust in the human respiratory tract. Therefore, effects of the size on the dust characteristics are likely to affect the toxicity of coal dust particles because the size of particles governs the settling location and residence time in the lung. The first objective of this thesis is to test the hypothesis that the elemental composition of airborne coal mine dust varies with the size of the dust.

Control of certain toxic characteristics of airborne coal mine dust through engineering measures may be possible if locational variation of those characteristics can be identified. Therefore, significance of the locational variability of the elemental characteristics of airborne coal mine dust is tested in the subsequent section. In addition, the relationship between the characteristics of airborne coal mine dust and the materials being cut is also studied. Based upon the results, effects of continuous miner, roof bolter and other secondary sources of dust on the elemental composition of the airborne dust are analyzed. Finally, applicability of the size and elemental information for dust source identification is discussed.

5.1 Selection of an Analytical Method

Analytical methods that have seen application to coal include virtually every method developed for elemental analysis. These can be categorized into chemical methods, optical methods, electron microscopy, X-ray analysis, and nuclear methods including nuclear activation and mass spectroscopy (Valkovic, 1983). Most of these methods have been applied to coal ash, while applications to raw coal were limited except several methods including X-ray fluorescence, atomic absorption, neutron activation and spectrophotometric methods (Simon and Huffman, 1977).

Among this variety of methods, only a few have been extensively used for the elemental characterization of coal mine dust. One of them is an optical method, emission spectroscopy, used for the analysis of heavy metals in the coal dust found in miners' lung tissues (Crable et al., 1966; Crable et al., 1968; Keenan et al., 1971). Spark source mass spectroscopy was used for elemental analysis of respirable coal mine dust (Kessler et al., 1971; Sharkey et al., 1975; Freedman, 1978). The atomic absorption method has also seen application to coal mine dust (Corn et al., 1973; Freedman, 1978) as well as coal dust in lung tissues (Keenan et al., 1971). The neutron activation technique has also been used for major element analysis for respirable coal mine dust (Wesson and Armstrong, 1975). Recently, scanning

electron microscopy is also being studied for the elemental analysis of coal mine dust.

Selection of a method for elemental analysis of the airborne coal mine dust collected by cascade impactors took into consideration several requirements associated with the availability of samples and the objectives of the future research. As indicated in Appendix 4, the weight of the sample from an individual stage of a multi-stage impactor is usually in the range of 0.05 to 1.00 mg. Samples from the backup filter are seldom greater than 0.010 mg while few samples from the first stage weigh more than 1.00 mg. Furthermore, except for that from the backup filter, a sample on each stage is divided into six or twelve submasses of dust due to the design of the cascade impactor stages as shown in Figure 8. Therefore, methods such as atomic absorption which cannot be easily used for multi-element analysis (Davison et al., 1974) are excluded because these methods require large samples for multi-element analysis.

This study is based upon an ongoing long-term research project aimed at identifying various characteristics of airborne coal mine dust. Therefore, another requirement for the method selection was that the dust samples collected for this study are to be preserved for the determination of other dust parameters. Some of the methods such as atomic absorption, spark source mass spectroscopy, and neutron activation methods require ashing or chemical treatments of the samples. Thus, application of these methods will destroy or alter some of the dust characteristics.

The problems described previously can be solved by the introduction of proton induced X-ray emission spectroscopy (PIXE) (Ahlberg et al., 1978) which has been applied to atmospheric aerosols sampled by cascade impactors (Berg et al., 1977; Lawson and Winchester, 1978; Ahlberg et al., 1978; Orsini and Boueres, 1979; Hudson et al., 1980). While electron microscopy is a surface technique, proton beams used for excitation of the atoms of a sample in a PIXE pass through the thin layer of the sample. The characteristic X-rays emitted by the sample are measured. The number of counts in a peak is a measure of the amount of the corresponding element in the sample. Because the sample for PIXE is prepared as a layer thinner than 5 mg/cm^2, matrix absorption of characteristic X-rays is negligible (Orlic et al., 1981). Thickness of the samples from cascade impactors used for this study is invariably smaller than this figure. Another advantage of PIXE is that the variables related to the characteristic X-ray yield are known or can be experimentally determined (Johansson and Johansson, 1976). Therefore, it is an absolute method and does not require standard samples.

In addition to the application to thin samples, PIXE is well documented also for thick samples (Campbell and Cookson, 1984). Degradation of the proton energy as the beam traverses a thick sample was studied by using several levels of proton energies to simulate the situation (Chen et al., 1981). Therefore, PIXE can

be applied to coal mine dust samples from cascade impactors as well as channel samples taken from the face. Based upon the intrinsic advantages of such a nondestructive method and the capability to do rapid routine multi-element analysis of extremely small samples at nanogram sensitivity (Lawson and Winchester, 1979), the PIXE method was chosen for elemental analysis in this study.

5.2 Analysis of Elemental Data

The coal mine dust samples listed in Appendix 5 were analyzed along with the channel samples taken in the vicinity of the face. For the size dependency study, samples from the third (10-15 μm), fifth (3.5-6 μm) and seventh (0.9-2 μm) stages of the cascade impactors were analyzed. In addition, analyses were performed for only two masses of dust on each of those stages, primarily due to the available proton beam size and the high cost of analysis. The elemental analysis was performed at a commercial laboratory. Before deciding the number of dust masses on each stage for analysis, possible variation of the element compositions among the six masses of dust on the same stage was tested.

5.2.1 Cross-Sectional Variation of Element Compositions on Impactor Stages

For this purpose, a sample collected in the immediate return of the continuous miner (Mine Code 141-1-1) was used. Because one slot on each stage was left ungreased as an experiment, only five sample masses on greased spots were subject to the analysis. Their elemental data in terms of the weight percentage of each element are included in Appendix 8.

Variation of each element among the five masses was measured by the coefficient of variance (CV). As shown in Table 12, analysis of the third-stage sample indicates that none of the major elements other than Mg shows a CV greater than 10% while some of the trace elements with very small relative concentration levels such as V, Cr, As and Mo have relatively high CVs. In the fifth stage, two major elements, K and Ca, show relatively high CVs (17% and 33%) compared to the other major elements. However, even these values are much smaller than those for some of the trace elements such as V, Cr, Cu, Zr and Pb. In the seventh stage, most of the major and trace elements have relatively high CVs compared to the data from the other stages. However, no CV for a major element is greater than 100%. Most of the trace elements have higher variations than the major elements, similar to the pattern found in the other stages. The relatively high variations of the trace elements must be interpreted cautiously because a large portion of the high CVs is due to the extremely low concentrations of trace elements. If the concentration of an element is near the detection limit, the CV for the two masses of dust with the concentration levels just below and above the detection limit is likely to be greater than its true value.

Table 12. Cross-Sectional Variation of the Elemental Compositions on Impactor Stages.

	Impactor Stages					
	3		5		7	
Elements	Mean	CV	Mean	CV	Mean	CV
Major Elements						
Mg	1.581	16.76	1.757	7.17	2.779	17.25
Al	18.106	7.20	15.130	9.22	13.241	22.35
Si	25.745	7.80	21.953	6.26	20.929	23.60
P	1.147	6.56	1.297	8.28	3.678	10.46
S	13.064	6.70	7.613	5.28	10.295	5.55
K	2.367	7.00	2.609	16.98	9.695	99.24
Ca	3.343	8.02	3.262	33.37	10.787	57.29
Ti	0.557	6.73	0.424	9.94	0.473	21.82
Fe	6.095	5.30	3.445	7.87	4.902	36.50
Trace Elements						
Cl	1.001	5.85	0.810	17.68	2.019	34.21
V	0.003	226.51	0.004	223.61	0.	
Cr	0.009	101.45	0.004	139.75	0.014	149.07
Mn	0.042	37.95	0.038	75.98	0.124	57.91
Ni	0.007	17.28	0.006	61.44	0.014	101.79
Cu	0.073	39.98	0.148	148.64	0.171	109.77
Zn	0.313	26.30	0.340	51.02	0.811	31.48
Ga	0.028	38.22	0.022	86.14	0.062	110.41
Ge	0.		0.		0.	
As	0.003	137.60	0.004	93.38	0.006	138.70
Br	0.034	18.65	0.030	16.55	0.050	21.36
Rb	0.015	63.64	0.009	60.88	0.026	84.29
Sr	0.029	19.72	0.022	18.46	0.025	73.68
Zr	0.016	64.52	0.005	137.60	0.037	121.39
Mo	0.010	137.60	0.		0.	
Pb	0.032	41.75	0.022	125.90	0.005	223.61

Note: The units for the mean and CV are 10^2 x % and % by weight, respectively.

Tables A.8.1 through A.8.3 in Appendix 8 show the ratios of major elements using the weight percentage of Si as the basis. This ratio is intended to indirectly test the similarity in the compositions of inorganic fractions among the different masses of dust. Even though K and Ca show relatively high variations in the seventh stage, remarkable resemblences are shown in the correlations of the major elements. Therefore, based upon the coefficients of variation for the major and trace elements and the ratios of the major elements, analyzing two sample masses from each stage is not expected to raise questions concerning the representativeness of samples.

5.2.2 Size Dependency of Elemental Compositions

All the elemental data used for this study are relative values expressed as weight percentages. Therefore, the problems associated with giving more weight to a sample with high levels of certain elements in the analysis can be eliminated. In this section, the possibility of a size dependency of elemental composition of coal mine dust is tested using some of the univariate and multivariate statistical methods described in Section 3.

Data from the same sampling location are tested by the analysis of variance (ANOVA) method to find the elements showing significant variability with size. At each sampling location, a multiple F-test designated as the REGW test is performed along with the ANOVA test to compare the elemental compositions on the three different stages. The differences in the overall compositions of all elements are then tested by the multivariate analysis of variance (MANOVA) test. As discussed in Section 2, the following analyses are performed on the major and trace element groups separately.

Tables 13 and 14 contain the elements showing significant size dependency at an alpha level (probability of rejecting a hypothesis when it should be accepted) of 5% and the results of the equality tests by the REGW multiple-F test for each sampling location. Also, the significance of the differences in the centroids of the 9 major and 21 trace elements are tested by MANOVA.

5.2.2.1 Size Dependency of the Major Elements

As shown in the results of the MANOVA tests, dust samples at all locations show significant size effects on the elemental compositions, while samples from the intake airway of the roof bolter have relatively weak size dependency compared to those from other locations. At all locations except in the intake of the continuous miner, a significant size effect is observed in the two major elements most common in the clay minerals, Al and Si. In the samples from the immediate returns of the miner and bolter operations, these two elements show highest concentrations in the third stage, while in the other samples, their

Table 13. Effects of Size on the Major Element Compositions.

Elements[1]	Comparison[2]	Stage/ Mean[3]
Sampling Location: CI		
Si	5,3>3,7	5/ 55.676, 3/ 41.517, 7/ 9.513
S	3,5>7	3/ 16.850, 5/ 13.288, 7/ 6.102
Ca	3,5>5,7	3/ 83.128, 5/ 46.313, 7/ 5.333
Ti	3,5>7	3/ 2.274, 5/ 1.567, 7/ 0.202
Fe	3>5,7	3/ 36.981, 5/ 14.616, 7/ 2.533
MANOVA Test		
Wilks' Lambda = 0.036		F(18,366) = 1.68 Pr>F = 0.0001
Pillai's Trace = 2.526		F(18,448) = 1.61 Pr>F = 0.0002
Sampling Location: CR		
Al	3>5>7	3/ 52.123, 5/ 30.384, 7/ 10.208
Si	3>5>7	3/ 92.256, 5/ 47.916, 7/ 14.394
P	7>5,3	7/ 2.090, 5/ 1.116, 3/ 1.000
S	3>5,7	3/ 16.538, 5/ 9.247, 7/ 6.545
K	3>5,7	3/ 8.939, 5/ 5.608, 7/ 3.593
Ca	3,5>5,7	3/ 31.507, 5/ 19.325, 7/ 6.108
Ti	3>5>7	3/ 4.391, 5/ 2.299, 7/ 0.496
Fe	3,5>7	3/ 19.223, 5/ 14.696, 7/ 3.040
Wilks' Lambda = 0.183		F(18,92) = 6.84 Pr>F = 0.0001
Pillai's Trace = 0.987		F(18,94) = 5.09 Pr>F = 0.0001
Sampling Location: RI		
Al	5,3>7	5/ 66.296, 3/ 58.844, 7/ 17.022
Si	5,3>7	5/120.350, 3/116.320, 7/ 22.400
S	3>5>7	3/ 21.693, 5/ 12.183, 7/ 5.302
Ca	3,5>5,7	3/ 31.078, 5/ 21.509, 7/ 4.815
Wilks' Lambda = 0.106		F(18,26) = 2.99 Pr>F = 0.0055
Pillai's Trace = 1.267		F(18,28) = 2.69 Pr>F = 0.0093

Table 13. (Continued).

Sampling Location: RR

Elements[1]	Comparison[2]	Stage/ Mean[3]
Mg	3,5>5,7	3/ 2.947, 5/ 1.517, 7/ 0.574
Al	3>5>7	3/ 61.936, 5/ 41.807, 7/ 15.187
Si	3>5>7	3/113.760, 5/ 72.140, 7/ 22.070
S	3>5,7	3/ 19.137, 5/ 8.242, 7/ 6.397
K	3>5>7	3/ 14.989, 5/ 9.953, 7/ 3.323
Ca	3>5,7	3/ 43.562, 5/ 20.357, 7/ 5.590
Ti	3,5>7	3/ 4.041, 5/ 2.802, 7/ 0.799
Fe	3,5>7	3/ 36.894, 5/ 24.860, 7/ 6.639

MANOVA Test

Wilks' Lambda = 0.101	F(18,50) = 5.95	Pr>F = 0.0001
Pillai's Trace = 1.269	F(18,52) = 5.02	Pr>F = 0.0001

Sampling Location: 2X

Mg	3,5>5,7	3/ 1.673, 5/ 1.199, 7/ 0.294
Al	3,5>7	3/ 47.591, 5/ 36.000, 7/ 9.310
Si	3,5>7	3/ 80.187, 5/ 58.695, 7/ 13.814
S	3>5,7	3/ 30.219, 5/ 18.714, 7/ 7.595
K	3,5>7	3/ 10.292, 5/ 8.322, 7/ 1.945
Ca	3>5,7	3/ 42.408, 5/ 14.579, 7/ 5.182
Ti	3,5>7	3/ 5.626, 5/ 4.099, 7/ 0.600

Wilks' Lambda = 0.089	F(18,38) = 4.96	Pr>F = 0.0001
Pillai's Trace = 1.370	F(18,40) = 4.83	Pr>F = 0.0001

Table 13. (Continued).

Sampling Location: 4X

Elements[1]	Comparison[2]	Stage/ Mean[3]
Al	5,3>7	5/ 35.579, 3/ 31.965, 7/ 8.143
Si	5,3>7	5/ 57.216, 3/ 54.495, 7/ 11.305
S	3,5>7	3/ 19.045, 5/ 17.081, 7/ 6.877
K	5,3>7	5/ 7.710, 3/ 7.249, 7/ 1.546
Ca	3>5,7	3/ 37.649, 5/ 17.557, 7/ 4.436
Ti	3,5>7	3/ 3.234, 5/ 2.983, 7/ 0.410
Fe	3,5>5,7	3/ 52.753, 5/ 26.702, 7/ 2.749

MANOVA Test

Wilks' Lambda = 0.010	F(18,26) = 12.57	Pr>F = 0.0001
Pillai's Trace = 1.329	F(18,28) = 3.08	Pr>F = 0.0037

Notes: (1) Only the elements showing significant size effects at an alpha risk of 5 percent by ANOVA are listed.
(2) Comparisons are based upon the multiple F-test, REGW. Stages connected by a comma indicate no significant difference between them.
(3) The unit for the mean values is 10^2 x % by weight.

Table 14. Effects of Size on the Trace Element Compositions.

Elements[1]	Comparison[2]	Stage/ Mean[3]
Sampling Location: CI		
Mn	3,5>7	3/ 0.319, 5/ 0.152, 7/ 0.029
Ni	3>5,7	3/ 0.132, 5/ 0.024, 7/ 0.007
Br	3>5,7	3/ 0.105, 5/ 0.035, 7/ 0.006
Sr	3>5,7	3/ 0.447, 5/ 0.123, 7/ 0.017
Zr	3>5,7	3/ 0.194, 5/ 0.033, 7/ 0.013
MANOVA Test		
Wilks' Lambda = 0.060	F(32,24) = 2.31	Pr>F = 0.0185
Pillai's Trace = 1.307	F(32,26) = 1.31	Pr>F = 0.1336
Sampling Location: CR		
Cl	3>5,7	3/ 2.433, 5/ 1.298, 7/ 0.795
V	3>5>7	3/ 0.137, 5/ 0.079, 7/ 0.002
Cr	3,5>7	3/ 0.081, 5/ 0.059, 7/ 0.008
Ni	3,5>7	3/ 0.037, 5/ 0.036, 7/ 0.008
Br	3,5>7	3/ 0.074, 5/ 0.038, 7/ 0.022
Rb	3,5>7	3/ 0.101, 5/ 0.068, 7/ 0.024
Sr	3>5>7	3/ 0.248, 5/ 0.130, 7/ 0.021
Zr	3>5>7	3/ 0.120, 5/ 0.066, 7/ 0.023
Mo	3>5,7	3/ 0.044, 5/ 0.007, 7/ 0.003
Pb	3,5>7	3/ 0.078, 5/ 0.049, 7/ 0.011
Wilks' Lambda = 0.215	F(32,78) = 2.81	Pr>F = 0.0001
Pillai's Trace = 1.045	F(32,80) = 2.74	Pr>F = 0.0001
Sampling Location: RI		
None of the elements shows significant variation among the three different size fractions.		

Table 14. (Continued).

Sampling Location: RR

Elements[1]	Comparison[2]	Stage/ Mean[3]
V	3>5,7	3/ 0.148, 5/ 0.068, 7/ 0.005
Mn	3,5>7	3/ 0.394, 5/ 0.281, 3/ 0.084
Ge	7>3,5	7/ 0.002, 3/ 0. , 5/ 0.
Br	3,5>5,7	3/ 0.049, 5/ 0.035, 7/ 0.021
Rb	3,5>5,7	3/ 0.201, 5/ 0.120, 7/ 0.027
Sr	3>5>7	3/ 0.213, 5/ 0.125, 7/ 0.036
Zr	5,3>7	3/ 0.121, 5/ 0.109, 7/ 0.024
Pb	3>5,7	3/ 0.176, 5/ 0.099, 7/ 0.038

MANOVA Test

Wilks' Lambda = 0.135	F(32,36) = 1.94	Pr>F = 0.0279
Pillai's Trace = 1.242	F(32,38) = 1.95	Pr>F = 0.0250

Sampling Location: 2X

Cl	3>5>7	3/ 2.892, 5/ 1.685, 7/ 0.547
Cu	3,5>5,7	3/ 0.678, 5/ 0.442, 3/ 0.067
Sr	3>5,7	3/ 0.700, 5/ 0.196, 7/ 0.019

Wilks' Lambda = 0.037	F(32,24) = 3.17	Pr>F = 0.0023
Pillai's Trace = 1.586	F(32,26) = 3.11	Pr>F = 0.0020

Sampling Location: 4X

Cl	5,3>3,7	5/ 2.304, 3/ 1.766, 7/ 0.650
V	5,3>3,7	5/ 0.075, 3/ 0.038, 7/ 0.003
Cr	5,3>7	5/ 0.093, 3/ 0.060, 7/ 0.013
Mn	3,5>5,7	3/ 0.449, 5/ 0.229, 7/ 0.022
Ni	3,5>5,7	3/ 0.109, 5/ 0.056, 7/ 0.011
Zn	3>5,7	3/ 6.852, 5/ 1.373, 7/ 0.622
Sr	3>5,7	3/ 0.360, 5/ 0.157, 7/ 0.016
Pb	3,5>7	3/ 0.286, 5/ 0.238, 7/ 0.012

Wilks' Lambda = 0.002	F(32,12) = 8.21	Pr>F = 0.0002
Pillai's Trace = 1.780	F(32,14) = 3.53	Pr>F = 0.0075

Note: See the notes in Table 13.

concentrations do not show differences between the third and fifth stages. Meanwhile, the size effects on Al are insignificant in the intake of the miner. Si, S and Ca show significant size effects in the dust samples collected from all locations.

The distinctive difference between the immediate returns of the miner and bolter is that Mg, which is a major component in rock dust, shows a significant size dependency in the immediate return of the bolter. Its size dependency can also be detected at two crosscuts outby the operation. A noticeable difference between the intake and return airways of the mining operations is that the number of elements showing significant size dependency increases in the return airways.

Weight percentages of most of the major elements show no differences between the third and fifth stages while, those on the seventh stage are relatively smaller. The only element with the highest weight percentage in the finest size range is P which shows a significant size dependency in the immediate return of the miner operation.

5.2.2.2 Size Dependency of the Trace Elements

While the nine major elements showed significant size dependency at all locations, the multivariate tests for the trace elements by MANOVA indicate that the overall compositions of trace elements at the intake airways of the miner and bolter operations are not significantly different in the three different size ranges. However, as shown in the samples from the immediate returns, the miner and bolter operations generate significant size effects on the element compositions, even though the size effects due to the roof bolter operation is much smaller.

As was the case for the major elements, the elemental compositions in the samples from the immediate return of the miner operation show the most significant size dependency and the largest number of elements contribute to this significant size effect. The size effects in the return airway samples are much more significant than the samples from the bolter operation.

Even though the weight is less than 70 ppm in all samples, Sr shows very distinctive size effects at most of the locations except the intake airways of the miner and bolter operations. Its concentration increases with size. In the immediate return of the miner, more elements are observed to have significant size dependency compared to the immediate return of the bolter. Cl, Cr, Ni and Mo show significant size effects only in the return of the miner while V, Br, Rb, Sr, Zr and Pb show size effects also in the immediate return of the bolter. In the samples from the immediate return of the bolter, only Ge has the highest concentration in the finest size range. In general, as size increases, higher concentrations of the trace elements were shown.

5.2.3 Locational Variation of Elemental Composition

As shown in Tables 15 through 18, almost the same statistical methods as in the previous section are employed to test the possibility of variation in the elemental compositions with sampling locations. The significance of differences in the overall elemental compositions are tested using MANOVA, and the concentrations of each element are compared by ANOVA to test the locational variability. Comparisons of an element among all the locations are made based upon a multiple F-test designated as REGW.

In order to reconstitute the elemental composition of the total airborne dust in the entire size range at a sampling location, it is necessary to calculate a weighted average elemental composition for the total dust using the weight percentage on each stage as the weighting factor. Therefore, weighting by the same weight is likely to overemphasize the elemental composition on the third stage which usually contains the largest sample among the three stages considered in this study. In addition, in the size range of interest in this study (0.9-15 μm), interactions of the particles in different size fractions, mainly due to agglomeration, are not expected. Hence, all the comparisons are made only for the samples from the same stage. This will provide better information, since particles in a certain size range are likely to remain in the same size range as the dust-laden air flows through the mining section.

5.2.3.1 Locational Variation of the Major Elements

All the samples from the three different stages show significant locational variation in the elemental compositions. In the samples in the size range of 10 to 15 μm, three elements (P, S and K) show significant differences in the weight percentages among the seven different sampling locations. P and S have the highest percentages in the intake air samples, while the sample from the immediate return of miner appears to contain the lowest levels of these two elements even though the differences are not statistically significant among the locations except for the location in the intake airway. Also, as shown in the results of the stepwise discriminant analysis, these three elements indicate significant locational variability in the size range of 10 to 15 μm even when the correlation among the major elements are considered.

In the size range of 3.5 to 6 μm, Si and K show significant locational variability based upon the results of ANOVA and discriminant analysis. These two elements show higher percentages at the locations near the roof bolter operation. The other element showing locational variability in this size range is Ca which has higher weight percentages in the intake air samples. In the size range from 0.9 to 2 μm, the samples collected near the bolter and miner operations contain significantly higher percentages of Al and Si. In addition, it

Table 15. MANOVA Tests for Locational Variation of the Major Element Compositions.

Elements[1]	Comparison[2]	Location/ Mean[3]		
On the Third Stage (10-15 μm)				
P	IN> the other locations	IN/ 36.921	CI/ 2.200	RR/ 2.110
		RI/ 1.666	4X/ 1.650	2X/ 1.563
		CR/ 1.000		
S	IN> the other locations	IN/140.880	2X/ 30.220	RI/ 21.690
		RR/ 19.140	4X/ 19.050	CI/ 16.850
		CR/ 16.54		
K	RI,RR,2X,CR> RR,2X,CR,4X> 2X,CR,4X,CI,IN	RI/ 17.182	RR/ 14.989	2X/ 10.292
		CR/ 8.938	4X/ 7.248	CI/ 4.673
		IN/ 0.894		
MANOVA Test				
Wilks' Lambda = 0.122		F(54,300) = 2.84	Prob>F = 0.0001	
Pillai's Trace = 1.632		F(54,378) = 2.62	Prob>F = 0.0001	
On the Fifth Stage (3.5-6 μm)				
Mg	RI,CI,RR,2X, 4X,CR>CI,RR, 2X,4X,CR,IN	RI/ 3.694	CI/ 2.693	RR/ 1.517
		2X/ 1.199	4X/ 0.939	CR/ 0.532
		IN/ 0.000		
Si	IN,RI,RR>RI, RR,2X,4X,CI,CR	IN/130.290	RI/120.350	RR/ 72.140
		2X/ 58.700	4X/ 57.220	CI/ 55.680
		CR/ 47.920		
P	IN> the other locations	IN/ 22.672	CI/ 2.815	4X/ 1.346
		RI/ 1.340	2X/ 1.124	CR/ 1.116
		RR/ 1.029		
S	IN> the other locations	IN/129.400	2X/ 18.710	4X/ 17.080
		CI/ 13.290	RI/ 12.180	CR/ 9.250
		RR/ 8.240		
K	RI,RR>RR,2X, 4X,CI,IN,CR	RI/ 18.939	RR/ 9.953	2X/ 8.322
		4X/ 7.710	CI/ 7.000	IN/ 6.239
		CR/ 5.608		
Ca	IN,CI>CI,RI, RR,CR,4X,2X	IN/ 78.123	CI/ 46.313	RI/ 21.509
		RR/ 20.357	CR/ 19.325	4X/ 17.557
		2X/ 14.579		
Fe	IN,RI,2X,4X, RR>RI,2X,4X, RR,CR,CI	IN/ 78.334	RI/ 54.023	2X/ 37.764
		4X/ 26.702	RR/ 24.860	CR/ 14.696
		CI/ 14.616		
Wilks' Lambda = 0.048		F(54,300) = 4.52	Prob>F = 0.0001	
Pillai's Trace = 1.878		F(54,378) = 3.19	Prob>F = 0.0001	

Table 15. (Continued).

On the Seventh Stage (0.9-2 μm)

Elements[1]	Comparison[2]	Location/ Mean[3]		
Al	RI,RR,CR>RR, CR,2X,4X>CR, 2X,4X,CI,IN	RI/ 17.022	RR/ 15.187	CR/ 10.208
		2X/ 9.310	4X/ 8.143	CI/ 5.896
		IN/ 3.751		
Si	RI,RR>RR,CR> 2X,4X,CI,IN	RI/ 22.399	RR/ 22.072	CR/ 14.394
		2X/ 13.814	4X/ 11.305	CI/ 9.513
		IN/ 7.768		
Fe	RR,2X,RI,IN> 2X,RI,IN,CR, 4X,CI	RR/ 6.639	2X/ 5.138	RI/ 4.133
		IN/ 3.436	CR/ 3.040	4X/ 2.749
		CI/ 2.533		

MANOVA Test

Wilks' Lambda = 0.234	F(54,300) = 1.83	Prob>F = 0.0009
Pillai's Trace = 1.131	F(54,378) = 1.63	Prob>F = 0.0053

Notes: (1) This column contains the elements showing significant locational variability at an alpha risk of 5 percent by ANOVA.
(2) Comparisons are made based upon the multiple F-test, REGW. All the locations connected by commas indicate no significant difference between them.
(3) The unit for the means is 10^2 x % by weight.

Table 16. MANOVA Tests for Locational Varition of the Trace Element Compositions.

On the Third Stage (10-15 μm)

Elements[1]	Comparison[2]	Location/ Mean[3]					
Cl	IN> the other locations	IN/ 15.602	2X/ 2.892	CR/ 2.433	CI/ 2.162	4X/ 1.766	RR/ 1.656
		RI/ 1.399					
V	2X,RR,RI,CR, CI>RR,RI,CR, CI,4X,IN	2X/ 0.434	RR/ 0.148	RI/ 0.141	CR/ 0.137	CI/ 0.042	4X/ 0.048
		IN/ 0.000					
Cu	no difference	2X/ 0.678	CI/ 0.533	RI/ 0.297	IN/ 0.295	4X/ 0.292	RR/ 0.240
		CR/ 0.140					
Zn	IN> the other locations	IN/ 17.120	4X/ 6.852	CI/ 3.942	2X/ 3.801	RI/ 1.533	RR/ 1.271
		CR/ 0.669					
Sr	2X,CI,4X,CR, RR>CI,4X,CR, RR,RI,IN	2X/ 0.700	CI/ 0.447	4X/ 0.360	CR/ 0.248	RR/ 0.213	RI/ 0.154
		IN/ 0.014					

MANOVA Test
Wilks' Lambda = 0.089 F(96,295) = 1.64 Prob>F = 0.0009
Pillai's Trace = 1.899 F(96,336) = 1.62 Prob>F = 0.0010

On the Fifth Stage (3.5-6 μm)

Cl	IN> the other locations	IN/ 12.402	RI/ 2.458	4X/ 2.304	2X/ 1.685	CI/ 1.666	RR/ 1.528
		CR/ 1.298					
Mn	IN,RI,RR>RI, RR,2X,4X,CI,CR	IN/ 0.793	RI/ 0.565	RR/ 0.281	2X/ 0.247	4X/ 0.229	CI/ 0.152
		CR/ 0.114					
Cu	IN,2X,CI,RI, 4X>2X,CI,RI, 4X,CR,RR	IN/ 0.788	2X/ 0.442	CI/ 0.357	RI/ 0.321	4X/ 0.246	CR/ 0.143
		RR/ 0.108					
As	2X> the other locations	2X/ 0.040	CI/ 0.010	RR/ 0.006	4X/ 0.006	RI/ 0.005	CR/ 0.004
		IN/ 0.000					
Rb	RI,2X,RR,4X> 2X,RR,4X,CR, CI,IN	RI/ 0.328	2X/ 0.187	RR/ 0.120	4X/ 0.109	CR/ 0.068	CI/ 0.035
		IN/ 0.007					
Zr	IN,2X>2X,RI, 4X,RR,CR,CI	IN/ 0.497	2X/ 0.209	RI/ 0.183	4X/ 0.141	RR/ 0.121	CR/ 0.066
		CI/ 0.033					

Table 16. (Continued).

MANOVA Tests on the Fifth Stage

Wilks' Lambda = 0.037 F(96,295) = 2.42 Prob>F = 0.0001
Pillai's Trace = 2.400 F(96,336) = 2.33 Prob>F = 0.0001

On the Seventh Stage (0.9-2 μm)

Elements[1]	Comparison[2]	Location/ Mean[3]					
Mn	no difference	RR/	0.084	RI/	0.049	IN/	0.047
		CR/	0.045	CI/	0.029	2X/	0.028
		4X/	0.022				
Zn	2X,IN,CI,RR,	2X/	0.944	IN/	0.922	CI/	0.826
	4X,CR>CI,RR,	RR/	0.722	4X/	0.622	CR/	0.602
	4X,CR,RI	RI/	0.505				
As	2X,4X>4X,IN,	2X/	0.025	4X/	0.011	IN/	0.009
	RR,CI,RI,CR	RR/	0.007	CI/	0.004	RI/	0.003
		CR/	0.002				
Br	CR,IN,RR,2X,	CR/	0.022	IN/	0.021	RR/	0.021
	CI,RI>IN,RR,	2X/	0.018	CI/	0.017	RI/	0.005
	2X,CI,RI,4X	4X/	0.005				
Mo	IN,2X,RR,CI,	IN/	0.033	2X/	0.024	RR/	0.015
	RI>2X,RR,CI,	CI/	0.013	RI/	0.003	CR/	0.003
	RI,CR,4X	4X/	0.000				

MANOVA Test

Wilks' Lambda = 0.096 F(96,295) = 1.58 Prob>F = 0.0021
Pillai's Trace = 1.798 F(96,336) = 1.50 Prob>F = 0.0049

Notes: (1) This column contains the elements showing significant locational variability at an alpha risk of 5 percent by ANOVA.
(2) Comparisons are made based upon the multiple F-test, REGW. All the locations connected by comma indicate no significant difference between them.
(3) The mean is in unit of 10^2 x % by weight.

Table 17. Stepwise Discriminant Analysis for Locational Variability of the Major and Trace Elements.

For the Major Elements

On the Third Stage (10-15 μm)

Step	Selected[1] Elements	F Statistic	Prob>F	Wilk's Lambda	Prob>Wilk's Lambda
1	P	5.363	0.0001	0.672	0.0001
2	K	4.845	0.0004	0.464	0.0000
3	Si	3.958	0.0020	0.339	0.0000
4	S	3.551	0.0043	0.253	0.0000
5	Ca	3.186	0.0086	0.193	0.0000

On the Fifth Stage (3.5-6 μm)

1	K	3.679	0.0033	0.475	0.0000
2	Si	5.628	0.0001	0.311	0.0000
3	Al	15.359	0.0001	0.126	0.0000
4	Ti	3.445	0.0053	0.105	0.0000
5	Ca	2.747	0.0197	0.083	0.0000

On the Seventh Stage (0.9-2 μm)

1	Si	6.691	0.0001	0.622	0.0000
2	Mg	2.320	0.0432	0.512	0.0000
3	Al	2.195	0.0548	0.425	0.0000

Table 17. (Continued).

For the Trace Elements

Step	Selected[1] Elements	F Statistic	Prob>F	Wilk's Lambda	Prob>Wilk's Lambda
On the Third Stage (10-15 μm)					
1	Sr	2.834	0.0163	0.594	0.0004
2	V	3.508	0.0046	0.447	0.0000
3	Zn	2.656	0.0232	0.357	0.0000
4	As	1.933	0.0894	0.300	0.0000
5	Mn	1.893	0.0965	0.253	0.0000
6	Ni	3.615	0.0040	0.186	0.0000
On the Fifth Stage (3.5-6 μm)					
1	Cl	3.617	0.0037	0.753	0.0037
2	As	2.922	0.0138	0.593	0.0004
3	Rb	2.802	0.0175	0.469	0.0000
On the Seventh Stage (0.9-2 μm)					
1	As	3.811	0.0025	0.743	0.0025
2	Mo	2.811	0.0171	0.590	0.0004
3	Mn	2.384	0.0385	0.482	0.0001
4	Br	2.746	0.0196	0.382	0.0000
5	Cr	2.478	0.0326	0.308	0.0000
6	Cu	1.927	0.0906	0.259	0.0000

Note: The selected elements denote the final selection of elements excluding all the removed elements at an alpha risk of 15 percent.

Table 18. ANOVA Tests for Locational Variability of the Total Weight Fractions of the Major and Trace Elements and Organic Component.

Variables	Comparison[1]	Location/ Mean[2]	
On the Third Stage (10-15 μm)			
Major Elements	no difference		
Trace Elements	IN> the other locations	IN/ 35.261 4X/ 11.180 RR/ 4.795 CR/ 4.337	2X/ 13.183 CI/ 8.830 RI/ 4.673
Organic Fraction	no difference		
On the Fifth Stage (3.5-6 μm)			
Major Elements	IN,RR>RI,RR, 2X,CI,4X,CR	IN/510.370 RR/182.710 CI/172.370 CR/131.120	RI/304.400 2X/180.500 4X/167.110
Trace Elements	IN> the other locations	IN/ 30.905 RI/ 6.288 CI/ 5.107 CR/ 2.888	2X/ 6.686 4X/ 5.362 RR/ 3.486
Organic Fraction	CR,4X,CI,RR, 2X,RI>RI,IN	CR/ 98.660 CI/ 98.225 2X/ 98.128 IN/ 94.587	4X/ 98.275 RR/ 98.138 RI/ 96.893
On the Seventh Stage (0.9-2 μm)			
Major Elements	RR,RI,CR,2X> CR,2X,4X,IN, CI	RR/ 62.349 CR/ 47.205 4X/ 37.579 CI/ 33.270	RI/ 62.075 2X/ 45.551 IN/ 33.538
Trace Elements	no difference		
Organic Fraction	CI,IN,4X,2X, CR>2X,CR,RI, RR	CI/ 99.649 4X/ 99.610 CR/ 99.511 RR/ 99.360	IN/ 99.645 2X/ 99.527 RI/ 99.365

Notes: (1) Comparisons are made based upon the multiple F-test, REGW. Locations connected by a comma indicate no significant difference between them.
(2) The unit is 10^2 x % by weight except in the organic component; % by weight for the organic component.

is shown that the roof bolter operation generates airborne dust significantly enriched in these two elements compared to the other locations including the miner operation.

As shown in Table 18, there is no difference among the sampling locations in the weight fractions of the 9 major elements in the size range of 10 to 15 μm. The differences become significant as the size of particles gets smaller. In general, in the size ranges below 6 μm, the roof bolter operation produces higher percentages of the major elements compared to the miner operation.

5.2.3.2 Locational Variation of the Trace Elements

Based upon the results from MANOVA, the samples in all three different size fractions show significant locational variation in the elemental compositions. In the size range of 10 to 15 μm, V, Zn, and Sr are the trace elements with significant locational variability according to the ANOVA tests and the stepwise discriminant analysis. V is highly concentrated in the samples near the face operations, while Sr shows smaller percentages near the face. The intake air has the highest percentages of Zn. Even though the differences of the levels of V between the samples from the roof bolter and miner operations are not statistically significant, it appears that the roof bolter operation produces airborne dust relatively enriched in V in this largely nonrespirable size range.

In the size range of 3.5 to 6 μm, Cl, As and Rb show significant locational variability, while the samples from the roof bolter operation contain significantly higher concentrations of Rb. In the size range of 0.9 to 2 μm, As, Br and Mo are the three trace elements with significant locational differences based upon the ANOVA and the stepwise discriminant analysis. Arsenic (As) is less enriched in the samples from the return airways. Br is more concentrated in the return of the miner operation, and, in general, it is enriched near the face operation. Meanwhile, the samples from the vicinity of the roof bolter operation show higher percentages of Mo.

As shown in Table 18, the total weight fraction of the trace elements in all the size ranges does not vary significantly with the sampling locations. However, the intake air dust samples in the size range above 3.5 μm show relatively higher weight fractions of the trace elements.

5.2.4 Discussion on the Size Dependency and Locational Variation of Elemental Composition

Significant size dependency of the overall composition of major elements was observed at all sampling locations, while those of the trace elements did not show significant size effects in the samples taken from the intake airways for the miner and bolter operations. Among the 9 major elements, the

concentrations of Al, Si, S and Ca showed significant variation with size at all locations except the intake air of the face operation. In general, their concentrations were higher in the coarser size ranges. However, concentrations of Al, Si and S in the size ranges of 10 to 15 μm and 3.5 to 6 μm did not show noticeable differences. In the samples from the immediate returns of the miner and bolter operations, their concentrations were much higher in the size range of 10 to 15 μm. In the samples from various locations, Ca, another major element showing size dependency was found to have almost the same concentrations in the samples in the size ranges of 3.5 to 6 μm and 0.9 to 2 μm. One distinctive difference of the elemental compositions of the samples from the intake airways of the face is that Ca was highly enriched in the size fractions above 3.5 μm.

The overall composition of 21 trace elements in the samples from the intake airways to the face operator were almost the same in all the size ranges. However, when individual element concentrations were studied, Sr showed a strong size dependency at most of the sampling locations; in general, less concentration occurred in the finer size ranges. Several trace elements such as V, Br, Rb, Sr and Zr varied significantly with size in the immediate returns of the miner as well as the bolter. Concentrations of these trace elements increased in the coarser size ranges.

The size dependency of the major and trace elements was more significant near the continuous miner operation than near the roof bolter operation. In addition, the airborne dust from the immediate returns of the face operations indicated more significant size effects on the elemental compositions that that from the intake airways.

The concentrations of the 9 major and 21 trace elements in all three size ranges varied significantly among the different sampling locations. The elements showing significant locational variability were different in each size range. In the size range below 3.5 μm, Si was found to be highly enriched in the immediate return of the roof bolter operation compared to the other sampling locations. In general, the roof bolter operation contained higher concentrations of most of the elements showing significant locational variability. Trace elements are known to be highly concentrated in the top and bottom materials of the coal seam. Therefore, higher trace element concentrations near the roof bolter operation can be expected.

In the samples from the intake air, P, S and Ca showed much higher concentrations in the size range above 3.5 μm. Apparently this resulted in higher concentrations of these elements in the sample from the immediate intake of the face operation. Concentrations of the trace elements, V, Rb, and Mo, were considerably different at different locations in the size ranges of 10 to 15 μm, 3.5 to 6 μm and 0.9 to 2 μm, respectively; the concentrations were higher near the roof bolter operation. Zn,

Sr, As and Cl varied significantly among the different sampling locations in the size range of 10 to 15 μm and showed less concentration near the face operations. As and Cl showed the same trend in the size range of 3.5 to 6 μm. Meanwhile, the concentrations of Br showed significant locational variability in the size range of 0.9 to 2 μm. The intake air samples were found to have higher concentrations of Cl and Zn in the size range of 10 to 15 μm; Cl, Mn, Cn and Zr in the size range of 3.6 to 6 μm; and Mo in the size range of 0.9 to 2 μm. The results of the analyses of size dependency and locational variability are summarized in Tables 19 and 20.

The differences in the total weight fractions of the 9 major elements among the samples from 7 different sampling locations were significant in the fine size range below 3.6 μm, while insignificant differences were observed in the nonrespirable size range of 10 to 15 μm. Higher weight percentage of the 9 major elements in total were found in the samples near the roof bolter operation in the size range below 3.6 μm. While there was no significant locational variation in the total weight percentages of the trace elements in all three size ranges, the amounts of the organic component (coal) in the size range below 3.5 μm were significantly different among the sampling locations. In general, a greater organic fraction was found in the finer size fractions of the samples collected near the continuous miner operations when compared with those from the roof bolter operation. In addition, the organic fractions accounted for greater weight percentages of the total coal mine dust in the finer size ranges at all sampling locations. The data to support this are shown in Table 21.

Comparing the elemental concentrations at two and four crosscuts outby the face, usually 160 to 200 feet apart, all the major and trace elements showing significant locational variation had higher concentrations at two crosscuts outby. However, the differences were not statistically significant for the major elements, while some of the trace elements such as V on the third stage, As and Zr on the fifth stage and As, Br and Mo on the seventh stage showed significant differences between these two locations in the return airways.

The source of significant variations in some of the major and trace element concentrations with the size and location are not always clear. Association of the trace elements in coal with minerals has been studied by many researchers (Miller, 1974; Miller, 1977; Swaine, 1976) and close affinities of some of the trace elements with the organic coals were also reported (Zubovic et al., 1960; Nicholls, 1968; Ruch et al., 1977; Gluskoter et al., 1977). However, many of the results were contradictory and largely dependent upon the coal samples used. Therefore, use of those sources to aid in element source identification may create serious errors. In the following section, the differences in the elemental compositions among the samples from various locations

Table 19. Summary of the Size Dependency of Elemental Composition.

Elements	Trend
Al, Si, S	1. Significant at all sampling locations except the intake air of the miner operation. 2. In the immediate returns of the miner and bolter operations, highest concentration in the size range of 10 to 15 μm; no difference between the size ranges of 3.5 to 6 μm and 0.9 to 2 μm. 3. In the other locations, lowest in the size range of 0.9 to 2 μm; no difference between the size ranges of 10 to 15 μm and 3.5 to 6 μm.
Ca	1. Significant at all sampling locations except the intake of the miner operation. 2. Higher concentrations in the size range above 3.5 μm in the intake airway and immediate intake of the miner operation. 3. Highest concentration in the size range of 10 to 15 μm; no difference between the size ranges of 3.5 to 6 μm and 0.9 to 2 μm.
Sr	1. Significant at all locations except the intake of the miner operation. 2. Higher concentration in the coarser size range.
V, Br, Rb, Sr, Zr, Pb	1. Significant at the immediate returns of the miner and bolter operations. 2. Higher concentration in the coarser size range.
Cl, Cr, Ni, Mo	1. Significant at the immediate return of the miner operation. 2. Higher concentration in the coarser size range.

Table 20. Summary of the Locational Variation of Elemental Composition.

Elements	Trend
P, S, Ca	1. In the intake airway, highly concentrated in the size range above 3.5 μm.
Si	1. Near the bolter operation, highly concentrated in the size range below 6 μm.
V, Rb, Mo	1. Significant locational variability for V in the size range of 10 to 15 μm, for Rb in the size range of 3.5 to 6 μm, and for Mo in the size range of 0.9 to 2 μm. 2. Higher concentrations near the bolter operation.
Zn, Sr, As, Cl	1. Significant in the size range of 10 to 15 μm. 2. Lower concentrations near the face operations.
As, Cl	1. Significant in the size range of 3.5 to 6 μm. 2. Lower concentrations near the face operations.
Br	1. Significant in the size range of 0.9 to 2 μm. 2. Higher concentration near the face operations.

Table 21. Variation in the Total Weight Fractions of the Major and Trace Elements and the Organic Components of Coal Mine Dust.

	Weight Percentages[2]								
	Major Elements			Trace Elements			Organic Components		
Stage[1]	3	5	7	3	5	7	3	5	7
IN	485.31/	510.37/	33.54	35.26/	30.91/	1.98	94.79/	94.59/	99.65
CI	213.14/	172.37/	33.27	8.83/	5.11/	1.93	97.78/	98.23/	99.65
CR	227.16/	131.03/	47.21	4.34/	2.89/	1.65	97.69/	98.66/	99.51
RI	286.51/	304.40/	62.08	4.67/	6.29/	1.40	97.09/	96.89/	99.37
RR	299.38/	182.71/	62.35	4.80/	3.49/	1.60	98.21/	98.14/	99.36
2X	387.19/	180.50/	45.55	13.18/	6.69/	1.78	96.00/	98.13/	99.53
4X	209.93/	167.11/	37.58	11.18/	5.36/	1.46	97.79/	98.28/	99.61

Notes: (1) The columns headed by 3, 5 and 7 indicate the weight percentages on the third, fifth and seventh stages in the cascade impactors.
(2) The unit for the major and trace elements is 10^2 x % by weight; % by weight for the organic components.

in each section are analyzed by measuring their associations with each other and with the channel samples.

5.3 Association Between Samples

So far in this section, all the analyses were performed on the relationships between variables such as the size and the elemental composition. Most of the statistical methods employed are based upon the structure of the covariance or correlation matrices of the variables. In this section, the degree of similarity between the samples are analyzed in order to identify the possible associations among the dust samples taken at various locations and also to compare the characteristics of the materials being cut with those of the airborne coal mine dust.

The interrelationships between samples with multiple variables can be quantified by the coefficient of proportional similarity (Imbrie and Purdy, 1962) defined as follows:

$$\cos \Theta_{m,n} = \frac{\sum_{j=1}^{p} X_{mj} X_{nj}}{\sum_{j=1}^{p} X_{mj}^2 \sum_{j=1}^{p} X_{mj}^2} \qquad (5.1)$$

where

p is the number of constituents (elements), and m and n denote the two samples, m and n.

This coefficient is merely the cosine of the angle between the two sample vectors in p-dimensional space. As implied by the mathematical expression, one limitation in applying this measure to the samples used in this study is that the importance of trace elements (usually with much smaller weight fractions) is likely to be ignored in determining the coefficient when they are considered along with major elements (with higher weight fractions). Therefore, the trace elements are treated separately in the calculation of the coefficient of proportional similarity.

In this study, the size of coal mine dust is defined by the aerodynamic diameter. Even though airborne coal mine dust is a heterogeneous mixture composed mainly of coal and minerals with different physical and chemical characteristics, particles with the same aerodynamic diameter can be assumed to exhibit similar aerodynamic behavior. Therefore, the influence of one sample on the others downstream can be studied by comparing the characteristics of the particles in the same size range. The association matrices containing the coefficients of proportional similarity for the samples from each section are included in Appendix 9. In the following sections, each association matrix is discussed with respect to the interrelationships among the

dust samples taken at various locations and those between the channel and dust samples. The trace element compositions in the rock dust samples are not taken into consideration, since it was found that they vary significantly even among samples from the same mine.

5.3.1 Sample Set B (Mine Code 142-1-1)

The high similarity coefficients between the samples from the immediate return of the miner operation (the CR samples) and the channel samples indicate that the two bottom coal benches in the coal seam were the major sources of the elements found in the CR samples. However, even though the major element compositions of the samples from the immediate return of the bolter operation (the RR samples) show close associations with the two top benches containing the roof materials, the trace element compositions show very low similarities with the two top noncoal benches, particularly in the size range of 0.9 to 6 μm. In turn, the RR samples in this size range are similar to those from the intake airways of the miner and bolter operations (the CI and RI samples) which are closely associated with none of the benches in the coal seam. Therefore, this implies that in the immediate return of bolter, trace elements in the fine particles in the size range of 0.9 to 6 μm may have originated in the intake.

Comparisons of the RR and CR samples with the channel samples show:

1. The trace element compositions of the CR samples in all size fractions are much closer to those of the coal bench which accounted for the major portion of the coal seam, even though the major element compositions show relatively high similarities between the CR sample and all four benches of the channel samples.
2. The trace element compositions of the RR samples in the size range of 3.5 to 15 μm show high similarity with the two top benches which were mixtures of the roof rock and coal.

The high similarity coefficient between the CI samples and the rock dust indicates possible contamination of the samples in the size range of 10 to 15 μm by rock dust.

The trace element compositions of the fine particles in the samples taken at two crosscuts outby the face operation (the 2X samples) is much closer to those of the RR samples. This may be an indication that the influence of the miner operation was not significant in the fine size range of 0.9 to 2 μm. The results of the size analysis indicated a presence of the fine-size modes at about 2.5 μm in the RI, RR and 2X samples. Considering the high similarity coefficients among these samples in the size ranges of 0.9 to 2.0 μm and 3.5 to 6 μm, particles in these fine size ranges appear to be transportable through the working area.

5.3.2 Sample Set C (Mine Code 03-3-1)

The two benches in the coal seam show very high (0.99) coefficients of similarity in terms of the major as well as the trace elements. In this section, the intake air was contaminated by the belt haulage and had a relatively high concentration of dust compared to the other mines. As shown in Table A.9.2 in Appendix 9, the major element compositions of the intake air samples (the IN samples) are similar to those of the coal seam, while the similarity coefficients of the trace element composition with the coal seam and rock dust are relatively low. The similarity with the coal seam is lower in the range of 0.9 to 2.0 μm. The influence of the intake air on the samples from the intake side of the miner and bolter operations (the CI/RI samples) can be observed in the high similarity coefficient with the IN samples in the size range of 0.9 to 2 μm and the relatively low similarities between the CI/RI samples in the same fine size range and the coal seam, while almost all other samples in this size range show much higher similarity coefficients with the coal seam. Therefore, this indicates the importance of the intake air as a potential dust source, particularly in the fine size range of 0.9 to 2 μm which may be contaminated before it reaches the section.

Even though separate splits of air were used for the miner and bolter operations, shuttle cars were employed in their intake airways. The effects of reentrainment of dust by shuttle car movement were observed in the size analysis through the presence of a relatively coarse mode at about 10 μm. Its effects on the return airways can be also noticed in terms of the high similarity coefficients among most of the samples from both splits of air, in spite of different dust levels measured in the different splits of air. The first several stages of the cascade impactor assigned to four crosscuts outby the face operation (the 4XRR sampling location) was seriously overloaded. Relatively high similarities of the 4XRR samples with the rock dust coupled with low similarities with the other samples in the size range of 10 to 15 μm and with the coal seam indicate that these stages were contaminated mainly by the rock dust from the roof.

5.3.3 Sample Set D (Mine Code 30-7-1)

The differences in the elemental compositions of the various benches in the coal seam are clearly shown in Table A.9.3 in Appendix 9. The two coal benches separated by slates have very similar major and trace element compositions, while the two slate benches significantly different from the coal benches in terms of their elemental compositions also show high similarity. The relationships between the samples from the immediate return of the miner operation (the CR1 samples) and the channel samples are different from the previous sections. The trace element compositions in the fine size fraction (0.9-2 μm) of the CR1 samples show low associations with the coal benches, while in the

size range of 10 to 15 μm, the coal benches appear to be the major source for both the major and trace elements.

As stated previously, the CR2 samples were taken during the floor cleanup cycle. In the fine size range of 0.9 to 2 μm, the CR1 and CR2 samples are almost identical in their elemental compositions. All three size fractions in the CR2 samples are poorly associated with the coal benches in the coal seam, while the coarse size fractions above 3.5 μm show high similarities with the noncoal benches. The trace elements in the fine size fractions of the CR1 and CR2 samples are not likely to be generated from the coal seam.

5.3.4 Sample Set E (Mine Code 200-2-1)

In this section, the samples from the first and sixth stages of the cascade impactors were also analyzed along with the samples from the third, fifth and seventh stages. Because no noncoal benches were found in the coal seam, only the whole-seam channel samples were taken. Comparison of the dust samples from the immediate return of the miner operation (the CR1 and CR2 samples) with the channel samples indicates that in the size range of 2 to 15 μm, the coal is the major source of the major and trace element concentrations. In the size range above 21 μm, the similarities of the major and trace element compositions between the CR and channel samples are very low, while in the size range of 0.9 to 2 μm, only the trace element compositions show low similarities. These trends can be found in the CR1 sample as well as in the CR2 sample.

The discrepancy between the CR and channel samples in the size range of 0.9 to 2 μm can be explained through the relatively high similarities of the CR samples with the intake air samples (the CI/RI samples) which in turn suggest the possible association of the fine particles in the CR and CI/RI samples. The differences in the size range above 21 μm may be created by cutting some roof material. However, since the roof rock was not sampled, this cannot be proved. The coarse particles above 21 μm in the CI/RI and RR samples show relatively high similarity coefficients with rock dust and indicate possible contaminations. However, low similarities between the coarse dust particles in the CI/RI and CR samples imply that the rock dust is not likely to be the major source of the coarse size fractions of the CR samples.

Even though the CR1 and CR2 samples were taken from different cuts and during different sampling times, the size consists and elemental compositions are remarkably similar. In this mine section, separate auxiliary fans were employed for the miner and bolter operations in a single split of air. In spite of the fact that the roof bolter was downstream of the miner for approximately half of the sampling time, the dust concentration measured in the immediate return of the bolter was very low (1.3 mg/m^3) compared to that in the other mines. However, considering

the high similarities between the CR and RR samples in the size range of 2 to 15 μm, the miner operation appears to be the major source of dust in the RR samples. The size analysis suggested possible presence of the fine-size modes at about 4 μm in all the samples. The association matrix in Table A.9.4 in Appendix 9 indicates high similarity coefficients among the samples in this range.

5.3.5 Sample Set F (Mine Code 11-2-1)

The similarities of the major and trace element compositions among the four benches in the coal seam show that the top bench containing roof rock is similar to the bottom bench and the second bony coal bench is closer to the third soft coal bench. The associations of these benches with the samples from the immediate return of the miner operation (the CR samples) are contradictory to those found in the previous section. As shown in Table A.9.5 in Appendix 9, the consistent relationships observed in this section are that the CR samples in the fine size range of 0.9 to 2 μm is similar to the benches primarily made up of coal, while the samples in the coarse range show similarity with the noncoal benches.

The mine dust taken from the intake airways of the miner and bolter operations (the CI and RR samples) showed similar size modes at about 3 μm in Section 4. However, their elemental compositions do not show high similarities in this size range. In spite of the low similarity coefficients, the similarities may not be sufficient reason to reject the significance of the fine-size mode because the relatively high similarities of the CI samples with the rock dust indicate possible contamination.

As shown in Appendix 5, the bolter operation did not significantly increase the dust level. Since the bolter spent approximately half of the sampling time downstream of miner, the significant effects of the dust originating from the miner operation are expected. The effects of the miner operation on the dust near the bolter are shown in the high similarity coefficients between the CR samples and the samples from the intake and immediate return of the bolter operation (the RI and RR samples). The insignificant dust generating potential of the bolter operation can be also detected in the relatively low similarities with the two top noncoal benches and also with high similarities with the coal benches.

5.3.6 Sample Set G (Mine Code 63-7-1)

The two top benches of the channel samples composed mainly of roof rock, bony coal and draw slate show extremely low similarities of the trace element composition with the coal bench, even though their major element compositions are relatively similar. The effects of mining the top noncoal benches can be detected in the trace element compositions of the samples from the immediate return of the miner operation (the CR

samples). The similarity coefficients of the CR samples with the coal bench based upon the trace element compositions clearly become smaller in the finer size ranges. Therefore, it can be estimated that a considerable amount of the trace elements in the CR samples originated from the noncoal benches of the seam.

The samples from the immediate returns of the miner and bolter operations (the CR and RR samples) show high similarities in all size fractions. However, the trace element compositions of the RR samples show very low similarity coefficients with all the benches from the coal seam; much lower in the size range of 0.9 to 2 μm. However, the close association with the intake air samples (the ININ and INOUT samples) indicate that in this size range, the major source of the trace elements in the RR samples might be the intake air.

According to the size analysis, the fine modes at about 3.5 μm were present in all the samples. As shown in Table A.9.6, the samples in the size range of 0.9 to 6 μm generally share higher similarities than those in the size range of 10 to 15 μm. None of the samples indicates possible association with the rock dust.

5.3.7 Discussion

The relationship between the characteristics of airborne coal mine dust and the materials being cut can be studied by comparing the characteristics of the samples from the immediate return of the miner operation (the CR samples) and the channel samples. The study indicated, in general, that the major element concentrations in all size fractions (0.9 to 15 μm) of the CR samples were closely associated with the coal seam regardless of the presence of noncoal bands in the coal seam. However, consistent similarities in the trace element compositions of the CR samples with the coal seam were not observed. In Sample Sets B and C, the coal benches were the major sources of trace elements in the CR samples in all size fractions while Sample Set G indicated that none of the coal and noncoal benches appeared to be closely associated with the trace element compositions of the CR samples in the size range of 0.9 to 2 μm. In Sample Set F, the trace element compositions of the CR samples in the size range of 0.9 to 2 μm were much closer to the coal benches than the noncoal benches, while high similarities in the trace element compositions between the coal bench and the CR samples from Sample Set E were observed only in the size range of 10 to 15 μm. These discrepancies might be due to the differences in the modes of occurrence of the trace elements as minerals or impurities in the organic coal and depend upon the effects of the miner operation on liberating the particles containing the trace elements from the coal seam.

In most of the sections, significant effects of employing shuttle cars in the intake airways were observed. When double splits of air were used for face ventilation, the major and trace

element compositions of the samples taken in separate return airways showed high similarities. This seems to be due to reentrainment of dust in the size range below 6 μm along the shuttle car route which subsequently contaminated both return airways. When the bolter operation was well ventilated by line brattice or auxiliary fan and tubings, the levels of dust generated by the bolter operation were low, but the elemental compositions of the fine dust in the range of 0.9 to 2 μm near the operation were very similar to those in the samples from the intake airway (the RI samples).

Potential of the intake air as a significant dust source was seen in the sections where dust levels in the intake air were considerable higher than in the other sections. Particularly in the size range of 0.9 to 2 μm, it can be shown through the high similarities that the intake air samples (the IN samples) were the major source of the trace elements on the samples from the intake airways to the miner and bolter operations (the CI and RI samples). In almost all sections sampled in this study, the fine-size modes commonly found in the size range of 2 to 4 μm shared similar elemental compositions. This may support the presence of the fine-size modes in the airborne coal mine dust size distributions.

Considering the influences of the intake air dust on the mine dust near the face operation and those of the reentrainment dust on the return airway dust, dust particles carrying various elements, particularly in the size range below 6 μm, seem to be transportable through the entire working area. The distance between the intake air sampling location and the face was usually near 500 feet. The last sampling location in the return airway was about 400 feet outby the nearest face operation.

6. CONCLUSIONS

6.1 Summary

Based upon the significance of airborne coal mine dust on safety and health concerns in underground coal mines, the main objective of this thesis was to analyze two basic characteristics of the airborne coal mine dust, size and elemental composition. A dust sampling strategy was established to provide airborne coal mine samples for characterization purposes. The Sierra Model 298 eight-stage cascade impactors were chosen for airborne coal mine dust sampling and extensively tested for their applicability in underground coal mines.

Selection of an impaction medium and determination of the optimal sampling times under various concentrations of dust were made based upon experiments in the dust chamber. A mixture of pure petroleum jelly and toluene was chosen to minimize the problems associated with particle bounce and blow-off. For a dust level of about 1 mg/m^3 (in the size range below 10 μm), none of the impactors with sampling times between 180 and 270 minutes experienced problems associated with either underloading or overloading, while 180 minutes was shown as the appropriate sampling time under a dust level of approximately 2 mg/m^3. At high dust levels above 4 mg/m^3 similar to situations in the immediate return of the continuous miner operation, the time required for completion of a cut (usually less than an hour for a 20-foot advance) was found to be an appropriate sampling time for cascade impactors.

Comparison between the isokinetic and nonisokinetic samples showed that the differences in the size distribution as well as dust concentration were not significant compared to the variation expected from side-by-side samplers. Therefore, dust samples taken by cascade impactors with standard nonisokinetic cowls and visors were assumed to be representative of the total airborne coal mine dust at various locations in the working area of underground coal mines.

The size data based upon the aerodynamic diameter were obtained directly from the samplers. Analytical representation of the airborne coal mine dust size was performed through empirical as well as lognormal distributions. The first objective of this section on the size analysis was to examine the two assumptions implicitly made in the current practice for coal mine dust size presentation: lognormality and unimodality in the mass size distribution. In addition, the second objective was to study locational variability and effects of the mining operation on the coal mine dust size distribution. The Chebychev approximation function and cubic-spline interpolation were employed to find mathematical expressions for the continuous cumulative mass size distributions and the subsequently corresponding mass size frequency distributions from their first derivatives.

The lognormal distribution models were obtained based upon the generalized histograms. Possible presence of polymodality in the mass size distribution was taken into consideration. Approximation of component distributions from a composite mass size distribution was made by two nonlinear least-squares methods, the Marquardt and DUD methods. These two methods were found to be insensitive to arbitrary selection of the starting values.

Comparison between the empirical and lognormal frequency distributions showed that the lognormal model was able to detect all the major modal patterns observed in the empirical distributions. However, this was the case only under the assumption of bimodality which was indicated in most of the dust samples taken at 11 different continuous miner development sections. An implication of this result is that analytical representation of airborne coal mine dust by assuming only one mode in their distributions may result in seriously biased inferences.

The size distributions of dust samples from various locations showed several characteristics that may be important in control of dust in underground coal mines. One of those was that significant presence of fine modes in the size range of 2 to 4 μm were observed in almost all dust samples. Because most of the particles in these fine modes with the geometric standard deviations less than 3 are respirable, the significance of these fine modes can be recognized. Even though dust samples from the immediate return of the miner had their major modes in the size range of 12 to 18 μm, the mass percentage of the dust associated with the fine modes below 5 μm was normally more than 10%. Therefore, considering the high dust concentrations originating from the miner operation, the significance of the fine modes as a major source for respirable dust can be realized because the geometric standard deviations of the fine modes were approximately 2.

Apparent reentrainment of dust due to shuttle car movement was noticed in the presence of relatively coarse modes at about 10 μm in the samples obtained along the shuttle car route which was usually in the intake airway of the face operation. It can be seen that a considerable portion of the particles in these modes with a geometric standard deviation of 1 to 2.5 are also respirable. In some sections, the roof bolter was found to generate insignificant amounts of dust and did not significantly change the size consists of the airborne dust coming to the operation. Presence of coarse modes greater than 12 μm was consistently observed in the samples from the returns two and four crosscuts outby the face operation.

Differences in the elemental compositions of coal among three Pennsylvania coalfields with different ranks of coal and different incidences of CWP were analyzed to study possible association between the elemental characteristics and development

of CWP. The statistical tests based upon 10 major and 11 trace elements showed significant differences in elemental composition among the three coalfields. Concentrations of Al, Si, Ti, Cr, Ni, Rb, V and Zr were higher in the coalfields with higher ranks of coal, while Fe, S and Sr showed the opposite trend.

Dust samples from 7 different sections were analyzed by the PIXE method. As an important topic for study of toxicity of particles in the human respiratory tract, the size dependency of elemental composition of airborne coal mine dust was tested. Overall compositions reflected by the 9 major elements in the airborne dust samples from three different size fractions (0.9 to 2 μm, 3.5 to 6 μm, and 10 to 15 μm) were found to be significantly different, while overall compositions reflected by the 21 trace elements showed significant size dependency at all the locations except the intake airways for the miner and bolter. Concentrations of Al, Si, S, Ca and Sr showed significant variation with size at almost all locations. The size effects were more significant in the immediate return of the miner where Cl, Cr, Ni, Mo, V, Br, Rb, Sr, Zr and Pb showed significant variation with size. In general, concentrations of these elements were higher in the coarser size ranges.

Locational variation of the overall compositions of the major and trace elements was also significant. Bolters generated higher concentrations of Si in the size range below 3.5 μm. In the coarser size range above 3.5 μm, P, S and K varied at different sampling locations; Si and Fe varied in the finer size range. P and S were highly concentrated in the intake airways, while K, Si and Fe showed higher concentrations near the roof bolter operation. Concentrations of V, Rb and Mo were significantly different in the size range of 10 to 15 μm, 3.5 to 6 μm and 0.9 to 2 μm, respectively. All these trace elements had higher concentrations near the roof bolter operation. Differences in the elemental compositions as well as concentrations of most of the elements at two and four crosscuts outby the face operation were not significant. In general, weight percentages of the organic components of coal mine dust were higher in the finer size ranges and near the continuous miner operation.

Associations among the dust and channel samples were measured in terms of the elemental compositions. The results were analyzed to study the relationship between the characteristics of airborne coal mine dust and the materials being cut and to study the source and transportability of airborne coal mine dust. The major elements in all the size fractions of airborne coal mine dust were found to be closely associated with the coal seam, independent of the presence or absence of noncoal bands. However, the relationship of the trace elements was not consistent. It was affected by the presence of noncoal bands in the coal seam and was different in different size fractions of airborne coal mine dust.

In some sections where relatively high concentrations of dust occurred in the intake airways, the dust in the intake airways was found to be a significant source of trace elements in the downwind sampling locations. The fine size fraction of reentrainment dust along the shuttle car route was found to influence the entire working area. The fine-size modes commonly observed in the size range of 2 to 4 μm throughout the working sections showed a strong similarity in their elemental compositions. Based upon these observations, it seems that airborne coal mine dust in the respirable size range can flow through the working area without a significant amount of deposition.

6.2 Conclusions

The airborne coal mine dust samples collected by multi-stage cascade impactors were found to be reliable for size characterization and the study of the association between the size and elemental characteristics. The use of the PIXE method appears to be quite useful and reliable for this type of research work. The mass size distributions of airborne coal mine dust from various locations in the working areas of the continuous miner development sections were well approximated by bimodal lognormal distributions.

The elemental composition of airborne coal mine dust varied with the size of dust particle and it was also different at different locations. This implies that, depending upon the job location, mine workers are likely to be exposed to mine dust with different size and elemental characteristics. The significance of the intake air dust as a potential source for elemental contamination of airborne coal mine dust at the face was observed. Dust reentrained along the shuttle car route was also found to be a significant dust source. Airborne coal mine dust in the respirable size range appears to be transportable through the working area without significant deposition.

6.3 Limitations

From the beginning of this thesis project, the principal limitation was the amount of dust sample available from the impactors. Because of this intrinsic limitation in the samplers, all the subsequent analyses were to be based upon the extremely small amount of sample. Therefore, careful attention has to be paid to the topic of data reproducibility. Employment of multiple side-by-side samplers is an alternative. However, if the variation in the characteristics of dust is significant, a high-volume sampler will be a better selection to provide samples for characterization purposes.

Other limitations in the data analysis were due to limited information on the characteristics of dust samples. For example, because only two size fractions below 1 μm exist in an impactor, the possibility of the presence of a third mode observed in many

samples in this range could not be studied. In addition, to identify the sources for bimodality associated with either the coal seam, dust control measures, or the mining process itself, more information on the other characteristics of coal mine dust such as mineralogical and morphological characteristics is necessary.

6.4 Some Implications of the Research and Recommendations for Future Research

The results of the analysis of size and elemental composition of airborne coal mine dust indicated presence of fine-size modes in the range of 2 to 5 μm in the mass size distributions of most of the dust samples. Considering that the mass percentages of these modes are significant and particles in these modes are mostly respirable, dust control measures must be engineered to handle these fine-size modes. At the same time, the sources for these modes must be identified by analyzing the other characteristics of airborne coal mine dust.

Size-dependency of the elemental characteristics of airborne coal mine dust was established in this research. The same approach for researching the other characteristics of airborne coal mine dust is desirable to identify a size range that should be targeted in the fight against CWP.

The importance of the roof bolter operation and intake air dust as significant sources for elements in airborne coal mine dust was established. If some elements have adverse effects on health concerns, more efforts must be exerted for dust control measures for the roof bolter operation and intake air.

Regardless of the floor conditions and dust control measures employed in continuous miner sections, dust reentrainment by shuttle cars was found to contaminate the face and return airways. Because most of the face workers are likely to be exposed to this type of dust, measurement and characterization of the reentrained dust must be studied for control purposes.

The significance of size dependency and locational variability of elemental characteristics must be taken into consideration in coal dust used for medical studies on the development of CWP. Difference between the characteristics of airborne coal mine dust and coal itself is another reason for this necessity.

The association between the rank and elemental characteristics of coal was found to be significant. However, this association can be either direct or synergistic with other dust characteristics. More detailed studies on the other characteristics of coal should be pursued to analyze the relationship between the rank of coal and regional differences in the incidence of CWP.

REFERENCES

Ahlberg, M. S., Leslie, A. C. D., and J. W. Winchester, 1978, Environmental and Occupational Health Analysis Using Proton-Induced X-Ray Emission," Ch. 4 in Electron Microscopy and X-Ray Applications to Environmental and Occupational Health Analysis, Russell, P. A., and A. E. Hutchings, Eds., Ann Arbor Science, Ann Arbor, MI.

Allen, T., 1981, Particle Size Measurement, Chapman and Hall, NY.

Anon., 1980, "Report of the Committee on Measurement and Control of Respirable Dust," Report NMAB-363, National Academy of Sciences, Washington, DC.

Anon., 1980, "Trace-Element Geochemistry of Coal Resource Development Related to Environmental Quality and Health," U.S. National Committee for Geochemistry, Panel on the Trace Element Geochemistry of Coal Resource Development Related to Health, National Academy Press, Washington, DC.

Anon., 1981, Technical Highlights: Health and Safety Research 1970-1980, U.S. Bureau of Mines special publication.

Anon., 1985, SAS User's Guide: Statistics, Version 5 Edition, SAS Institute, Inc., Cary, NC.

Anon., 1985, Instructional Manual for the Marple Cascade Impactors, Anderson Samplers, Inc., Bulletin No. 290 I.M.-3-82.

Anon., 1985, Occupational Medicine Report 1984, Institute of Occupational Medicine, Edinburgh, U.K.

Anon., 1985, "Reducing Dust Exposure of Roof Bolter Operators," U.S. Bureau of Mines Technology News, No. 219.

Attfield, M. D., 1984, "Recent Results and Forthcoming Studies in the Epidemiology of Coal Workers' Pneumoconiosis in Underground Miners," Proceedings of the Coal Mine Dust Conference, West Virginia University, Morgantown, WV, pp. 156-162.

Baier, E. J., and R. Diakun, 1963, "Environmental Dust Study of Anthracite Coal Mines of Eastern Pennsylvania," J. of Occupational Medicine, Vol. 5, No. 8, pp. 396-403.

Bennett, J. G., Dick, J. A., Kaplan, Y. S., Shand, P. A., Shennan, D. H., Thomas, D. J., and J. S. Washington, 1979, "The Relationship Between Coal Rank and The Prevalence of Pneumoconiosis," British J. of Industrial Medicine, Vol. 36, pp. 206-210.

Berg, W. W., Sage, R. V. L., Sato, K., Pilotte, J. O., Cohn, S. L., Winchester, J. W., and J. W. Nelson, 1977, "Hourly Variation of Aerosol Composition in the Great Lake Basin," J. of Great Lakes Research, Vol. 3 and 4, pp. 278-290.

Bowman, J. D., Busch, K. A., and S. A. Schulman, 1983, "Statistical Evaluation of Sampling Strategies for Coal Mine Dust," Ch. 23 in Aerosols in the Mine and Industrial Work Environments, Marple, VA, and B. Y. H. Liu, Eds., Ann Arbor Science, Ann Arbor, MI.

Brain, J. D., 1977, "Anesthesia and Respiratory Defense Mechanisms," International Anesthesia Clinics, Vol. 15, pp. 169-198.

Bray, J. H., and S. E. Maxwell, 1982, Multivariate Analysis of Variance, Series in Quantitative Applications in the Social Sciences, Sage Publications, Beverly Hills, CA.

Breslin, J. A., and G. E. Niewiadomski, 1982, "Improving Dust Control Technology for U.S. Mines," U.S. Bureau of Mines Impact Report.

Brezovec, D., 1981, "Managers Spur Productivity Gains," Coal Age, Vol. 86, No. 12, pp. 55-59.

Burkhart, J. E., McCawley, M. A., and R. W. Wheeler, 1983, "Particle Size Distributions in Underground Coal Mines," A paper presented at American Industrial Hygiene Association Conference, Philadelphia, PA.

Campbell, J. L., and J. A. Cookson, 1984, "PIXE Analysis of Thick Targets," Nuclear Instruments and Methods in Physical Research, Vol. B3, North-Holland Publishing Co., Amsterdam, Netherlands, pp. 185-197.

Carlberg, J. R., Crable, J. V., Limhaco, L. P., Norris, H. B., Holtz, J. L., Mauer, P. A., and F. R. Wolowicz, 1971, "Total Dust, Coal, Free Silica, and Trace Metal Concentrations in Bituminous Coal Miners' Lungs," American Industrial Hygiene Association J., Vol. 32, No. 7, pp. 432-440.

Chen, C. Y., 1955, "Filtration of Aerosols by Fibrous Media," Chemistry Reviews, Vol. 55, pp. 595-602.

Chen, J. R., Kneis, H., Martin, B., Nobiling, R., Traxel, K., Chao, E. C. T., and J. A. Minkin, 1981, "Trace Elemental Analysis of Bituminous Coals Using the Heidelberg Proton Microprobe," Nuclear Instruments and Methods, Vol. 181, North-Holland Publishing Co., Amsterdam, Netherlands, pp. 151-157.

Cheng, L., 1973, "Collection of Airborne Dust by Water Spray," Industrial and Engineering Chemistry Process Design and Development, Vol. 12, No. 2, pp. 221-225.

Cheng, L., 1977, "Dynamic Spreading of Drops Impacting onto a Solid Surface," Industrial and Engineering Chemistry Process Design and Development, Vol. 16, No. 2, pp. 192-197.

Coenen, W., 1966, Staub, Vol. 26 (Title and particulars of reference unavailable).

Conte, S. D., and C. D. Boor, 1980, Elementary Numerical Analysis; An Algorithm Approach, McGraw-Hill Co., NY.

Corn, M., Stein, F., Hammad, Y., Manekshaw, S., and W. Bell, 1972, "Physical and Chemical Properties of Respirable Coal Mine Dust," Final Report, U.S. Bureau of Mines Grant No. C0101742, Available as NTIS Report No. PB 222-490, National Technical Information Service, Springfield, VA.

Corn, M., Stein, F., Hammad, Y., Manekshaw, S., and Freedman, R., and A. M. Hartstein, 1973, "Physical and Chemical Properties of Respirable Coal Dust from Two United States Mines," American Industrial Hygiene Association J., Vol. 33, No. 7, pp. 295-285.

Crable, J. V., Keenan, R. G., Wolowicz, F. R., Knott, M. J., Holtz, J. L., and C. H. Gorski, 1967, "The Mineral Content of Bituminous Coal Miners' Lungs," American Industrial Hygiene Associate J., Vol. 28, No. 1, pp. 8-12.

Crable, J. V., Keenan, R. G., Kinser, R. E., Smallwood, A. W., and P. A. Mauer, 1968, "Metal and Mineral Concentrations in Lungs of Bituminous Coal Miners," American Industrial Hygiene Association J., Vol. 29, No. 2, pp. 106-110.

Daniel, J. H., 1984, "Respirable Dust Control Research - The Bureau of Mines Program," Proceedings of the Coal Mine Dust Conference, West Virginia University, Morgantown, WV, pp. 1-7.

Davies, C. N., 1974, "Size Distribution of Atmospheric Particles," J. of Aerosol Science, Vol. 5, No. 3, pp. 293-300.

Davison, R. L., Natusch, D. F. S., Wallace, J. R., and C. A. Evanse, 1974, "Trace Elements in Flyash - Dependence of Concentration on Particle Size," Environmental Science and Technology, Vol. 8, pp. 1107-1123.

Deepak, A., and G. P. Box, 1982, "Representation of Aerosol Size Distribution Data by Analytical Methods," Atmospheric Aerosols: Their Formation, Optical Properties, and Effects, A. Deepak, Ed., Spectrum Press, Hampton, VA.

Divers, E. F., and J. J. Janosik, 1978, "Comparison of Five Types of Low-Energy Scrubbers for Dust Control," U.S. Bureau of Mines RI 8289.

Divers, E. F., and J. McClelland, 1984, "Maintain Filters to Control Roof Dust," Coal Age, Vol. 89, pp. 141-142.

Emmerling, J. E., and R. J. Seibel, 1975, "Dust Suppression with Water Sprays During Continuous Coal Mining Operations," U.S. Bureau of Mines RI 8064.

Esmen, N. A., and T. C. Lee, 1980, "Distortion of Cascade Impactor Measured Size Distributions Due to Bounce and Blow-Off," American Industrial Hygiene Association J., Vol. 41, No. 6, pp. 410-419.

Esmen, N. A., and Y. Y. Hammad, 1979, "Log-Normality of Environmental Sampling Data," J. of Environmental Science and Health, A12, pp. 29-41.

Esmen, N. A., 1983, "Mathematical Basis for an Efficient Sampling Strategy," Aerosols in the Mining and Industrial Work Environments, Marple, V. A., and B. Y. H. Liu, Eds., Ann Arbor Science, Ann Arbor, MI, pp. 271-283.

Freedman, R. W., 1978, "Procedures for Analysis of Respirable Dust as Relted to Coal Workers' Pneumoconiosis," Ch. 28 in Analytical Methods for Coal and Coal Products, Vol. II, K. Clarence, Jr., Ed., Academic Press Inc., NY.

Friedlander, S. K., 1977, Smoke, Dust and Haze Fundamentals of Aerosol Behavior, John Wiley & Sons, Inc., NY.

Gerencher, J. J., 1984, "Multivariate Study of the Interrelationships Among Selected Variables of the Organic Fraction of Samples of United States' Coals," Unpublished D.Ed. Thesis, The Pennsylvania State University, University Park, PA.

Given, P. H., 1973, "How May Coals Be Characterized for Practical Use?" A paper presented at Short Course on Coal Characteristics and Coal Conversion Processes, The Pennsylvania State University, University Park, PA.

Glick, D. C., 1984, "Variability in the Inorganic Content of United States' Coals, A Multivariate Statistical Study," Unpublished M.S. Thesis, The Pennsylvania State University, University Park, PA.

Gluskoter, H. G., Ruch, R. R., Miller, W. G., Cahill, R. A., Dreher, G. B., and J. K. Kuhn, 1977, "Trace Elements in Coal: Occurrence and Distribution," Illinois State Geological Survey Circular 499.

Green, P., 1978, Analyzing Multivariate Data, Dryden Press, Hinsdale, IL.

Grigal, D., Ufken, G., Sandstedt, J., Blom, M., Johnson, D., 1982, "Development of Improved Scrubbers for Coal Mine Applications," Final Report, U.S. Bureau of Mines Contract No. H0199055, Donaldson Co., Inc., Available as NTIS Report No. PB 83-205385, National Technical Information Service, Springfield, VA.

Hamilton, R. J., and G. Knight, 1958, "Some Studies of Dust Size Distribution and the Relationship Between the Dust Formation and Coal Strength," Proceedings of a Conference on Mechanical Properties of Non-Metallic Brittle Materials, Butterworth Scientific Publishing Co., London, U.K.

Hamilton, R. J., 1985, Industrial Health and Safety, a synthesis report on research supported by the Commission of the European Community during the period 1977-82, Luxembergh.

Hammad, Y., Corn, M., and V. Dharmarajan, 1981, "Environmental Characterization," Ch. 12 in Occupational Lung Diseases: Research Approaches and Methods, Weill, H., and M. Turner-Warwick, Ed., Marcel Dekker, Inc., NY.

Hartman, I., Nagy, J., and J. K. Rauschenberger, 1954, "Lessons from Intensive Dust Sampling of a Coal Mine," U.S. Bureau of Mines RI 5054.

Heppelston, A. G., 1947, "The Essential Lesion of Pneumoconiosis in Welsh Coal Workers," J. of Pathology and Bacteriology, Vol. 59, No. 7, pp. 453-460.

Herdan, 1960, Small Particle Statistics, Butterworth & Co., London, U.K.

Hertzberg, M., Cashdollar, K. L., and J. Opferman, 1979, "The Flammability of Coal Dust-Air Mixtures: Lean-Limit, Flame Temperatures, Ignition Energies, and Particle Size Effects," U.S. Bureau of Mines RI 8360.

Heyder, J., Gebhart, J., and W. Stahlhofen, 1980, "Inhalation of Aerosols: Particle Deposition and Retention," Ch. 3 in Generation of Aerosols, K. Willeke, Ed., Ann Arbor Science, Ann Arbor, MI.

Hicks, D., Fay, J. W. T., Ashford, J. R., and S. Rae, 1961, "The Relationship Between Pneumoconiosis and Environmental Conditions," National Coal Board, Pneumoconiosis Field Research, London, U.K.

Hodkinson, J. R., 1958, "A Note on the Particle-Size Distribution of Microscopic Coal and Rock Dusts," Safety in Mines Research Establishment Research Report, No. 153, Ministry of Fuel and Power, London, U.K.

Hogg, R., 1984, "Particle Technology Laboratory Lecture Notes and Laboratory Manual," Department of Mineral Engineering, The Pennsylvania State University, University Park, PA.

Hudson, G. M., Kaufmann, H. C., Nelson, J. W., and M. A. Bonacci, 1980, "Advances in the Use of PIXE and PESA for Air Pollution Sampling," Nuclear Instruments and Methods, Vol. 168, North-Holland Publishing Co., Amsterdam, Netherlands, pp. 259-263.

Huggins, C. W., Johnson, S. N., Segreti, J. M., and J.G. Synder, 1985, "Determination of Alpha Quartz Particle Distribution in Respirable Coal Mine Dust Samples and Reference Standards," U.S. Bureau of Mines RI 8975.

Hurley, J. F., Burns, J., Copland, L., Dodgson, J., and M. Jacobsen, 1982, "Coalworkers' Simple Pneumoconiosis and Exposure to Dust at 10 British Coalmines," British J. of Industrial Medicine, Vol. 39, pp. 120-127.

Imbrie, J., and E. Purdy, 1962, "Classification of Modern Bahamian Carbonate Sediments," Classification of Carbonate Rocks, Vol. 7, pp. 253-272.

Ishii, H., Sato, T., and K. Tachibana, 1978, "Observation of Crustal Movements at the Akita Geophysical Observatory (3)-Application of Chebychev Approximation Function for Data Observed by Extensometers and Tiltmeter," J. of the Geodetic Society of Japan, Vol. 24, No. 3, pp. 122-131.

Ito, P. K., 1980, "Robustness of ANOVA and MANOVA Test Procedures," Handbook of Statistics, Vol. I; Analysis of Variance, P. R. Krishnaiah, Ed., North-Holland Publishing Co., NY.

Jacobsen, M., Rae, S., Walton, W. H., and J. M. Rogan, 1970, "New Dust Standards for British Coal Mines," Nature, Vol. 227, No. 5257, pp. 445-447.

Jacobsen, M., Rae, S., Walton, W. H., and J. M. Rogan, 1971, "The Relationship between Pneumoconiosis and Dust Exposure in British Coal Miners," Inhaled Particles and Vapours III, W. H. Walton Ed., Unwin Bros., Oldwoking (Surrey), U.K., pp. 903-919.

Jaenicke, R., and C. N. Davies, 1976, "The Mathematical Expression of the Size Distribution of Atmospheric Aerosols," J. of Aerosol Science, Vol. 7, No. 3, pp. 255-260.

Jayaraman, N. I., Schroeder, W. E., and F. N. Kissell, 1986, "Studies of Dust Knockdown by Water Sprays Using a Full-Scale Model Mine Entry," Society of Mining Engineers of AIME, Transactions, Vol. 278, pp. 1875-1882.

Johansson, S. A. E., and T. B. Johansson, 1976, "Analytical Application of Particle-Induced X-Ray Emission," Nuclear Instrument and Methods, Vol. 137, North Holland Publishing Co., Amsterdam, Netherlands, pp. 473-516.

Johnson, R., and D. Wichern, 1982, Applied Multivariate Statistical Analysis, Prentice-Hall, Englewood Cliffs, NJ.

Kapadia, A., 1980, "Data Reduction for Aerosol Size Distribution Measuring Instruments," Unpublished Ph.D. Thesis, University of Minnesota, MN.

Keenan, R. G., Crable, J. V., Smallwood, A. W., and J. R. Carlberg, 1971, "Chemical Composition of the Coal Miners' Lung," American Industrial Hygiene Association J., Vol. 32, No. 6, pp. 392-397.

Kessler, T., Sharkey, A. G., Jr., and R. A. Friedel, 1971, "Spark-Source Mass Spectrometer Investigation of Coal Particles and Coal Ash," U.S. Bureau of Mines TPR 42.

Kessler, T., Sharkey, A. G., Jr., and R. A. Friedel, 1973, "Analysis of Trace Elements in Coal by Spark-Source Mass Spectrometry," U.S. Bureau of Mines RI 7714.

Knutson, E. O., and P. J. Lioy, 1983, "Measurement and Presentation of Aerosol Size Distributions," Air Sampling Instruments for Evaluation of Atmospheric Contaminants, American Conference of Governmental Industrial Hygienists, Cincinnati, OH, pp. G.1-G.12.

Kost, J. A., Colinet, J. F., and G. A. Shireey, 1981, "Field Survey of Float Dust in Coal Mining Operations," Final Report, U.S. Bureau of Mines Contract No. J0308030, Bituminous Coal Research Inc., Monroeville, PA.

Kost, J. A., Shirley, G. A., and C. T. Ford, 1980, "In-Mine Tests for Wetting Agent Effectiveness," U.S. Bureau of Mines OFR 30-82.

Lawson, D. R., and J. W. Winchester, 1978, "Sulfur and Crustal Reference Elements in Nonurban Aerosols from Squaw Mountain Colorado," Environmental Science and Technology, Vol. 12, pp. 716-721.

Lee, C., and J. M. Mutmansky, 1986, "A Strategy for Coal Mine Respirable Dust Sampling Using Multi-Stage Impactors for Characterization Purpose," Proceedings of the Symposium on Engineering Health and Safety in Coal Mining, A. W. Khair, Ed., Society of Mining Engineers of AIME, Littleton, CO.

Leiteritz, H., Einbrandt, H., and W. Klosterkotter, 1967, "Grain Size and Mineral Content of Lung Dust of Coal Miners Compared with Mine Dust," Inhaled Particles and Vapours III, Davies, C. N., Ed., Pergamon Press, London, U.K., pp. 381-392.

Lepeltier, C., 1969, "A Simplified Statistical Treatment of Geochemical Data by Geophysical Representative," Economic Geology, Vol. 64, pp. 538-550.

Liu, B. Y. H., Pui, D. Y. H., and K. L. Rubow, 1983, "Characteristics of Air Sampling Filter Media," Ch. 70 in Aerosols in the Mine and Industrial Work Environments, Marple, V. A., and B. Y. H. Liu, Eds., Ann Arbor Science, Ann Arbor, MI.

Loinhart, W. S., 1969, "Roentgenographic Evidence of Coal Workers' Pneumoconiosis in Three Geographic Areas in the United States," J. of Occupational Medicine, Vol. 11, No. 8, pp. 399-408.

Malinowski, E. R., and D. G. Howery, 1980, Factor Analysis in Chemistry, John Wiley and Sons, Inc., NY.

Marple, V. A., Liu, B. Y. H., and K. L. Rubow, 1978, "A Dust Generator for Laboratory Use," American Industrial Hygiene Association J., Vol. 39, No. 1, pp. 26-32.

Marple, V. A., and K. L. Rubow, 1983, "An Aerosol Chamber for Instrument Evaluation and Calibration," American Industrial Hygiene Association J., Vol. 44, No. 5, pp. 361-367.

Matta, J. E., 1976, "Effect of Location and Type of Water Sprays for Respirable Dust Suppression on a Continuous-Mining Machine," U.S. Bureau of Mines Coal Mine Health and Safety Research Program TPR 96.

McBride, W. W., Pendergrass, E., and J. Lieben, 1963, "Pneumoconiosis Study of Western Pennsylvania Bituminous Coal Miners," J. of Occupational Medicine, Vol. 5, No. 8, pp. 376-388.

McBride, W. W., Pendergrass, E., and J. Lieben, 1966, "Pneumoconiosis of Pennsylvania Anthracite Miners," J. of Occupational Medicine, Vol. 8, No. 7, pp. 365-376.

McNown, J. A., and J. Malaika, 1950, "Effects of Particle Shape on Settling Velocity at Low Reynolds Number," Transactions of American Geophysical Union, Vol. 19, pp. 74-82.

Mercer, T. T., 1975, "The Deposition Model of the Task Group on Lung Dynamics: A Comparison with Recent Experimental Data," Health Physics, Vol. 29, pp. 673-680.

Miller, R. N., 1977, "Geochemical Study of the Inorganic Constituents in Some Low-Rank Coals," Unpublished Ph.D. Thesis, The Pennsylvania State University, University Park, PA.

Miller, W. G., 1974, "Relationships Between Minerals and Selected Trace Elements in Some Pennsylvania Age Coals of Western Illinois," Unpublished M.S. Thesis, University of Illinois, Urbana-Champaign, IL.

Morgan, W. K. C., 1971, "Coal Workers' Pneumoconiosis," American Industrial Hygiene Association J., Vol. 32, No. 1, pp. 29-34.

Morgan, W. K. C., Reger, R. B., Burgess, D. B., and E. P. Schoub, 1972, "A Comparison of the Prevalence of Coal Workers' Pneumoconiosis and Respiratory Impairment in Pennsylvania Bituminous and Anthracite Miners," Annals of New York Academy of Science, NY, pp. 252-259.

Morgan W. K.C., Burgess, D. B., Jacobson, G., O'Brien, R. J., Pendergrass, E., Reger, R. B., and E. P. Schoub, 1973, "The Prevalence of Coal Workers' Pneumoconiosis in U.S. Coal Miners," Archives of Environmental Health, Vol. 27, No. 4, pp. 221-226.

Mutmansky, J. M., and C. Lee, 1984, "An Analysis of Coal and Geological Variables Related to Coal Workers' Pneumoconiosis," Proceedings of the Coal Mine Dust Conference, West Virginia University, Morgantown, WV, pp. 235-249.

Naeye, R. L., Mahon, J. K., and W. S. Dellinger, 1971, "Rank of Coal and Coal Workers' Pneumoconiosis," American Review of Respiratory Disease, Vol. 103, pp. 350-355.

Nagelschmidt, G., 1965, "The Study of Lung Dust in Pneumoconiosis," American Industrial Hygiene Association J., Vol. 26, No. 1, pp. 1-7.

Neter, J., and W. Wasserman, 1974, Applied Linear Statistical Models: Regression, Analysis of Variance, and Experimental Designs, Richard D. Irwin, Inc., Homewood, IL.

Nicholls, G. D., 1968, "The Geochemistry of Coal-Bearing Strata," Coal and Coal-Bearing Strata, Murchison, D., and T. Stanley, Eds., Inter-Univerity Geological Congress, American Elsevier Publishing Co., NY.

Niewiadomski, G. E., 1983, "Improving Dust Control Technology," Proceedings of the Symposium on Control of Respirable Coal Mine Dust, Mine Safety and Health Administration, Beckley, WV.

O'Gorman, J. V., 1971, "Studies on Mineral Matter and Trace Elements in North American Coals," Unpublished Ph.D. Thesis, The Pennsylvania State University, University Park, PA.

Oldham, P. D., 1953, "The Nature of the Variability of Dust Concentrations at the Coal Face," British J. of Industrial Medicine, Vol. 10, pp. 227-234.

Olsen, C. L., 1974, "Comparative Robustness of Six Tests in Multivariate Analysis of Variance," J. of the American Statistical Association, Vol. 69, pp. 894-908.

Orlic, I., Pavlic, M., Rendic, D., Marijanovic, P., Vakovic, V., Budran, M., and L. Cindro, 1981, "Determination of Trace Elements in Coal by X-Ray Emission Spectroscopy," A paper presented at International Congress of Analytical Techniques in Environmental Chemistry, Barcelona, Spain.

Orsini, C. M. Q., and L. C. S. Boueres, 1979, "Atmospheric Aerosol Characterization by Means of Impactor Samples Analyzed by PIXE," A paper presented at International Congress of Analytical Techniques in Environmental Chemistry, Barcelona, Spain.

Otsu, H., Kubota, R., and Y. Matsuda, 1983, "Determination of Statistical Frequency Distribution of Geochemical Data," Mining Geology of Japan, Vol. 33, No. 6, pp. 427-431.

Otsu, H., Kubota, R., and Y. Matsuda, 1984, "Partition of Statistical Frequency Distribution of Geochemical Data," Mining Geology of Japan, Vol. 34, No. 1, pp. 51-56.

Page, S., Hughes, B., and S. Monroe, 1984, "Water-Powered Scrubber Aids Ventilation," World Mining Equipment, Vol. 8, No. 12, pp. 67-68.

Perera, F. P., and A. K. Ahmed, 1979, "Respirable Particles: Impact of Airborne Fine Particles on Health and Environment, Ballinger Publishing Co., Cambridge, MA.

Piperno, E., 1973, "Trace Element Emission: Aspects of Environmental Toxicology," Trace Elements in Fuel, Advances in Chemistry Series, No. 141, S. P. Babu, Ed., American Chemistry Society, Chicago, IL.

Ralston, M. L., and R. I. Jennrich, 1978, "DUD, A Derivative-Free Algorithm for Nonlinear Least Squares," Technometrics, Vol. 20, No. 1, pp. 7-13.

Rankin, R. L., and S. L. Rodgers, 1980, "Study of Respirable Dust Outby the Working Face of a Coal Mine," Final Report, U.S. Bureau of mines Contract No. J0366022, Mine Safety Appliances Co., Available as NTIS Report No. PB 81-236762, National Technical Information Service, Springfield, VA.

Rankin, R. L., Rodgers, S. J., and E. V. Polite, 1983, "Effects of Engineering Parameters on the Control of Respirable Dust," Final Report, U.S. Bureau of Mines Contract No. J0387226, Mine Safety Appliances Co., Available as NTIS Report No. PB 83-232207, National Technical Information Service, Springfield, VA.

Reisner, M. T. R., 1971, "Results of Epidemiological Studies of Pneumoconiosis in Western German Coal Mines," W. H. Walton, Ed., Unwin Bros., Oldwoking (Surrey), U.K., pp. 921-929.

Rocketle, H., 1977, "Motality Among Coal Miners Covered by the UMWA Health and Retirement Funds," U.S. National Institute of Occupational Safety and Health Contract No. HSM 99-73-80.

Roepke, W. W., and B. D. Hanson, 1986, "Interactive Computer Program for Analyzing Respirable Dust Generation by Drum-Type Cutting Machines," Proceedings of the Symposium on Engineering Health and Safety in Coal Mining, A. W. Khair, Ed., Society of Mining Engineers of AIME, Littleton, CO.

Roscoe, B. A., and P. K. Hopke, 1980, "Determination of Mineral Matter in Coal by Target Transformation Factor Analysis," Proceedings of the 4th International Conference on Nuclear Methods in Environmental and Energy Research, Columbia, MO.

Rubow, K. L., Marpel, V. A., Olin, J., and M. A. McCawley, 1985, "A Personal Cascade Impactors: Design, Evaluation and Calibration," University of Minnesota Particle Technology Laboratory Publication No. 469.

Rubow, K. L., 1985, Personal communication.

Ruch, R. R., Cahill, R. A., Frost, J. K., Camp, L. R., and H. J. Gluskoter, 1977, "Survey of Trace Elements in Coal and Coal-Related Materials by Neutron Activation Analysis," J. of Radioanalytical Chemistry, Vol. 38, pp. 415-424.

Seibel, R. J., 1976, "Dust Control at a Transfer Point Using Foam and Water Sprays," U.S. Bureau of Mines Coal Mine Health and Safety Research Program TPR 97.

Shapiro, S. S., and M. B. Wilk, 1965, "An Analysis of a Variance Test for Normality (Complete Sample)," Biometrika, Vol. 52, No. 3 and 4, pp. 591-611.

Sharkey, A. G., Jr., Kessler, T., and R.A. Friedel, 1975, "Trace Elements in Coal Dusts by Spark-Source Mass Spectrometry," Ch. 4 in Trace Elements in Fuel, Advances in Chemistry Series No. 141, Babu, S. P., Ed., American Chemistry Society, Chicago, IL.

Shen, A. J., and T. A. Ring, 1984, "Distinguishing Between Two Aerosol Size Distributions," Unpublished paper, Massachusetts Institute of Technology, MA.

Simon, F. O., and C. Huffman, 1977, "Analytical Methods Used by the U.S. Geological Survey for Determining the Chemical Composition of Coal," American Chemical Society, Division of Petroleum Chemistry, Preprint 22, Washington, DC.

Sinclair, A. J., 1976, Application of Probability Paper in Mineral Exploration, Special Volume No. 4, Association of Exploration Geochemists, Amsterdam, Netherlands.

Smoot, L. D., Horton, M. D., and G. Williams, 1977, "Propagation of Laminar, Pulverized Coal-Air Flames," Proceedings of the Sixteenth International Symposium on Combustion, pp. 375-387.

Soo, S. L., 1967, Fluid Dynamics of Multiphase Systems, Blaisdell, Waltham, MA.

Sorenson, J. J., Kober, T. E., and H.G. Petering, 1974, "The Connection of Cd, Cu, Fe, Ni, Pb and Zn in Bituminous Coals from Mines with Differing Incidences of Coalworkers' Pneumoconiosis," American Industrial Hygiene Association J., Vol. 35, No. 2, pp. 93-98.

Spencer, B. B., and B. E. Lewis, 1980, "HP-67/69 and TI-59 Programs to Fit the Normal and Log-Normal Distribution Functions by Linear Regression," Powder Technology, Vol. 27, pp. 219-226.

Sutherland, W. H., 1986, "Federal Program - Coal Mine Quartz Analysis and Evaluation," Proceedings of the Symposium on Engineering Health and Safety in Coal Mining, A. W. Khair, Ed., Society of Mining Engineers of AIME, Littleton, CO.

Swaine, D. J., 1976, "Trace Elements in Coal," Recent Contributions to Geochemistry and Analytical Chemistry, A. E. Tugarinov, Ed., John Wiley and Sons, NY.

Sweet, D. V., Crouse, W. E., Crable, J. V., Carlberg, J. R., and W. S. Lainhart, 1974, "The Relationship of Total Dust, Free Silica, and Trace Metal Concentrations to the Occupational Respiratory Disease of Bituminous Coal Miners," American Industrial Hygiene Association J., Vol. 35, No. 8, pp. 479-485.

Thimons, E. D., and J. L. Kohler, 1985, "Measurement of Air Velocity in Mines," U.S. Bureau of Mines RI 8971.

Timbrell, V., 1965, "The Inhalation of Fibrous Dusts," Annals of New York Academy of Science, No. 132, pp. 255-273.

Tokuhata, G. K., Dessauer, P., Pendergrass, E., Hartman, T., Digon, E., and W. Miller, 1970, "Pneumoconiosis Among Anthracite Coal Miners in Pennsylvania, American J. of Public Health, Vol. 60, No. 3, pp. 441-451.

Tomb, T. F., Emmerling, J. E., and R. H. Kellner, 1972, "Experimental Investigation on the Collection of Airborne Coal Mine Dust by Water Spray in a Horizontal Duct," A paper presented at American Industrial Hygiene Association Conference, San Francisco, CA.

Tuggle, R. M., 1981, "The NIOSH Decision Scheme," American Industrial Hygiene Association J., Vol. 42, No. 7, pp. 493-498.

Twomey, S., 1975, "Comparison of Constrained Linear Inversion and an Iterative Nonlinear Algorithm Applied to the Indirect Estimation of Particle Size Distribution," J. of Comput. Phy., Vol. 18, pp. 188-200.

Volkovic, V., 1983, Trace Elements in Coal, CRC Press, Boca Raton, FL.

Volkwein, J. C., Thimons, E. D., and G. Haflinger, Jr., 1985, "Extended Advance of Continuous Miner Successfully Ventilated with a Scrubber in a Blowing Section," Proceedings of the Second U.S. Ventilation Symposium, P. Mousset-Jones, Ed., A. A. Balkema, Boston, MA, pp. 741-745.

Walton, W. H., and A. Woolcock, 1960, "The Suppression of Airborne Dust with Water Sprays," Aerodynamic Capture of Particles, E. G. Richardson, Ed., Pergamon Press, NY.

Welker, R. W., Eisenberg, W., Semmler, R. A., and G. J. Yucuis, 1982, "Mine Particle Size Characterization," U.S. Bureau of Mines Contract No. J0199086, Fine Particle Research Section, IIT Research Institute.

Wesson, T. C., and F. E. Armstrong, 1975, "Elemental Composition of Coal Mine Dust," U.S. Bureau of Mines RI 7992.

Whitby, K. T., 1974, "Modeling of Multimodal Aerosol Distributions," Proceedings of the 1974 Conference on Aerosols in Nature, Medicine and Technology, Vorderhinderland, FRG.

Whitby, K. T., 1983, "Workplace Aerosol Size Distribution and their Interpretation," Ch. 27 in Aerosols in the Mining and Industrial Work Environments, Marple, V.A., and B. Y. H. Liu, Eds., Ann Arbor Science, MI.

Willeke, K., Whitby, K. T., Clark, W. E., and V. A. Marple, 1974, "Size Distribution of Denver Aerosols-A Comparison of Two Sites," Atmospheric Environment, Vol. 8, pp. 609-633.

Willeke, K., and P. A. Tufto, 1983, "Sampling Efficiency Determination of Aerosol Sampling Inlets," Ch. 25 in Aerosols in the Mining and Industrial Work Environments, Marple, V. A., and Y. H. Liu, Eds., Ann Arbor Science, Ann Arbor, MI.

Willis, H. S., 1930, "Pneumoconiosis and Tuberculosis," Medicine, Vol. 9, No. 12, pp. 413-419.

Wynn, A. H. A., and J. G. Dawes, 1951, "The Size Classification of Airborne Dusts in Mines," Safety in Mines Research Establishment Research Report, No. 28, Ministry of Fuel and Power, London, U.K.

Zubovic, P., Stadnichenko, T., and N. B. Sheffey, 1960, "The Association of Minor Elements with Organic and Inorganic Phases of Coal," Professional Paper 400-B, U.S. Geological Survey.

APPENDIX 1

DISTRIBUTION OF DATA ON PENNSYLVANIA COALS FROM THE PENN STATE COAL DATA BASE

Penn State Sample No.	County	Seam	Rank
80	Schuylkill	Buck Mountain	Anthracite
83	Northumberland	Pa #8	Semi-Anthracite
84	Northumberland	Pa #8	Semi-Anthracite
85	Northumberland	Pa #8	Anthracite
379	Sullivan	P&M 'B'	Semi-Anthracite
383	Sullivan	P&M 'A'	Semi-Anthracite
384	Sullivan	P&M 'B'	Semi-Anthracite
627	Northumberland	PA #2	Semi-Anthracite
867	Schuylkill	Primrose	Anthracite
871	Luzerne	Wharton	Anthracite
873	Luzerne	Patlor	Anthracite
874	Luzerne	Ross	Anthracite
126	Cambria	Lower Kittanning	Low-Volatile
317	Somerset	Lower Freeport	Low-Volatile
318	Somerset	Upper Freeport	Low-Volatile
319	Somerset	Upper Kittanning	Low-Volatile
615	Bedford	Kelly	Low-Volatile
619	Bedford	Barnett	Low-Volatile
620	Bedford	Twin	Low-Volatile
631	Lycoming	n.a.	Low-Volatile
632	Lycoming	n.a.	Low-Volatile
633	Lycoming	#1 Seam-Rider	Low-Volatile
875	Lycoming	Bloss	Low-Volatile
879	Lycoming	One Foot	Low-Volatile
880	Lycoming	Bear Creek	Low-Volatile
1014	Somerset	Lower Kittanning	Low-Volatile
1015	Somerset	Lower Kittanning	Low-Volatile
1016	Somerset	Lower Kittanning	Low-Volatile
1030	Bedford	Kelly	Low-Volatile
1031	Bedford	Kelly	Low-Volatile
1032	Bedford	Twin	Low-Volatile
1033	Bedford	Fulton	Low-Volatile
1201	Somerset	Lower Kittanning	Low-Volatile
253	Clearfield	Brookville	Medium-Volatile
254	Clearfield	Lower Kittanning	Medium-Volatile
255	Clearfield	Lower Kittanning	Medium-Volatile
257	Clearfield	Upper Freeport	Medium-Volatile
258	Clearfield	Upper Kittanning	Medium-Volatile
259	Clearfield	Upper Kittanning	Medium-Volatile
260	Clearfield	Middle Kittanning	Medium-Volatile

(continued)

Penn State Sample No.	County	Seam	Rank
320	Somerset	Pittsburgh	Medium-Volatile
323	Clearfield	Brookville	Medium-Volatile
324	Clearfield	Middle Kittanning	Medium-Volatile
634	Tioga	n.a.	Medium-Volatile
635	Tioga	Bloss	Medium-Volatile
1010	Fayette	Lower Kittanning	Medium-Volatile
1024	Centre	Lower Kittanning	Medium-Volatile
1025	Centre	Lower Kittanning	Medium-Volatile
1026	Clearfield	Lower Kittanning	Medium-Volatile
1027	Clearfield	Mercer	Medium-Volatile
1028	Clearfield	Clarion	Medium-Volatile
1029	Clearfield	Clarion	Medium-Volatile
1137	Clearfield	Lower Kittanning	Medium-Volatile
1138	Clearfield	Upper Kittanning	Medium-Volatile
1139	Clearfield	Lower Kittanning	Medium-Volatile
1144	Clearfield	Lower Kittanning	Medium-Volatile
1192	Clearfield	Lower Kittanning	Medium-Volatile
1194	Cambria	Lower Kittanning	Medium-Volatile
1195	Cambria	Lower Kittanning	Medium-Volatile
1196	Centre	Lower Kittanning	Medium-Volatile
1197	Somerset	Lower Kittanning	Medium-Volatile
1261	Fayette	Lower Kittanning	Medium-Volatile
102	Washington	Pittsburgh	High-Volatile
325	Armstrong	Middle Kittanning	High-Volatile
326	Armstrong	Upper Kittanning	High-Volatile
328	Beaver	Upper Freeport	High-Volatile
329	Lawrence	Brookville	High-Volatile
330	Lawrence	Middle Kittanning	High-Volatile
331	Mercer	Brookville	High-Volatile
332	Lawrence	Lower Kittanning	High-Volatile
341	Jefferson	Clarion	High-Volatile
345	Clarion	Lower Kittanning	High-Volatile
353	Clarion	Upper Clarion	High-Volatile
354	Clarion	Lower Kittanning	High-Volatile
355	Lawrence	Lower Kittanning	High-Volatile
614	Clarion	Lower Clarion	High-Volatile
1011	Jefferson	Lower Kittanning	High-Volatile
1012	Jefferson	Lower Kittanning	High-Volatile
1013	Jefferson	Lower Kittanning	High-Volatile
1017	Armstrong	Lower Kittanning	High-Volatile

(continued)

Penn State Sample No.	County	Seam	Rank
1018	Armstrong	Lower Kittanning	High-Volatile
1019	Armstrong	Lower Kittanning	High-Volatile
1020	Lawrence	Lower Kittanning	High-Volatile
1021	Lawrence	Lower Kittanning	High-Volatile
1022	Lawrence	Lower Kittanning	High-Volatile
1023	Jefferson	Lower Freeport	High-Volatile
1034	Jefferson	Lower Freeport	High-Volatile
1035	Jefferson	Lower Freeport	High-Volatile
1099	Washington	Pittsburgh	High-Volatile
1141	Jefferson	Lower Kittanning	High-Volatile
1142	Jefferson	Lower Kittanning	High-Volatile
1143	Armstrong	Lower Kittanning	High-Volatile
1166	Venango	Lower Kittanning	High-Volatile
1167	Lawrence	Lower Kittanning	High-Volatile
1168	Lawrence	Lower Kittanning	High-Volatile
1169	Clarion	Lower Kittanning	High-Volatile
1170	Clarion	Lower Kittanning	High-Volatile
1171	Butler	Lower Kittanning	High-Volatile
1300	Clearfield	Lower Kittanning	High-Volatile

APPENDIX 2

SELECTION OF THE UPPER AND LOWER LIMIT SIZES FOR THE SIZE DATA FROM CASCADE IMPACTORS

Derivation of the histograms and frequency distributions from the impactor size data requires knowledge of upper and lower limit sizes for the impactor. Since these two methods for size representation are based upon the weight fraction of each interval and the geometric mean of the corresponding interval, selection of the upper size of the first stage and the lower size of the last stage are very important. Furthermore, these two limit sizes affect the overall shape and parameters of the mass size distribution.

A conventional method suggests 50 μm and 0.25 μm (half of the cut size of the eighth stage) for the upper and lower limit sizes of cascade impactors, respectively (Anderson Samplers Inc., 1985). A paper by Burkhart et al. (1983) shows 100 μm and 0.01 μm for the coal mine dust size representation. The selection in this paper was based upon the comparison of the geometric mean estimated from the cumulative plot on lognormal probability paper with that estimated from the corresponding mass size frequency distribution. The coal mine dust sample was prepared and found to have one mode.

The airborne coal mine dust size varies with the sampling location. Near the continuous miner operation, coarse size fractions account for more weight percentages compared to other locations. Therefore, arbitrary selection of the upper and lower limit sizes may overemphasize or underemphasize the coarse and fine size fractions. Table A.2.1 contains the size distributions of samples from the immediate return of the miner operation and four crosscuts outby the face operations. As shown, significant differences in the coarse size fractions can be noticed. These two size distributions were found to possess relatively weak bimodality. Table A.2.2 shows the geometric means and geometric standard deviations of these sample size data. The upper limit size varies from 50 μm to 150 μm, while the lower limit size is in the range of 0.01 μm to 0.25 μm. Estimation of the distribution parameters by cumulative plots and lognormal distributions is based upon the methods used in Chapter 4.

As shown, lognormal frequency distributions based upon the upper limit sizes in the range of 50 to 150 μm do not result in significant differences in the geometric mean and geometric standard deviation. This is also the case for the lower limit sizes in the range of 0.01 to 0.25 μm. The following Table A.2.3 shows the collection efficiency of the backup filters (Millipore PVC with 5-μm pore size) used for cascade impactors. The table indicates relatively high (>98%) collection efficiency even below 0.1 μm. As indicated in Chapter 4, it is intended to give significant meanings only to the mass size modes in the range of the impactor cut size. Therefore, in this thesis 100 μm and 0.1 μm are chosen as hypothetical upper and lower limit sizes for the size data from cascade impactors.

Table A.2.1. Size Distribution of the Coal Mine Dust Samples Samples Used for Selection of the Upper and Lower Limit Sizes.

Stage Number	Cut Size (μm)	Cumulative Percentage (Finer Than %)	
		CR Sample	4X Sample
1	21	66.73	88.73
2	15	50.59	67.70
3	10	30.24	53.55
4	6	14.90	35.47
5	3.5	6.69	17.35
6	2	1.49	4.39
7	0.9	0.84	1.79
8	0.5	0.64	0.82

Note: CR and 4X denote the immediate return of the miner operation and four crosscuts outby the face operations, respectively.

Table A.2.2. Variation in the Geometric Mean and Geometric Standard Deviation with Different Upper and Lower Sizes.

	From Cumulative Plots	Upper Limit Sizes (μm) 150	100	75	50
Sample ID: CR					
X_g (μm)	16.10	16.60	15.85	15.14	14.13
S_g^g	2.22	2.29	2.25	2.24	2.24
Sample ID: 4X					
X_g (μm)	9.24	9.14	8.91	8.71	8.32
S_g^g	3.00	2.95	2.88	2.88	2.82
	From Cumulative Plots	Lower Limit Sizes (μm) 0.25	0.13	0.06	0.01
Sample ID: CR					
X_g (μm)	16.10	15.85	15.85	15.85	15.85
S_g^g	2.22	2.25	2.25	2.25	2.25
Sample ID: 4X					
X_g (μm)		8.91	8.91	8.91	8.91
S_g^g		2.88	2.88	2.88	2.88

Notes: (1) 100 μm and 0.01 μm were used for the base in the sensitivity analysis in this table.
(2) X_g and S_g denote the geometric mean and geometric standard deviation.

Table A.2.3. Collection Efficiency of the Backup Filters.

Pressure Drop (cm Hg)	1	3
Particle Size (μm)	Collection Efficiency (%)	
0.035	97.80	97.00
0.100	98.50	98.60
0.300	99.70	99.89
1.000	99.91	99.89

Note: (1) The data is from Liu et al. (1983).
(2) Total pressure drop in the Sierra Model 298 cascade impactor is 1.8 cm Hg.

APPENDIX 3

DATA FOR THE STUDY ON ISOKINETIC SAMPLING WITH CASCADE IMPACTORS

Table A.3.1. Samples from Section H (Mine Code 101-7-1).

Sampling Location: 4 feet outby the inby end of tubing
Air Velocity: 97 feet per minute
Dust Concentration: 33.34 mg/m³

Sampler Stage	Averaged Sample Weight (mg) Isokinetic (1)	Nonisokinetic (2)	Ratio (1)/(2)
1	0.699	0.319	2.19
2	0.277	0.567	0.49
3	0.628	0.751	0.84
4	0.946	1.052	0.90
5	0.581	0.585	0.99
6	0.599	0.424	1.41
7	0.290	0.231	1.26
8	0.076	0.082	0.93
Backup	0.057	0.056	1.02
Total Dust Wt.	4.153	4.067	1.02
Dust Wt.< 6 µm	1.603	1.378	1.16

Table A.3.2. Samples from Section K (Mine Code 104-7-1).

Sampling Location: 4 feet outby the inby end of tubing
Air Velocity: 103 feet per minute
Dust Concentration: 8.75 mg/m³

Sampler Stage	Averaged Sample Weight (mg) Isokinetic (1)	Nonisokinetic (2)	Ratio (1)/(2)
1	0.294	0.193	1.52
2	0.095	0.144	0.66
3	0.101	0.179	0.56
4	0.185	0.191	0.97
5	0.176	0.203	0.87
6	0.246	0.220	1.12
7	0.070	0.072	0.97
8	0.028	0.030	0.93
Backup	0.028	0.028	1.00
Total Dust Wt.	1.223	1.260	0.97
Dust Wt.< 6 µm	0.548	0.553	0.99

Table A.3.3. Samples from Section O (Mine Code 111-2G-1).

Sampling Location: immediate return of the miner operation
Air Velocity: 230 feet per minute
Dust Concentration: 35.76 mg/m³

Sampler Stage	Averaged Sample Weight (mg) Isokinetic (1)	Nonisokinetic (2)	Ratio (1)/(2)
1	0.651	0.830	0.78
2	0.385	0.574	0.67
3	0.503	0.803	0.63
4	0.912	0.975	0.94
5	0.588	0.872	0.67
6	0.353	0.470	0.75
7	0.259	0.222	1.17
8	0.098	0.094	1.04
Backup	0.014	0.023	0.61
Total Dust Wt.	3.763	4.863	0.77
Dust Wt.< 6 µm	1.312	1.681	0.78

Table A.3.4. Samples from Section O (Mine Code 111-2G-1).

Sampling Location: two crosscuts outby the face operation
Air Velocity: 192 feet per minute
Dust Concentration: 3.87 mg/m³

Sampler Stage	Averaged Sample Weight (mg) Isokinetic (1)	Nonisokinetic (2)	Ratio (1)/(2)
1	0.038	0.089	0.43
2	0.038	0.152	0.25
3	0.149	0.302	0.49
4	0.317	0.392	0.81
5	0.301	0.397	0.76
6	0.330	0.314	1.05
7	0.116	0.089	1.30
8	0.041	0.020	2.05
Backup	0.015	0.073	0.21
Total Dust Wt.	1.345	1.827	0.74
Dust Wt.< 6 µm	0.803	0.893	0.90

Table A.3.5. Samples from Section P (Mine Code 112-2G-1).

Sampling Location: immediate return of the miner operation
Air Velocity: 205 feet per minute
Dust Concentration: 32.14 mg/m³

Sampler Stage	Averaged Sample Weight (mg) Isokinetic (1)	Nonisokinetic (2)	Ratio (1)/(2)
1	1.774	1.388	1.28
2	0.333	0.697	0.48
3	0.537	0.804	0.67
4	0.793	0.880	0.90
5	0.582	0.484	1.20
6	0.380	0.419	0.91
7	0.197	0.140	1.41
8	0.079	0.044	1.80
Backup	0.023	0.029	0.79
Total Dust Wt.	4.698	4.885	0.96
Dust Wt.< 6 µm	1.261	1.116	1.30

Table A.3.6. Samples from Section P (Mine Code 112-2G-1).

Sampling Location: two crosscuts outby the face operation
Air Velocity: 195 feet per minute
Dust Concentration: 6.05 mg/m³

Sampler Stage	Averaged Sample Weight (mg) Isokinetic (1)	Nonisokinetic (2)	Ratio (1)/(2)
1	0.094	0.085	1.11
2	0.070	0.150	0.47
3	0.253	0.329	0.77
4	0.490	0.500	0.98
5	0.339	0.430	0.79
6	0.396	0.268	1.48
7	0.272	0.096	2.83
8	0.032	0.029	1.10
Backup	0.029	0.017	1.71
Total Dust Wt.	1.975	1.924	1.03
Dust Wt.< 6 µm	1.068	0.840	1.27

Table A.3.7. Samples from Section L (Mine Code 111-EG-1).

Sampling Location: four crosscuts outby the face operation
Air Velocity: 210 feet per minute
Dust Concentration: 7.10 mg/m³

Sampler Stage	Averaged Sample Weight (mg) Isokinetic (1)	Nonisokinetic (2)	Ratio (1)/(2)
1	0.098	0.177	0.55
2	0.080	0.326	0.25
3	0.302	0.567	0.53
4	0.505	0.828	0.61
5	0.521	0.559	0.93
6	0.551	0.433	1.27
7	0.173	0.175	0.99
8	0.061	0.074	0.82
Backup	0.011	0.055	0.20
Total Dust Wt.	2.302	3.194	0.72
Dust Wt.< 6 µm	1.317	1.296	1.02

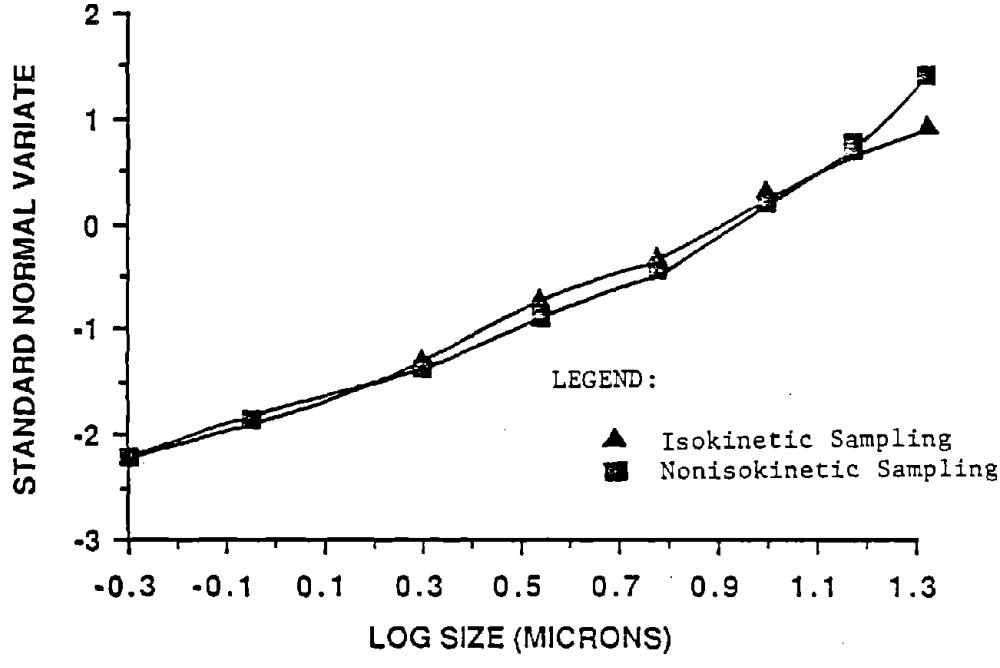

1. Lognormal Plot of the Data in Table A.3.1.

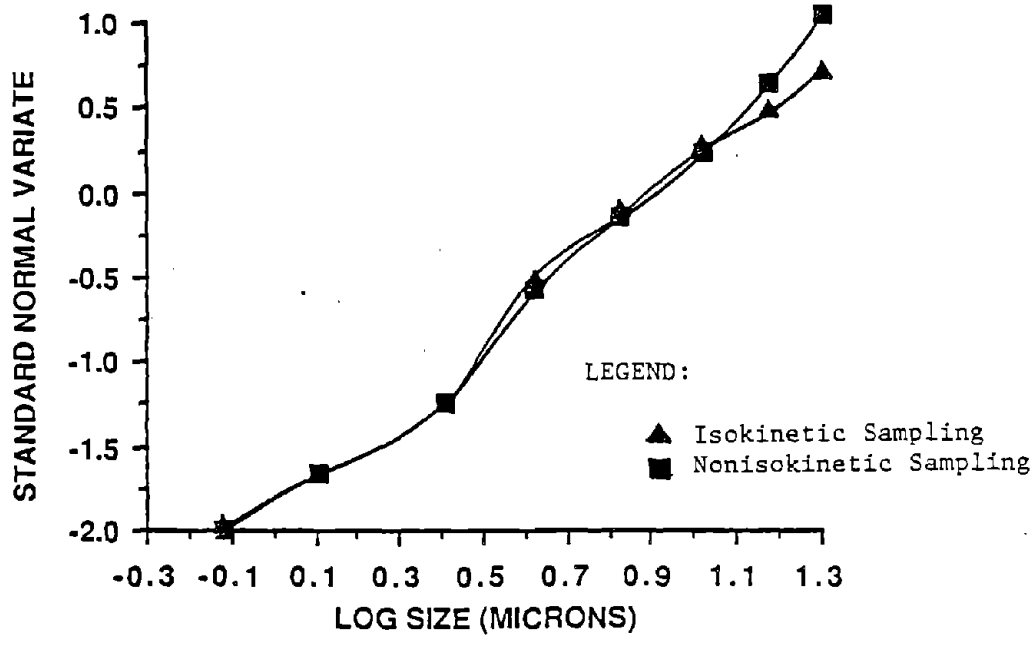

2. Lognormal Plot of the Data in Table A.3.2.

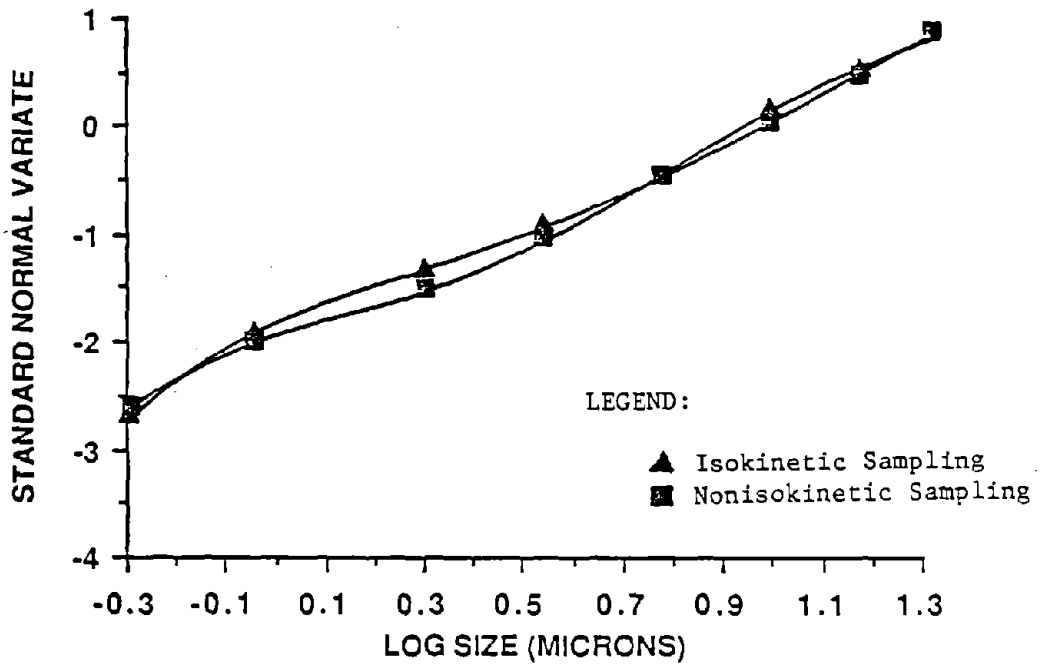

3. Lognormal Plot of the Data in Table A.3.3.

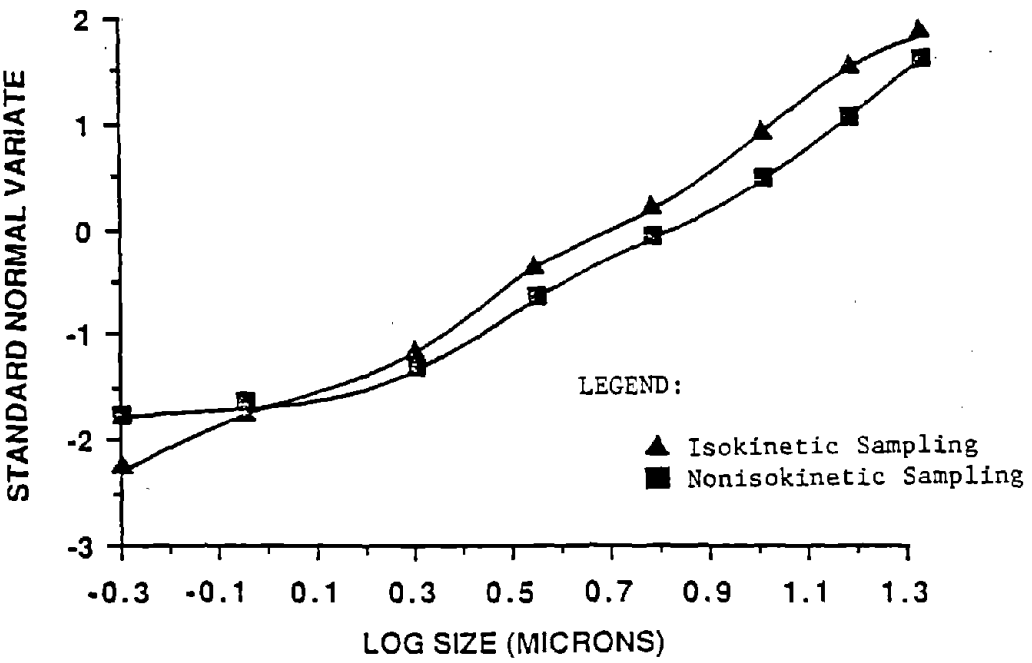

4. Lognormal Plot of the Data in Table A.3.4.

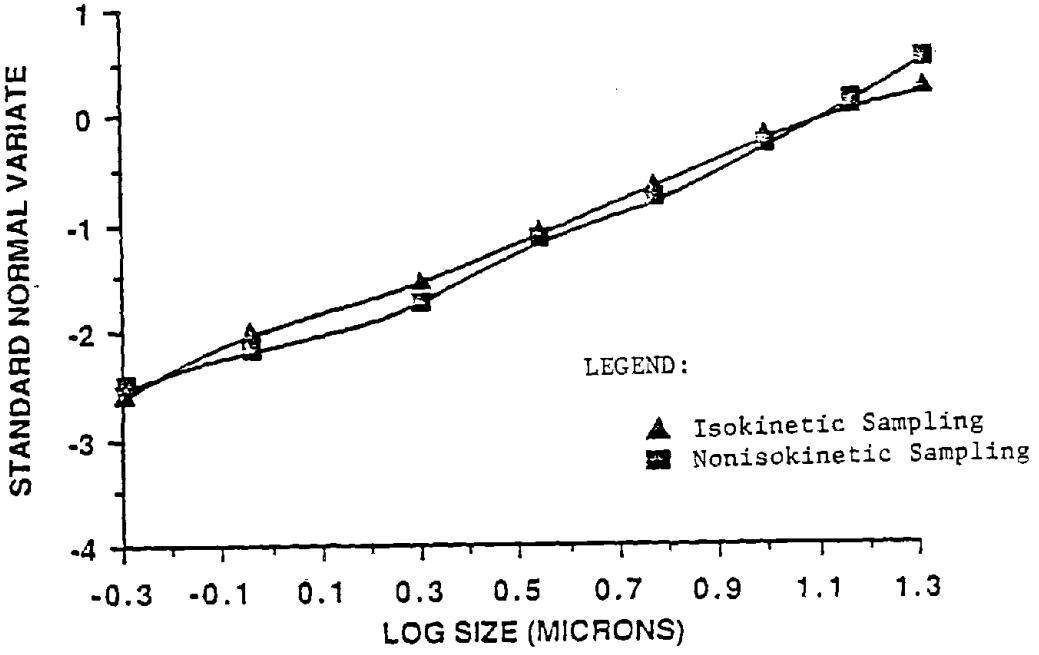

5. Lognormal Plot of the Data in Table A.3.5.

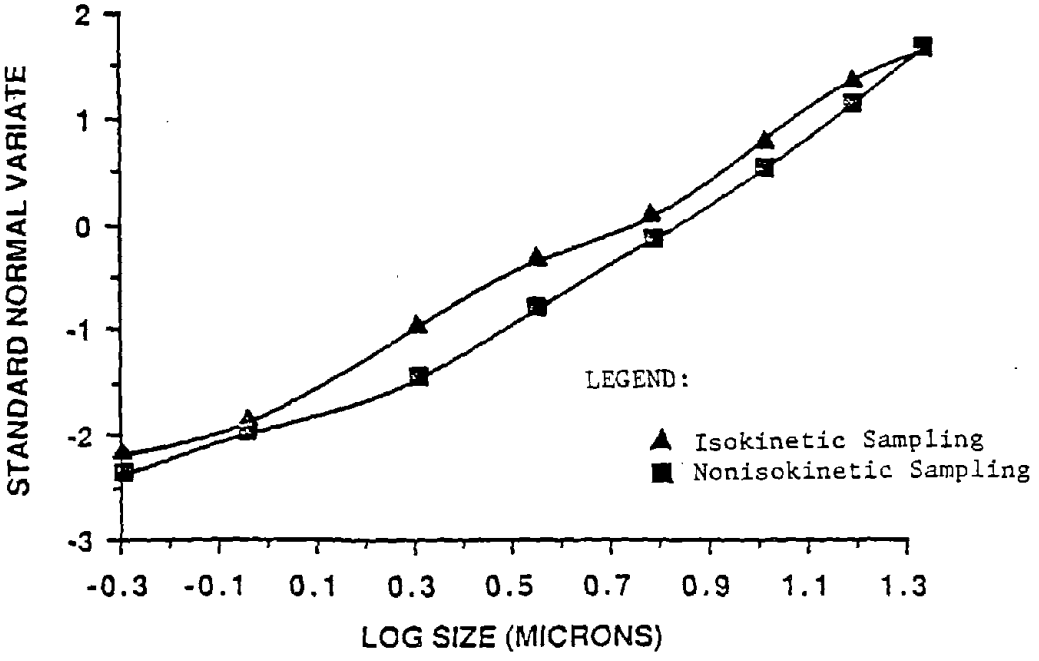

6. Lognormal Plot of the Data in Table A.3.6.

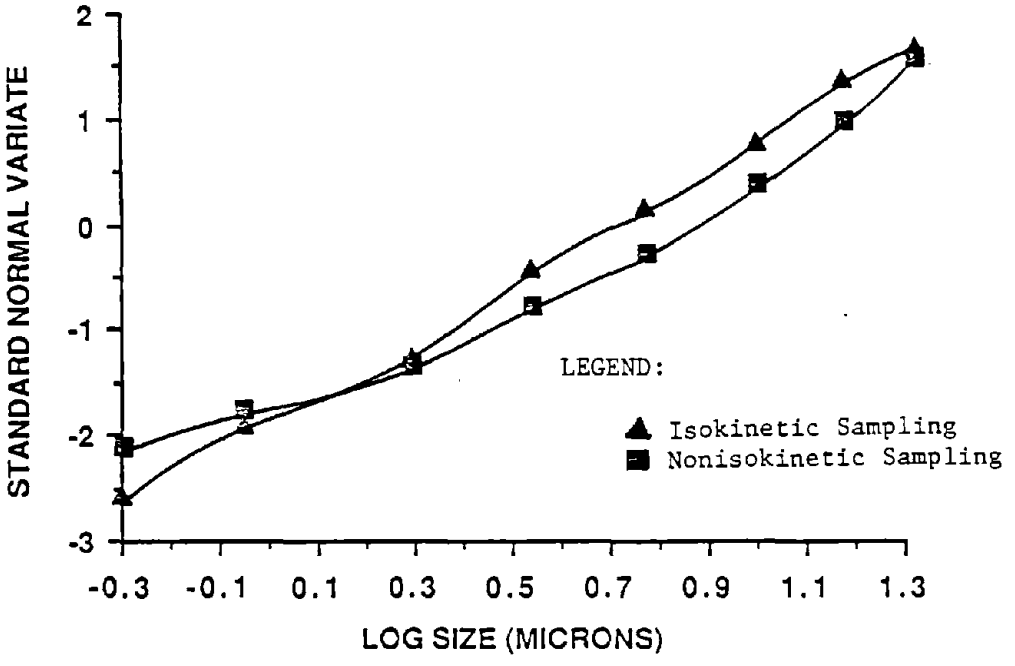

7. Lognormal Plot of the Data in Table A.3.7.

APPENDIX 4

DESCRIPTION OF THE SECTIONS

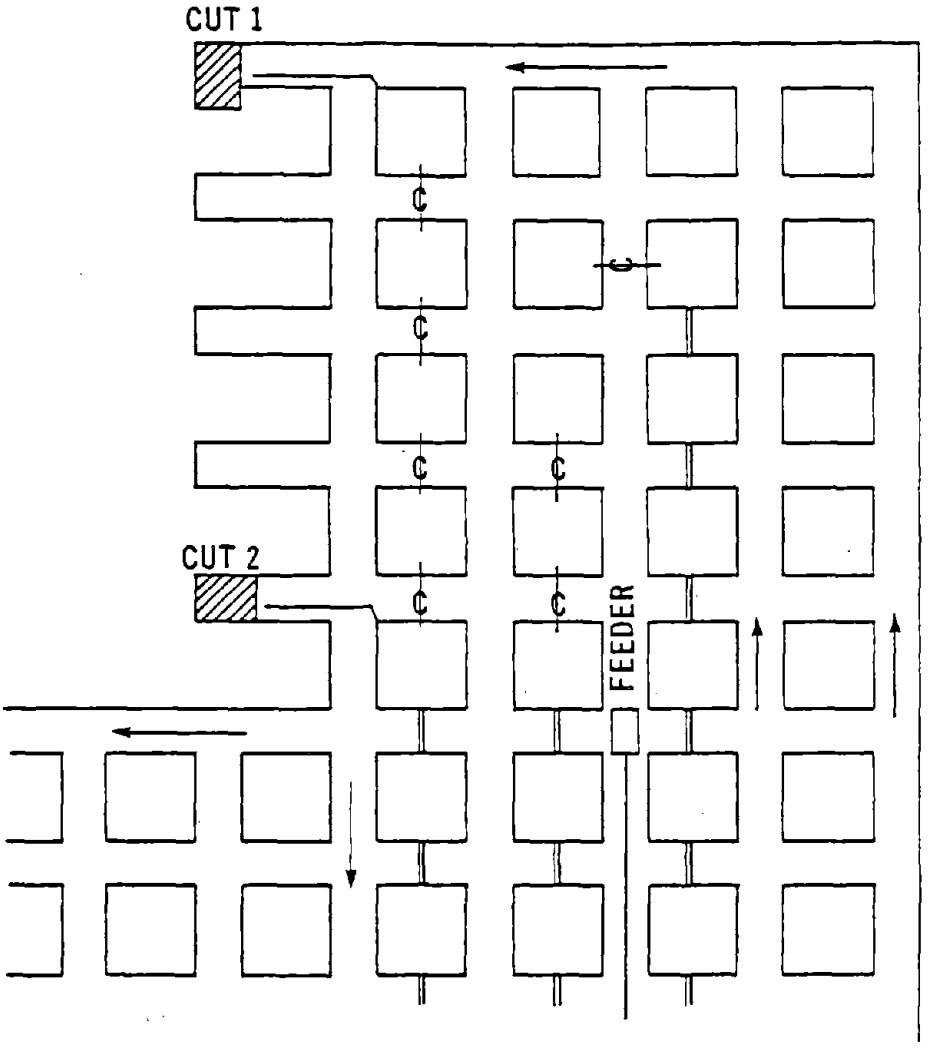

1. Section A (Mine Code 141-1-1).

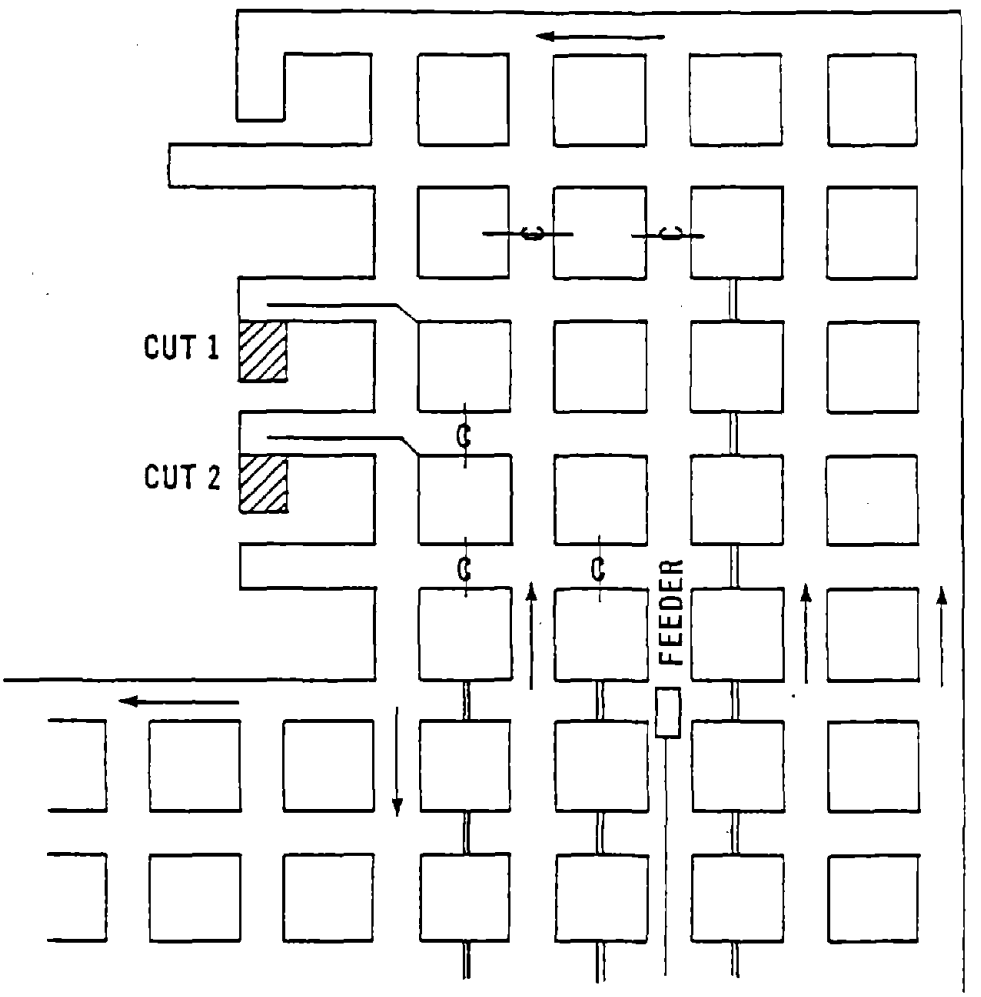

2. Section B (Mine Code 142-1-1).

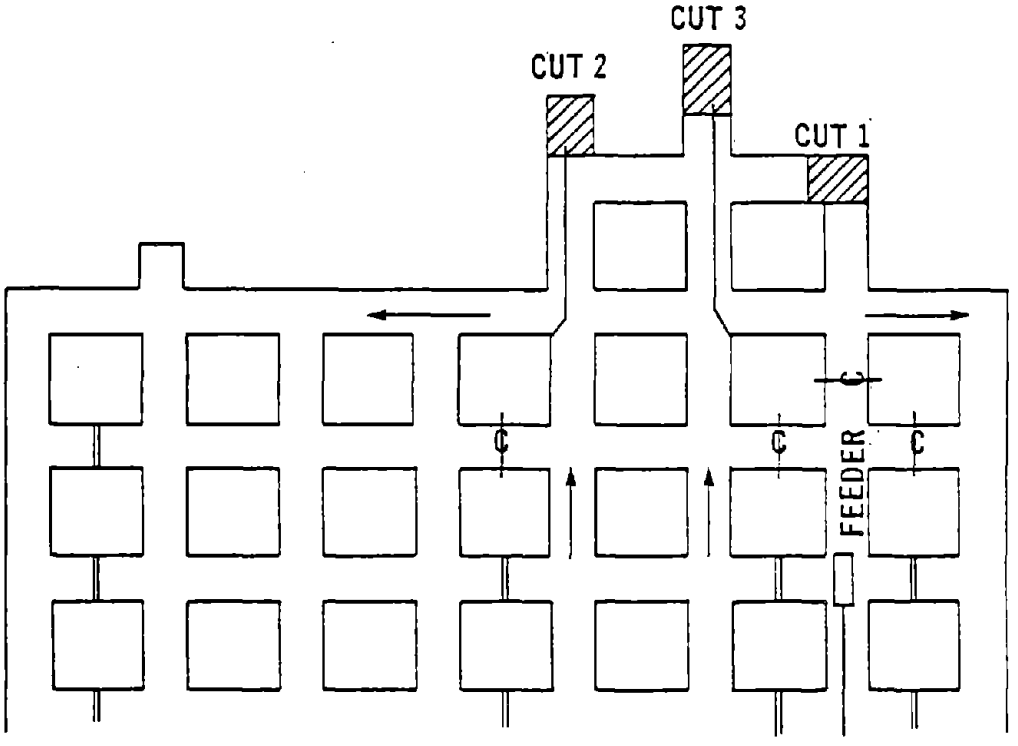

3. Section C (Mine Code 03-3-1).

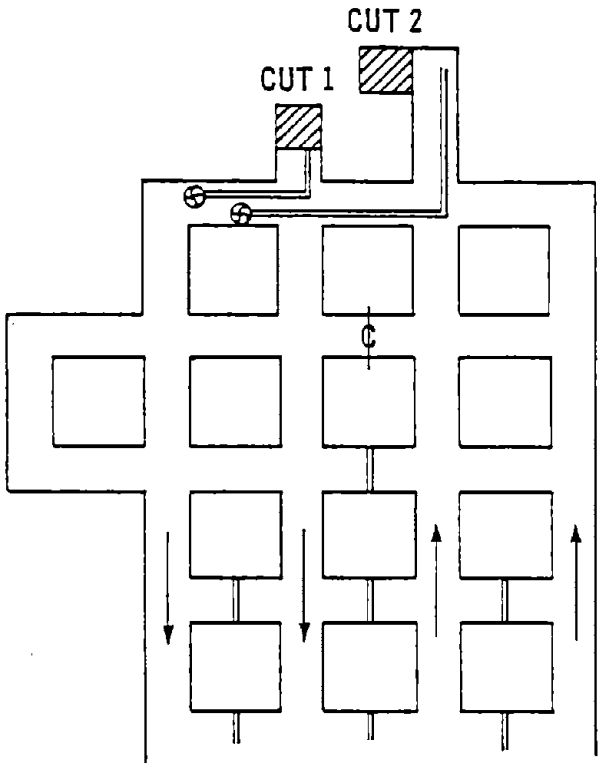

4. Section D (Mine Code 30-7-1).

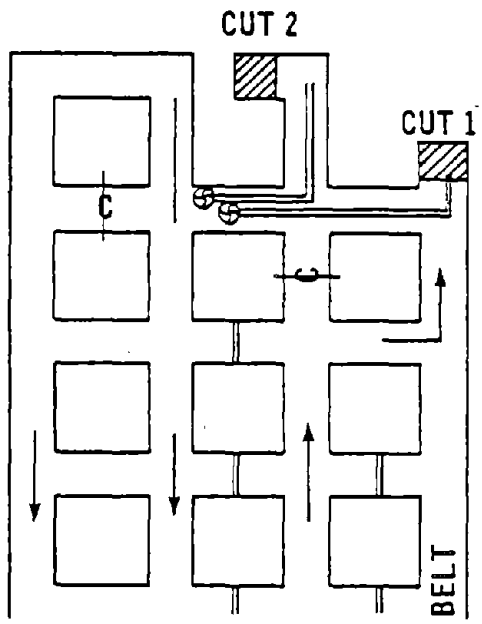

5. Section E (Mine Code 200-2-1).

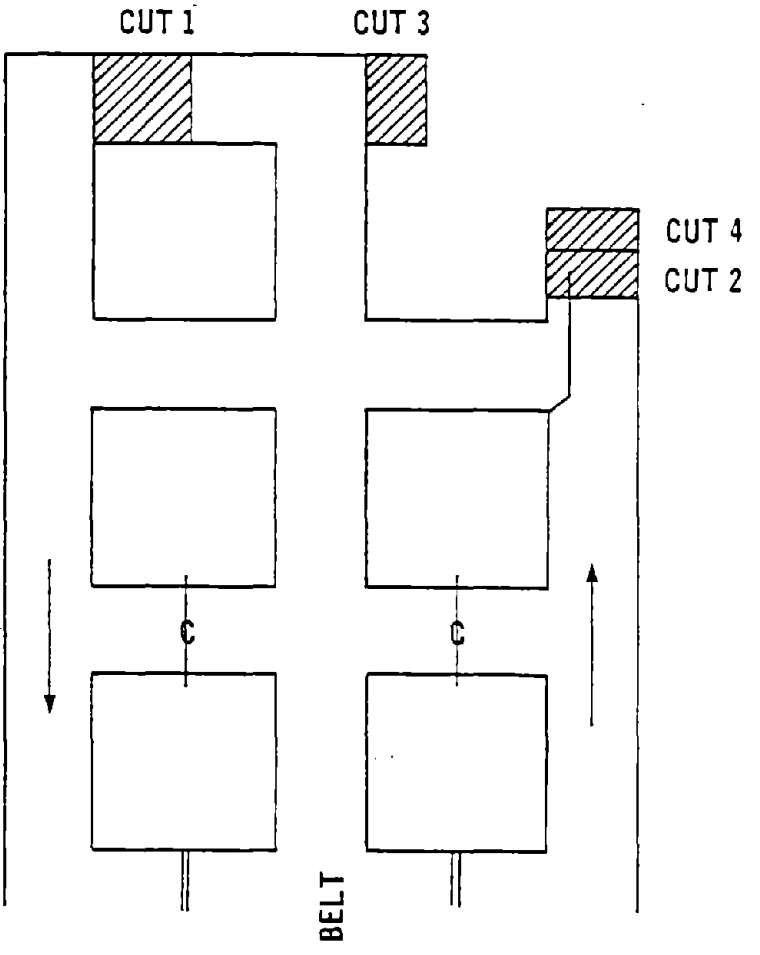

6. Section F (Mine Code 11-2-1).

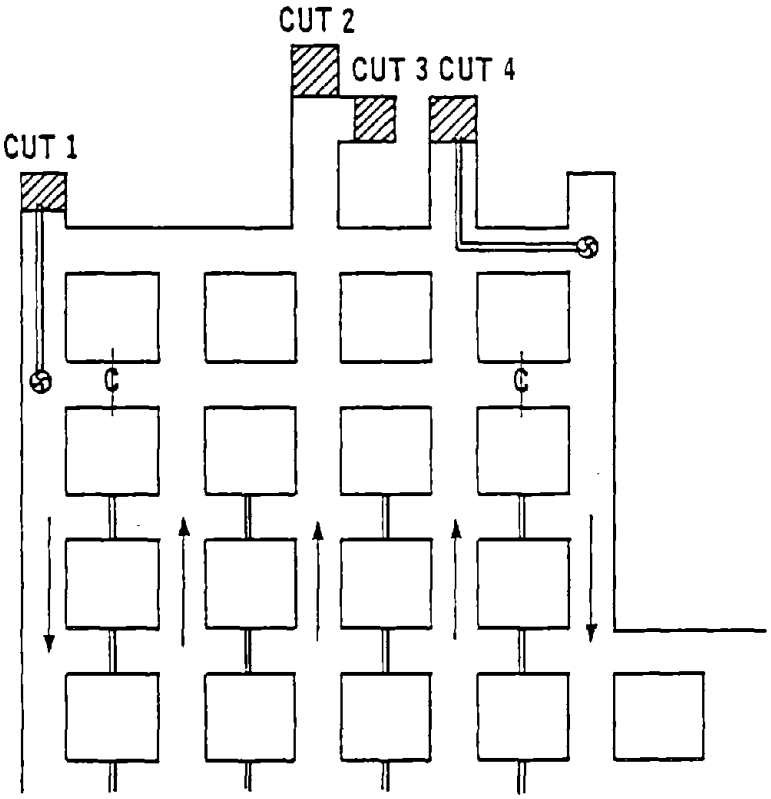

7. Section G (Mine Code 63-7-1).

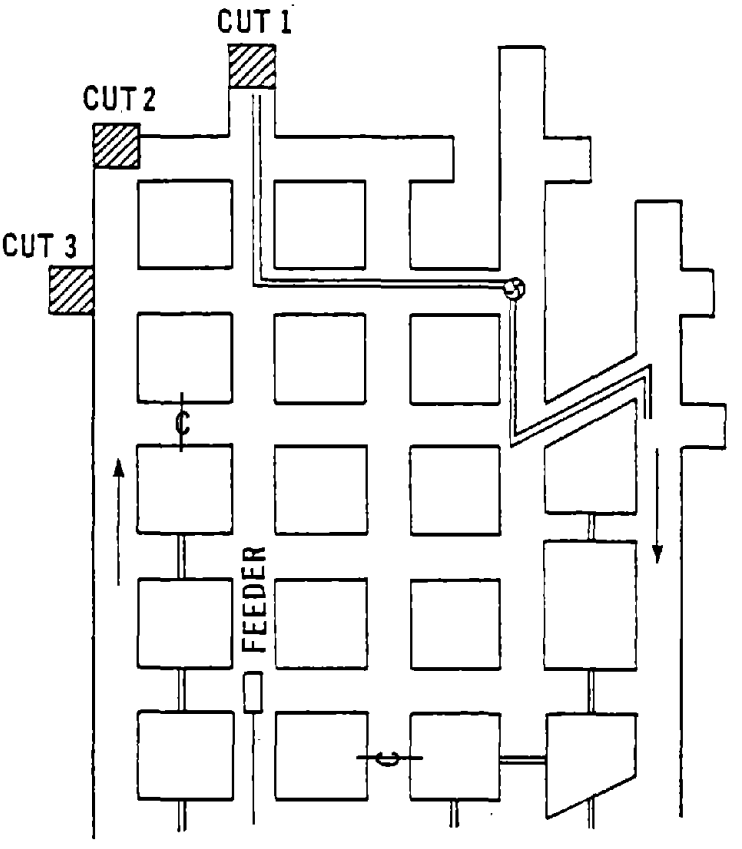

8. Section H (Mine Code 101-7-1).

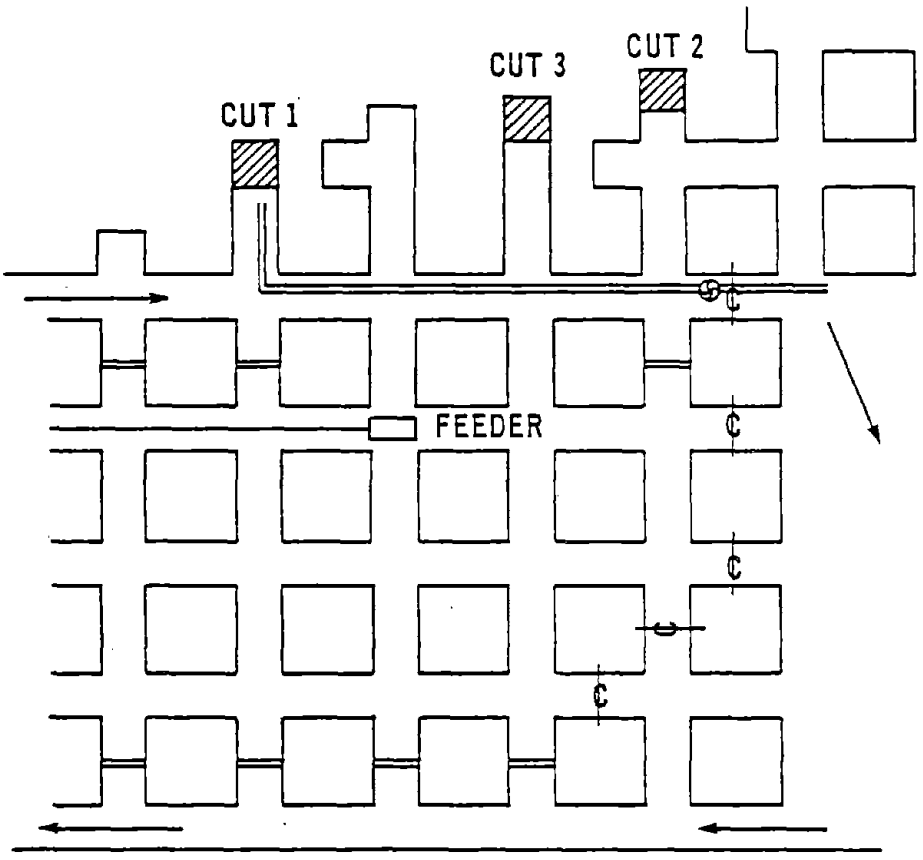

9. Section I (Mine Code 102-7-1).

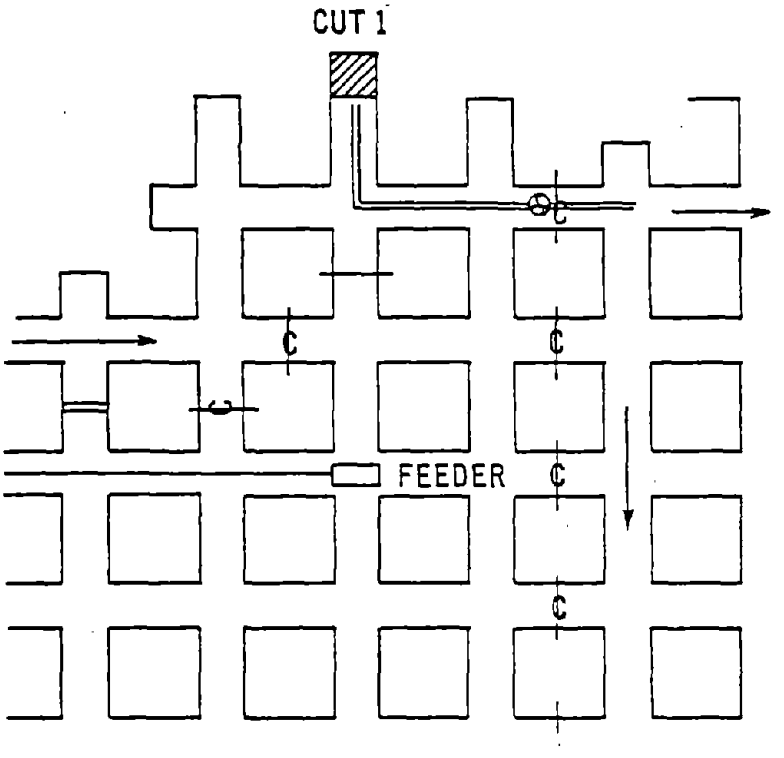

10. Section J (Mine Code 103-7-1).

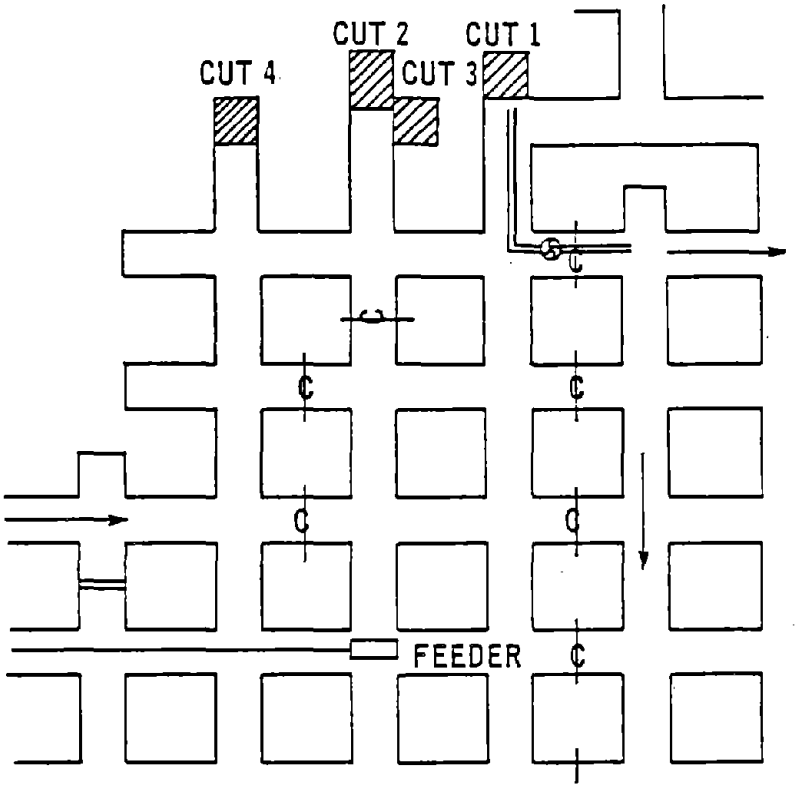

11. Section K (Mine Code 104-7-1).

Mine and Section Code: 141-1-1 and 142-1-1
Location (State): Pennsylvania Coal Seam: Brookville (A)
Entry Dimensions: 5 ft x 20 ft
Face Ventilation: Single split with line brattices for miner and roof bolter,
Ventilation Measurements: 113 ft/min at the last open crosscut; 356 ft/min in the immediate return of the miner (behind the brattice). temperature (°F): 59 dry, 58.5 wet
Mine and Section Code: 03-3-1
Location (State): Pennsylvania Coal Seam: Upper Freeport "E" Seam
Entry Dimensions: 4 ft x 18.5 ft
Face Ventilation: Fish-tail system with line brattices for the miner and roof bolter; no. 2 and no. 3 venturi spray on continuous miner.
Ventilation Measurements: 313 ft/min at one crosscut outby the face; 205 ft/min at two crosscuts outby the face.

(continued)

Mine and Section Code: 30-7-1
Location (State): Pennsylvania Coal Seam: Pittsburgh
Entry Dimensions: 5.5 ft x 15 ft
Face Ventilation: Single split with the tubings and auxiliary fans for the miner and roof bolter
Mine and Section Code: 200-2-1
Location (State): West Virginia Coal Seam: Lower Kittanning
Entry Dimensions: 4.8 ft x 17 ft
Face Ventilation: Single split with 16-in tubings and 25-hp auxiliary fans for the miner and roof bolter.
Ventilation Measurements: 80 ft/min in the last open crosscut; temperature (°F): 59 dry, 58 wet
Mine and Section Code: 11-2-1
Location (State): Pennsylvania Coal Seam: Lower Kittanning "B" Seam
Entry Dimensions: 5.5 ft x 18 ft
Face Ventilation: Single split with line brattice for the miner
Ventilation Measurements: 13,400 cfm at the last open crosscut; temperature (°F): 64 dry, 62 wet

(continued)

Mine and Section Code: 63-7-1
Location (State): Pennsylvania Coal Seam: Pittsburgh
Entry Dimensions: 8 ft x 16 ft
Face Ventilation: Fish-tail ventilation with 18-in tubings for the miner; 50-hp auxillary fan.
Ventilation Measurements: 142 ft/min in the intake airway; 54,500 cfm at the last open crosscut. temperature (°F): 63 dry, 62 wet
Mine and Section Guide Code: 101-7-1, 102-7-1, 103-7-1 and 104-7-1
Location (State): Ohio Coal Seam: Pittsburgh
Entry Dimensions: 16 ft x 7 ft at 101-7-1; 19 ft x 6 ft at 102-7-1, 103-7-1 and 104-7-1
Face Ventilation: single-split ventilation with tubings with a 50-hp auxiliary fan for the miner operation.
Ventilation Measurements: (1) at 101-7-1: 151 fpm at the intake airway and 9300 cfm inside the tubings; (2) at 102-7-1: 103 fpm at the intake airway and 8850 cfm inside the tubings; (3) at 103-7-1: 112 fpm at the intake airway; (4) at 104-7-1: 114 fpm at the intake airway and 10400 cfm inside the tubings.

APPENDIX 5

MINE DUST SIZE DATA FROM CASCADE IMPACTORS

Stage Number	Cut Size (μm)	Cumulative Percentage (Finer Than %)				
		Sampling Locations at Section A (Mine Code 141-1-1)				
		CI	RI	RR	2X	4X
1	21	71.08	90.08	80.19	87.20	85.97
2	15	52.53	81.19	66.28	71.84	77.45
3	10	38.88	66.20	49.02	50.73	63.47
4	6	26.86	46.03	30.71	29.82	43.08
5	3.5	16.03	28.62	19.36	15.37	21.23
6	2.0	5.64	11.67	8.11	2.04	5.46
7	0.9	4.01	3.77	2.91	1.48	2.26
8	0.5	2.67	1.03	1.14	0.56	1.04
Total Dust Level (mg/m^3)		1.48	9.09	16.67	4.37	4.76
Sampling Time (minutes)		227	222	229	225	223

		Sampling Locations at Section B (Mine Code 142-1-1)				
		CI	CR	RI	RR	2X
1	21	67.01	78.29	90.38	83.47	84.41
2	15	53.01	55.63	82.36	68.24	68.60
3	10	39.42	37.41	67.10	51.70	49.39
4	6	21.86	18.94	48.18	27.87	28.60
5	3.5	10.69	9.63	28.68	16.90	16.12
6	2.0	1.87	1.25	6.13	1.97	1.48
7	0.9	1.22	0.40	0.98	0.82	0.30
8	0.5	0.49	0.04	0.39	0.47	0.17
Total Dust Level (mg/m^3)		2.12	21.99	2.54	5.61	4.99
Sampling Time (minutes)		291	64	302	302	298

(continued)

Stage Number	Cut Size (μm)	Cumulative Percentage (Finer Than %)						
		Sampling Locations at Section C (Mine Code 03-3-1)						
		IN	CI/RI	CR	2XCR	4XCR	RR	2XRR
1	21	93.58	85.04	75.65	79.39	61.09	84.94	76.81
2	15	92.78	73.60	61.78	64.73	50.00	70.83	70.44
3	10	88.36	53.75	39.41	43.96	35.78	52.21	53.16
4	6	63.86	26.76	20.16	19.69	21.98	28.95	32.89
5	3.5	43.78	13.26	9.15	11.01	8.56	10.21	16.56
6	2.0	12.45	3.95	2.13	1.50	2.02	2.05	2.27
7	0.9	4.02	2.69	1.26	0.60	1.22	1.23	1.16
8	0.5	2.41	2.03	0.91	0.32	1.01	0.94	0.61
Total Dust Level (mg/m^3)		0.36	5.31	8.36	9.84	6.28	8.29	3.24
Sampling Time (minutes)		342	283	138	219	229	147	279

Stage Number	Cut Size (μm)	Sampling Locations at Section D (Mine Code 30-7-1)	
		CR1	CR2
1	21	77.12	87.08
2	15	56.00	74.87
3	10	34.72	57.22
4	6	16.46	35.16
5	3.5	5.96	18.68
6	2.0	1.35	4.17
7	0.9	0.62	1.15
8	0.5	0.03	0.02
Total Dust Level (mg/m^3)		11.79	4.87
Sampling Time (minutes)		68	45

(continued)

Stage Number	Cut Size (μm)	Cumulative Percentage (Finer Than %)			
		Sampling Locations at Section E (Mine Code 200-2-1)			
		CR1	CR2	RI	RR
1	21	76.58	82.53	86.95	74.54
2	15	58.07	64.88	83.74	62.01
3	10	39.23	45.91	80.53	54.62
4	6	21.91	26.15	59.55	44.99
5	3.5	10.42	13.16	31.19	20.58
6	2.0	2.67	2.54	5.48	2.90
7	0.9	0.47	0.52	2.46	0.14
8	0.5	0.27	0.19	0.95	0.13
Total Dust Level (mg/m^3)		20.77	14.73	0.90	1.31
Sampling Time (minutes)		154	195	294	290

Stage Number	Cut Size (μm)	Sampling Locations at Section F (Mine Code 11-2-1)					
		CI/RI	CR	RI	RR	2X	4X
1	21	81.63	82.92	88.29	88.83	94.16	95.40
2	15	60.34	64.84	74.37	77.49	84.43	88.53
3	10	38.77	41.91	54.45	58.44	63.36	69.78
4	6	21.29	20.30	31.39	33.93	33.90	45.64
5	3.5	12.35	11.27	15.01	17.03	16.85	19.29
6	2.0	5.46	12.84	4.84	7.78	5.37	6.75
7	0.9	2.15	0.49	1.01	3.77	1.82	2.02
8	0.5	1.32	0.04	0.72	3.05	0.45	0.33
Total Dust Level (mg/m^3)		3.26	43.92	8.76	9.90	10.67	8.24
Sampling Time (minutes)		281	56	271	268	239	258

(continued)

Stage Number	Cut Size (μm)	Cumulative Percentage (Finer Than %)						
		Sampling Locations at Section G (Mine Code 63-7-1)						
		ININ	INOUT	CI	CR1	CR2	RI	RR
1	21	95.39	98.34	82.84	69.38	72.33	86.96	84.51
2	15	82.03	95.69	66.17	47.24	48.25	69.76	65.48
3	10	60.60	86.09	51.52	26.46	29.29	51.61	45.92
4	6	43.09	74.17	38.64	12.43	15.41	34.41	22.56
5	3.5	28.57	49.00	25.76	6.86	5.40	21.03	12.74
6	2.0	11.57	24.50	17.17	2.58	2.86	7.97	9.82
7	0.9	4.61	17.22	9.59	0.74	1.11	2.87	4.69
8	0.5	0.23	7.95	0.25	0.11	0.51	0.01	0.09
Total Dust Level (mg/m³)		0.75	0.52	0.78	34.44	8.09	0.62	8.56
Sampling Time (minutes)		290	291	255	80	134	255	66

Stage Number	Cut Size (μm)	Sampling Locations at Section H (Mine Code 101-7-1)			
		CI	CR	2X	4X
1	21	90.00	83.01	88.81	84.73
2	15	80.64	77.97	73.74	70.70
3	10	67.09	64.74	56.87	50.74
4	6	48.82	37.26	38.85	31.14
5	3.5	34.73	22.10	22.24	18.17
6	2.0	8.09	9.72	5.29	6.71
7	0.9	3.82	3.71	2.09	2.54
8	0.5	2.09	1.56	1.07	1.38
Total Dust Level (mg/m³)		3.24	28.93	6.01	12.85
Sampling Time (minutes)		170	61	195	195

(continued)

Stage Number	Cut Size (μm)	Cumulative Percentage (Finer Than %)				
		Sampling Locations at Section I (Mine Code 102-7-1)				
		CI	CR1	CR2	2X	4X
1	21	83.32	65.82	78.50	92.16	92.16
2	15	70.45	42.66	67.89	80.97	81.45
3	10	50.38	20.86	51.83	61.59	63.34
4	6	27.04	12.48	35.16	41.78	45.84
5	3.5	14.72	7.56	23.95	22.33	23.24
6	2.0	4.14	2.69	8.19	6.89	0.87
7	0.9	3.05	1.45	5.46	2.44	3.28
8	0.5	2.40	0.70	3.94	0.80	0.96
Total Dust Level (mg/m^3)		2.62	31.75	6.60	28.88	19.45
Sampling Time (minutes)		175	65	25	227	225

		Sampling Locations at Section J (Mine Code 103-7-1)		
		CI	2X	4X
1	21	87.67	85.06	95.40
2	15	78.99	70.12	75.86
3	10	71.38	51.28	55.17
4	6	54.18	30.77	32.50
5	3.5	23.59	15.51	18.23
6	2.0	5.48	2.23	4.34
7	0.9	4.41	1.83	3.58
8	0.5	1.52	1.43	3.05
Total Dust Level (mg/m^3)		4.21	8.39	8.73
Sampling Time (minutes)		78	75	76

(continued)

Stage Number	Cut Size (μm)	Cumulative Percentage (Finer Than %)			
		Sampling Locations at Section K (Mine Code 104-7-1)			
		CI	CR	2X	4X
1	21	82.21	84.68	95.99	95.03
2	15	67.26	73.25	90.88	85.25
3	10	50.07	59.04	80.65	71.76
4	6	30.79	43.88	57.78	50.07
5	3.5	17.64	27.77	29.10	33.13
6	2.0	8.67	10.33	11.94	16.01
7	0.9	4.93	4.60	4.36	5.59
8	0.5	3.44	2.22	1.26	1.35
Total Dust Level (mg/m^3)		1.68	8.75	13.61	13.74
Sampling Time (minutes)		199	72	250	250

APPENDIX 6

RESULTS OF THE STATISTICAL TESTS

FOR COAL MINE DUST SIZE MODELING

Notes for Tables A.6.1 through A.6.11:

(1) "Curvi." denotes a curvilinear pattern of the residuals.
(2) "Linear" denotes a linear pattern of the residuals.
(3) gf1 and gf2 are the measures of the goodness of fit by Chi-square and modified Chi-square, respectively.
(4) GM1, GM2 and GM3 denote the first, second and third model values in microns, respectively, while GS1 and GS2 are the geometric standard deviations of the first and second modes, respectively. In the lognormal distribution, GM denotes the geometric mean.
(5) %1 denotes the mass percentage of the first mode.

Table A.6.1. Size Modeling of Coal Mine Dust from Section A (Mine Code 141-1-1).

Sampling Location	Residual Analysis	Analysis Results: Empirical Distribution: Chebychev Function	Analysis Results: Empirical Distribution: Spline Function	Analysis Results: Lognormal Distribution: Unimodal	Analysis Results: Lognormal Distribution: Bimodal
CI	Curvi.	GM1=17.78	GM1= 2.82 GM2=17.98	GM1=16.00 GS1= 2.60 gf1=13.87 gf2= 0.15	GM1= 4.23 GS1= 1.83 %1= 0.31 GM2= 21.00 GS2= 1.65 gf1=267.26 gf2= 0.05
RI	Curvi.	GM1= 5.96	GM1= 2.72 GM2= 8.22	GM1= 6.90 GS1= 1.37 gf1= 0.03 gf2= 0.02	GM1= 2.10 GS1= 1.37 %1= 0.13 GM2= 8.18 GS2= 2.42 gf1= 0.45 gf2= 0.04
RR	Curvi.	GM1=11.48	GM1= 2.47 GM2=14.25	GM1=11.56 GS1= 2.66 gf1= 0.45 gf2= 0.06	GM1= 2.27 GS1= 1.48 %1= 0.15 GM2= 13.02 GS2= 2.19 gf1= 97.69 gf2= 0.04
2X	Curvi.	GM1=10.23	GM1= 2.98 GM2=12.30	GM1=10.75 GS1= 2.29 gf1= 1.48 gf2= 0.08	GM1= 3.15 GS1= 1.32 %1= 0.18 GM2= 12.27 GS2= 1.86 gf1= 16418 gf2= 0.03
4X	Linear	GM1= 5.62	GM1= 6.31	GM1= 6.79 GS1= 2.57 gf1= 0.08 gf2= 0.04	GM1= 3.51 GS1= 1.57 %1= 0.18 GM2= 8.82 GS2= 2.49 gf1= 0.34 gf2= 0.02

Table A.6.2. Size Modeling of Coal Mine Dust from Section B (Mine Code 142-1-1).

Sampling Location	Residual Analysis	Analysis Results: Empirical Distribution: Chebychev Function	Analysis Results: Empirical Distribution: Spline Function	Analysis Results: Lognormal Distribution: Unimodal	Analysis Results: Lognormal Distribution: Bimodal
CI	Linear	GM1=17.80	GM1= 2.72 GM2= 7.50 GM3=17.78	GM1=13.93 GS1= 2.87 gf1= 0.08 gf2= 0.04	GM1= 8.86 GS1= 2.38 %1= 0.68 GM2= 27.55 GS2= 1.56 gf1= 0.27 gf2= 0.03
CR	Curvi.	GM1=17.38	GM1= 2.51 GM2= 8.13 GM3=17.38	GM1=15.37 GS1= 2.02 gf1=10.25 gf2= 0.14	GM1= 11.95 GS1= 2.47 %1= 0.85 GM2= 16.28 GS2= 1.17 gf1= 0.03 gf2= 0.02
RI	Curvi.	GM1=10.59	GM1= 2.57 GM2=15.85	GM1= 6.09 GS1= 2.62 gf1= 0.06 gf2= 0.06	GM1= 2.68 GS1= 1.45 %1= 0.29 GM2= 9.14 GS2= 2.11 gf1= 4.04 gf2= 0.02
RR	Curvi.	GM1=11.22	GM1= 2.51 GM2= 7.94 GM3=16.22	GM1=10.60 GS1= 2.46 gf1= 0.27 gf2= 0.08	GM1= 2.46 GS1= 1.11 %1= 0.06 GM2= 11.85 GS2= 2.21 gf1= 5.63 gf2= 0.02
2X	Curvi.	GM1= 8.91	GM1= 2.66 GM2=15.65	GM1=11.05 GS1= 2.39 gf1= 0.16 gf2= 0.07	GM1= 2.63 GS1= 1.01 %1= 0.04 GM2= 12.33 GS2= 2.17 gf1= 1.51 gf2= 0.01

Table A.6.3. Size Modeling of Coal Mine Dust from Section C (Mine Code 03-3-1).

Sampling Location	Residual Analysis	Analysis Results: Empirical Distribution — Chebychev Function	Analysis Results: Empirical Distribution — Spline Function	Analysis Results: Lognormal Distribution — Unimodal	Analysis Results: Lognormal Distribution — Bimodal
IN	Linear	GM1= 4.07	GM1= 2.47 GM2= 6.88	GM1= 3.89 GS1= 2.10 gf1= 1.25 gf2= 0.18	GM1= 2.07 GS1= 1.26 %1= 0.50 GM2= 6.36 GS2= 1.44 gf1= 0.64 gf2= 0.10
CI/RI	Curvi.	GM1=10.86	GM1= 2.72 GM2= 8.33	GM1= 9.77 GS1= 2.20 gf1=28.94 gf2= 0.04	GM1= 1.70 GS1= 1.10 %1= 0.02 GM2= 9.68 GS2= 2.16 gf1= 51.44 gf2= 0.05
CR	Curvi.	GM1= 5.84	GM1= 2.79 GM2=11.68	GM1=12.71 GS1= 2.27 gf1=13.92 gf2= 0.03	GM1= 2.86 GS1= 1.10 %1= 0.03 GM2= 12.97 GS2= 2.18 gf1= 54.60 gf2= 0.02
2XCR	Curvi.	GM1=13.80	GM1= 2.61 GM2= 9.11	GM1=11.98 GS1= 2.20 gf1= 2.86 gf2= 0.06	GM1= 2.89 GS1= 1.08 %1= 0.06 GM2= 12.26 GS2= 2.06 gf1= 48.48 gf2= 0.03
4XCR	Linear	GM1=19.50	GM1= 4.80 GM2=12.50	GM1=15.13 GS1= 3.20 gf1= 0.09 gf2= 0.04	GM1= 3.91 GS1= 1.38 %1= 0.08 GM2= 17.57 GS2= 2.85 gf1= 0.66 gf2= 0.01

Table A.6.3. (Continued).

Sampling Location	Residual Analysis	Analysis Results: Empirical Distribution: Chebychev Function	Analysis Results: Empirical Distribution: Spline Function	Analysis Results: Lognormal Distribution: Unimodal	Analysis Results: Lognormal Distribution: Bimodal
RR	Curvi.	GM1=10.96	GM1= 7.94 GM2=15.49	GM1= 9.91 GS1= 2.29 gf1= 2.54 gf2= 0.02	GM1= 5.02 GS1= 1.68 %1= 0.35 GM2= 14.40 GS2= 1.89 gf1= 12432 gf2= 0.01
2XRR	Linear	GM1= 7.59	GM1= 2.98 GM2=12.59 u3=38.90	GM1= 8.10 GS1= 2.75 gf1= 0.10 gf2= 0.11	GM1= 3.00 GS1= 1.08 %1= 0.12 GM2= 8.62 GS2= 2.42 gf1= 0.27 gf2= 0.08

Table A.6.4. Size Modeling of Coal Mine Dust from Section D (Mine Code 30-7-1).

		Analysis Results			
		Empirical Distribution		Lognormal Distribution	
Sampling Location	Residual Analysis	Chebychev Function	Spline Function	Unimodal	Bimodal
CR1	Curvi.	GM1=15.85	GM1=15.85	GM1=14.83 GS1= 2.00 gf1=12.23 gf2= 0.06	GM1= 6.04 GS1= 1.70 %1= 0.25 GM2= 17.64 GS2= 1.69 gf1=120.54 gf2= 0.03
CR2	Linear	GM1= 8.41	GM1= 2.78 GM2= 8.41	GM1= 9.04 GS1= 2.48 gf1= 0.04 gf2= 0.03	GM1= 2.74 GS2= 1.37 %1= 0.13 GM2= 10.49 GS2= 2.14 gf1= 0.23 gf2= 0.02

Table A.6.5. Size Modeling of Coal Mine Dust from Section E (Mine Code 200-2-1).

		Analysis Results			
		Empirical Distribution		Lognormal Distribution	
Sampling Location	Residual Analysis	Chebychev Function	Spline Function	Unimodal	Bimodal
CR1	Curvi.	GM1=16.79	GM1=16.79	GM1=14.11 GS1= 2.24 gf1= 3.36 gf2= 0.07	GM1= 4.69 GS1= 1.84 %1= 0.27 GM2= 17.39 GS2= 1.78 gf1= 5.74 gf2= 0.01
CR2	Curvi.	GM1=11.89	GM1= 3.26 GM2=16.79	GM1=12.26 GS1= 2.29 gf1= 0.43 gf2= 0.06	GM1= 3.35 GS2= 1.57 %1= 0.20 GM2= 14.29 GS2= 1.88 gf1= 1075 gf2= 0.02
RI	Linear	GM1= 4.37	GM1= 3.12 GM2=19.50	GM1= 4.22 GS1= 1.95 gf1= 5.03 gf2= 0.21	GM1= 4.24 GS1= 1.82 %1= 0.86 GM2= 30.31 GS2= 1.41 gf1= 16.35 gf2= 0.06
RR	Curvi.	GM1= 5.96	GM1= 3.86 GM2=18.84	GM1= 7.40 GS1= 3.46 gf1= 0.24 gf2= 0.28	GM1= 3.93 GS1= 1.55 %1= 0.52 GM2= 22.96 GS2= 1.61 gf1= 8688 gf2= 0.01

Table A.6.6. Size Modeling of Coal Mine Dust from Section F (Mine Code 11-2-1).

		Analysis Results			
		Empirical Distribution		Lognormal Distribution	
Sampling Location	Residual Analysis	Chebychev Function	Spline Function	Unimodal	Bimodal
CR	Curvi.	GM1=16.60	GM1= 2.82 GM2=16.60	GM1= 14.98 GS1= 1.96 gf1= 48611 gf2= 0.15	GM1= 5.64 GS1= 2.17 %1= 0.29 GM2= 16.93 GS2= 1.67 gf1= 2.56 gf2= 0.03
CI	Linear	GM1=15.14	GM1= 2.65 GM2=15.14	GM1= 13.07 GS1= 2.03 gf1= 2.55 gf2= 0.09	GM1= 2.60 GS1= 1.14 %1= 0.04 GM2= 13.26 GS2= 1.94 gf1= 25.11 gf2= 0.03
RI	Curvi.	GM1= 9.12	GM1=11.22	GM1= 9.99 GS1= 2.28 gf1= 1.64 gf2= 0.03	GM1= 3.16 GS1= 1.69 %1= 0.18 GM2= 11.55 GS2= 1.95 gf1= 74.67 gf2= 0.01
RR	Curvi.	GM1= 8.71	GM1= 8.71	GM1= 9.18 GS1= 2.29 gf1= 0.06 gf2= 0.01	GM1= 8.34 GS2= 2.57 %1= 0.80 GM2= 10.36 GS2= 1.59 gf1= 0.08 gf2= 0.01

Table A.6.6. (Continued).

Sampling Location	Residual Analysis	Analysis Results: Empirical Distribution: Chebychev Function	Analysis Results: Empirical Distribution: Spline Function	Analysis Results: Lognormal Distribution: Unimodal	Analysis Results: Lognormal Distribution: Bimodal
2X	Curvi.	GM1= 6.92	GM1= 8.41	GM1= 8.48 GS1= 2.05 gf1= 5.93 gf2= 0.05	GM1= 2.12 GS1= 1.33 %1= 0.13 GM2= 8.91 GS2= 1.79 gf1= 11842 gf2= 0.04
4X	Curvi.	GM1= 5.96	GM1= 4.73 GM2=10.23	GM1= 6.85 GS1= 2.14 gf1= 0.27 gf2= 0.03	GM1= 6.27 GS2= 1.98 %1= 0.87 GM2= 14.24 GS2= 1.11 gf1= 1.22 gf2= 0.04

Table A.6.7. Size Modeling of Coal Mine Dust from Section G (Mine Code 63-7-1).

		Analysis Results			
		Empirical Distribution		Lognormal Distribution	
Sampling Location	Residual Analysis	Chebychev Function	Spline Function	Unimodal	Bimodal
ININ	Curvi.	GM1= 6.61	GM1= 2.85 GM2=12.22	GM1= 9.25 GS1= 2.54 gf1= 0.37 gf2= 0.17	GM1= 3.13 GS1= 1.85 %1= 0.46 GM2= 13.00 GS2= 1.53 gf1= 0.23 gf2= 0.06
INOUT	Curvi.	GM1= 3.55	GM1= 3.55 GM2=11.68	GM1= 3.88 GS1= 2.44 gf1= 0.88 gf2= 0.17	GM1= 3.54 GS1= 1.32 %1= 0.24 GM2= 4.31 GS2= 3.34 gf1= 0.19 gf2= 0.12
CI	Curvi.	GM1=12.30	GM1= 4.90 GM2=16.79	GM1= 12.69 GS1= 2.87 gf1= 1.51 gf2= 0.23	GM1= 6.92 GS1= 4.28 %1= 0.82 GM2= 15.64 GS2= 1.19 gf1= 0.08 gf2= 0.06
CR1	Curvi.	GM1=22.91	GM1= 2.73 GM2=17.38	GM1= 17.45 GS1= 1.89 gf1= 20933 gf2= 0.11	GM1= 3.49 GS1= 1.67 %1= 0.08 GM2= 17.67 GS2= 1.80 gf1= 26.79 gf2= 0.03

Table A.6.7. (Continued).

Sampling Location	Residual Analysis	Analysis Results: Empirical Distribution: Chebychev Function	Analysis Results: Empirical Distribution: Spline Function	Analysis Results: Lognormal Distribution: Unimodal	Analysis Results: Lognormal Distribution: Bimodal
CR	Curvi.	GM1=22.39	GM1= 4.78 GM2=16.60	GM1= 17.47 GS1= 1.87 gf1=850845 gf2= 0.14	GM1= 5.73 GS1= 1.40 %1= 0.16 GM2= 19.11 GS2= 1.62 gf1=10xx14 gf2= 0.07
RI	Linear	GM1=10.23	GM1= 2.82 GM2=16.22	GM1= 11.56 GS1= 2.48 gf1= 0.51 gf2= 0.14	GM1= 3.76 GS1= 1.92 %1= 0.38 GM2= 16.03 GS2= 1.68 gf1= 0.32 gf2= 0.04
RR	Curvi.	GM1=16.79	GM1= 8.32 GM2=16.79	GM1= 13.16 GS1= 2.06 gf1= 27.62 gf2= 0.15	GM1= 0.92 GS1= 1.37 %1= 0.02 GM2= 13.35 GS2= 1.91 gf1= 24.43 gf2= 0.05

Table A.6.8. Size Modeling of Coal Mine Dust from Section H (Mine Code 101-7-1).

		Analysis Results			
		Empirical Distribution		Lognormal Distribution	
Sampling Location	Residual Analysis	Chebychev Function	Spline Function	Unimodal	Bimodal
CI	Curvi.	GM1= 4.44	GM1= 2.47 GM2= 5.62	GM1= 6.050 GS1= 2.88 gf1= 0.16 gf2= 0.13	GM1= 2.31 GS1= 1.09 %1= 0.17 GM2= 8.98 GS2= 2.53 gf1= 1.15 gf2= 0.03
CR	Curvi.	GM1= 7.59	GM1= 2.69 GM2= 7.59	GM1= 7.00 GS1= 2.55 gf1= 0.25 gf2= 0.11	GM1= 6.35 GS1= 3.06 %1= 0.79 GM2= 9.24 GS2= 1.15 gf1= 0.04 gf2= 0.03
2X	Curvi.	GM1= 7.76	GM1= 2.85 GM2=15.85	GM1= 9.28 GS1= 2.64 gf1= 0.21 gf2= 0.07	GM1= 3.22 GS1= 1.53 %1= 0.33 GM2= 13.69 GS2= 1.83 gf1=154815 gf2= 0.03
4X		GM1= 9.55	GM1=12.85 GM2=11.48	GM1= 11.00 GS1= 2.42 gf1= 2.51 gf2= 0.06	GM1= 2.59 GS1= 1.53 %1= 0.17 GM2= 12.40 GS2= 1.99 gf1= 3726 gf2= 0.03

Table A.6.9. Size Modeling of Coal Mine Dust from Section I (Mine Code 102-7-1).

Sampling Location	Residual Analysis	Analysis Results: Empirical Distribution: Chebychev Function	Analysis Results: Empirical Distribution: Spline Function	Analysis Results: Lognormal Distribution: Unimodal	Analysis Results: Lognormal Distribution: Bimodal
CI	Linear	GM1=11.09	GM1= 2.82 GM2= 9.77	GM1= 10.64 GS1= 2.32 gf1= 17.57 gf2= 0.05	GM1= 2.21 GS1= 1.22 %1= 0.08 GM2= 11.07 GS2= 2.11 gf1=457.69 gf2= 0.03
CR1	Curvi.	GM1=23.71	GM1= 3.16 GM2=16.60	GM1= 19.00 GS1= 1.77 gf1= & gf2= 0.16	GM1= 3.30 GS1= 1.32 %1= 0.07 GM2= 18.76 GS2= 1.72 gf1= & gf2= 0.05
CR2	Curvi.	GM1= 9.44	GM1= 2.69 GM2=11.22	GM1= 9.97 GS1= 3.11 gf1= 0.41 gf2= 0.08	GM1= 2.16 GS1= 1.23 %1= 0.15 GM2= 12.06 GS2= 2.50 gf1= 19.93 gf2= 0.05
2X	Curvi.	GM1= 6.70	GM1= 4.57 GM2=12.02	GM1= 8.15 GS1= 2.48 gf1= 0.16 gf2= 0.04	GM1= 3.46 GS1= 1.68 %1= 0.41 GM2= 12.20 GS2= 1.69 gf1=163.11 gf2= 0.04
4X	Curvi.	GM1= 6.68	GM1= 4.37 GM2=11.75	GM1= 7.69 GS1= 2.56 gf1= 0.11 gf2= 0.04	GM1= 5.46 GS1= 2.25 %1= 0.81 GM2= 14.63 GS2= 1.13 gf1= 0.04 gf2= 0.02

Table A.6.10. Size Modeling of Coal Mine Dust from Section J (Mine Code 103-7-1).

		Analysis Results			
		Empirical Distribution		Lognormal Distribution	
Sampling Location	Residual Analysis	Chebychev Function	Spline Function	Unimodal	Bimodal
CI	Linear	GM1= 5.13	GM1= 4.37 GM2=17.78	GM1= 5.12 GS1= 2.24 gf1= 0.64 gf2= 0.23	GM1= 4.45 GS1= 1.64 %1= 0.70 GM2= 21.61 GS2= 1.58 gf1= 37369 gf2= 0.07
2X	Curvi.	GM1=10.01	GM1= 2.95 GM2=14.79	GM1= 10.43 GS1= 2.42 gf1= 2.13 gf2= 0.07	GM1= 3.15 GS1= 1.32 %1= 0.16 GM2= 12.27 GS2= 2.01 gf1= 2714 gf2= 0.02
4X	Curvi.	GM1=10.23	GM1= 2.88 GM2= 8.71 u3=16.22	GM1= 11.35 GS1= 2.12 gf1=580.90 gf2= 0.16	GM1= 3.21 GS1= 1.35 %1= 0.20 GM2= 12.85 GS2= 1.76 gf1= & gf2= 0.05

Table A.6.11. Size Modeling of Coal Mine Dust from Section K (Mine Code 104-7-1).

		Analysis Results			
		Empirical Distribution		Lognormal Distribution	
Sampling Location	Residual Analysis	Chebychev Function	Spline Function	Unimodal	Bimodal
CI	Curvi.	GM1=11.89	GM1=15.49	GM1= 11.65 GS1= 2.50 gf1= 10.49 gf2= 0.06	GM1= 6.53 GS1= 2.44 %1= 0.55 GM2= 17.76 GS2= 1.82 gf1= 2.11 gf2= 0.03
CR	Curvi.	GM1= 6.46	GM1= 2.95 GM2=14.45	GM1= 7.97 GS1= 3.13 gf1= 0.08 gf2= 0.05	GM1= 2.92 GS1= 1.63 %1= 0.36 GM2= 14.00 GS2= 2.07 gf1= 1250 gf2= 0.05
2X	Curvi.	GM1= 4.90	GM1= 4.90	GM1= 5.52 GS1= 2.15 gf1= 0.62 gf2= 0.04	GM1= 5.49 GS1= 2.72 %1= 0.67 GM2= 5.15 GS2= 1.62 gf1= 0.03 gf2= 0.01
4X	Curvi.	GM1= 5.50	GM1= 2.75 GM2= 7.24 GM3=15.49	GM1= 6.59 GS1= 2.78 gf1= 0.07 gf2= 0.05	GM1= 2.80 GS1= 2.08 %1= 0.46 GM2= 10.89 GS2= 1.91 gf1= 0.11 gf2= 0.02

APPENDIX 7

EMPIRICAL AND LOGNORMAL DISTRIBUTIONS OF AIRBORNE COAL MINE DUST

Note: (1) The solid and dotted lines in the empirical distributions represent the mass size frequency distributions approximated by the Chebychev approximation function and the cubic-spline interpolation, respectively.
(2) The solid and dotted lines in the lognormal frequency distributions represent the component distribution and the composite distribution, respectively.

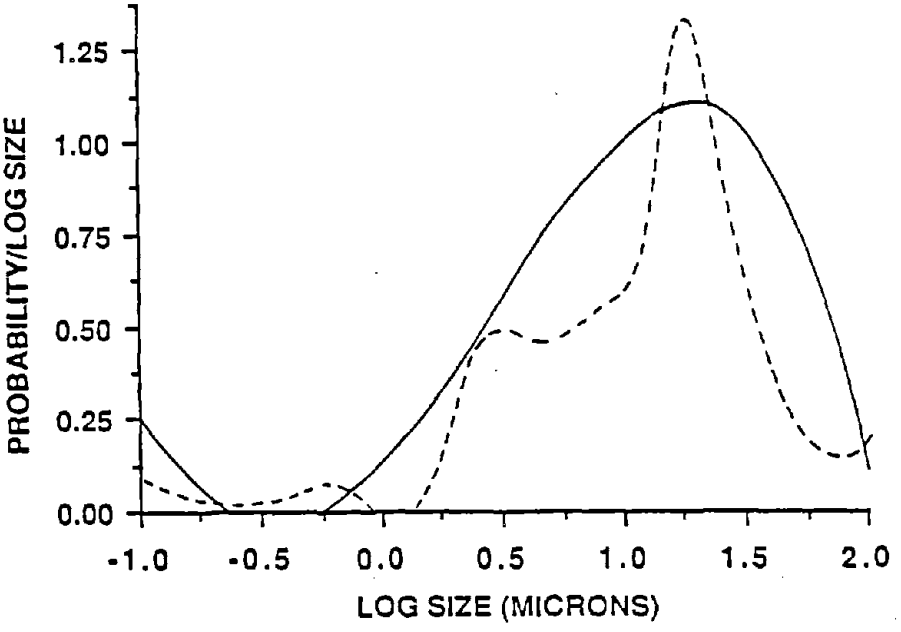

a. Empirical Frequency Distributions.

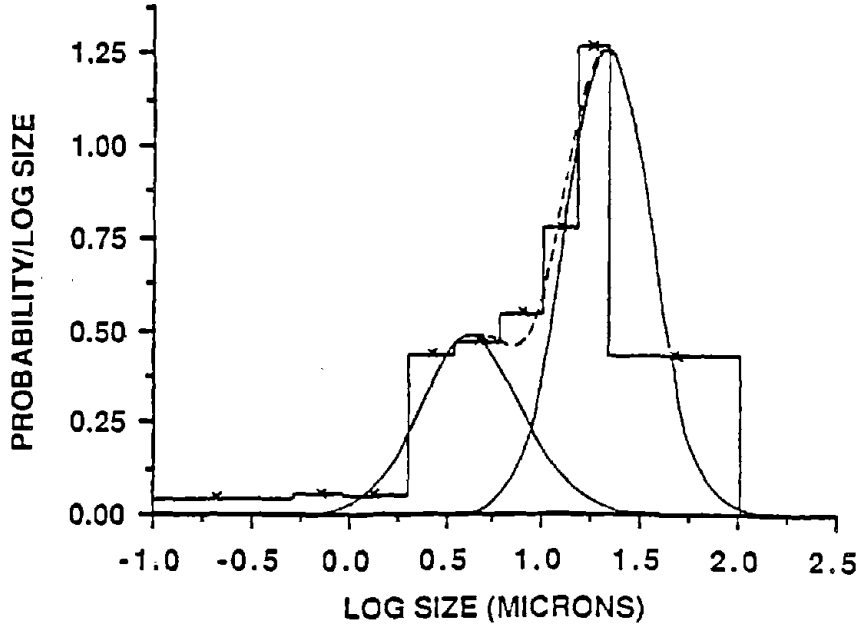

b. Lognormal Frequency Distributions.

1. Frequency Distributions of the CI Samples from Section A.

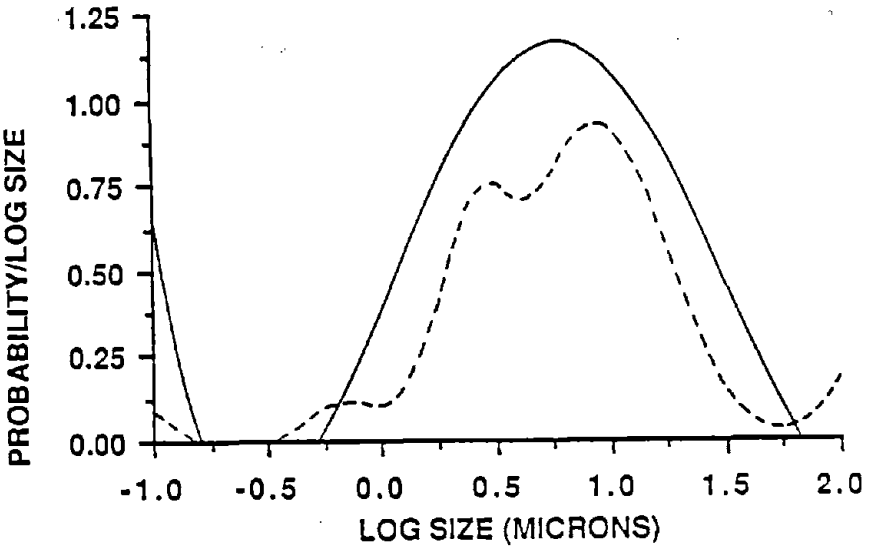

a. Empirical Frequency Distributions.

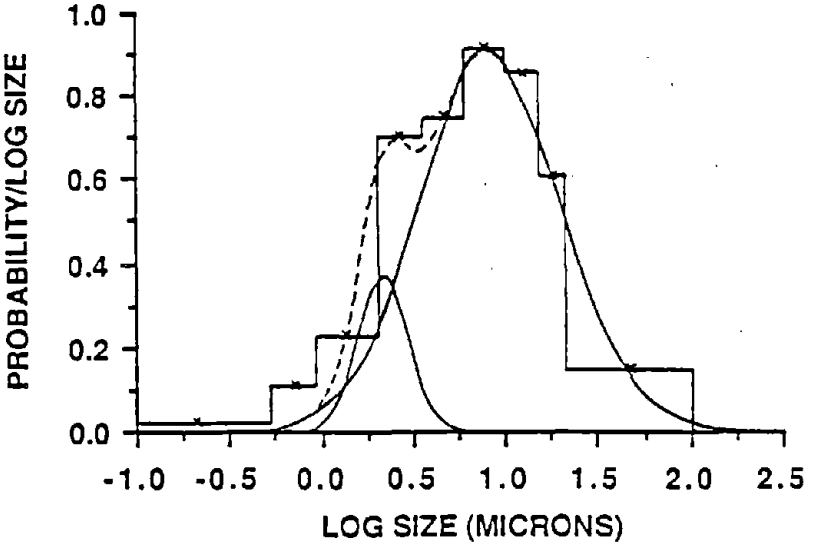

b. Lognormal Frequency Distributions.

2. Frequency Distributions of the RI Samples from Section A.

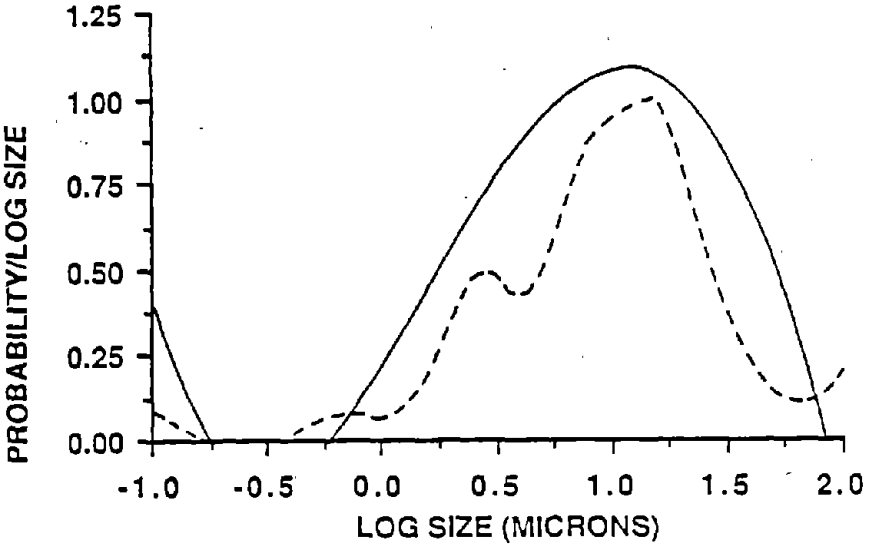

a. Empirical Frequency Distributions.

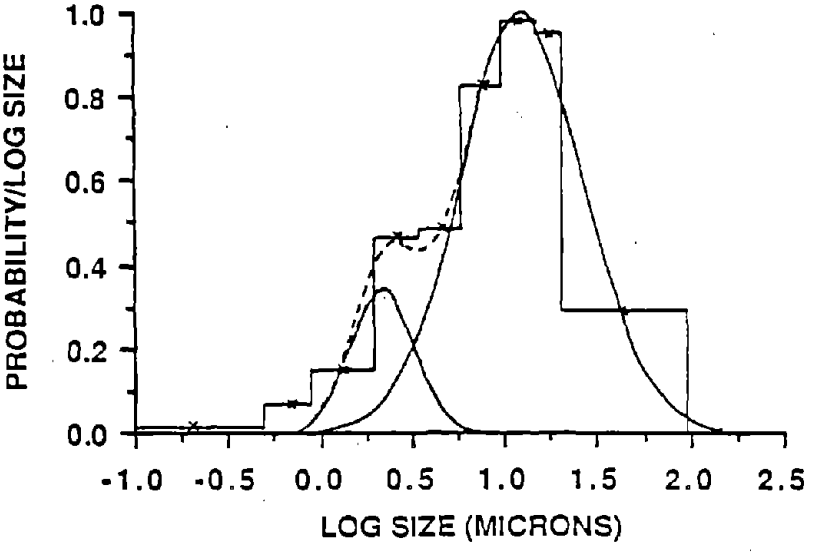

b. Lognormal Frequency Distributions.

3. Frequency Distributions of the RR Samples from Section A.

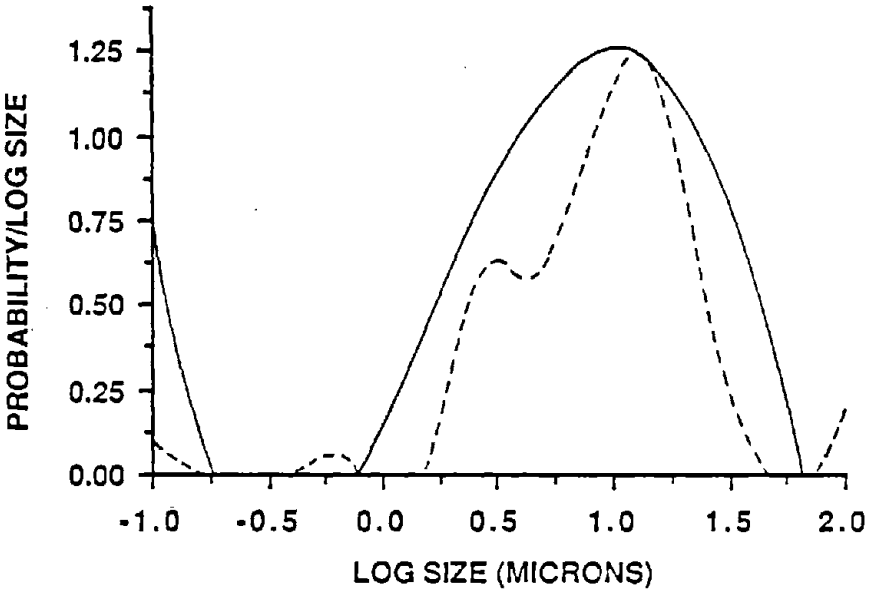

a. Empirical Frequency Distributions.

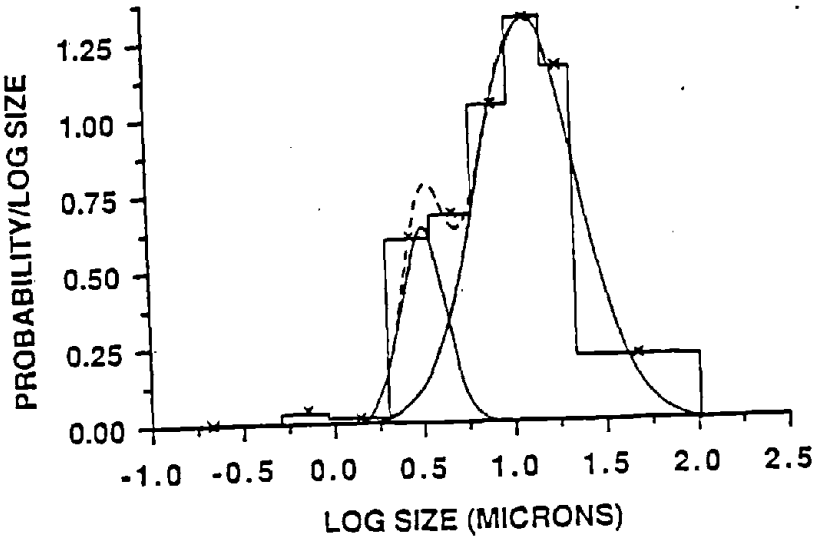

b. Lognormal Frequency Distributions.

4. Frequency Distributions of the 2X Samples from Section A.

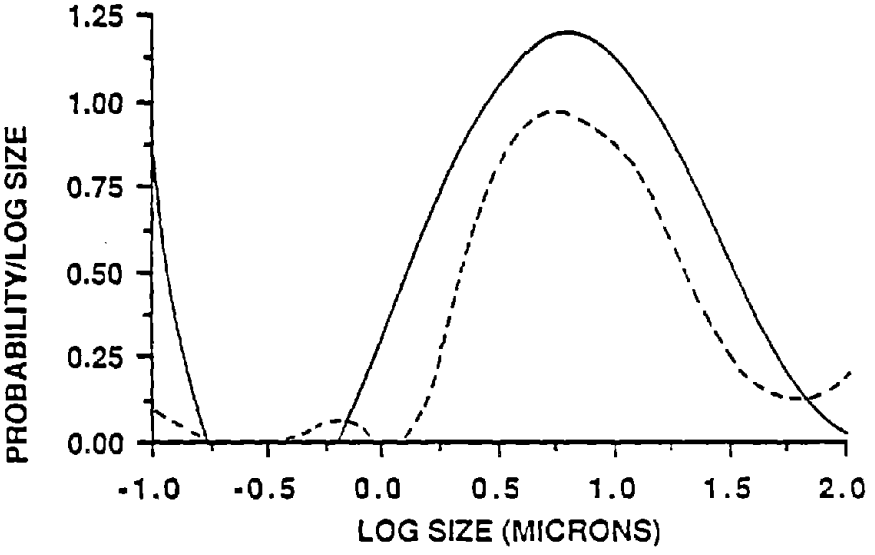

a. Empirical Frequency Distributions.

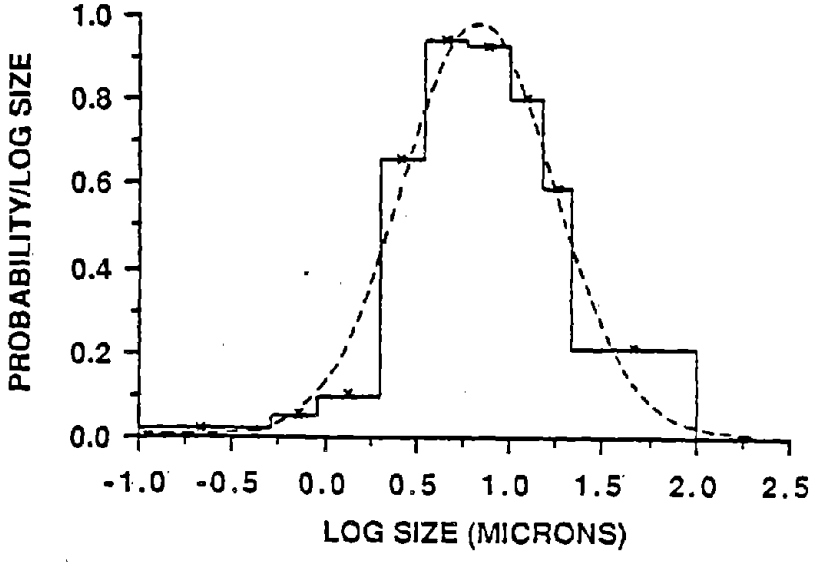

b. Lognormal Frequency Distributions.

5. Frequency Distributions of the 4X Samples from Section A.

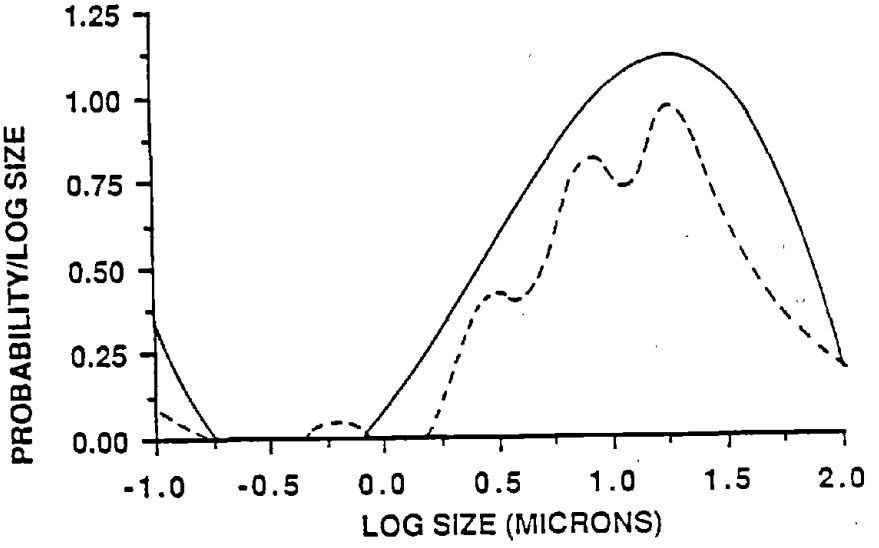

a. Empirical Frequency Distributions.

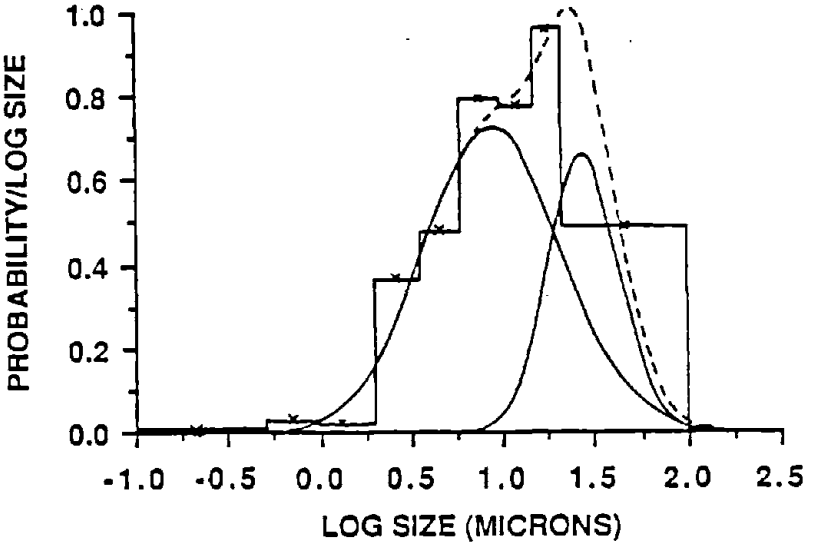

b. Lognormal Frequency Distributions.

6. Frequency Distributions of the CI Samples from Section B.

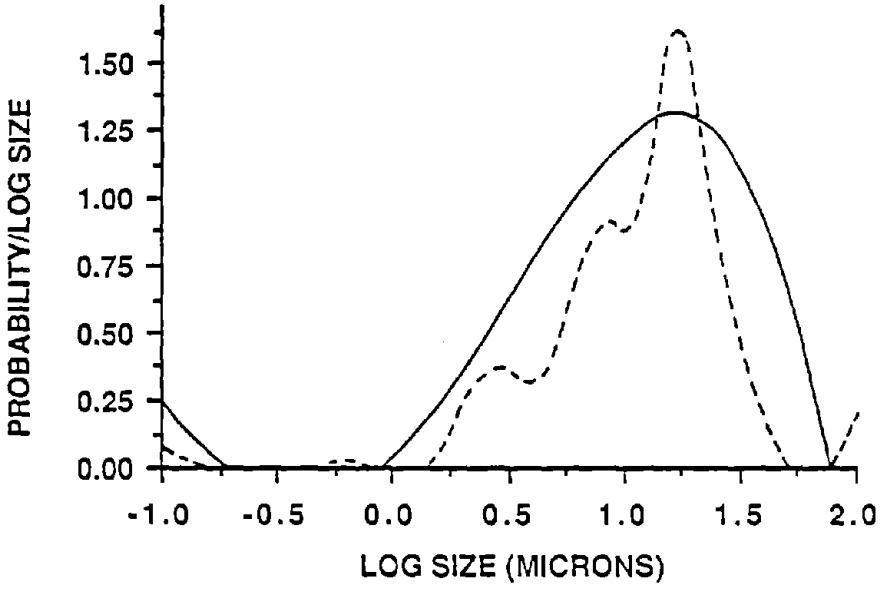

a. Empirical Frequency Distributions.

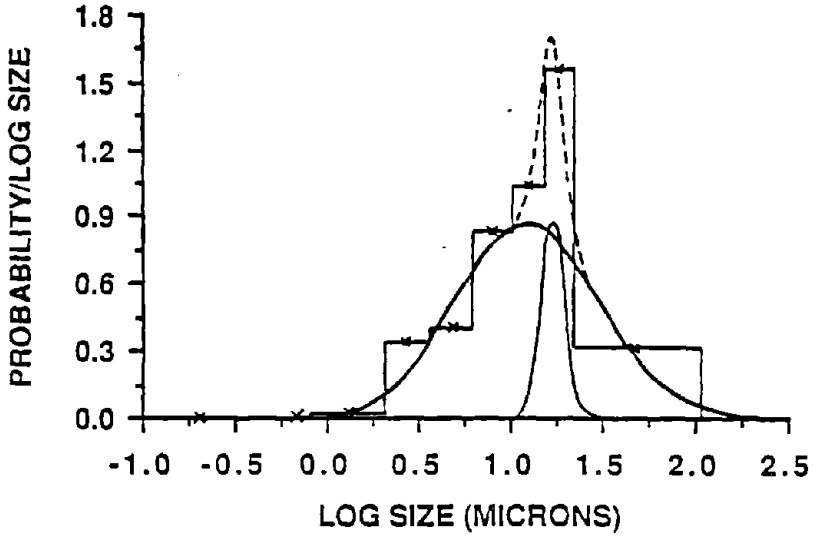

b. Lognormal Frequency Distributions.

7. Frequency Distributions of the CR Samples from Section B.

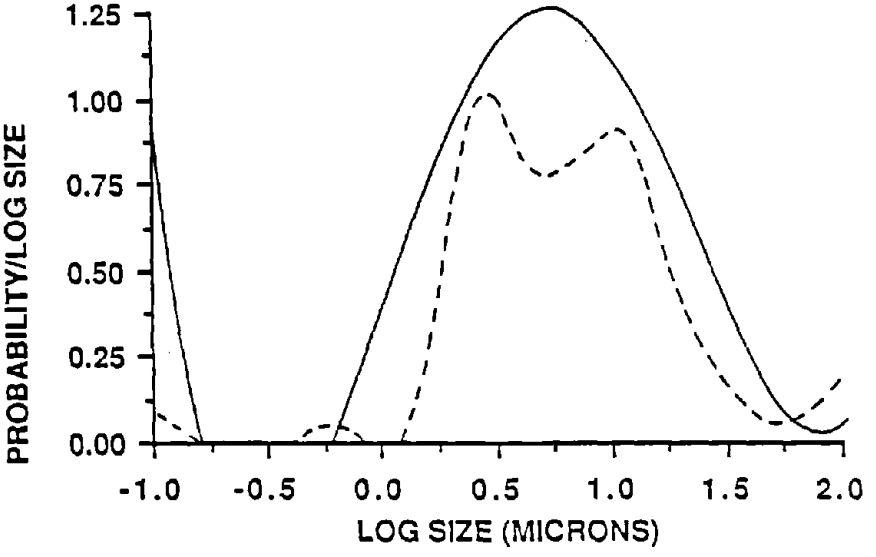

a. Empirical Frequency Distributions.

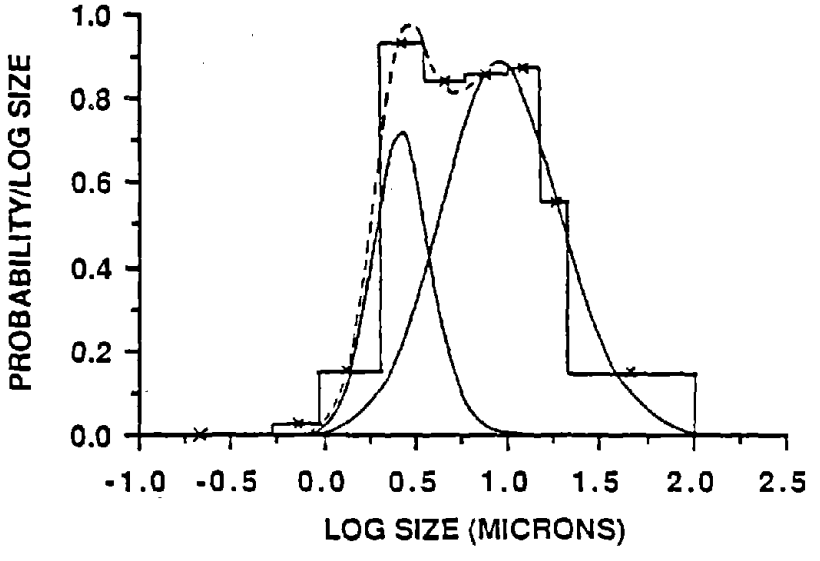

b. Lognormal Frequency Distributions.

8. Frequency Distributions of the RI Samples from Section B.

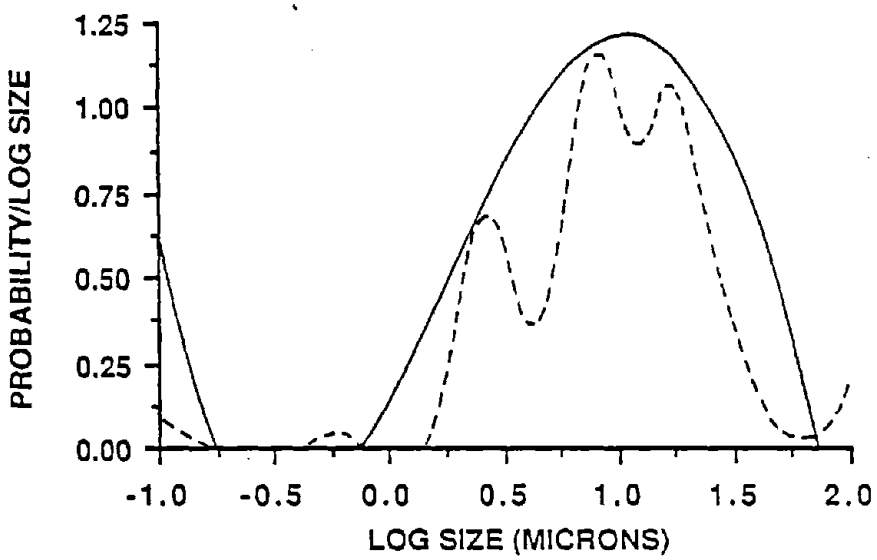

a. Empirical Frequency Distributions.

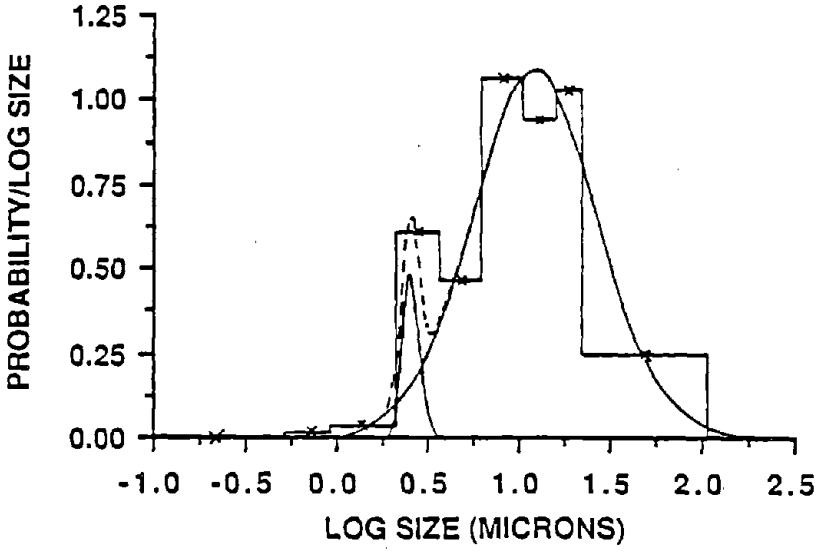

b. Lognormal Frequency Distributions.

9. Frequency Distributions of the RR Samples from Section B.

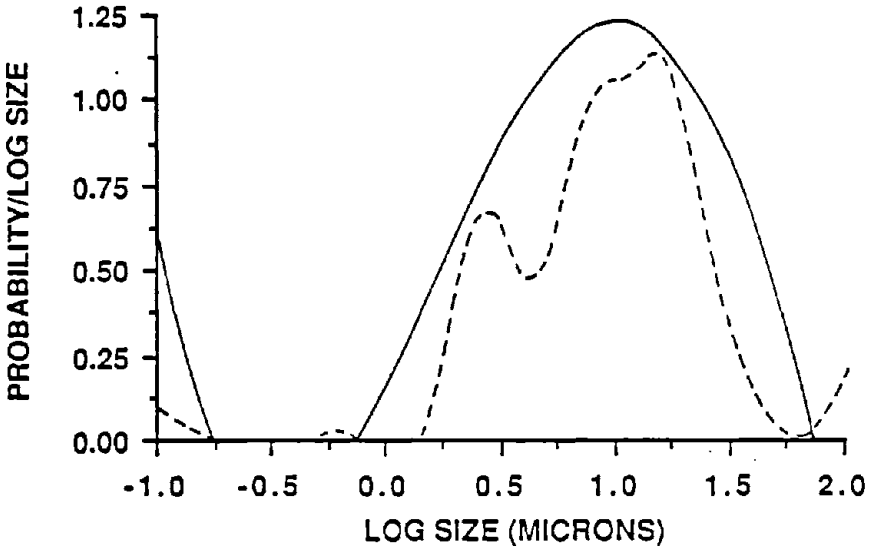

a. Empirical Frequency Distributions.

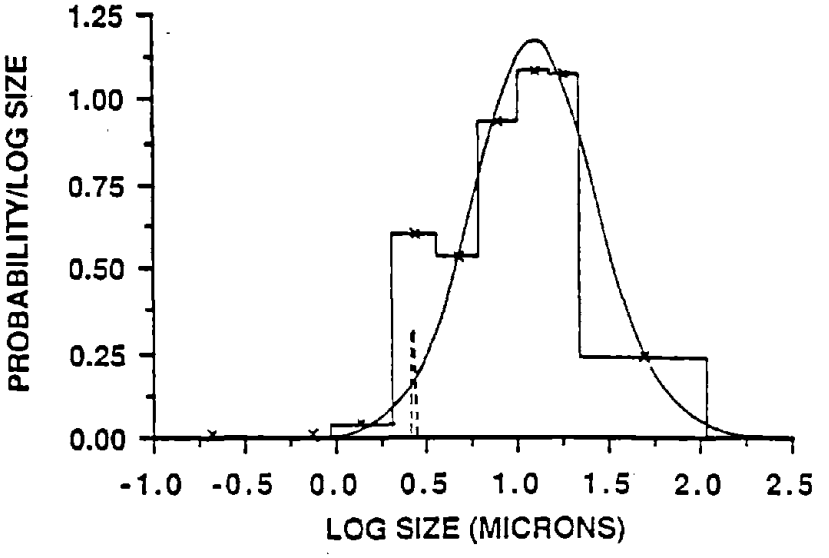

b. Lognormal Frequency Distributions.

10. Frequency Distributions of the 2X Samples from Section B.

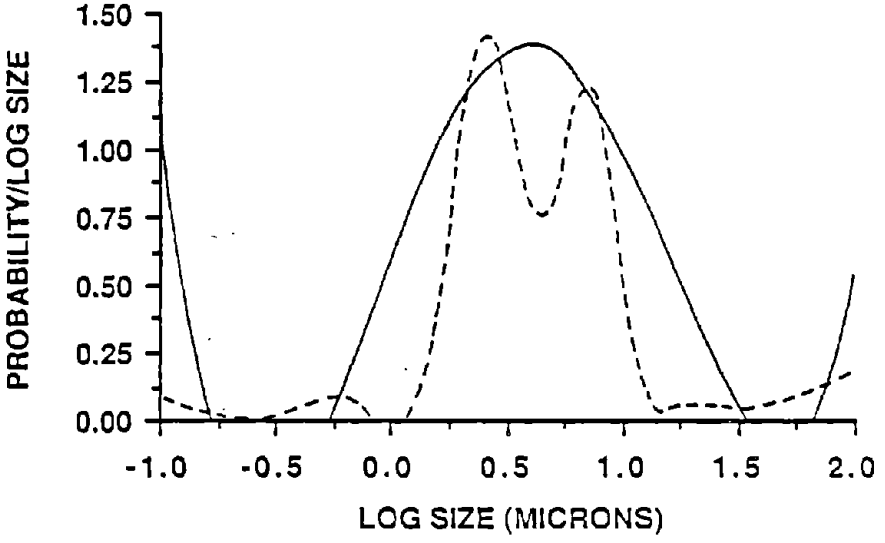

a. Empirical Frequency Distributions.

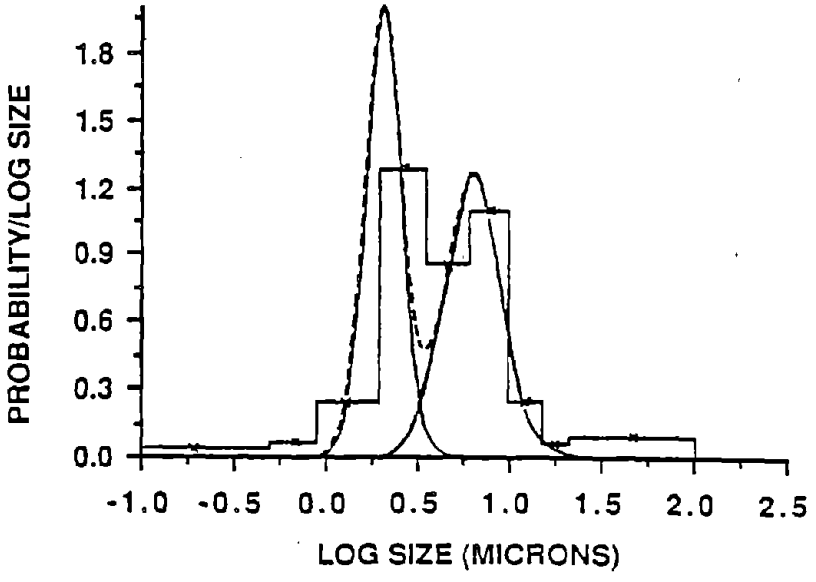

b. Lognormal Frequency Distributions.

11. Frequency Distributions of the IN Samples from Section C.

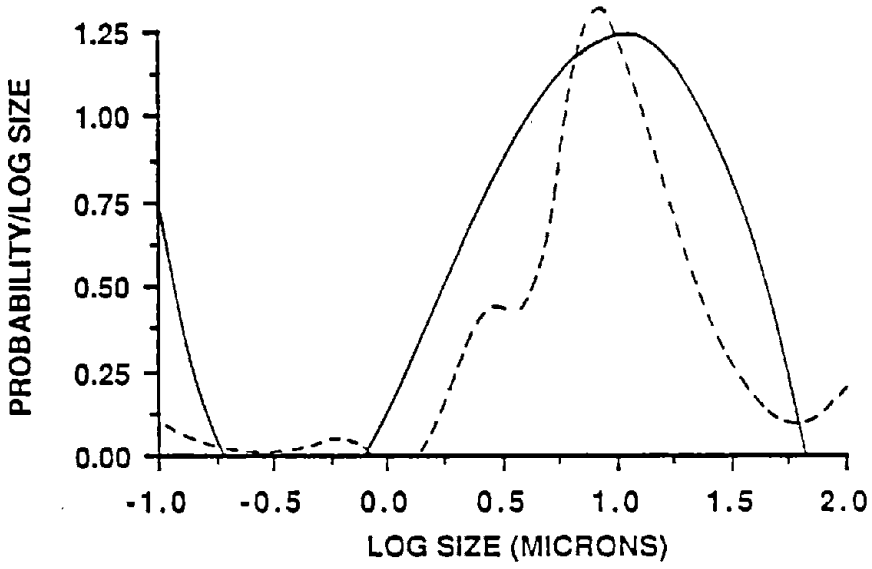

a. Empirical Frequency Distributions.

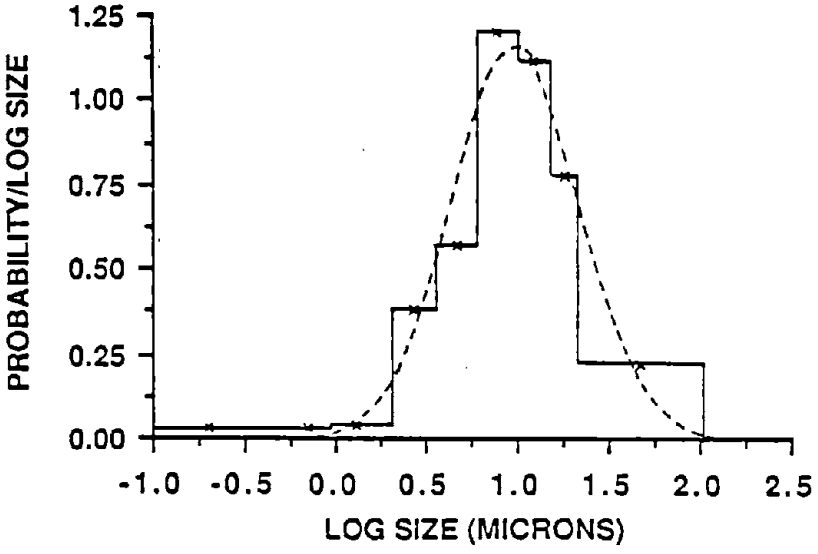

b. Lognormal Frequency Distributions.

12. Frequency Distributions of the CI/RI Samples from Section C.

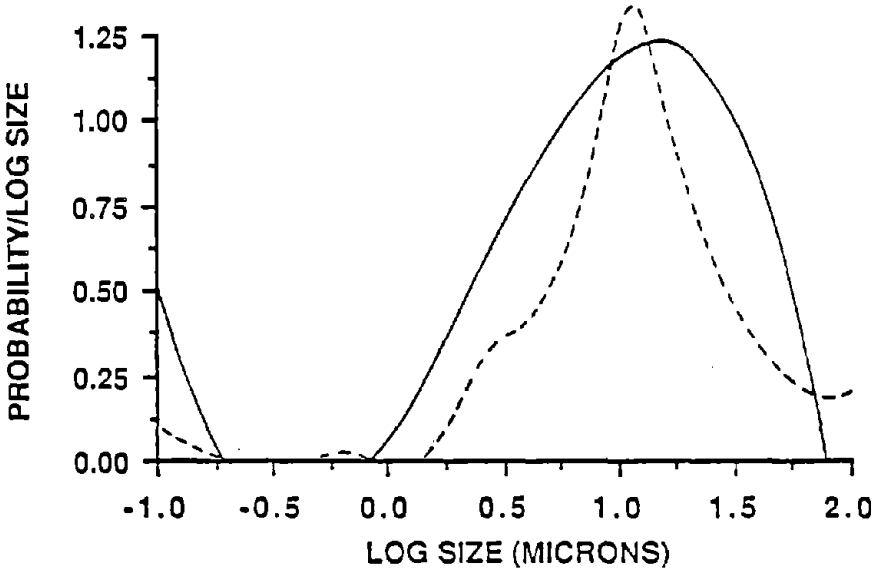

a. Empirical Frequency Distributions.

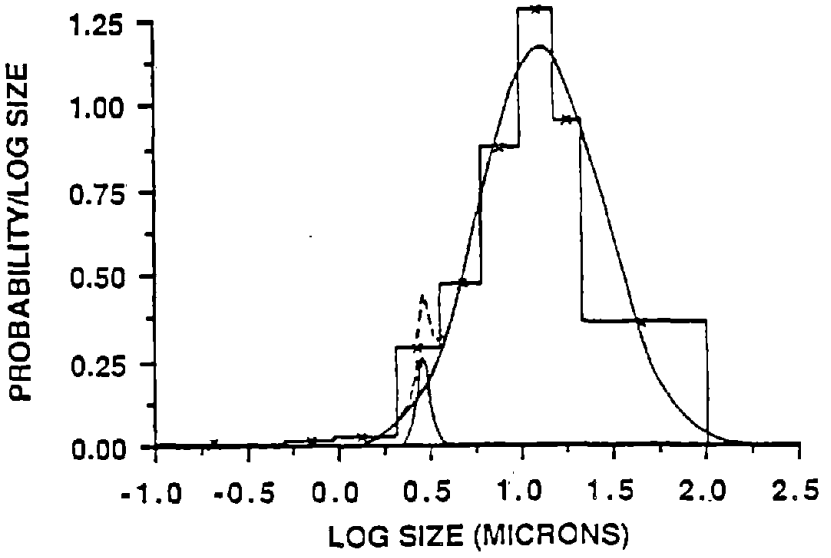

b. Lognormal Frequency Distributions.

13. Frequency Distributions of the CR Samples from Section C.

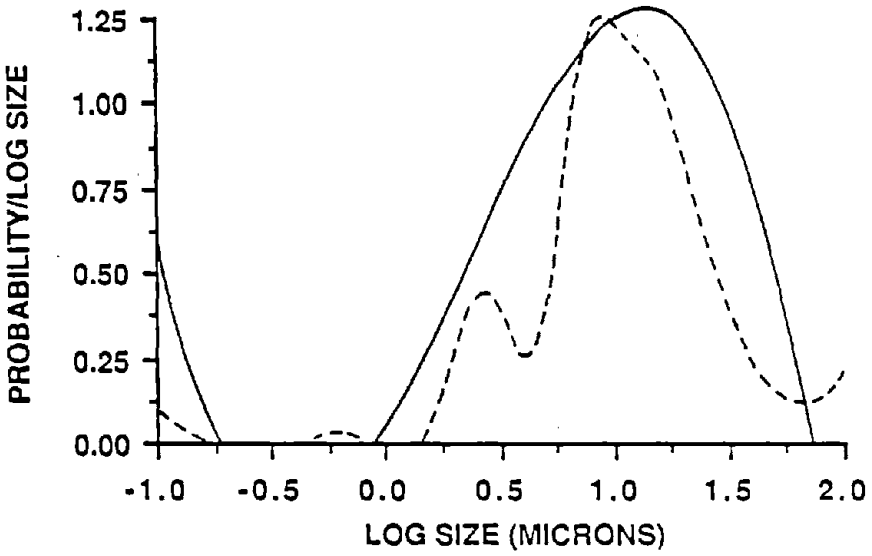

a. Empirical Frequency Distributions.

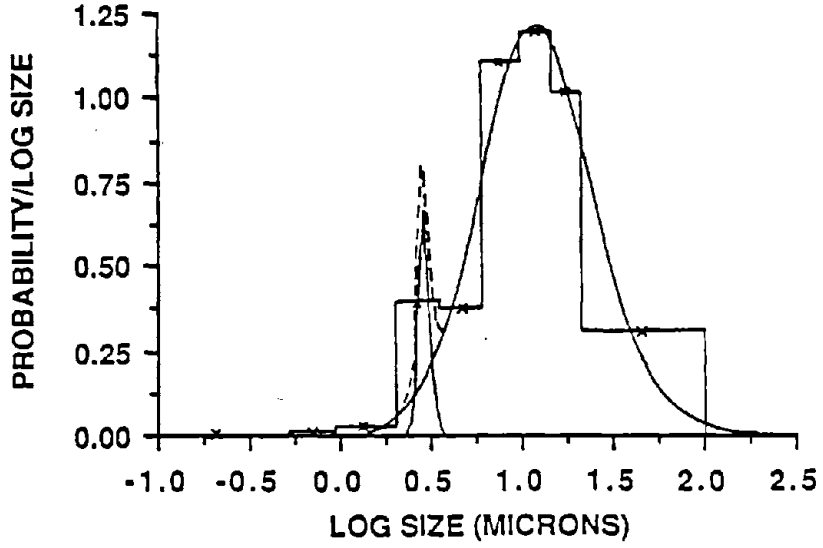

b. Lognormal Frequency Distributions.

14. Frequency Distributions of the 2XCR Samples from Section C.

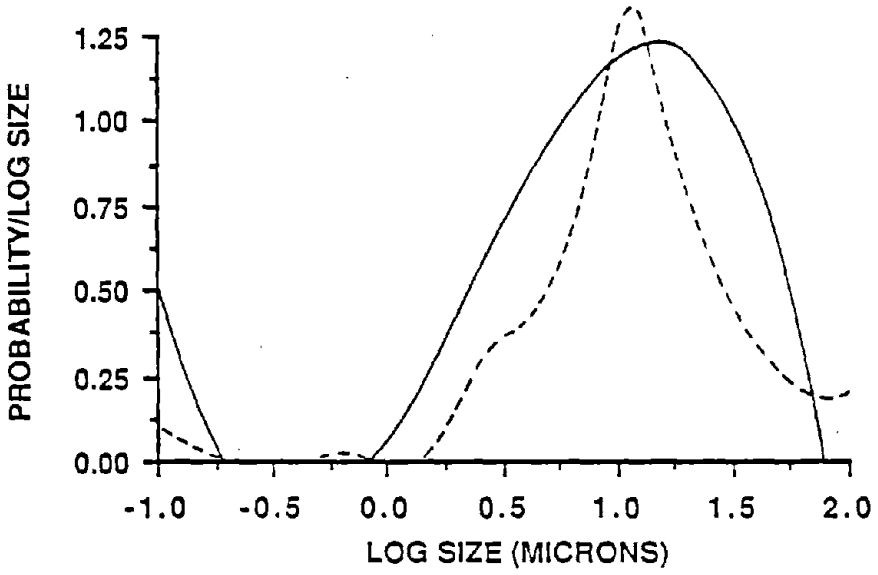

a. Empirical Frequency Distributions.

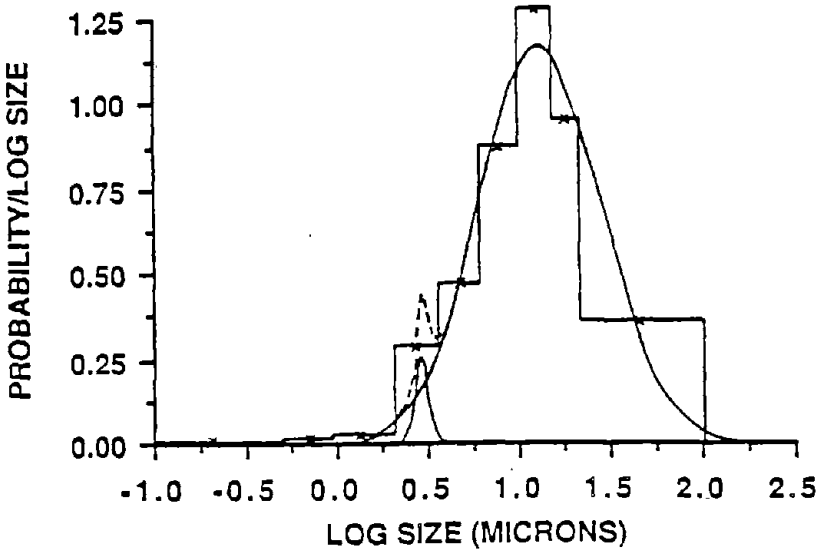

b. Lognormal Frequency Distributions.

13. Frequency Distributions of the CR Samples from Section C.

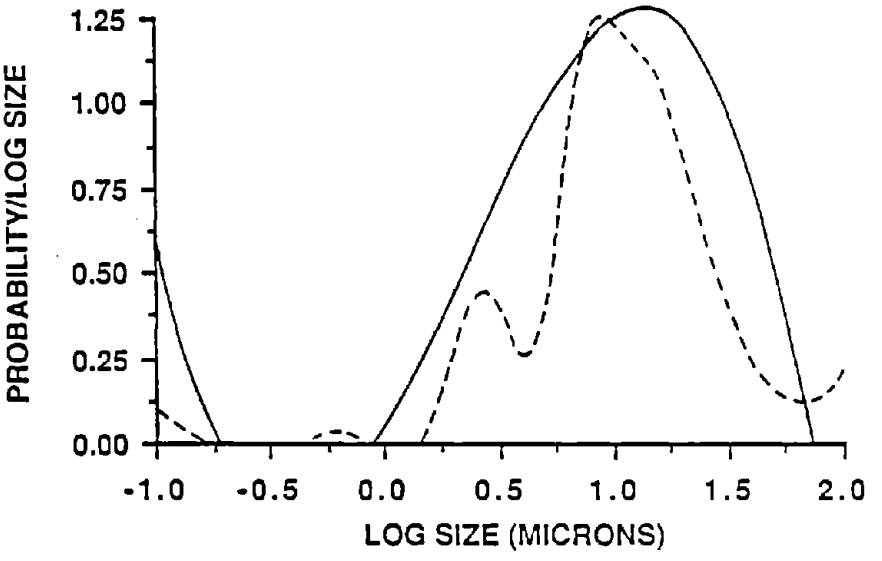

a. Empirical Frequency Distributions.

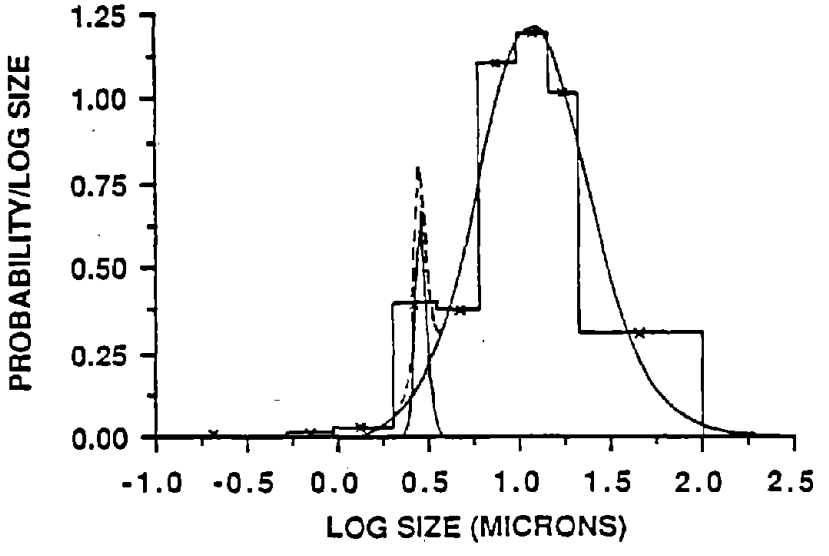

b. Lognormal Frequency Distributions.

14. Frequency Distributions of the 2XCR Samples from Section C.

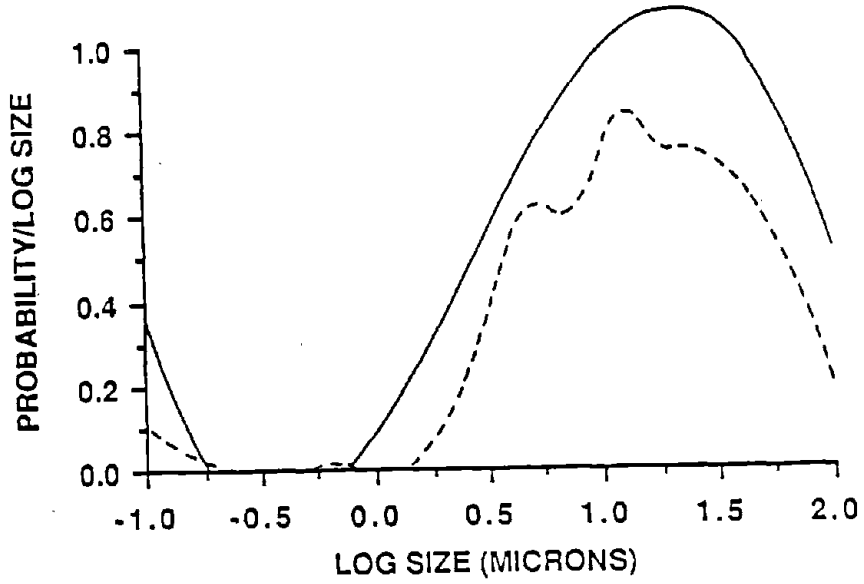

a. Empirical Frequency Distributions.

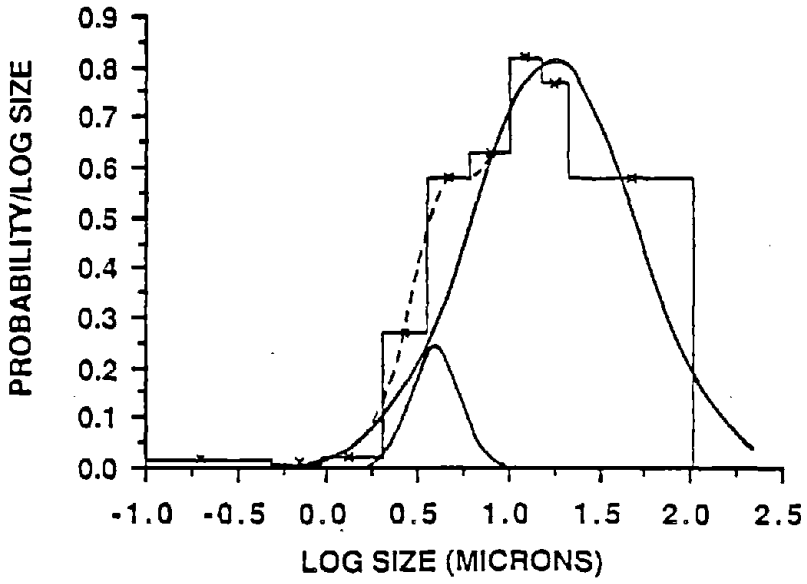

b. Lognormal Frequency Distributions.

15. Frequency Distributions of the 4XCR Samples from Section C.

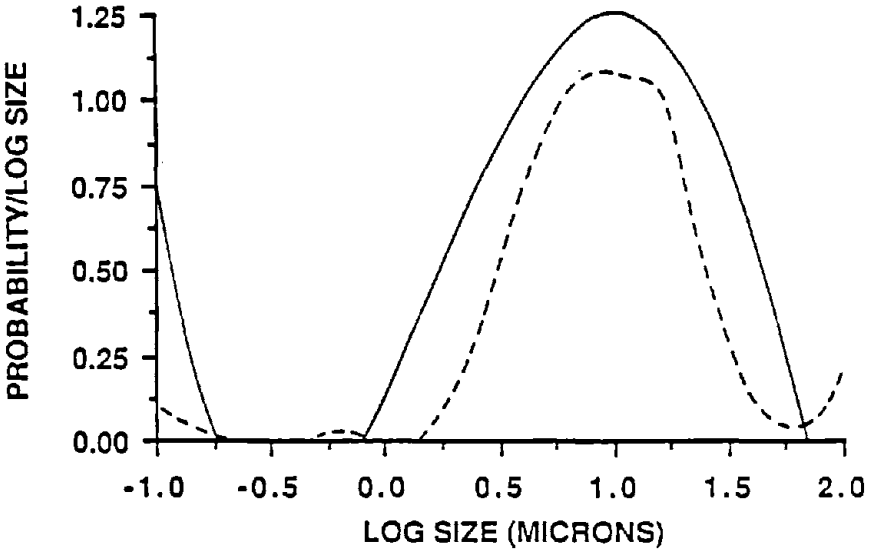

a. Empirical Frequency Distributions.

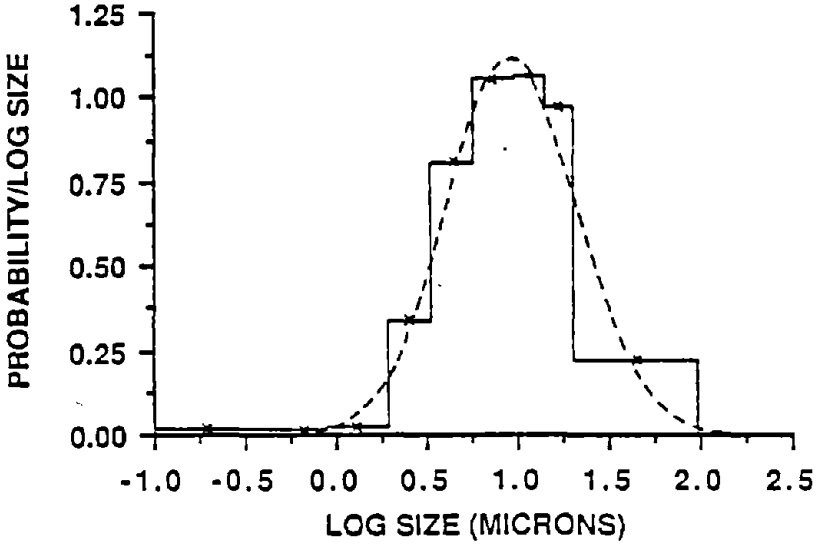

b. Lognormal Frequency Distributions.

16. Frequency Distributions of the RR Samples from Section C.

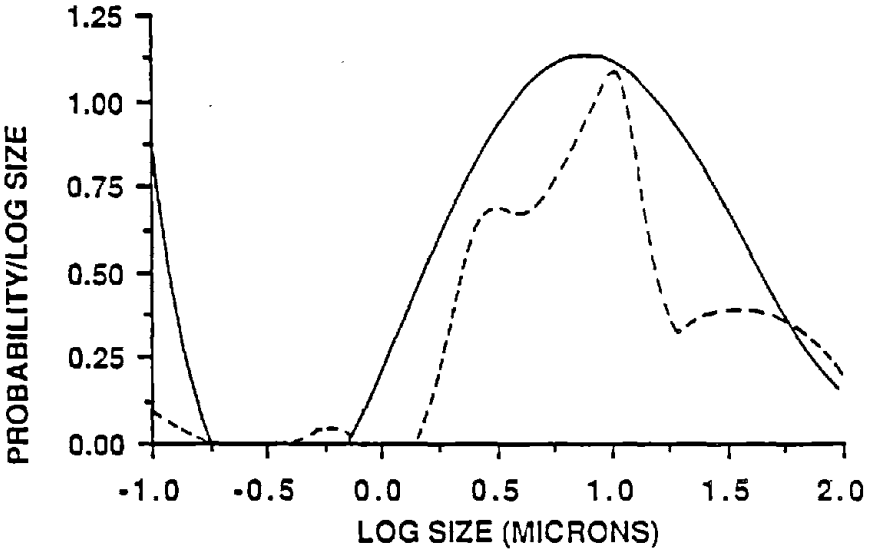

a. Empirical Frequency Distributions.

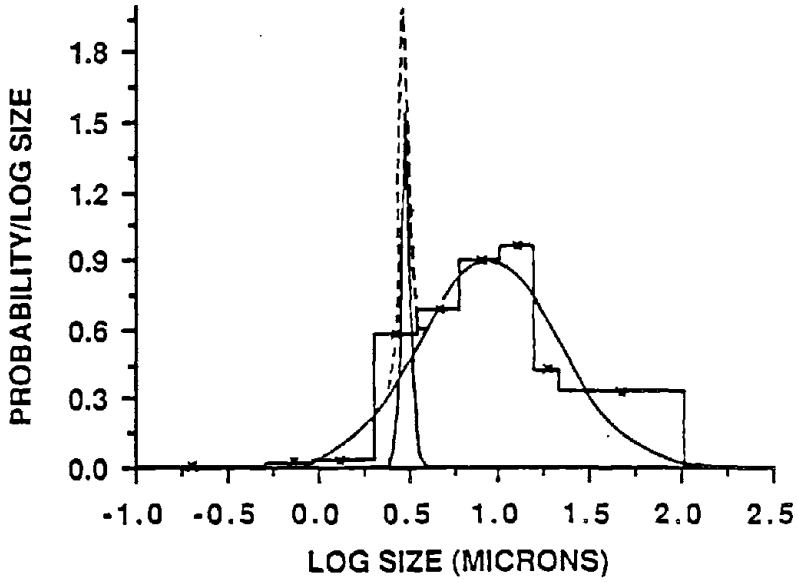

b. Lognormal Frequency Distributions.

17. Frequency Distributions of the 2XRR Samples from Section C.

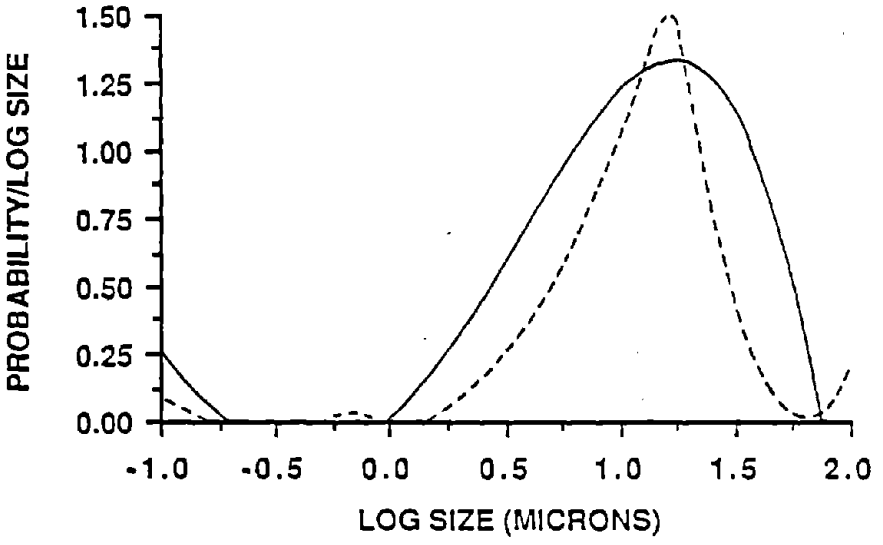

a. Empirical Frequency Distributions.

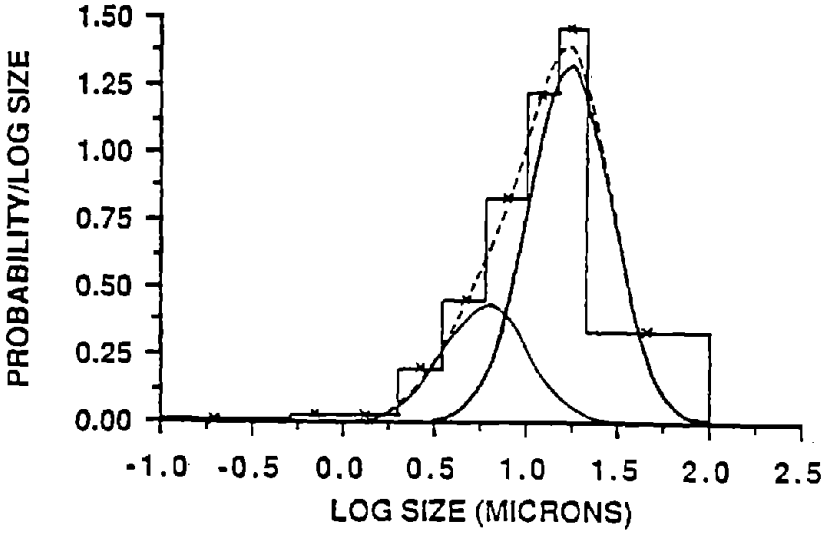

b. Lognormal Frequency Distributions.

18. Frequency Distributions of the CR1 Samples from Section D.

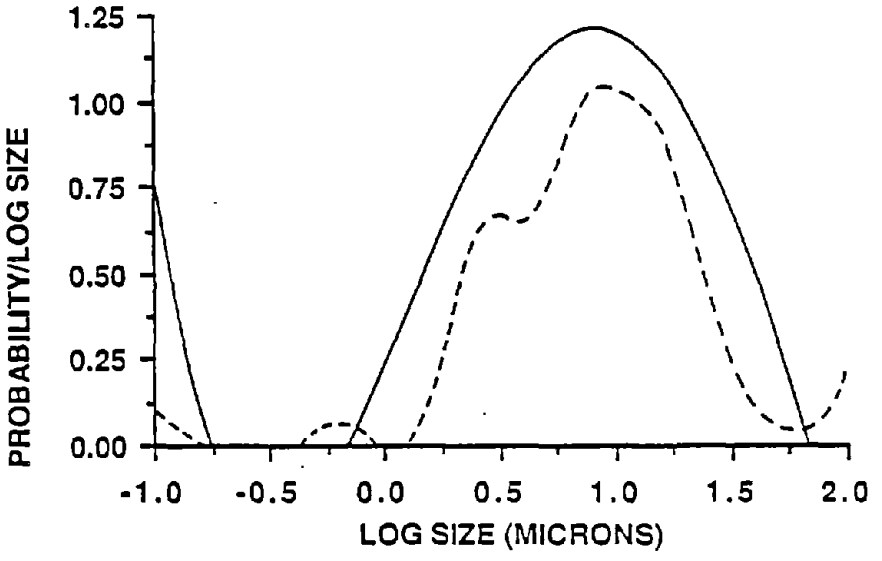

a. Empirical Frequency Distributions.

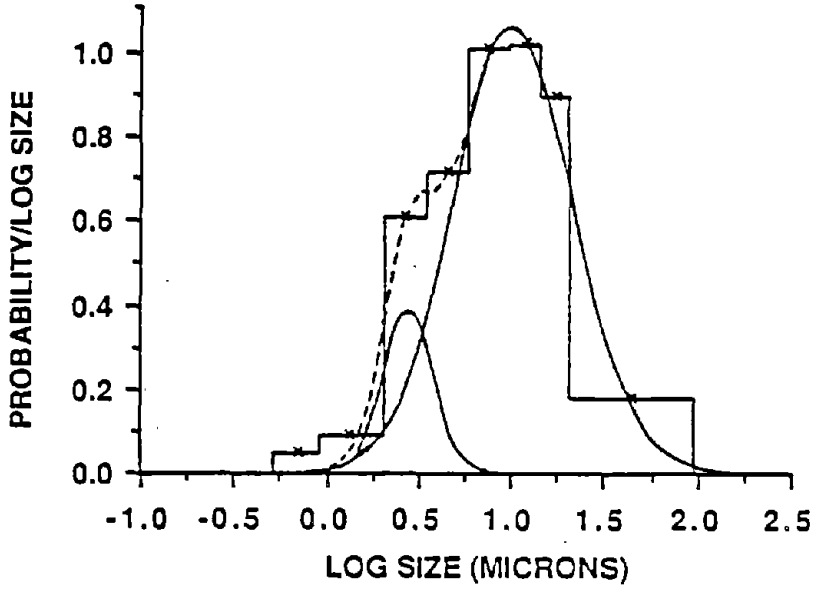

b. Lognormal Frequency Distributions.

19. Frequency Distributions of the CR2 Samples from Section D.

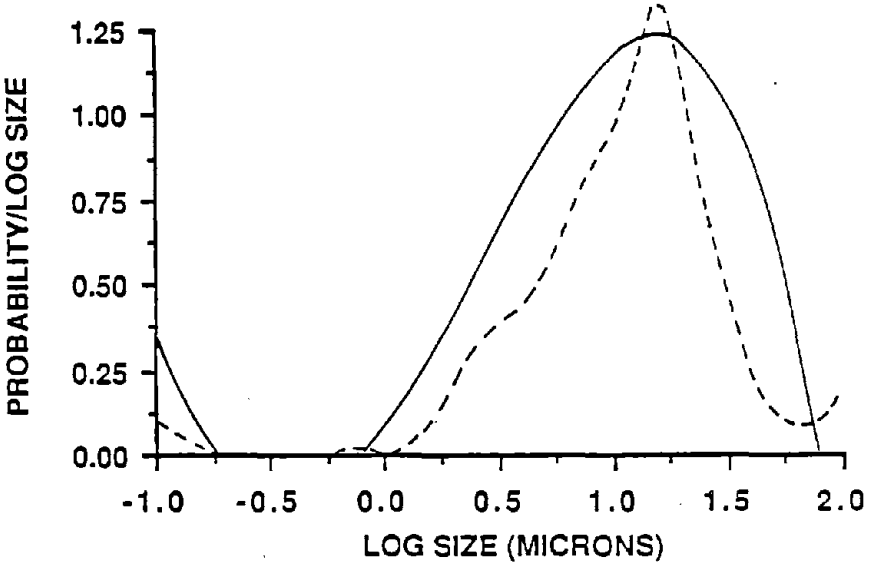

a. Empirical Frequency Distributions.

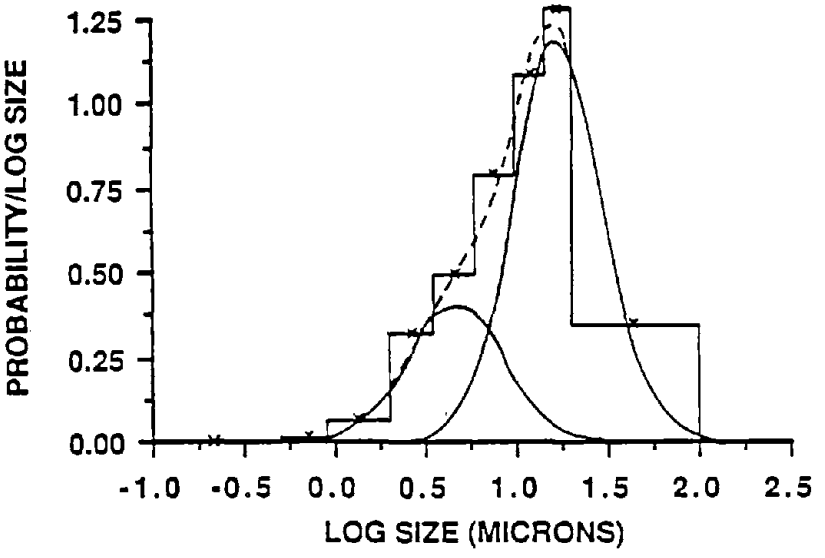

b. Lognormal Frequency Distributions.

20. Frequency Distributions of the CR1 Samples from Section E.

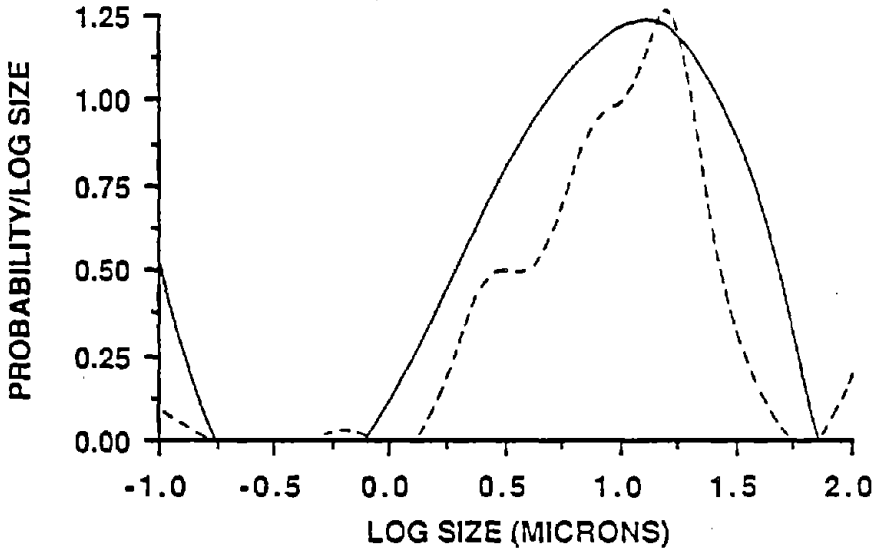

a. Empirical Frequency Distributions.

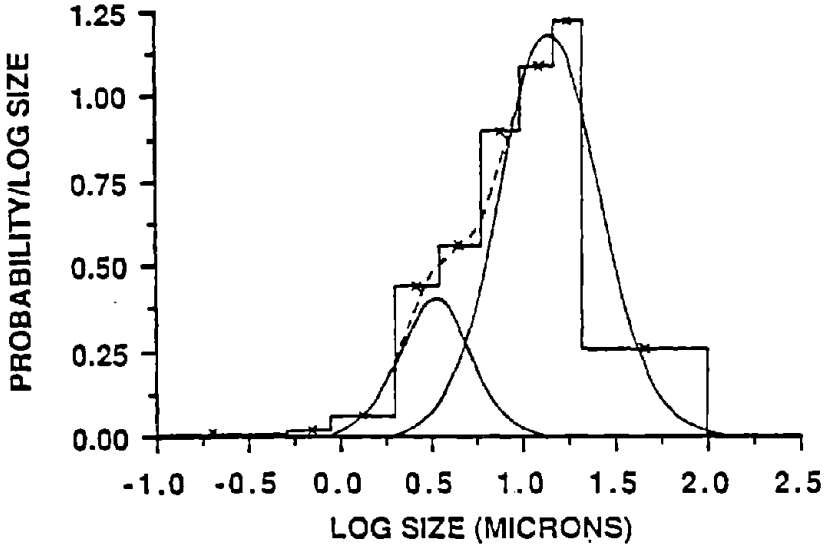

b. Lognormal Frequency Distributions.

21. Frequency Distributions of the CR2 Samples from Section E.

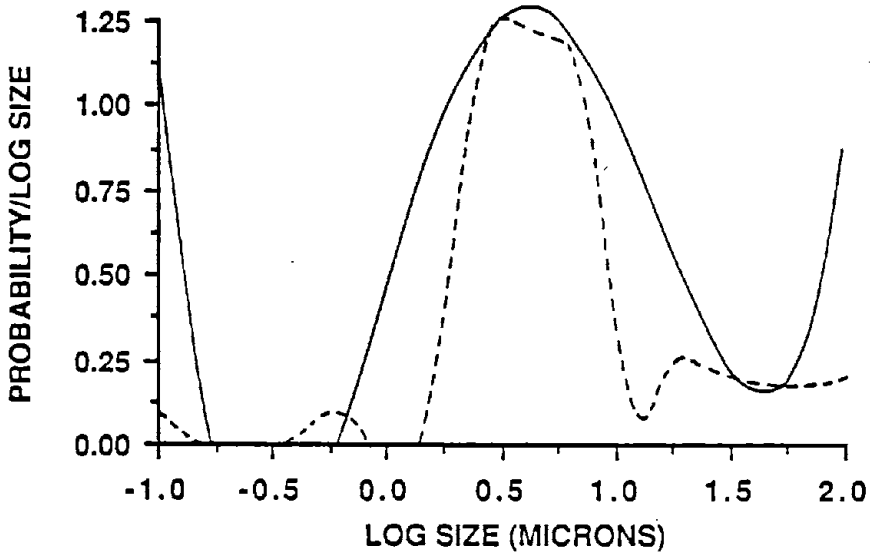

a. Empirical Frequency Distributions.

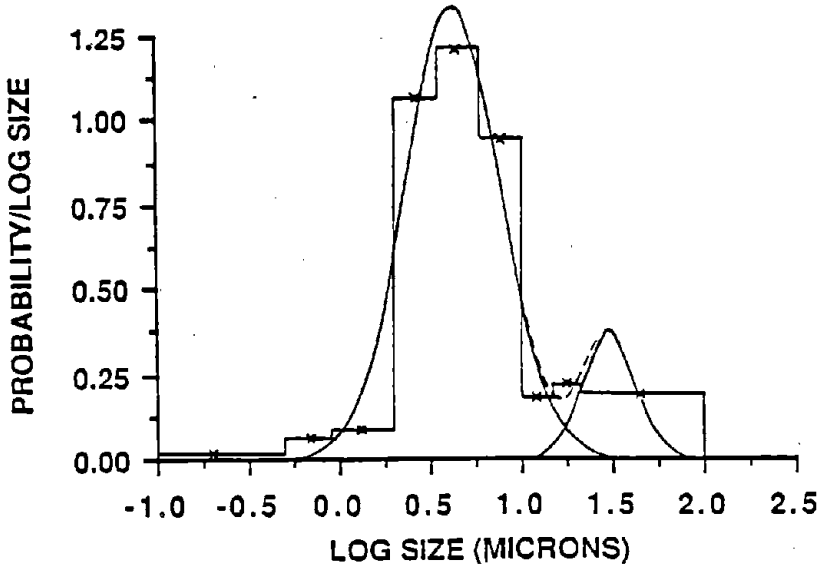

b. Lognormal Frequency Distributions.

22. Frequency Distributions of the RI Samples from Section E.

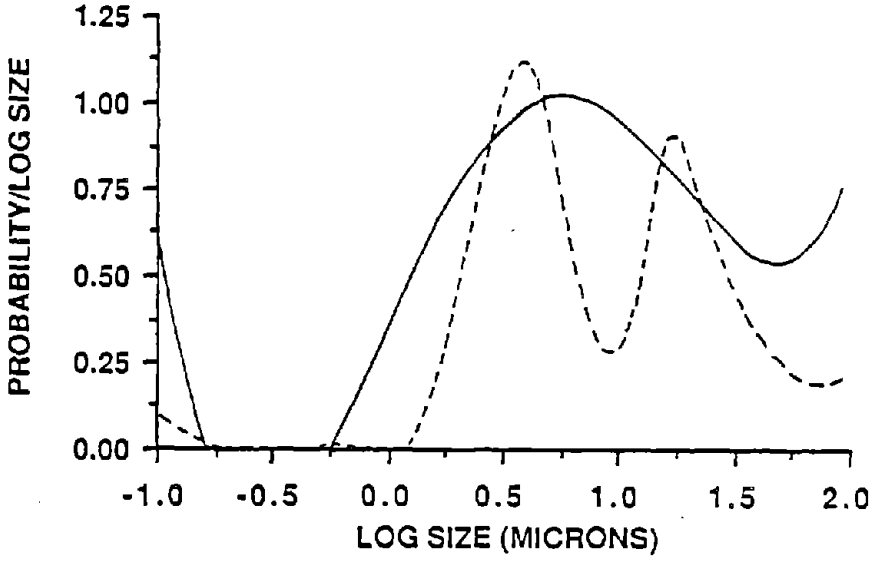

a. Empirical Frequency Distributions.

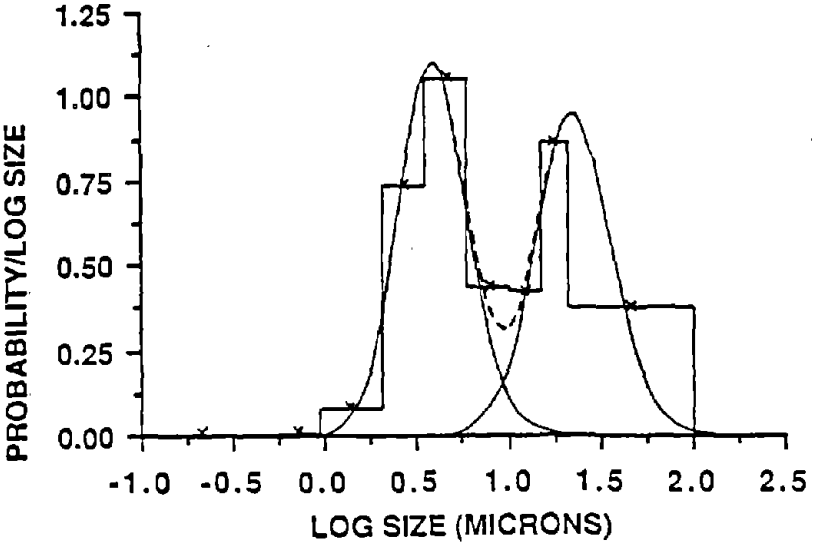

b. Lognormal Frequency Distributions.

23. Frequency Distributions of the RR Samples from Section E.

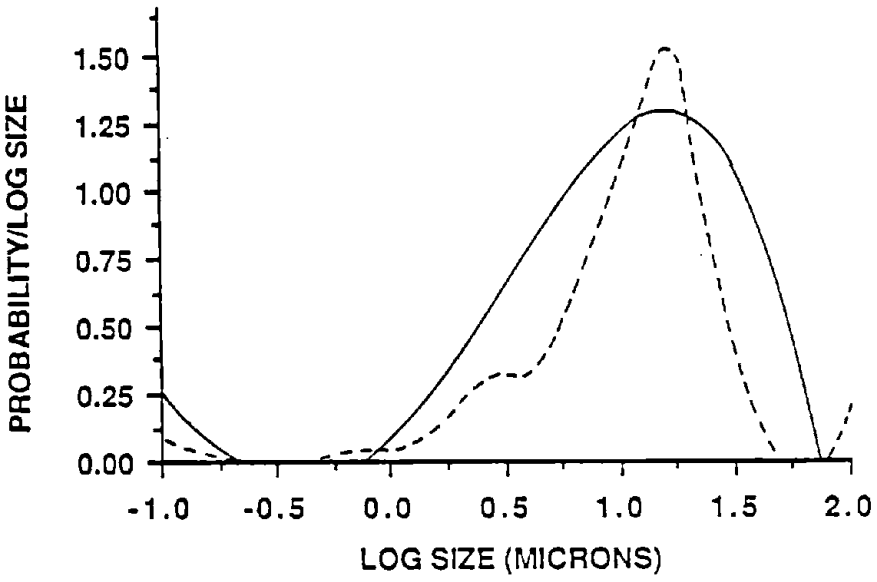

a. Empirical Frequency Distributions.

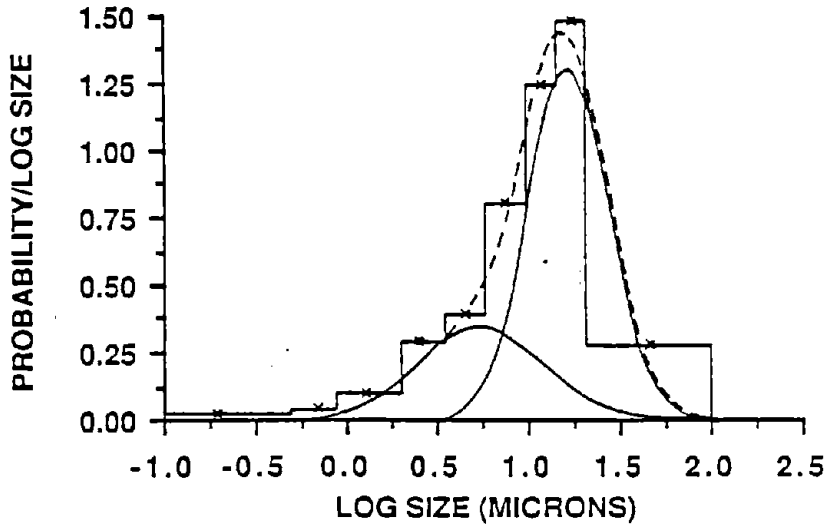

b. Lognormal Frequency Distributions.

24. Frequency Distributions of the CI Samples from Section F.

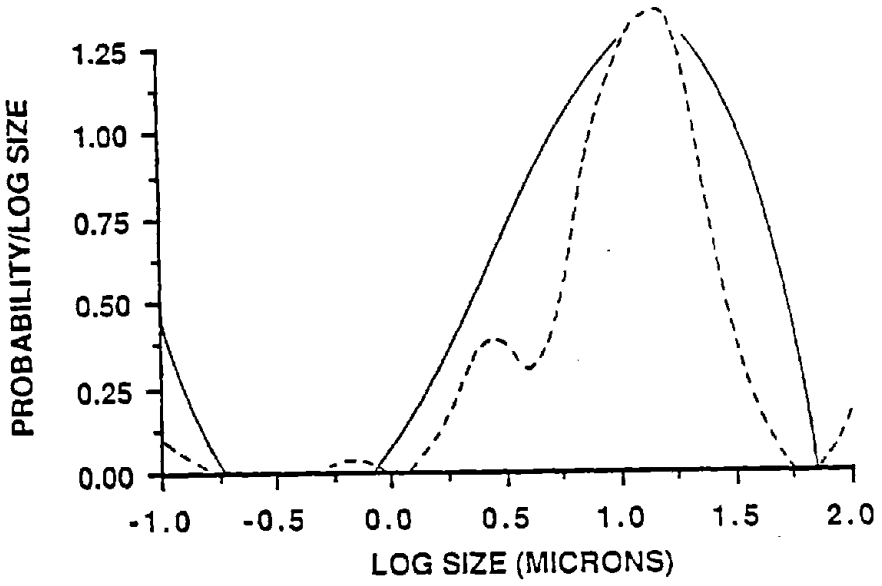

a. Empirical Frequency Distributions.

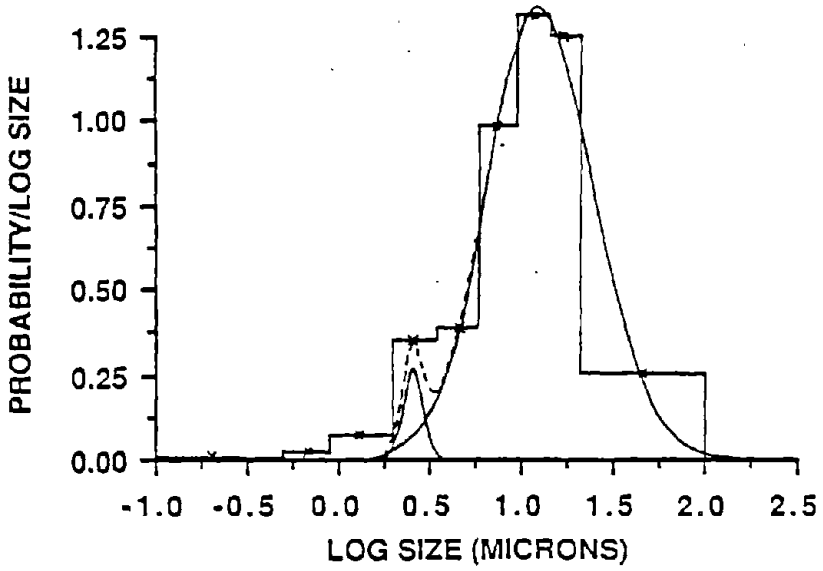

b. Lognormal Frequency Distributions.

25. Frequency Distributions of the CR Samples from Section F.

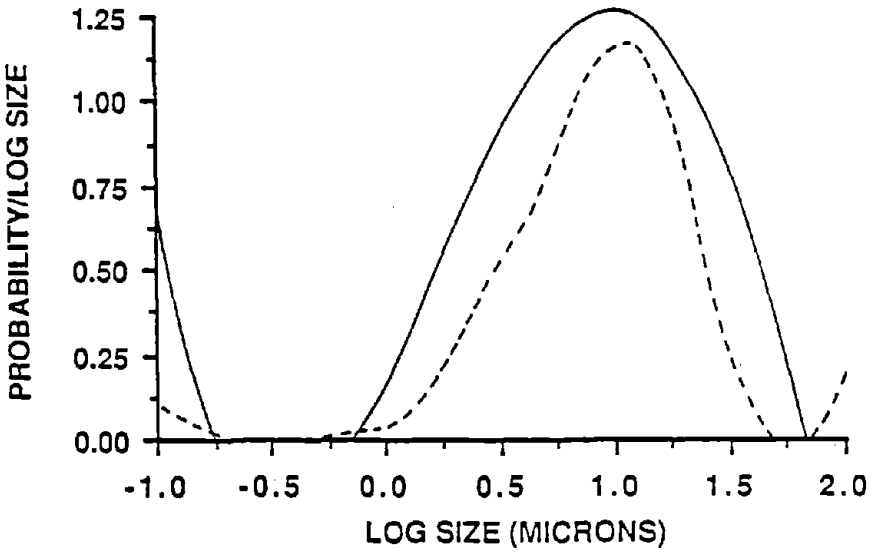

a. Empirical Frequency Distributions.

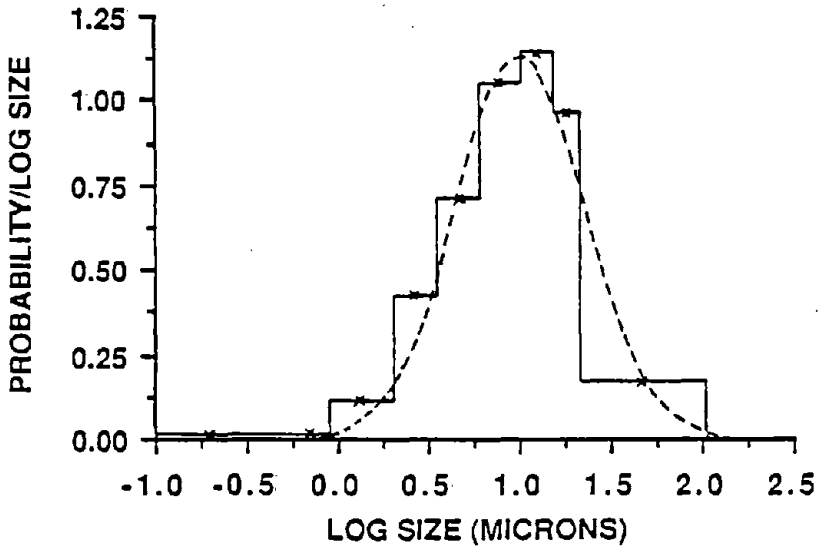

b. Lognormal Frequency Distributions.

26. Frequency Distributions of the RI Samples from Section F.

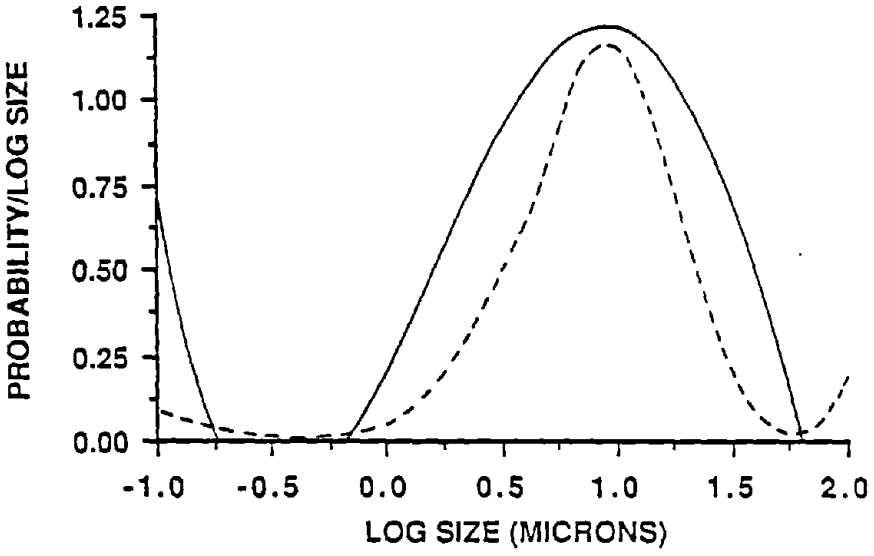

a. Empirical Frequency Distributions.

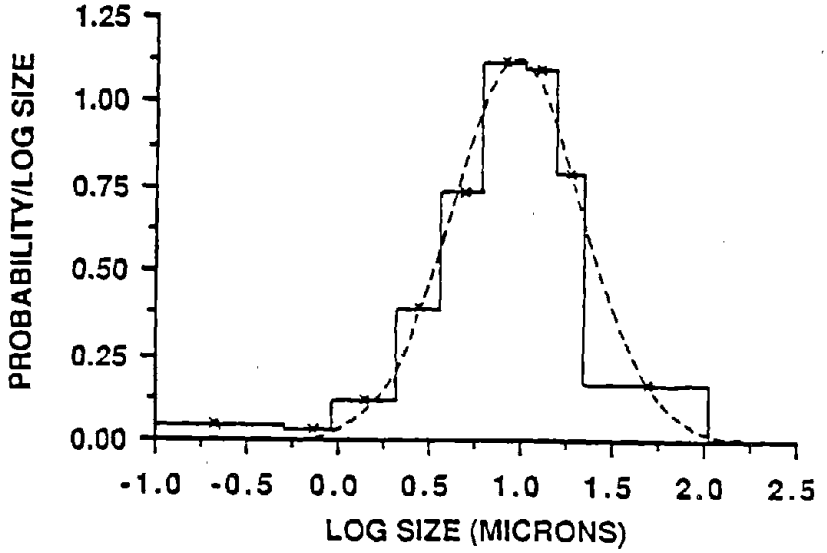

b. Lognormal Frequency Distributions.

27. Frequency Distributions of the RR Samples from Section F.

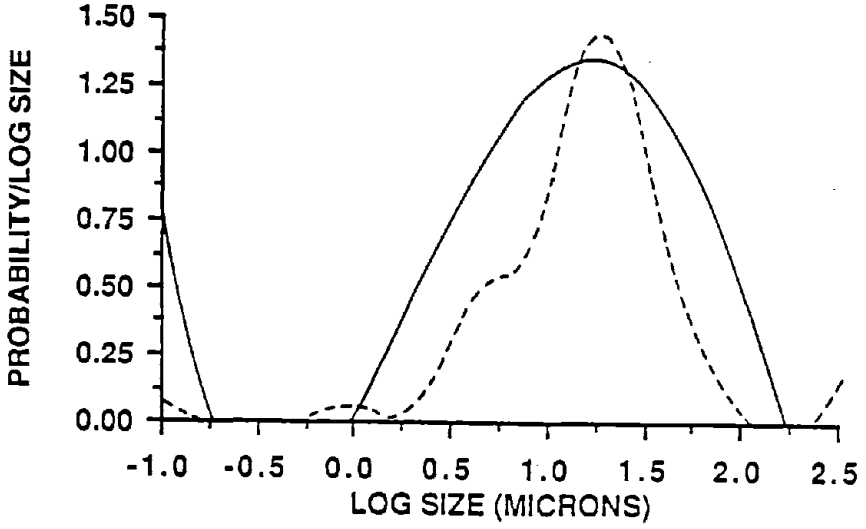

a. Empirical Frequency Distributions.

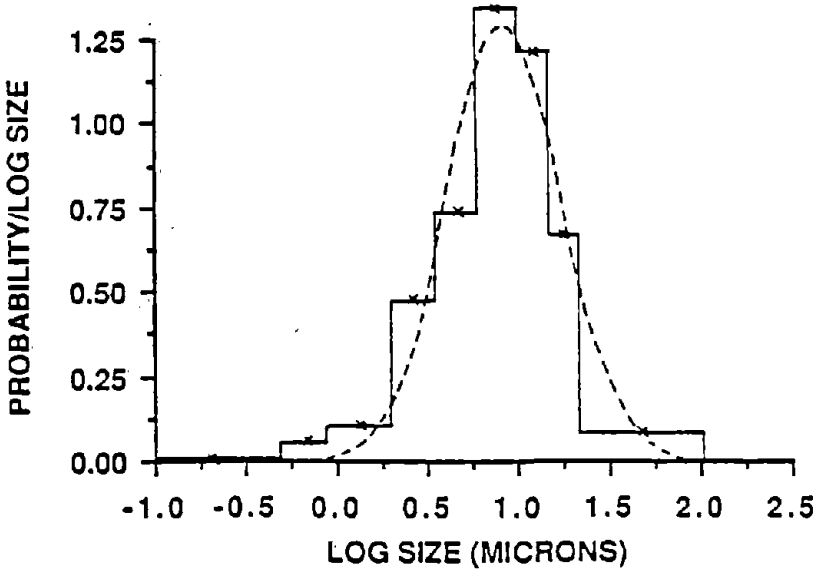

b. Lognormal Frequency Distributions.

28. Frequency Distributions of the 2X Samples from Section F.

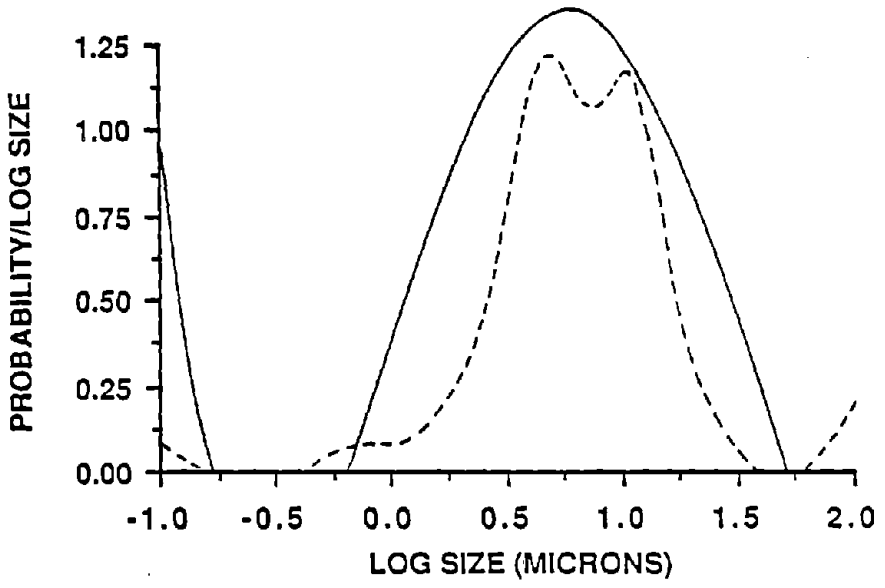

a. Empirical Frequency Distributions.

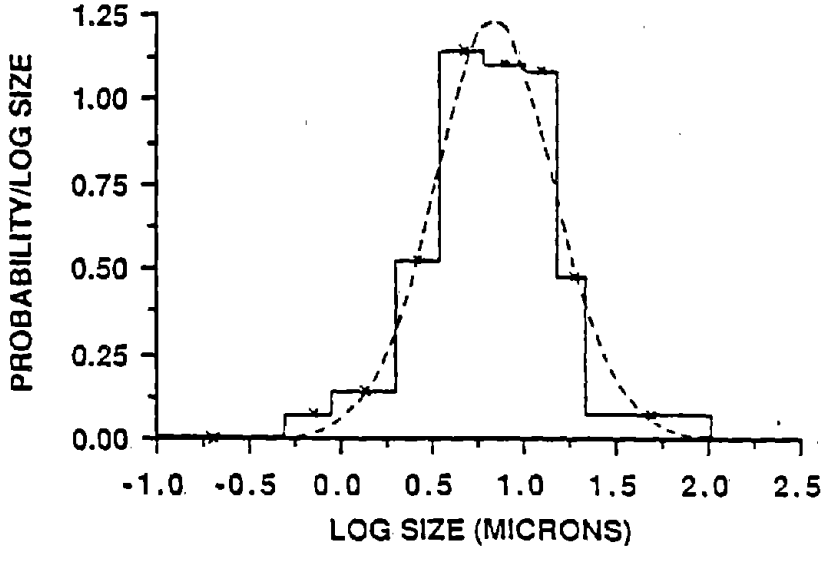

b. Lognormal Frequency Distributions.

29. Frequency Distributions of the 4X Samples from Section F.

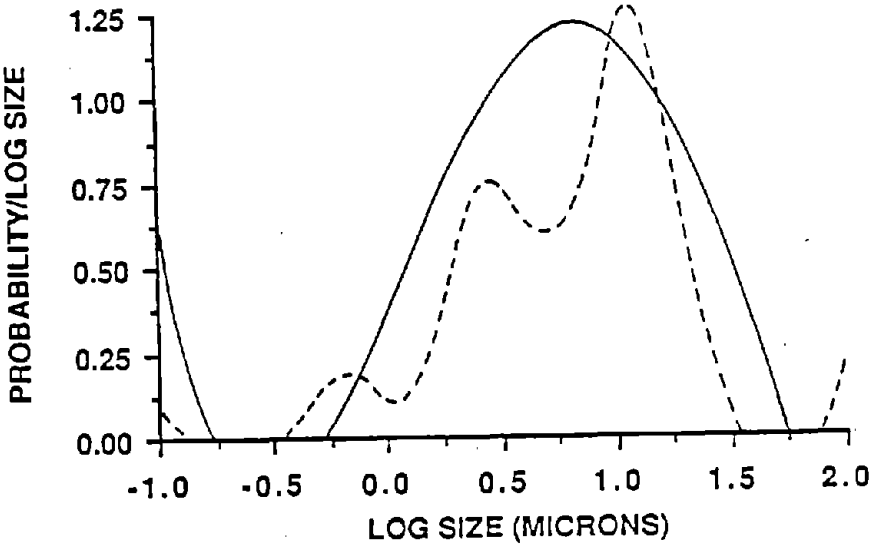

a. Empirical Frequency Distributions.

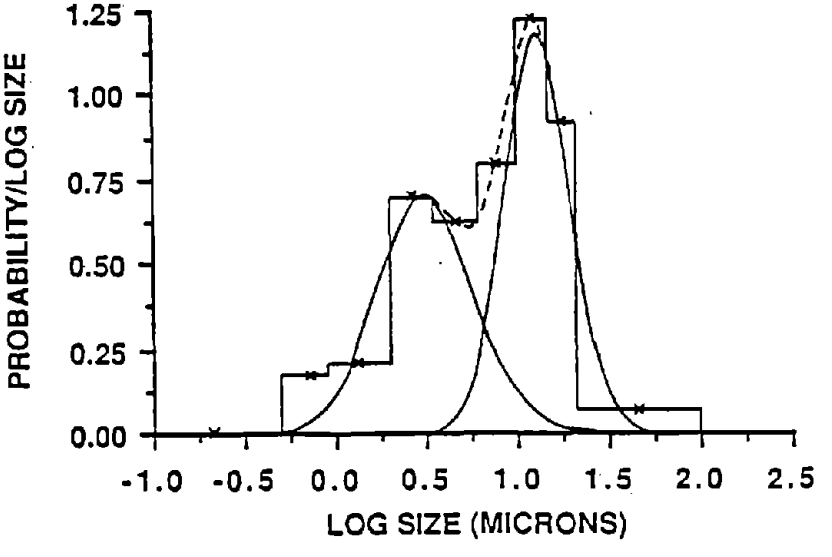

b. Lognormal Frequency Distributions.

30. Frequency Distributions of the ININ Samples from Section G.

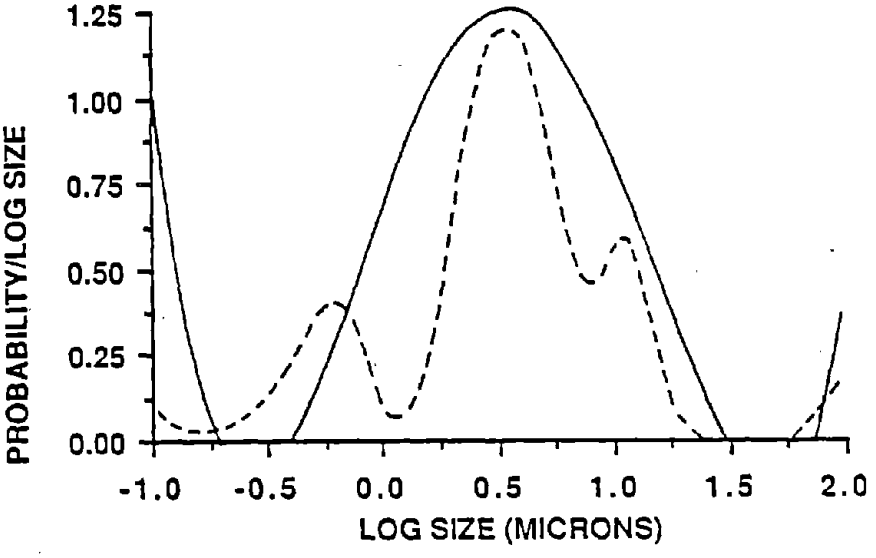

a. Empirical Frequency Distributions.

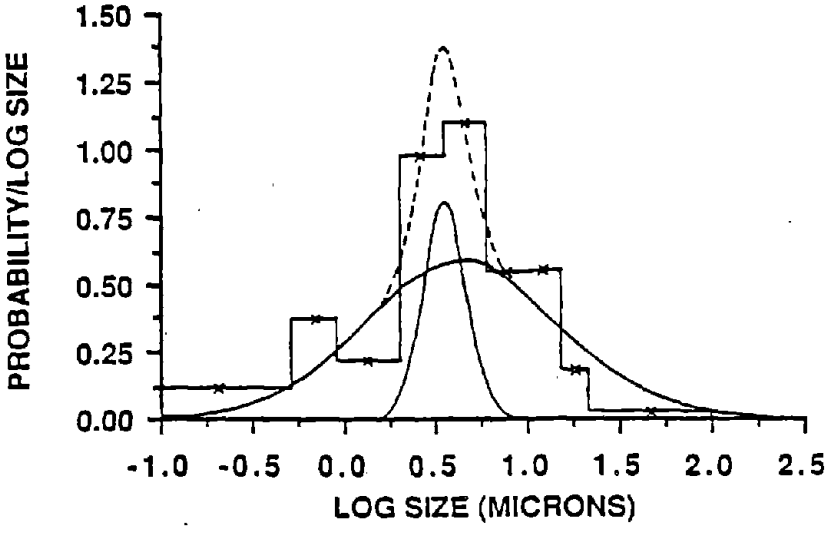

b. Lognormal Frequency Distributions.

31. Frequency Distributions of the INOUT Samples from Section G.

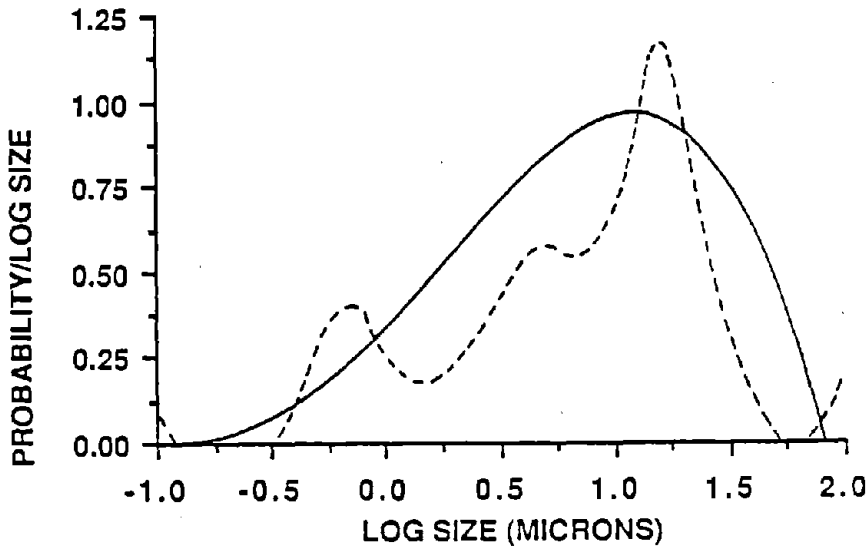

a. Empirical Frequency Distributions.

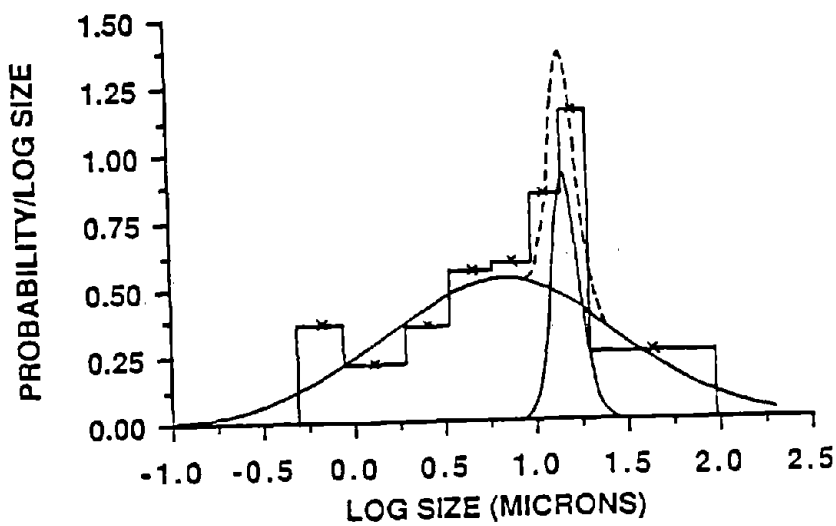

b. Lognormal Frequency Distributions.

32. Frequency Distributions of the CI Samples from Section G.

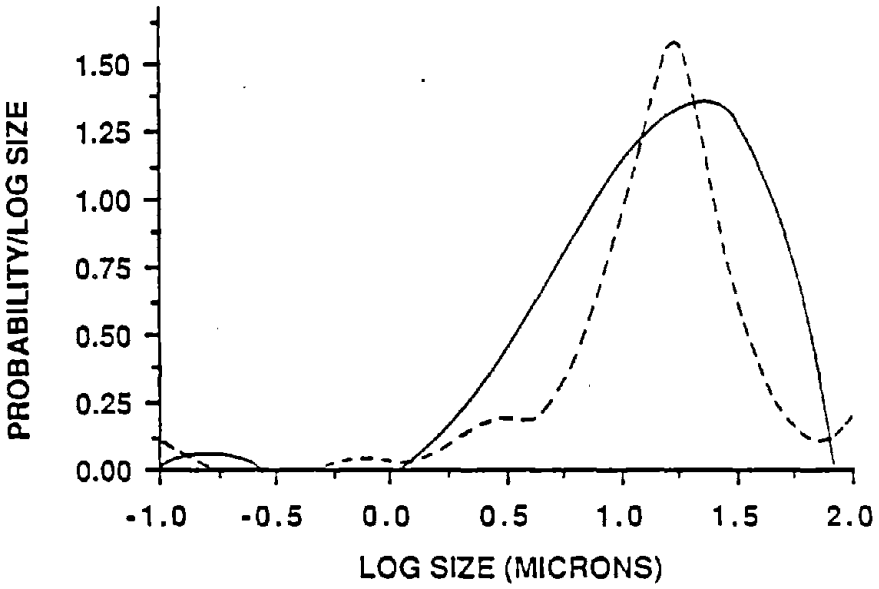

a. Empirical Frequency Distributions.

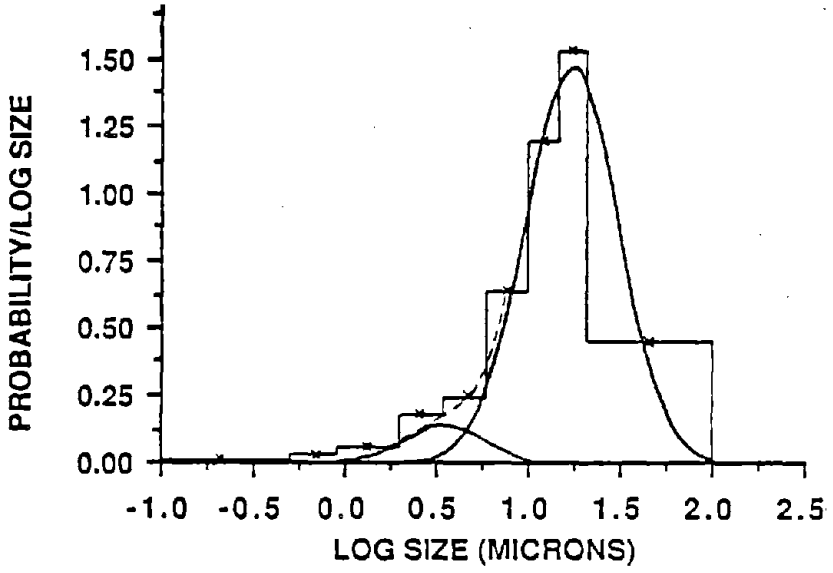

b. Lognormal Frequency Distributions.

33. Frequency Distributions of the CR1 Samples from Section G.

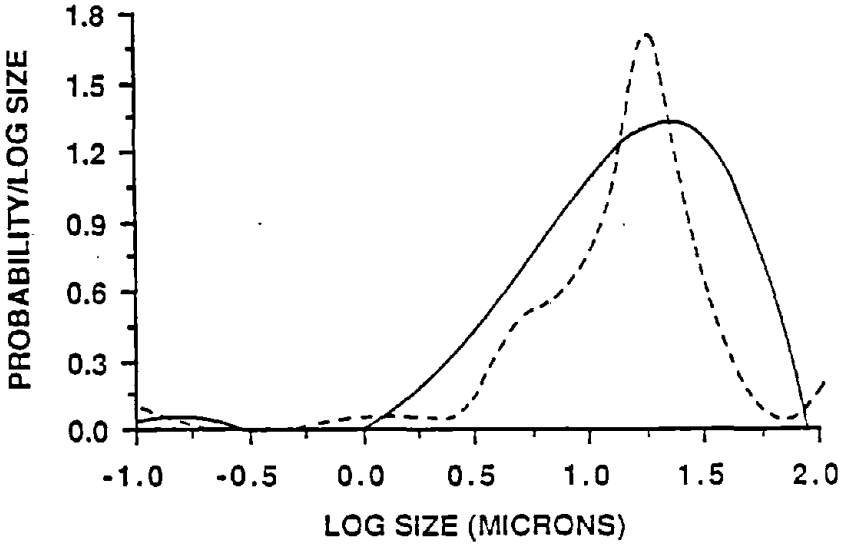

a. Empirical Frequency Distributions.

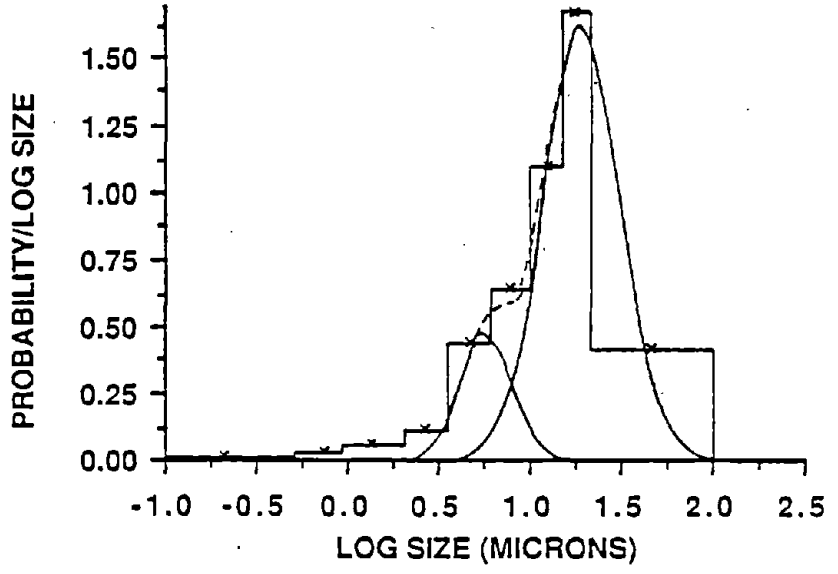

b. Lognormal Frequency Distributions.

34. Frequency Distributions of the CR2 Samples from Section G.

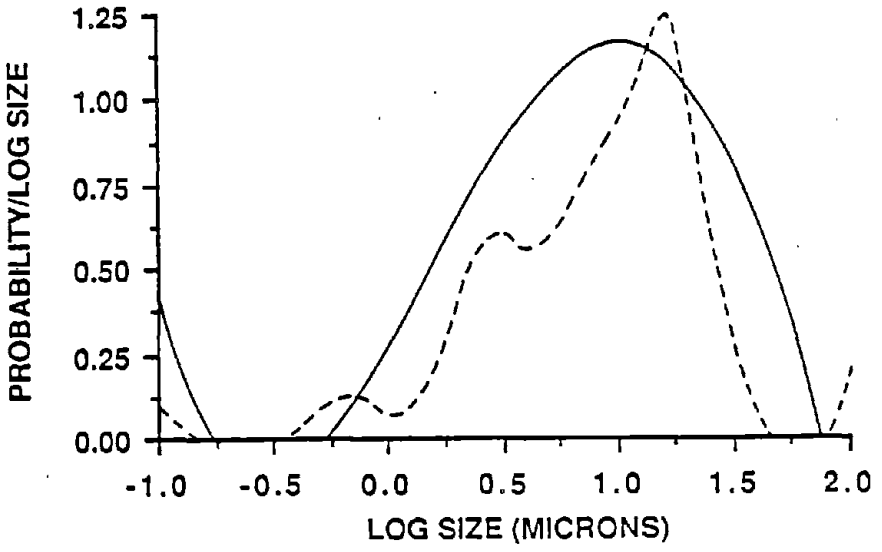

a. Empirical Frequency Distributions.

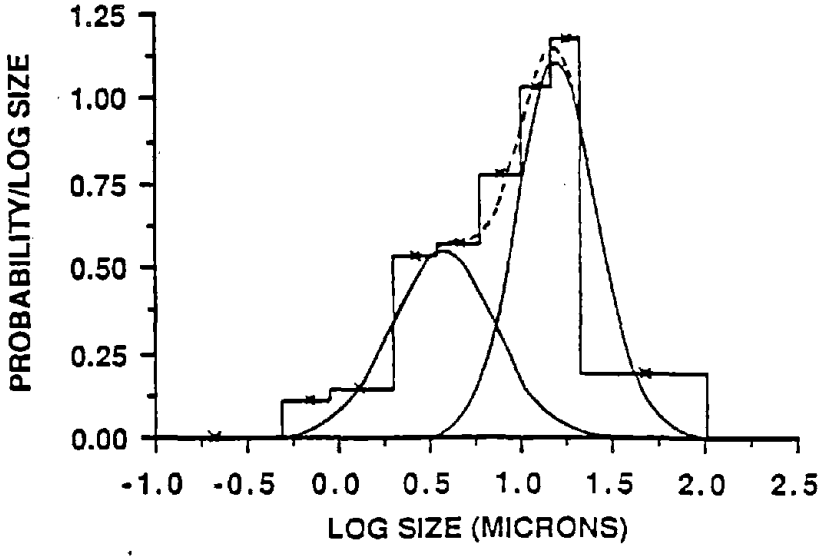

b. Lognormal Frequency Distributions.

35. Frequency Distributions of the RI Samples from Section G.

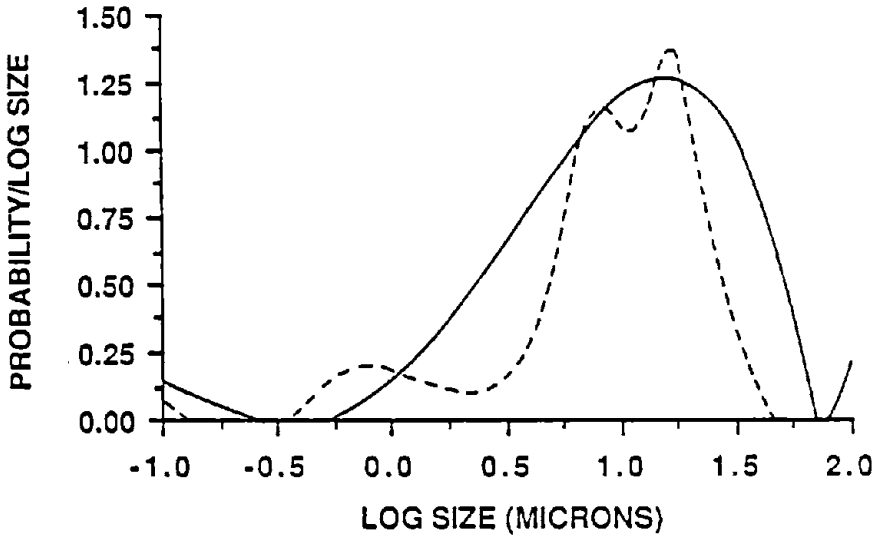

a. Empirical Frequency Distributions.

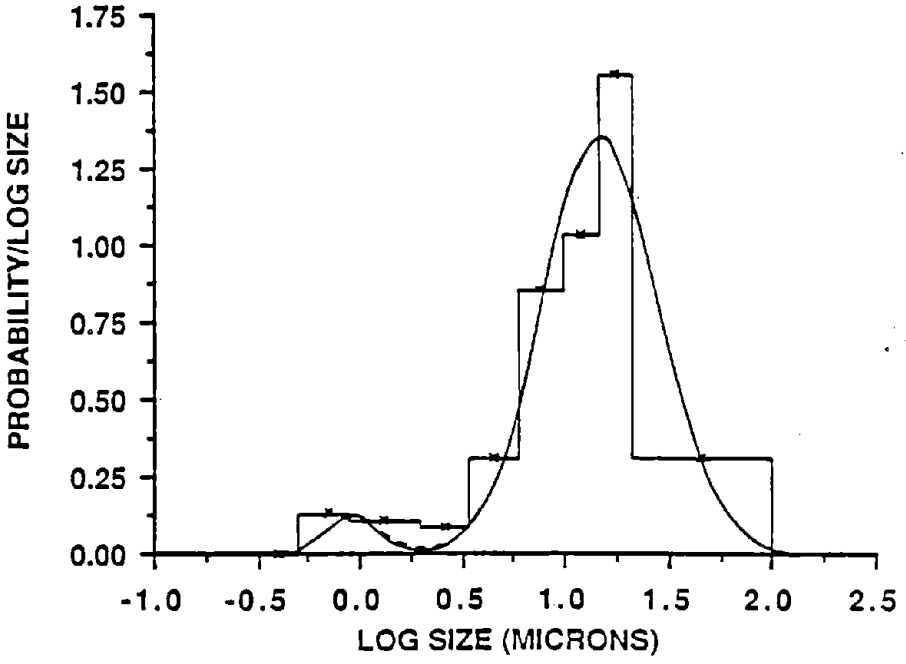

b. Lognormal Frequency Distributions.

36. Frequency Distributions of the RR Samples from Section G.

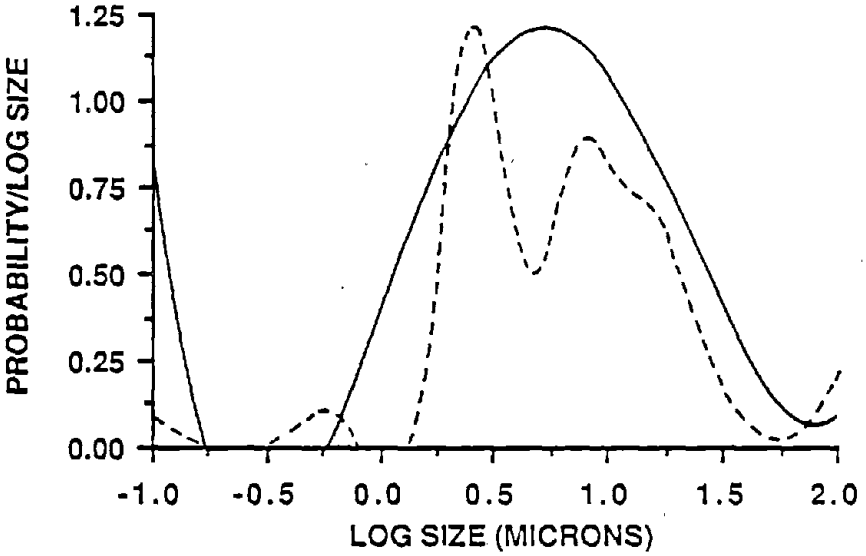

a. Empirical Frequency Distributions.

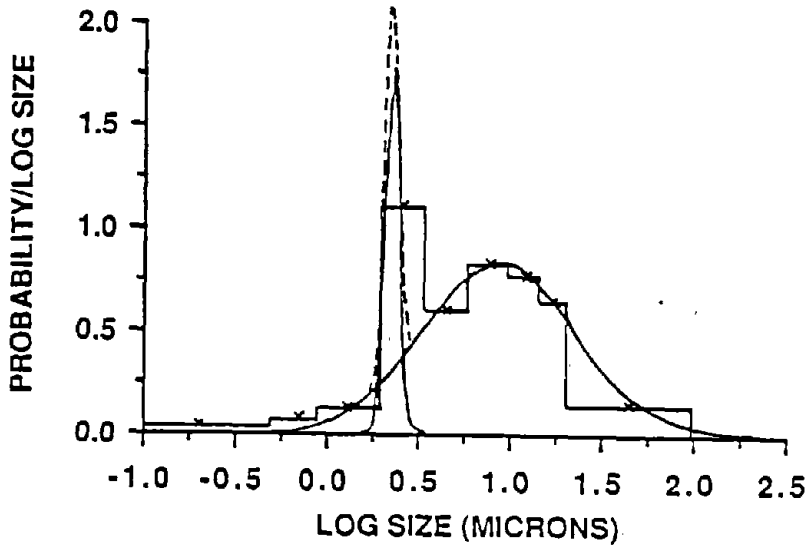

b. Lognormal Frequency Distributions.

37. Frequency Distributions of the CI Samples from Section H.

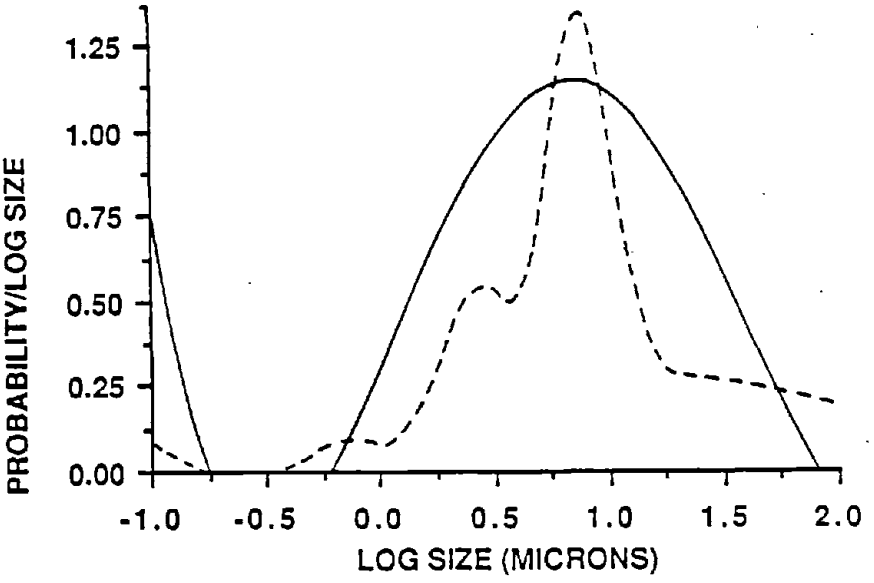

a. Empirical Frequency Distributions.

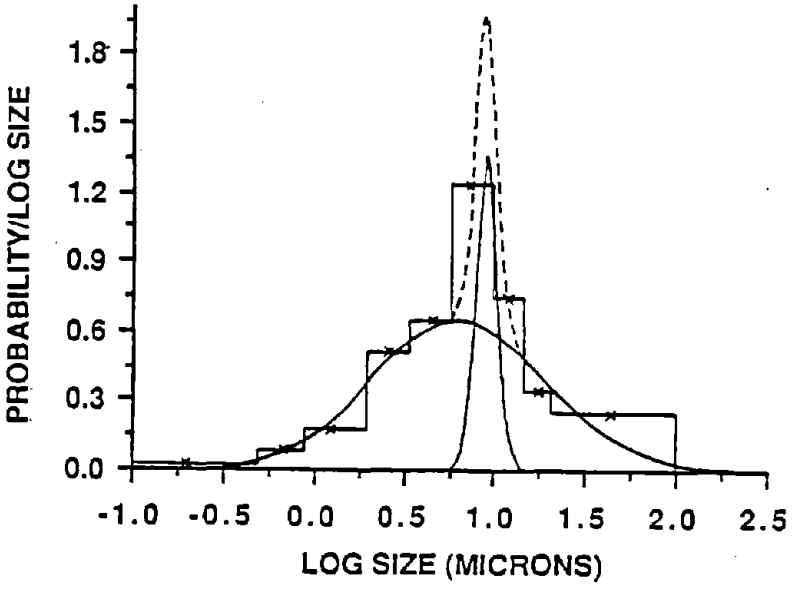

b. Lognormal Frequency Distributions.

38. Frequency Distributions of the CR Samples from Section H.

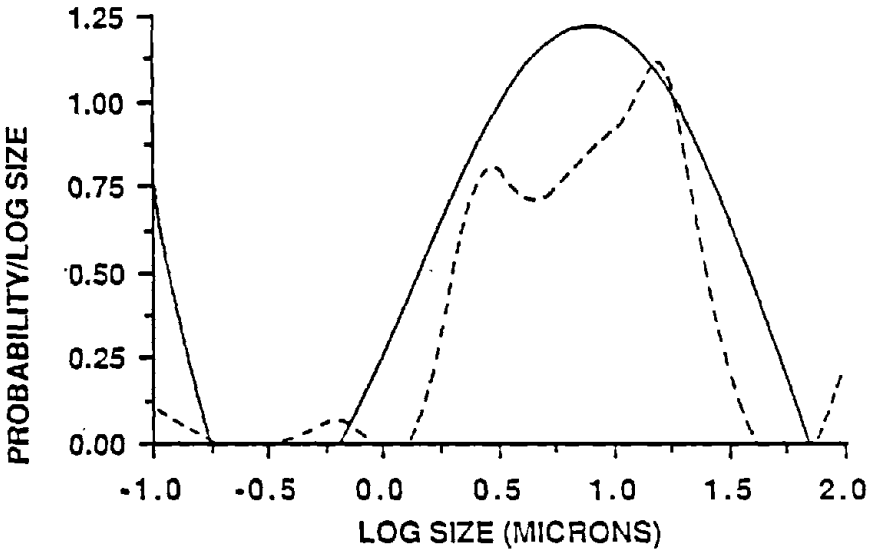

a. Empirical Frequency Distributions.

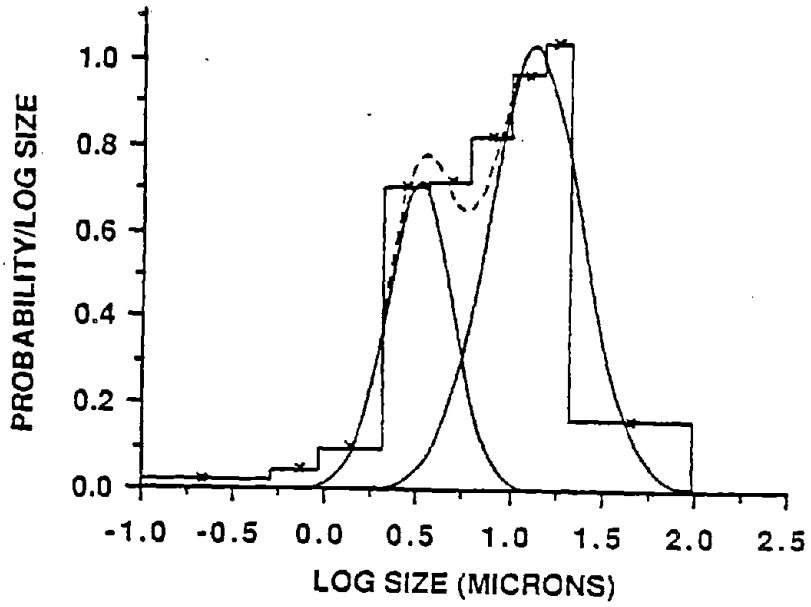

b. Lognormal Frequency Distributions.

39. Frequency Distributions of the 2X Samples from Section H.

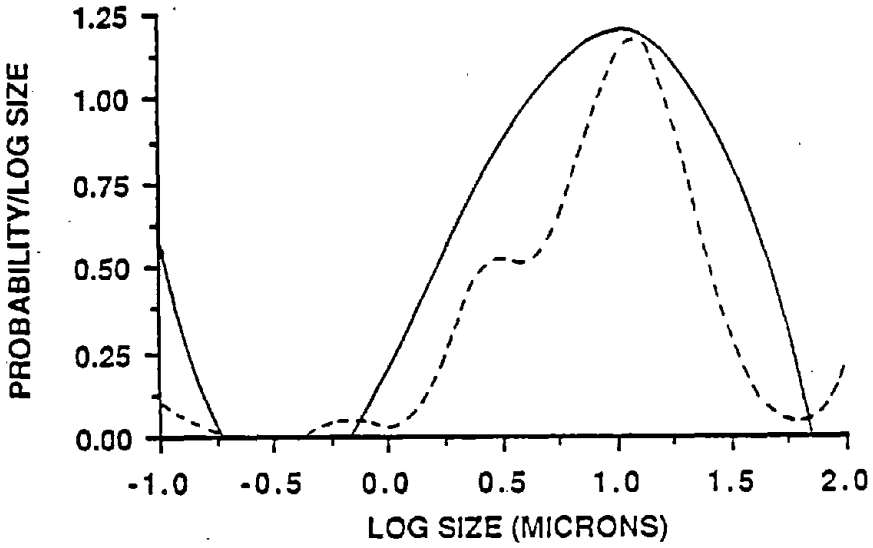

a. Empirical Frequency Distributions.

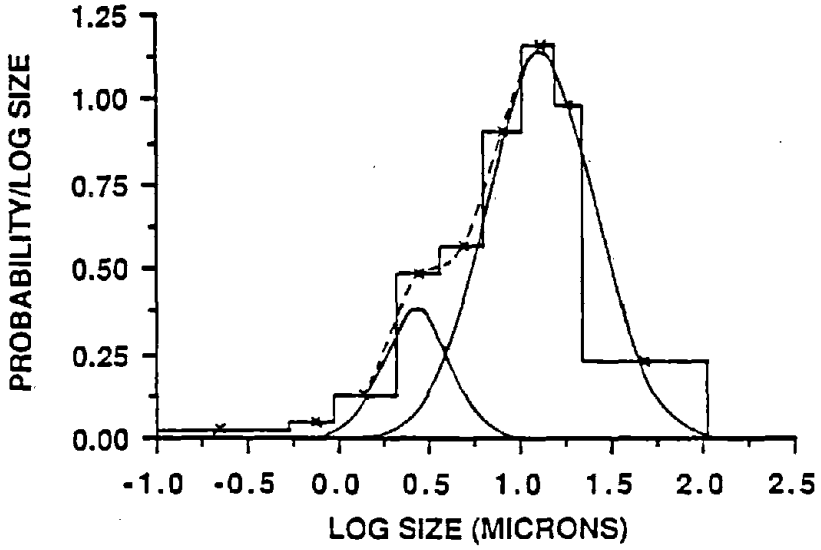

b. Lognormal Frequency Distributions.

40. Frequency Distributions of the 4X Samples from Section H.

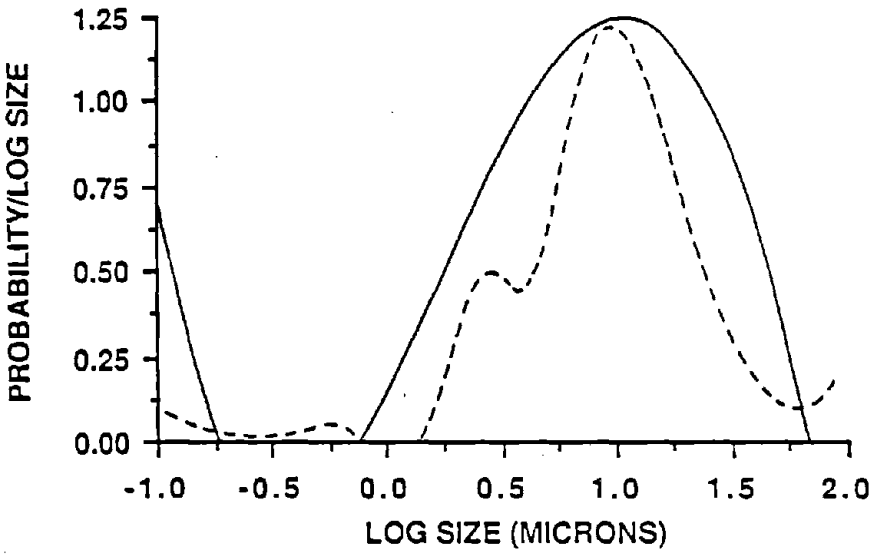

a. Empirical Frequency Distributions.

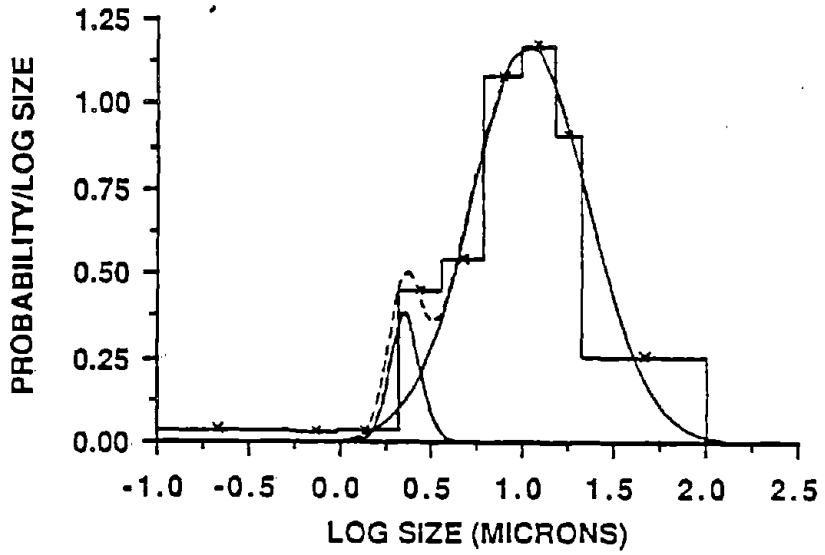

b. Lognormal Frequency Distributions.

41. Frequency Distributions of the CI Samples from Section I.

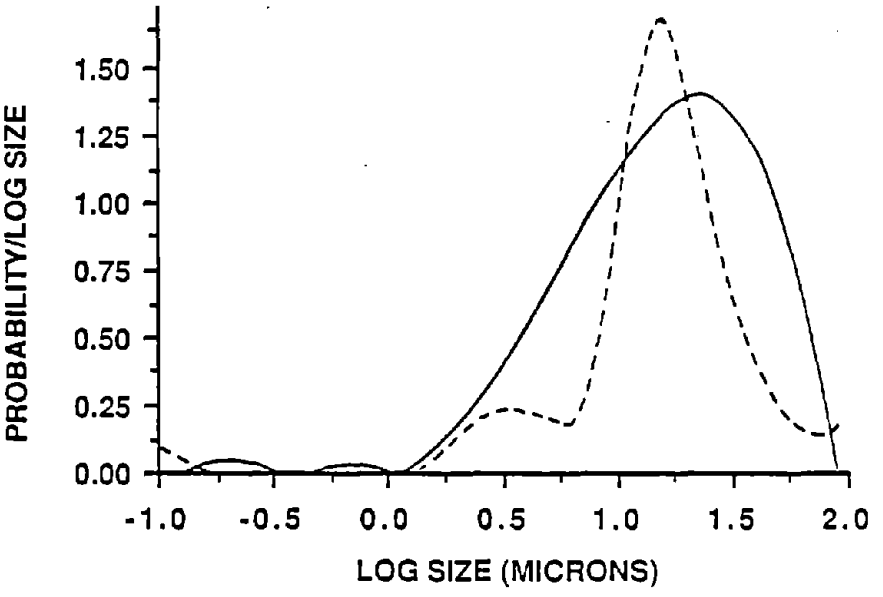

a. Empirical Frequency Distributions.

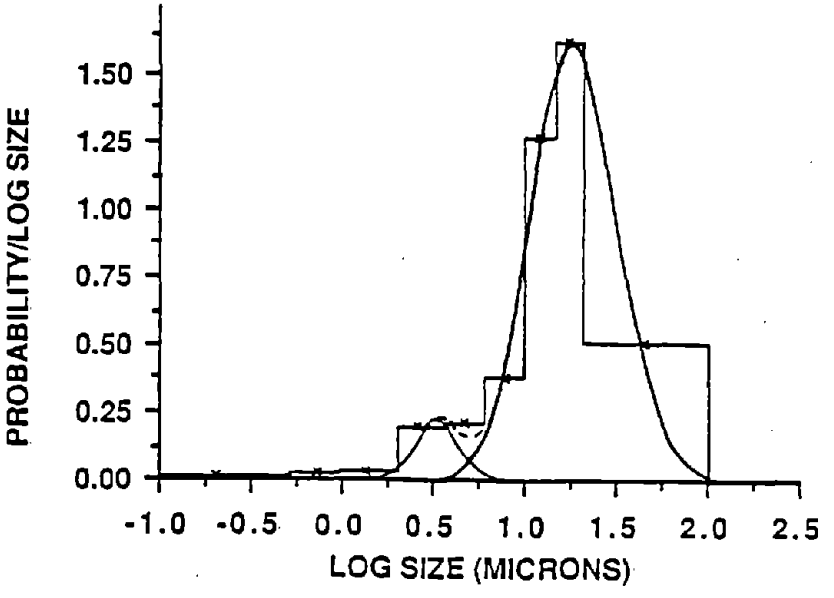

b. Lognormal Frequency Distributions.

42. Frequency Distributions of the CR1 Samples from Section I.

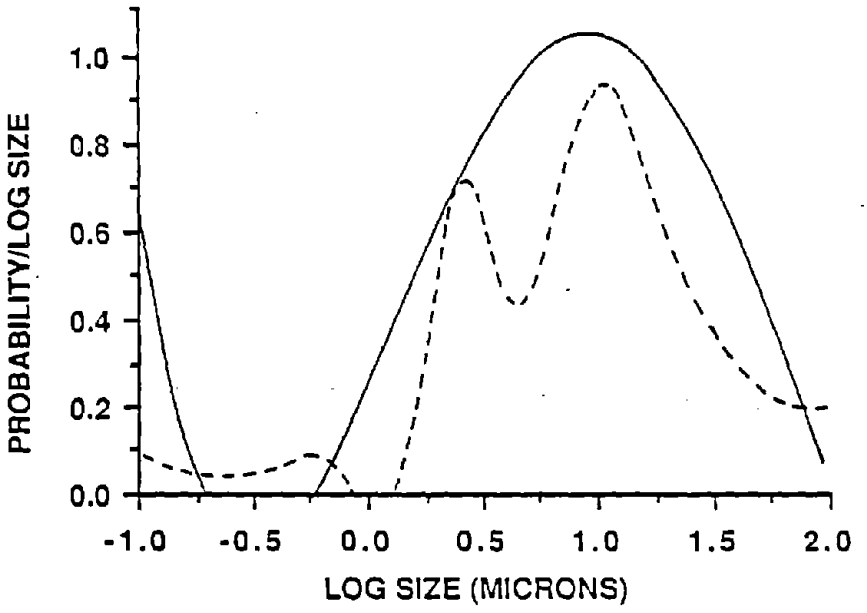

a. Empirical Frequency Distributions.

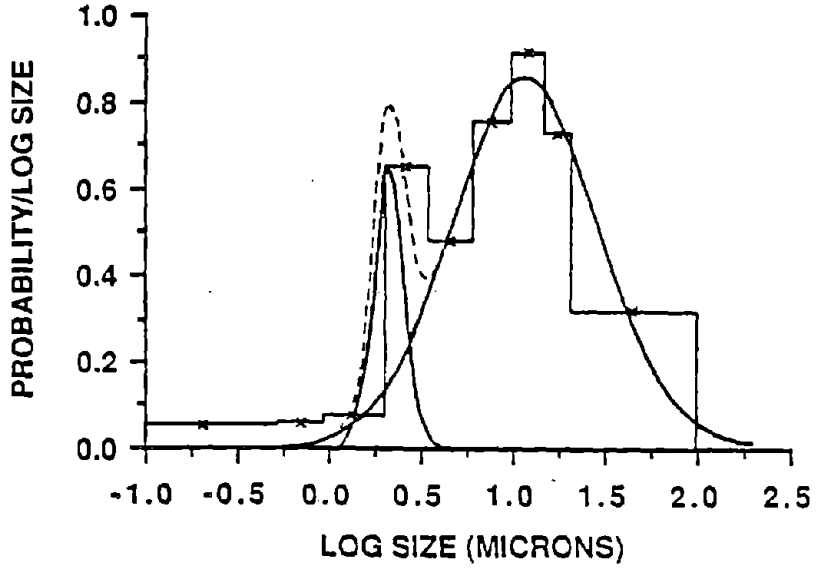

b. Lognormal Frequency Distributions.

43. Frequency Distributions of the CR2 Samples from Section I.

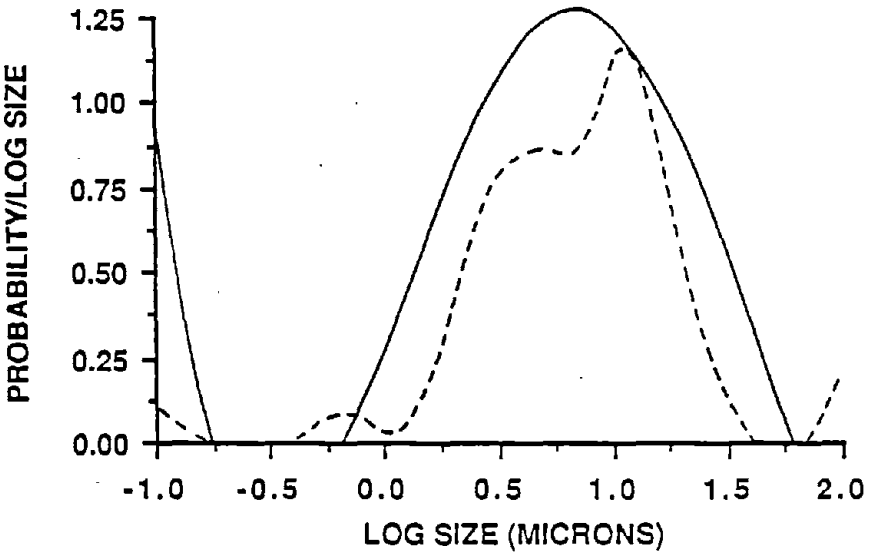

a. Empirical Frequency Distributions.

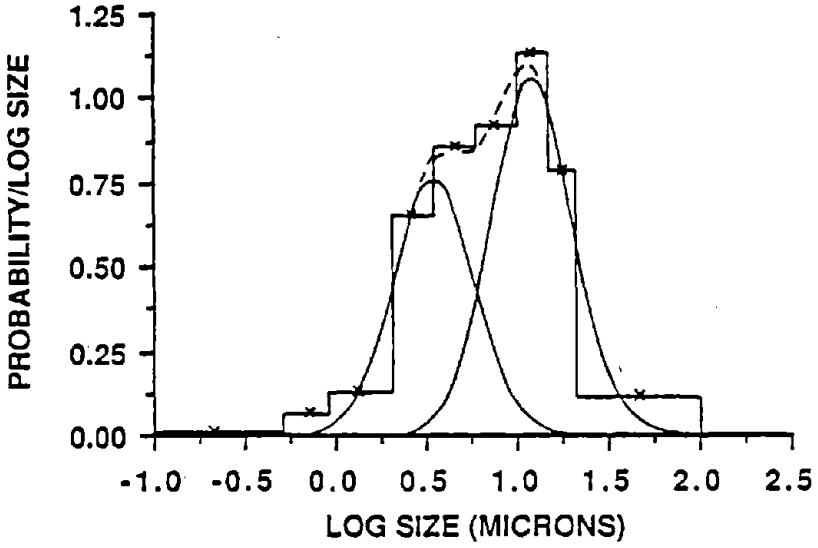

b. Lognormal Frequency Distributions.

44. Frequency Distributions of the 2X Samples from Section I.

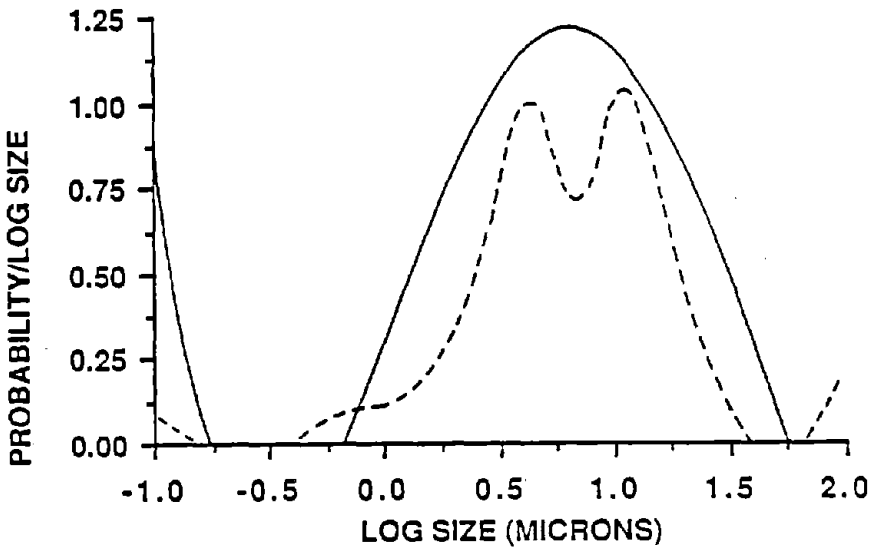

a. Empirical Frequency Distributions.

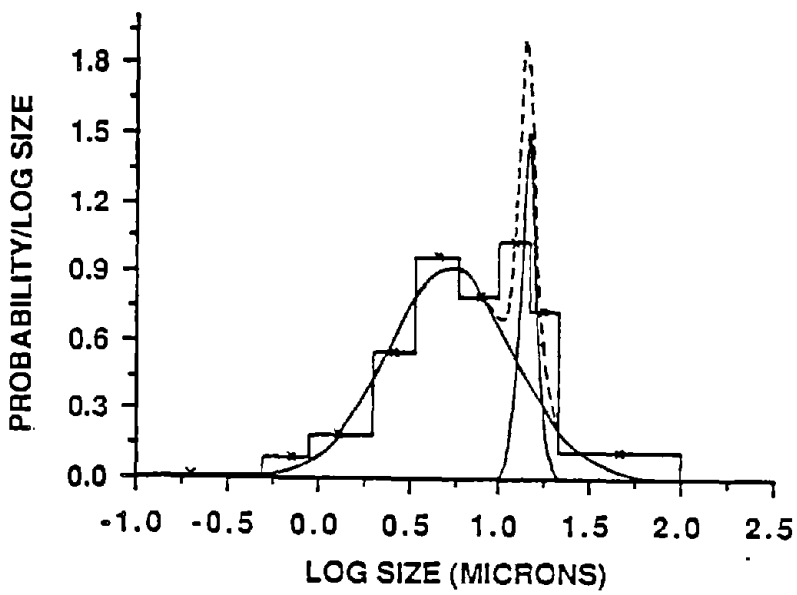

b. Lognormal Frequency Distributions.

45. Frequency Distributions of the 4X Samples from Section I.

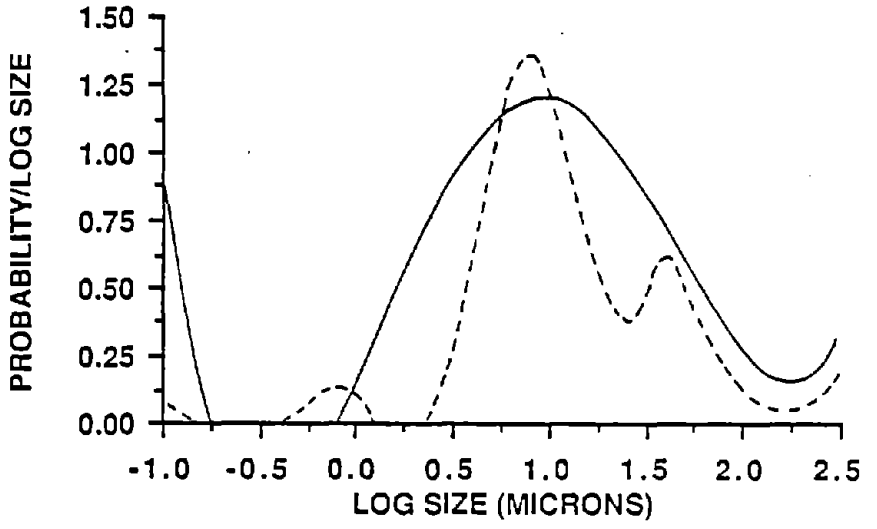

a. Empirical Frequency Distributions.

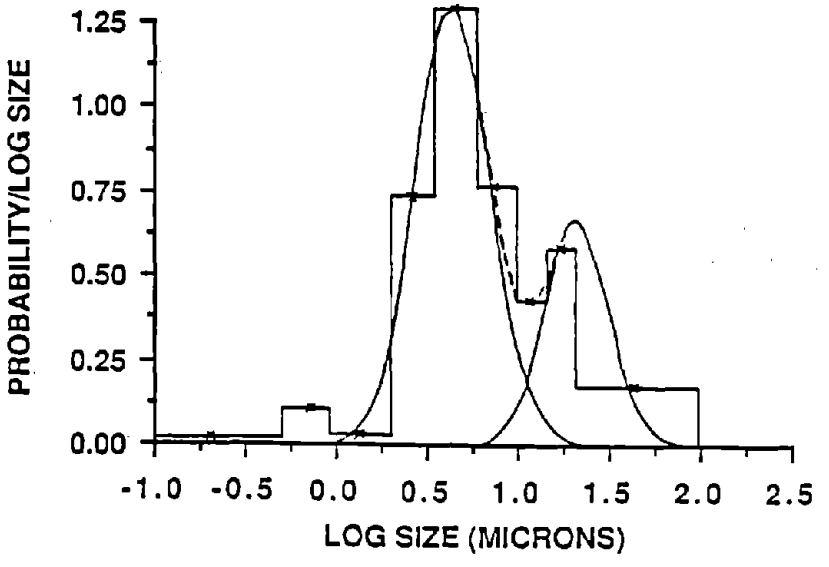

b. Lognormal Frequency Distributions.

46. Frequency Distributions of the CI Samples from Section J.

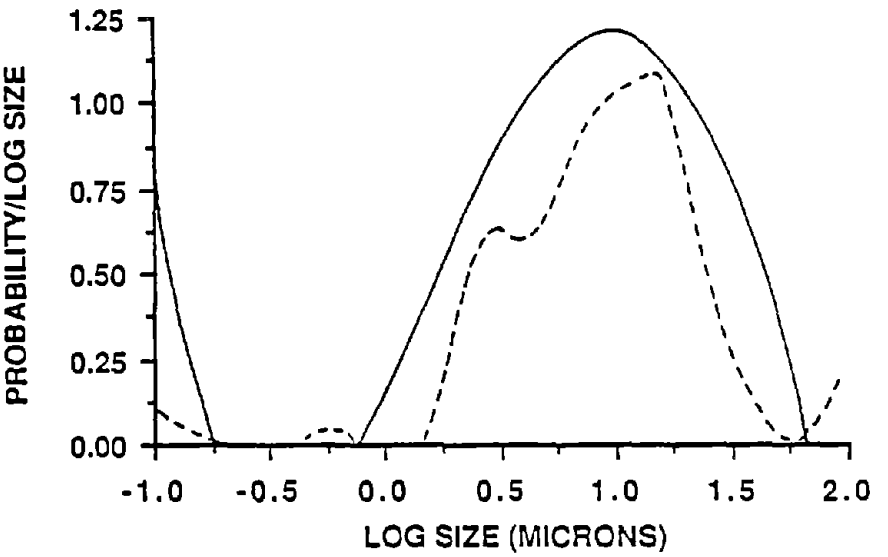

a. Empirical Frequency Distributions.

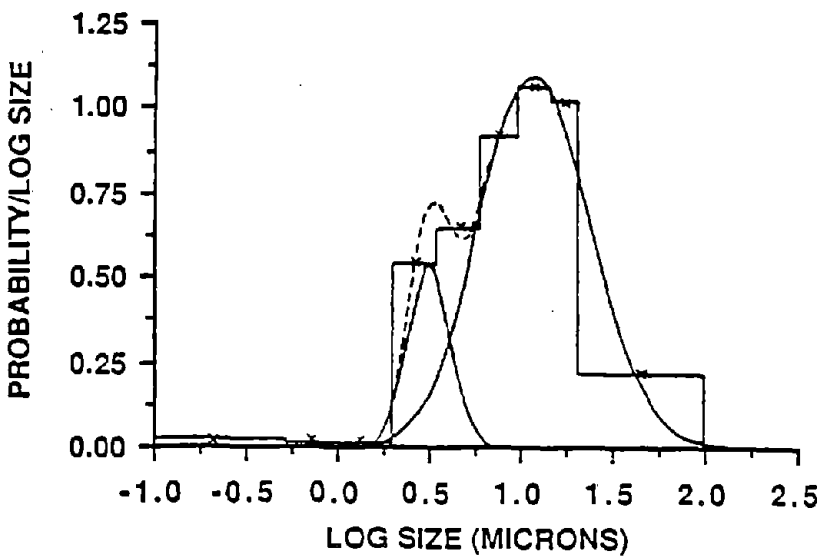

b. Lognormal Frequency Distributions.

47. Frequency Distributions of the 2X Samples from Section J.

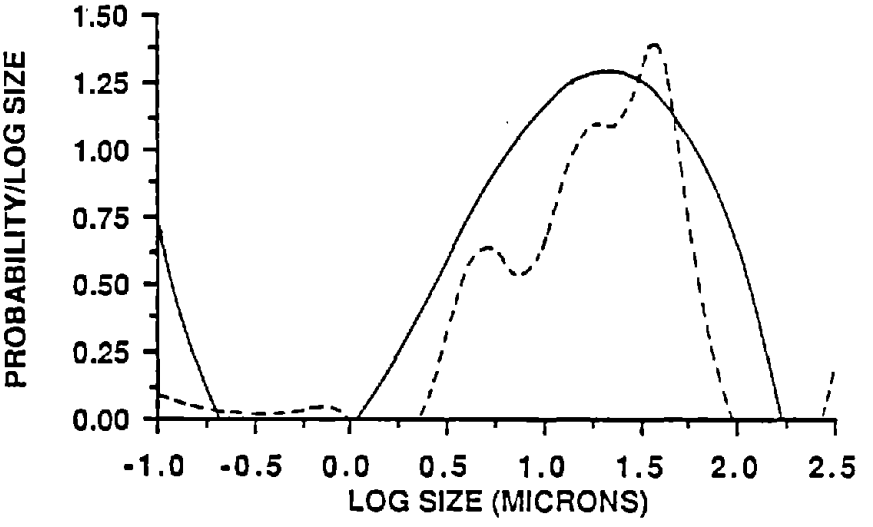

a. Empirical Frequency Distributions.

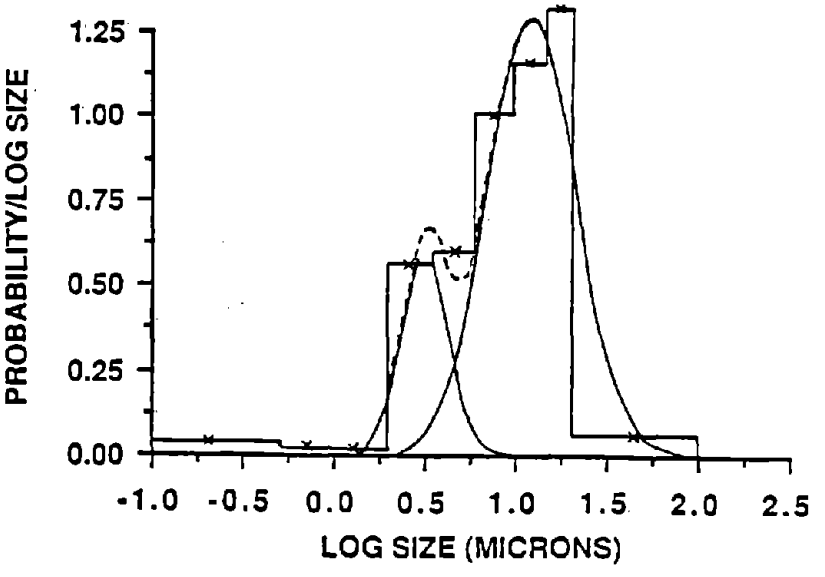

b. Lognormal Frequency Distributions.

48. Frequency Distributions of the 4X Samples from Section J.

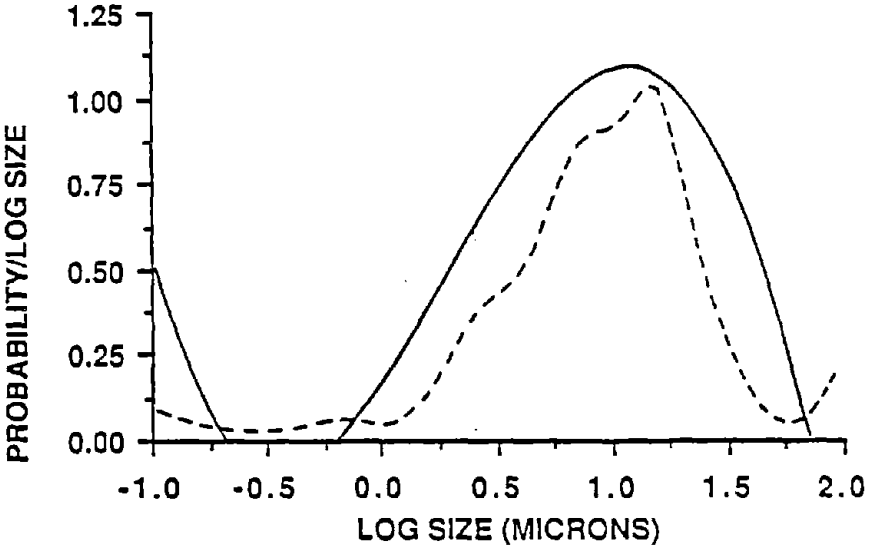

a. Empirical Frequency Distributions.

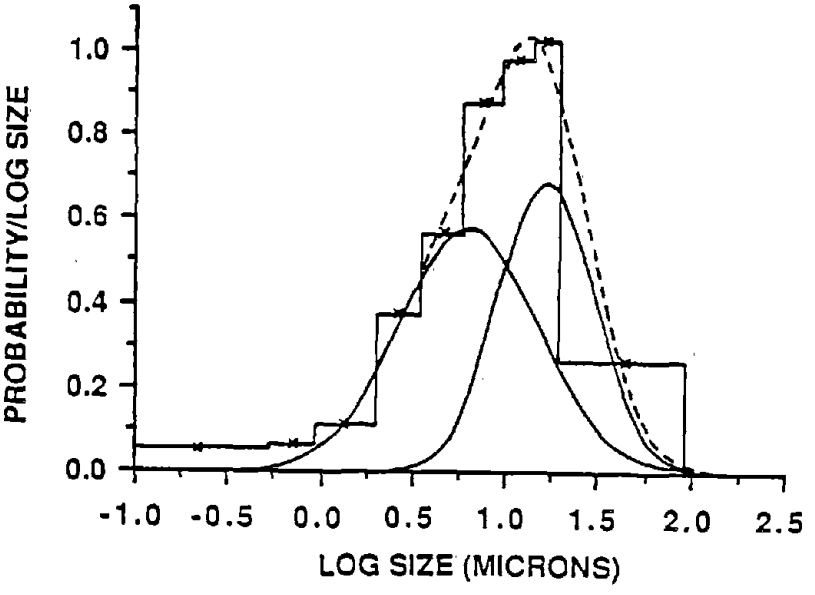

b. Lognormal Frequency Distributions.

49. Frequency Distributions of the CI Samples from Section K.

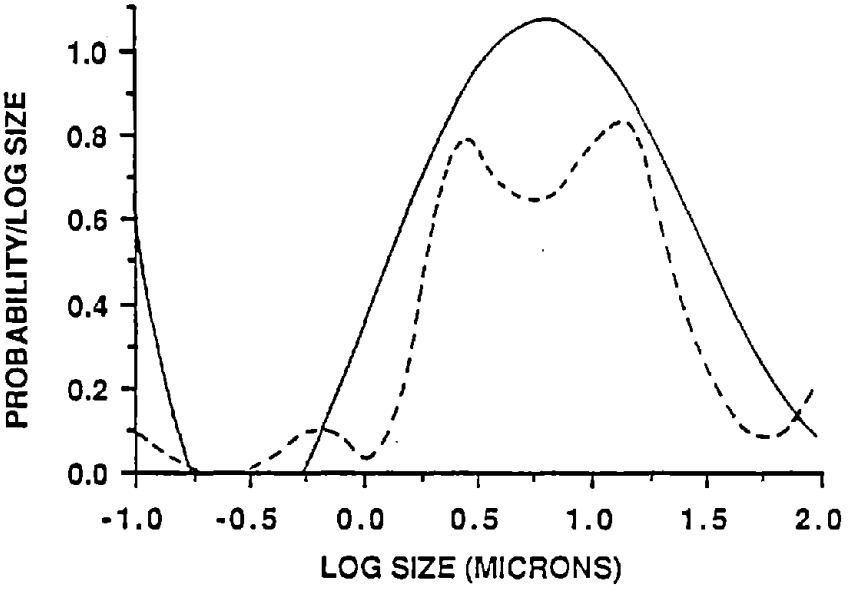

a. Empirical Frequency Distributions.

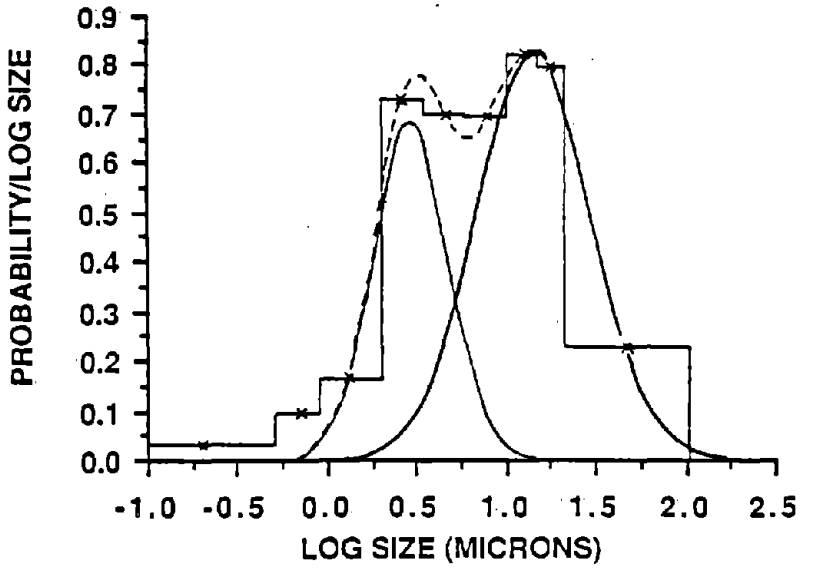

b. Lognormal Frequency Distributions.

50. Frequency Distributions of the CR Samples from Section K.

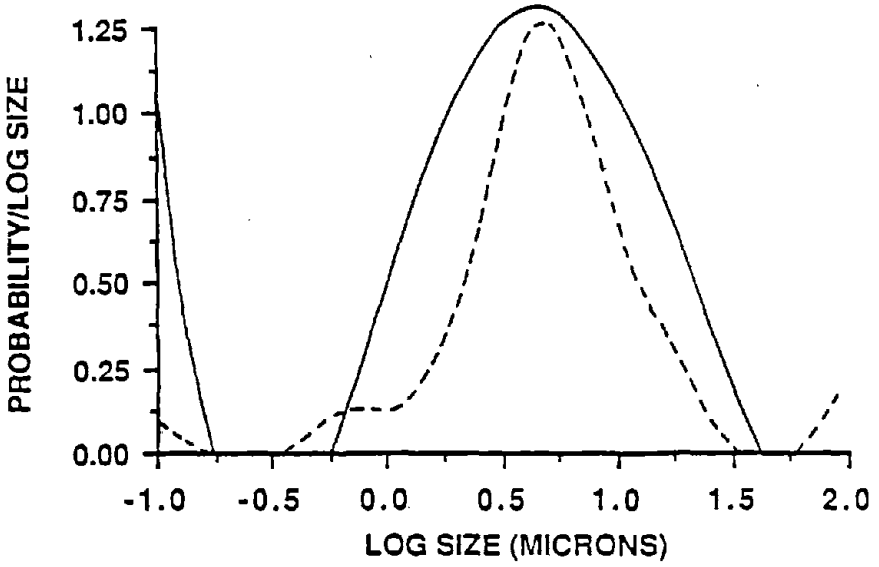

a. Empirical Frequency Distributions.

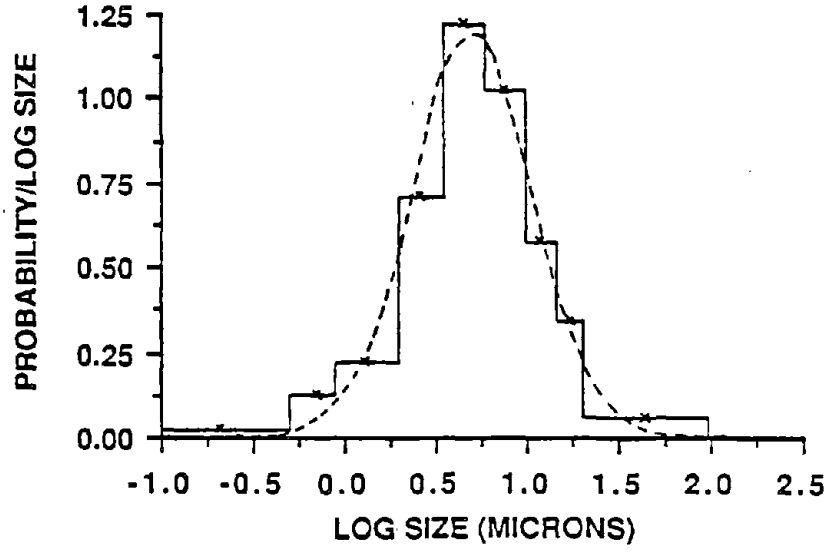

b. Lognormal Frequency Distributions.

51. Frequency Distributions of the 2X Samples from Section K.

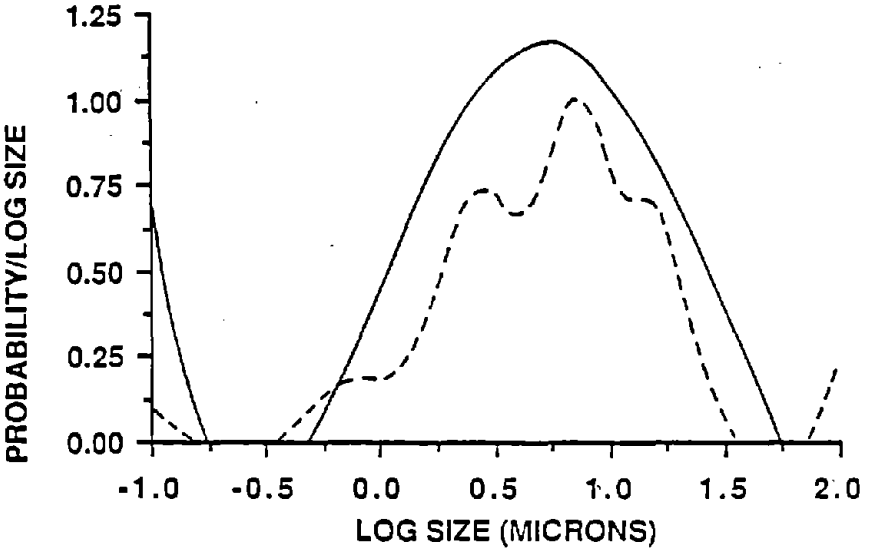

a. Empirical Frequency Distributions.

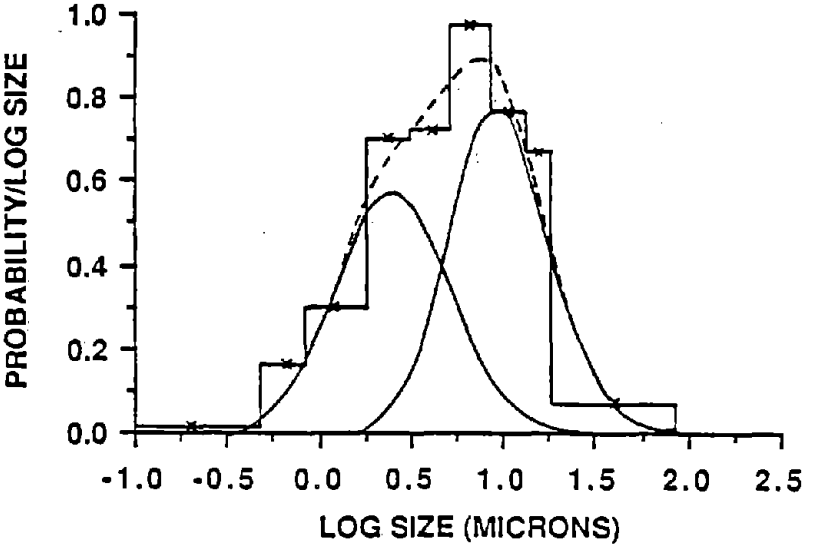

b. Lognormal Frequency Distributions.

52. Frequency Distributions of the 4X Samples from Section K.

APPENDIX 8

DATA FOR THE STUDY ON CROSS-SECTIONAL VARIATION OF ELEMENT COMPOSITIONS ON IMPACTOR STAGES

Table A.8.1. Cross-Sectional Variation of the Elemental Compositions on the Third Stage.

Elements	Weight Fractions (% x 10^2) / (Ratios)						
	Mass 1	Mass 2	Mass 3	Mass 4	Mass 5	Mean	CV
Mg	1.691	1.824	1.566	1.136	1.688	1.581	16.8
	(0.06)	(0.07)	(0.06)	(0.05)	(0.07)		
Al	9.220	19.361	18.202	17.552	16.193	18.106	7.2
	(0.69)	(0.71)	(0.70)	(0.70)	(0.72)		
Si	7.662	27.399	26.102	24.927	22.637	25.745	7.8
	(1.00)	(1.00)	(1.00)	(1.00)	(1.00)		
P	1.146	1.241	1.032	1.144	1.170	1.147	6.6
	(0.04)	(0.05)	(0.04)	(0.05)	(0.05)		
S	3.923	13.651	13.480	12.328	11.938	13.064	6.7
	(0.50)	(0.50)	(0.52)	(0.49)	(0.53)		
K	2.572	2.351	2.375	2.425	2.114	2.367	7.0
	(0.09)	(0.09)	(0.09)	(0.10)	(0.09)		
Ca	3.441	3.668	3.403	3.263	2.940	3.343	8.0
	(0.12)	(0.13)	(0.13)	(0.13)	(0.13)		
Ti	0.592	0.557	0.583	0.559	0.496	0.557	6.7
	(0.02)	(0.02)	(0.02)	(0.02)	(0.02)		
Fe	6.175	6.338	6.415	5.921	5.626	6.095	5.3
	(0.22)	(0.23)	(0.25)	(0.24)	(0.25)		
Cl	1.043	1.058	1.002	0.995	0.908	1.001	5.9
V	0.	0.	0.	0.	0.015	0.003	226.5
Cr	0.015	0.	0.009	0.	0.020	0.009	101.5
Mn	0.028	0.061	0.025	0.041	0.055	0.042	38.0
Ni	0.005	0.008	0.006	0.007	0.007	0.007	17.3
Cu	0.053	0.093	0.034	0.078	0.105	0.073	40.0
Zn	0.267	0.323	0.212	0.433	0.330	0.313	26.3
Ga	0.024	0.029	0.012	0.036	0.039	0.028	38.2
Ge	0.	0.	0.	0.	0.	0.	0.
As	0.	0.	0.007	0.006	0.	0.003	137.6
Br	0.033	0.039	0.024	0.040	0.035	0.034	18.7
Rb	0.017	0.026	0.014	0.017	0.	0.015	63.6
Sr	0.032	0.023	0.034	0.032	0.022	0.029	19.7
Zr	0.018	0.017	0.015	0.028	0.	0.016	64.5
Mo	0.	0.	0.	0.028	0.024	0.010	137.6
Pb	0.041	0.047	0.018	0.018	0.037	0.032	41.8

Notes: (1) CV denotes the coefficient of variation.
(2) Ratios given in the table are the ratios of the individual element to Si.

Table A.8.2. Cross-Sectional Variation of the Elemental Compositions on the Fifth Stage.

	Weight Fractions (% x 10^2) / (Ratios)						
Elements	Mass 1	Mass 2	Mass 3	Mass 4	Mass 5	Mean	CV
Mg	1.551 (0.08)	1.825 (0.08)	1.738 (0.08)	1.790 (0.08)	1.879 (0.08)	1.757	7.2
Al	12.987 (0.66)	15.445 (0.67)	15.012 (0.67)	15.334 (0.69)	16.873 (0.76)	15.130	9.2
Si	19.585 (1.00)	23.188 (1.00)	22.341 (1.00)	22.346 (1.00)	22.303 (1.00)	21.953	6.3
P	1.343 (0.07)	1.405 (0.06)	1.295 (0.06)	1.119 (0.05)	1.324 (0.06)	1.297	8.3
S	6.930 (0.35)	7.943 (0.34)	7.593 (0.34)	7.790 (0.35)	7.808 (0.35)	7.613	5.3
K	1.971 (0.10)	2.574 (0.11)	2.506 (0.11)	2.817 (0.13)	3.177 (0.14)	2.609	17.0
Ca	2.902 (0.15)	2.640 (0.11)	2.592 (0.12)	2.991 (0.13)	5.186 (0.23)	3.262	33.4
Ti	0.394 (0.02)	0.434 (0.02)	0.370 (0.02)	0.446 (0.02)	0.476 (0.02)	0.424	9.9
Fe	2.461 (0.13)	2.774 (0.12)	3.032 (0.14)	4.244 (0.19)	4.713 (0.21)	3.445	7.9
Cl	0.695	0.925	0.661	0.779	0.990	0.810	17.7
V	0.	0.	0.	0.021	0.	0.004	223.6
Cr	0.	0.	0.	0.008	0.011	0.004	140.0
Mn	0.018	0.017	0.018	0.060	0.079	0.038	76.0
Ni	0.002	0.009	0.003	0.005	0.010	0.006	61.4
Cu	0.018	0.027	0.034	0.129	0.537	0.148	148.6
Zn	0.216	0.222	0.236	0.413	0.614	0.340	51.0
Ga	0.007	0.008	0.010	0.043	0.044	0.022	86.1
Ge	0.	0.	0.	0.	0.	0.	0.
As	0.007	0.005	0.006	0.	0.	0.004	93.4
Br	0.025	0.027	0.032	0.038	0.030	0.030	16.6
Rb	0.014	0.	0.011	0.011	0.008	0.009	60.9
Sr	0.029	0.022	0.020	0.020	0.019	0.022	18.5
Zr	0.	0.014	0.012	0.	0.	0.005	137.6
Mo	0.	0.	0.	0.	0.	0.	0.
Pb	0.	0.012	0.008	0.021	0.071	0.022	125.9

Note: See the notes in Table A.8.1.

Table A.8.3. Cross-Sectional Variation of the Elemental Compositions on the Seventh Stage.

	Weight Fractions (% x 10^2) / (Ratios)						
Elements	Mass 1	Mass 2	Mass 3	Mass 4	Mass 5	Mean	CV
Mg	2.974 (0.16)	2.552 (0.12)	3.522 (0.17)	2.531 (0.12)	2.314 (0.10)	2.779	12.3
Al	11.889 (0.65)	14.783 (0.68)	8.645 (0.43)	15.258 (0.74)	15.359 (0.65)	13.241	22.4
Si	18.271 (1.00)	21.890 (1.00)	20.335 (1.00)	20.532 (1.00)	23.619 (1.00)	20.929	23.6
P	3.726 (0.20)	3.846 (0.18)	3.027 (0.15)	4.042 (0.20)	3.747 (0.16)	3.678	10.5
S	9.649 (0.53)	10.311 (0.47)	9.933 (0.49)	11.154 (0.54)	10.428 (0.44)	10.295	5.6
K	15.697 (0.86)	3.195 (0.15)	23.811 (1.17)	2.860 (0.14)	2.912 (0.12)	9.695	99.2
Ca	13.783 (0.75)	8.088 (0.37)	30.309 (1.49)	5.448 (0.27)	6.406 (0.27)	10.787	57.3
Ti	0.425 (0.02)	0.463 (0.02)	0.347 (0.02)	0.502 (0.02)	0.626 (0.02)	0.473	21.8
Fe	2.923 (0.16)	3.370 (0.15)	4.925 (0.24)	6.163 (0.30)	7.127 (0.30)	4.902	36.5
Cl	2.583	1.432	2.934	1.642	1.503	2.019	34.2
V	0.	0.	0.	0.	0.	0.	0.
Cr	0.	0.	0.	0.048	0.024	0.014	149.1
Mn	0.097	0.030	0.107	0.168	0.218	0.124	57.0
Ni	0.	0.016	0.	0.034	0.022	0.014	101.8
Cu	0.042	0.024	0.045	0.318	0.427	0.171	109.8
Zn	0.609	0.630	0.648	1.012	1.158	0.811	31.5
Ga	0.017	0.008	0.012	0.129	0.146	0.062	110.4
Ge	0.	0.	0.	0.	0.	0.	0.
As	0.	0.	0.014	0.	0.018	0.006	138.7
Br	0.041	0.037	0.063	0.053	0.055	0.050	21.4
Rb	0.039	0.017	0.018	0.	0.057	0.026	84.3
Sr	0.	0.019	0.051	0.024	0.033	0.025	73.7
Zr	0.	0.	0.109	0.043	0.032	0.037	121.4
Mo	0.	0.	0.	0.	0.	0.	0.
Pb	0.	0.	0.	0.025	0.	0.005	223.6

Note: See the notes in Table A.8.1.

APPENDIX 9

ASSOCIATION MATRICES OF THE INTERRELATIONSHIPS AMONG THE DUST AND CHANNEL SAMPLES

Table A.9.1. The Association Matrix of the Dust and Channel Samples at Section B (Mine Code 142-1-1).

Samples	CI3	CI5	CI7	CR3	CR5	CR7	RI3	RI5	RI7
CI3									
CI5	0.75 (0.97)								
CI7	0.59 (0.86)	0.97 (0.90)							
CR3	0.36 (0.61)	0.85 (0.70)	0.94 (0.90)						
CR5	0.37 (0.69)	0.87 (0.78)	0.96 (0.93)	0.99 (0.99)					
CR7	0.58 (0.66)	0.92 (0.74)	0.97 (0.93)	0.93 (0.99)	0.93 (0.99)				
RI3	0.49 (0.94)	0.94 (0.96)	0.98 (0.95)	0.95 (0.79)	0.97 (0.84)	0.94 (0.83)			
RI5	0.40 (0.88)	0.90 (0.88)	0.95 (0.69)	0.90 (0.47)	0.92 (0.55)	0.87 (0.52)	0.96 (0.86)		
RI7	0.39 (0.96)	0.89 (0.94)	0.94 (0.87)	0.95 (0.58)	0.97 (0.65)	0.90 (0.64)	0.97 (0.93)	0.98 (0.87)	
RR3	0.47 (0.88)	0.93 (0.87)	0.95 (0.72)	0.93 (0.50)	0.95 (0.57)	0.91 (0.55)	0.99 (0.87)	0.99 (0.99)	0.99 (0.88)
RR5	0.42 (0.92)	0.90 (0.90)	0.94 (0.80)	0.93 (0.57)	0.95 (0.63)	0.90 (0.62)	0.98 (0.92)	0.99 (0.96)	0.99 (0.94)
RR7	0.42 (0.92)	0.90 (0.87)	0.95 (0.76)	0.95 (0.41)	0.97 (0.49)	0.92 (0.48)	0.98 (0.84)	9.98 (0.82)	0.99 (0.87)
2X3	0.54 (0.89)	0.89 (0.93)	0.90 (0.98)	0.92 (0.90)	0.89 (0.94)	0.91 (0.93)	0.90 (0.78)	0.92 (0.83)	0.89 (0.75)
2X5	0.40 (0.85)	0.81 (0.91)	0.83 (0.90)	0.88 (0.86)	0.86 (0.90)	0.85 (0.88)	0.88 (0.93)	0.95 (0.82)	0.91 (0.80)
2X7	0.47 (0.95)	0.86 (0.93)	0.90 (0.86)	0.93 (0.56)	0.91 (0.64)	0.91 (0.63)	0.91 (0.91)	0.94 (0.82)	0.92 (0.99)
CH1	0.26 (0.47)	0.83 (0.47)	0.90 (0.37)	0.91 (0.33)	0.95 (0.35)	0.84 (0.35)	0.95 (0.52)	0.93 (0.75)	0.97 (0.44)
CH2	0.26 (0.39)	0.82 (0.38)	0.91 (0.32)	0.92 (0.36)	0.96 (0.37)	0.85 (0.36)	0.95 (0.43)	0.91 (0.61)	0.96 (0.31)
CH3	0.30 (0.36)	0.65 (0.46)	0.73 (0.73)	0.87 (0.95)	0.80 (0.91)	0.79 (0.93)	0.73 (0.58)	0.76 (0.24)	0.75 (0.32)
CH4	0.33 (0.36)	0.67 (0.46)	0.76 (0.73)	0.89 (0.95)	0.82 (0.91)	0.81 (0.93)	0.74 (0.58)	0.72 (0.24)	0.73 (0.32)
DUST	0.97 (0.33)	0.58 (0.19)	0.39 (0.06)	0.13 (0.06)	0.15 (0.06)	0.38 (0.05)	0.27 (0.16)	0.18 (0.27)	0.16 (0.15)

Table A.9.1. (Continued).

Samples	RR3	RR5	RR7	2X3	2X5	2X7	CH1	CH2	CH3
RR3									
RR5	0.99 (0.97)								
RR7	0.99 (0.83)	0.99 (0.89)							
2X3	0.92 (0.78)	0.90 (0.83)	0.92 (0.75)						
2X5	0.92 (0.83)	0.92 (0.84)	0.92 (0.66)	0.97 (0.95)					
2X7	0.94 (0.82)	0.92 (0.89)	0.94 (0.98)	0.99 (0.85)	0.98 (0.77)				
CH1	0.95 (0.75)	0.97 (0.67)	0.95 (0.36)	0.78 (0.45)	0.80 (0.61)	0.82 (0.38)			
CH2	0.94 (0.61)	0.96 (0.53)	0.95 (0.20)	0.78 (0.41)	0.78 (0.58)	0.81 (0.24)	0.99 (0.94)		
CH3	0.75 (0.28)	0.74 (0.34)	0.78 (0.12)	0.92 (0.73)	0.89 (0.71)	0.92 (0.29)	0.62 (0.26)	0.63 (0.34)	
CH4	0.73 (0.27)	0.71 (0.34)	0.76 (0.12)	0.90 (0.73)	0.83 (0.70)	0.88 (0.29)	0.63 (0.25)	0.65 (0.33)	0.98 (0.99)
DUST	0.25 (0.30)	0.18 (0.22)	0.19 (0.12)	0.32 (0.19)	0.18 (0.19)	0.24 (0.09)	0.04 (0.29)	0.04 (0.42)	0.09 (0.05)

Samples	CH4	DUST
CH3		
CH4		
DUST	0.12 (0.05)	

Notes:
(1) CH1 denotes the first roof bench in the channel sample.
(2) CH2 denotes the second roof bench in the channel sample.
(3) CH3 denotes the coal bench in the channel sample.
(4) CH4 denotes the bony coal and floor bench in the channel sample.
(5) DUST denotes the rock dust sample.
(6) The values in parentheses are based only upon the trace elements.
(7) The number affixed to the sample code denotes the impactor stage number.

Table A.9.2. The Association Matrix of the Dust and Channel Samples at Section C (Mine Code 03-3-1).

Samples	IN3	IN5	IN7	CI/RI3	CI/RI5	CI/RI7	CR3	CR5	CR7
IN3									
IN5	0.89 (0.99)								
IN7	0.98 (0.97)	0.93 (0.97)							
CI/RI3	0.85 (0.87)	0.89 (0.86)	0.78 (0.72)						
CI/RI5	0.88 (0.94)	0.93 (0.93)	0.79 (0.82)	0.98 (0.98)					
CI/RI7	0.99 (0.99)	0.98 (0.99)	0.97 (0.99)	0.81 (0.78)	0.85 (0.87)				
CR3	0.89 (0.86)	0.93 (0.86)	0.81 (0.72)	0.99 (0.99)	0.99 (0.98)	0.86 (0.78)			
CR5	0.82 (0.95)	0.91 (0.95)	0.73 (0.85)	0.96 (0.97)	0.96 (0.99)	0.82 (0.90)	0.97 (0.97)		
CR7	0.97 (0.97)	0.94 (0.96)	0.96 (0.88)	0.73 (0.96)	0.78 (0.99)	0.98 (0.92)	0.79 (0.96)	0.72 (0.99)	
2XCR3	0.84 (0.85)	0.91 (0.85)	0.73 (0.70)	0.96 (0.99)	0.99 (0.97)	0.82 (0.77)	0.98 (0.99)	0.97 (0.97)	0.75 (0.95)
2XCR5	0.86 (0.94)	0.93 (0.93)	0.76 (0.83)	0.93 (0.98)	0.98 (0.99)	0.86 (0.88)	0.97 (0.98)	0.95 (0.99)	0.80 (0.99)
2XCR7	0.96 (0.96)	0.99 (0.96)	0.89 (0.99)	0.94 (0.70)	0.97 (0.80)	0.95 (0.90)	0.97 (0.70)	0.94 (0.83)	0.90 (0.86)
4XCR3	0.87 (0.92)	0.87 (0.92)	0.84 (0.80)	0.98 (0.99)	0.94 (0.99)	0.82 (0.86)	0.96 (0.99)	0.89 (0.99)	0.75 (0.98)
4XCR5	0.80 (0.92)	0.90 (0.92)	0.68 (0.80)	0.92 (0.99)	0.95 (0.99)	0.80 (0.86)	0.95 (0.99)	0.98 (0.99)	0.81 (0.98)
4XCR7	0.98 (0.99)	0.97 (0.98)	0.92 (0.91)	0.86 (0.93)	0.91 (0.98)	0.96 (0.95)	0.90 (0.93)	0.83 (0.98)	0.95 (0.99)
RR3	0.80 (0.94)	0.84 (0.94)	0.70 (0.85)	0.97 (0.96)	0.98 (0.97)	0.75 (0.89)	0.97 (0.96)	0.91 (0.99)	0.68 (0.97)
RR5	0.78 (0.94)	0.85 (0.95)	0.68 (0.88)	0.98 (0.92)	0.98 (0.94)	0.74 (0.92)	0.98 (0.92)	0.95 (0.97)	0.66 (0.94)
RR7	0.98 (0.98)	0.96 (0.97)	0.93 (0.89)	0.85 (0.95)	0.90 (0.99)	0.96 (0.93)	0.89 (0.95)	0.82 (0.99)	0.96 (0.99)
2XRR3	0.86 (0.93)	0.88 (0.92)	0.79 (0.81)	0.98 (0.99)	0.98 (0.99)	0.80 (0.86)	0.98 (0.99)	0.90 (0.99)	0.75 (0.98)
2XRR5	0.84 (0.98)	0.92 (0.98)	0.73 (0.93)	0.96 (0.91)	0.99 (0.95)	0.82 (0.96)	0.98 (0.91)	0.98 (0.98)	0.74 (0.97)
2XRR7	0.99 (0.97)	0.98 (0.98)	0.96 (0.99)	0.84 (0.74)	0.89 (0.84)	0.99 (0.99)	0.89 (0.74)	0.82 (0.86)	0.98 (0.89)

Table A.9.2. (Continued).

Samples	IN3	IN5	IN7	CI/RI3	CI/RI5	CI/RI7	CR3	CR5	CR7
4XRR3	0.48	0.63	0.43	0.71	0.67	0.54	0.70	0.84	0.37
	(0.79)	(0.80)	(0.91)	(0.41)	(0.54)	(0.88)	(0.41)	(0.59)	(0.62)
4XRR5	0.88	0.92	0.79	0.97	0.99	0.85	0.99	0.94	0.79
	(0.90)	(0.90)	(0.77)	(0.99)	(0.99)	(0.83)	(0.99)	(0.99)	(0.98)
4XRR7	0.99	0.96	0.97	0.85	0.88	0.98	0.89	0.81	0.97
	(0.99)	(0.98)	(0.92)	(0.93)	(0.98)	(0.95)	(0.93)	(0.98)	(0.99)
CH1	0.83	0.90	0.71	0.81	0.90	0.84	0.87	0.86	0.81
	(0.69)	(0.67)	(0.48)	(0.94)	(0.89)	(0.56)	(0.94)	(0.85)	(0.84)
CH2	0.85	0.92	0.73	0.81	0.90	0.87	0.88	0.88	0.83
	(0.68)	(0.67)	(0.48)	(0.94)	(0.89)	(0.56)	(0.94)	(0.85)	(0.84)
DUST	0.44	0.37	0.54	0.60	0.46	0.37	0.51	0.40	0.32
	(0.05)	(0.09)	(0.07)	(0.12)	(0.10)	(0.08)	(0.15)	(0.14)	(0.05)

Samples	2XCR3	2XCR5	2XCR7	4XCR3	4XCR5	4XCR7	RR3	RR5	RR7
2XCR5	0.99								
	(0.97)								
2XCR7	0.95	0.96							
	(0.68)	(0.891							
4XCR3	0.90	0.86	0.91						
	(0.98)	(0.99)	(0.79)						
4XCR5	0.98	0.97	0.93	0.82					
	(0.99)	(0.99)	(0.78)	(0.99)					
4XCR7	0.89	0.92	0.97	0.86	0.83				
	(0.92)	(0.98)	(0.90)	(0.97)	(0.97)				
RR3	0.97	0.95	0.91	0.94	0.90	0.86			
	(0.96)	(0.97)	(0.83)	(0.99)	(0.98)	(0.96)			
RR5	0.98	0.95	0.91	0.92	0.94	0.83	0.99		
	(0.92)	(0.94)	(0.87)	(0.96)	(0.96)	(0.95)	(0.99)		
RR7	0.87	0.91	0.96	0.85	0.92	0.99	0.84	0.81	
	(0.94)	(0.99)	(0.88)	(0.98)	(0.98)	(0.99)	(0.97)	(0.95)	
2XRR3	0.95	0.93	0.93	0.97	0.87	0.89	0.99	0.97	0.88
	(0.98)	(0.99)	(0.79)	(0.99)	(0.99)	(0.97)	(0.98)	(0.96)	(0.98)
2XRR5	0.99	0.99	0.95	0.90	0.98	0.88	0.97	0.98	0.87
	(0.90)	(0.95)	(0.92)	(0.99)	(0.99)	(0.97)	(0.97)	(0.99)	(0.97)
2XRR7	0.86	0.89	0.93	0.85	0.82	0.99	0.81	0.79	0.99
	(0.72)	(0.85)	(0.99)	(0.82)	(0.82)	(0.93)	(0.86)	(0.89)	(0.91)
4XRR3	0.70	0.64	0.64	0.60	0.79	0.44	0.56	0.72	0.46
	(0.39)	(0.55)	(0.93)	(0.53)	(0.52)	(0.68)	(0.60)	(0.69)	(0.65)
4XRR5	0.99	0.98	0.97	0.94	0.94	0.92	0.98	0.98	0.91
	(0.99)	(0.99)	(0.75)	(0.99)	(0.99)	(0.96)	(0.97)	(0.93)	(0.97)
4XRR7	0.84	0.87	0.95	0.88	0.78	0.98	0.82	0.79	0.99
	(0.92)	(0.98)	(0.90)	(0.97)	(0.97)	(0.99)	(0.97)	(0.93)	(0.97)

Table A.9.2. (Continued).

Samples	2XCR3	2XCR5	2XCR7	4XCR3	4XCR5	4XCR7	RR3	RR5	RR7
CH1	0.92	0.96	0.91	0.73	0.92	0.91	0.84	0.85	0.90
	(0.95)	(0.89)	(0.45)	(0.89)	(0.90)	(0.79)	(0.83)	(0.74)	(0.82)
CH2	0.92	0.96	0.92	0.73	0.93	0.91	0.83	0.84	0.91
	(0.94)	(0.89)	(0.44)	(0.89)	(0.89)	(0.79)	(0.82)	(0.74)	(0.82)
DUST	0.37	0.29	0.42	0.26	0.24	0.37	0.52	0.47	0.37
	(0.15)	(0.10)	(0.10)	(0.17)	(0.13)	(0.05)	(0.17)	(0.19)	(0.07)

Samples	2XRR3	2XRR5	2XRR7	4XRR3	4XRR5	4XRR7	CH1	CH2
2XRR3								
2XRR5	0.95							
	(0.96)							
2XRR7	0.86	0.85						
	(0.83)	(0.94)						
4XRR3	0.56	0.72	0.46					
	(0.53)	(0.75)	(0.90)					
4XRR5	0.98	0.98	0.89	0.61				
	(0.99)	(0.93)	(0.79)	(0.47)				
4XRR7	0.88	0.83	0.99	0.44	0.89			
	(0.97)	(0.98)	(0.93)	(0.68)	(0.96)			
CH1	0.82	0.92	0.88	0.53	0.91	0.83		
	(0.89)	(0.72)	(0.51)	(0.10)	(0.92)	(0.79)		
CH2	0.82	0.92	0.89	0.57	0.90	0.84	0.99	
	(0.89)	(0.72)	(0.51)	(0.10)	(0.92)	(0.79)	(0.99)	
DUST	0.60	0.37	0.38	0.73	0.45	0.48	0.07	0.08
	(0.11)	(0.15)	(0.07)	(0.12)	(0.07)	(0.06)	(0.05)	(0.04)

Notes: (1) CH1 denotes the first coal bench in the channel sample.
(2) CH2 denotes the second coal bench in the channel sample.
(3) DUST denotes the rock dust sample.
(4) The values in parentheses are based only upon the trace elements.
(5) See Table A.9.1.

Table A.9.3. The Association Matrix of the Dust and Channel Samples at Section D (Mine Code 30-7-1).

Samples	CR13	CR15	CR17	CR23	CR25	CR27	CH1	CH2	CH3
CR13									
CR15	0.99 (0.91)								
CR17	0.92 (0.52)	0.94 (0.83)							
CR23	0.85 (0.32)	0.85 (0.37)	0.82 (0.34)						
CR25	0.80 (0.51)	0.81 (0.60)	0.79 (0.56)	0.99 (0.95)					
CR27	0.94 (0.56)	0.96 (0.85)	0.98 (0.99)	0.89 (0.34)	0.87 (0.58)				
CH1	0.99 (0.92)	0.99 (0.74)	0.93 (0.29)	0.85 (0.25)	0.79 (0.37)	0.94 (0.33)			
CH2	0.94 (0.10)	0.96 (0.08)	0.98 (0.04)	0.83 (0.95)	0.81 (0.81)	0.98 (0.04)	0.94 (0.09)		
CH3	0.99 (0.90)	0.99 (0.76)	0.96 (0.36)	0.84 (0.26)	0.79 (0.39)	0.96 (0.38)	0.99 (0.99)	0.98 (0.10)	
CH4	0.94 (0.04)	0.96 (0.03)	0.96 (0.01)	0.94 (0.94)	0.92 (0.79)	0.99 (0.01)	0.94 (0.04)	0.96 (0.99)	0.95 (0.04)
DUST	0.05 (0.60)	0.06 (0.48)	0.11 (0.16)	0.56 (0.17)	0.64 (0.24)	0.22 (0.17)	0.04 (0.39)	0.11 (0.07)	0.04 (0.38)

Samples	CH4	DUST
CH4		
DUST	0.32 (0.04)	

Notes:
(1) CH1 denotes the first coal bench in the channel sample.
(2) CH2 denotes the first slate bench in the channel sample.
(3) CH3 denotes the second coal bench in the channel sample.
(4) CH4 denotes the second slate bench in the channel sample.
(5) DUST denotes the rock dust sample.
(6) The values in parentheses are based only upon the trace elements.
(7) See Table A.9.1.

Table A.9.4. The Association Matrix of the Dust and Channel Samples at Section E (Mine Code 200-1-1).

Samples	CR11	CR13	CR15	CR16	CR17	CR21	CR23	CR25	CR26
CR11									
CR13	0.47 (0.41)								
CR15	0.44 (0.40)	0.99 (0.99)							
CR16	0.40 (0.37)	0.99 (0.99)	0.99 (0.99)						
CR17	0.39 (0.91)	0.99 (0.73)	0.99 (0.73)	0.99 (0.70)					
CR21	0.99 (0.91)	0.42 (0.57)	0.38 (0.56)	0.34 (0.55)	0.33 (0.90)				
CR23	0.48 (0.21)	0.95 (0.97)	0.99 (0.98)	0.99 (0.98)	0.98 (0.57)	0.42 (0.41)			
CR25	0.41 (0.39)	0.99 (0.99)	0.97 (0.99)	0.99 (0.99)	0.94 (0.72)	0.34 (0.55)	0.96 (0.98)		
CR26	0.39 (0.44)	0.95 (0.99)	0.98 (0.99)	0.97 (0.99)	0.99 (0.75)	0.33 (0.60)	0.98 (0.97)	0.93 (0.99)	
CR27	0.39 (0.90)	0.96 (0.76)	0.98 (0.75)	0.99 (0.73)	0.96 (0.99)	0.32 (0.89)	0.97 (0.60)	0.99 (0.74)	0.95 (0.78)
CI/RI1	0.44 (0.80)	0.83 (0.86)	0.85 (0.85)	0.82 (0.88)	0.80 (0.97)	0.36 (0.83)	0.86 (0.73)	0.92 (0.85)	0.78 (0.87)
CI/RI3	0.56 (0.71)	0.92 (0.91)	0.91 (0.90)	0.89 (0.89)	0.88 (0.93)	0.50 (0.78)	0.94 (0.81)	0.93 (0.89)	0.86 (0.92)
CI/RI5	0.43 (0.20)	0.99 (0.97)	0.99 (0.97)	0.97 (0.98)	0.98 (0.57)	0.37 (0.93)	0.99 (0.99)	0.94 (0.98)	0.98 (0.96)
CI/RI6	0.72 (0.42)	0.95 (0.99)	0.93 (0.99)	0.91 (0.99)	0.90 (0.75)	0.67 (0.57)	0.95 (0.97)	0.91 (0.99)	0.90 (0.99)
CI/RI7	0.39 (0.45)	0.87 (0.99)	0.86 (0.99)	0.84 (0.99)	0.85 (0.77)	0.29 (0.58)	0.89 (0.96)	0.88 (0.99)	0.82 (0.99)
RR1	0.45 (0.74)	0.73 (0.91)	0.78 (0.91)	0.75 (0.89)	0.70 (0.94)	0.38 (0.82)	0.77 (0.80)	0.89 (0.90)	0.67 (0.92)
RR3	0.52 (0.57)	0.96 (0.97)	0.94 (0.97)	0.95 (0.96)	0.95 (0.85)	0.47 (0.68)	0.97 (0.91)	0.91 (0.97)	0.95 (0.98)
RR5	0.46 (0.24)	0.99 (0.98)	0.99 (0.98)	0.98 (0.98)	0.98 (0.61)	0.40 (0.41)	0.99 (0.99)	0.96 (0.99)	0.98 (0.97)
RR6	0.66 (0.58)	0.97 (0.94)	0.96 (0.94)	0.95 (0.93)	0.94 (0.83)	0.60 (0.69)	0.97 (0.88)	0.93 (0.94)	0.94 (0.96)
RR7	0.46 (0.73)	0.97 (0.90)	0.97 (0.90)	0.95 (0.89)	0.95 (0.94)	0.40 (0.81)	0.98 (0.79)	0.96 (0.89)	0.94 (0.91)
CH1	0.49 (0.13)	0.97 (0.96)	0.93 (0.96)	0.94 (0.97)	0.96 (0.50)	0.44 (0.34)	0.96 (0.99)	0.85 (0.96)	0.96 (0.95)
DUST	0.12 (0.17)	0.31 (0.10)	0.39 (0.08)	0.37 (0.12)	0.29 (0.13)	0.06 (0.30)	0.36 (0.09)	0.59 (0.08)	0.27 (0.10)

Table A.9.4. (Continued).

Samples	CR27	CI/RI1	CI/RI3	CI/RI5	CI/RI6	CI/RI7	RR1	RR3	RR5
CR27									
CI/RI1	0.91 (0.98)								
CI/RI3	0.93 (0.94)	0.96 (0.98)							
CI/RI5	0.95 (0.60)	0.84 (0.73)	0.92 (0.80)						
CI/RI6	0.91 (0.77)	0.85 (0.87)	0.94 (0.91)	0.93 (0.97)					
CI/RI7	0.90 (0.79)	0.95 (0.89)	0.96 (0.92)	0.88 (0.96)	0.83 (0.99)				
RR1	0.86 (0.96)	0.95 (0.99)	0.87 (0.99)	0.72 (0.80)	0.79 (0.92)	0.81 (0.93)			
RR3	0.94 (0.87)	0.86 (0.94)	0.95 (0.98)	0.95 (0.91)	0.94 (0.98)	0.91 (0.98)	0.73 (0.97)		
RR5	0.97 (0.64)	0.85 (0.76)	0.92 (0.83)	0.99 (0.99)	0.95 (0.98)	0.86 (0.97)	0.77 (0.82)	0.94 (0.93)	
RR6	0.93 (0.84)	0.84 (0.91)	0.93 (0.94)	0.96 (0.87)	0.99 (0.94)	0.83 (0.94)	0.77 (0.94)	0.95 (0.97)	0.97 (0.89)
RR7	0.97 (0.95)	0.93 (0.98)	0.97 (0.99)	0.98 (0.79)	0.94 (0.91)	0.94 (0.93)	0.83 (0.99)	0.95 (0.97)	0.98 (0.89)
CH1	0.88 (0.54)	0.74 (0.68)	0.88 (0.75)	0.96 (0.99)	0.91 (0.95)	0.84 (0.94)	0.59 (0.75)	0.96 (0.87)	0.94 (0.99)
DUST	0.54 (0.13)	0.70 (0.07)	0.51 (0.06)	0.29 (0.01)	0.36 (0.06)	0.48 (0.03)	0.84 (0.10)	0.32 (0.06)	0.37 (0.02)

Samples	RR6	RR7	CH1	DUST
RR6				
RR7	0.95 (0.93)			
CH1	0.93 (0.85)	0.92 (0.74)		
DUST	0.35 (0.08)	0.45 (0.07)	0.12 (0.07)	

Notes: (1) CH1 denotes the whole seam channel sample.
(2) DUST denotes the rock dust sample.
(3) The values in parentheses are based only upon the trace elements.
(4) See Table A.9.1.

Table A.9.5. The Association Matrix of the Dust and Channel Samples at Section F (Mine Code 11-2-1).

Samples	CI3	CI5	CI7	CR3	CR5	CR7	RI3	RI5	RI7
CI5	0.99 (0.99)								
CI7	0.74 (0.79)	0.76 (0.76)							
CR3	0.53 (0.31)	0.51 (0.22)	0.68 (0.52)						
CR5	0.51 (0.63)	0.49 (0.55)	0.70 (0.75)	0.98 (0.92)					
CR7	0.54 (0.82)	0.51 (0.77)	0.75 (0.81)	0.95 (0.70)	0.91 (0.87)				
RI3	0.45 (0.32)	0.42 (0.23)	0.74 (0.57)	0.97 (0.99)	0.99 (0.93)	0.98 (0.74)			
RI5	0.90 (0.58)	0.90 (0.51)	0.70 (0.73)	0.97 (0.94)	0.99 (0.98)	0.99 (0.86)	0.99 (0.94)		
RI7	0.52 (0.32)	0.49 (0.24)	0.71 (0.56)	0.94 (0.88)	0.99 (0.89)	0.99 (0.79)	0.97 (0.93)	0.99 (0.86)	
RR3	0.87 (0.30)	0.85 (0.22)	0.80 (0.55)	0.87 (0.97)	0.87 (0.89)	0.88 (0.66)	0.93 (0.96)	0.88 (0.93)	0.86 (0.84)
RR5	0.62 (0.31)	0.59 (0.23)	0.73 (0.56)	0.97 (0.97)	0.99 (0.92)	0.99 (0.71)	0.99 (0.98)	0.99 (0.95)	0.98 (0.90)
RR7	0.53 (0.94)	0.51 (0.91)	0.72 (0.91)	0.95 (0.55)	0.99 (0.81)	0.99 (0.94)	0.98 (0.59)	0.99 (0.78)	0.99 (0.60)
2X3	0.70 (0.78)	0.68 (0.72)	0.77 (0.85)	0.96 (0.82)	0.97 (0.95)	0.97 (0.91)	0.99 (0.81)	0.98 (0.95)	0.96 (0.74)
2X5	0.55 (0.67)	0.53 (0.60)	0.71 (0.80)	0.97 (0.89)	0.99 (0.99)	0.99 (0.92)	0.99 (0.92)	0.99 (0.99)	0.99 (0.85)
2X7	0.55 (0.88)	0.53 (0.83)	0.75 (0.85)	0.95 (0.67)	0.99 (0.91)	0.99 (0.98)	0.99 (0.71)	0.99 (0.86)	0.99 (0.73)
4X3	0.70 (0.89)	0.68 (0.84)	0.77 (0.88)	0.96 (0.69)	0.97 (0.90)	0.97 (0.95)	0.99 (0.71)	0.98 (0.88)	0.96 (0.67)
4X5	0.55 (0.61)	0.52 (0.55)	0.71 (0.76)	0.96 (0.92)	0.99 (0.98)	0.99 (0.87)	0.99 (0.92)	0.99 (0.99)	0.99 (0.84)
4X7	0.75 (0.81)	0.53 (0.76)	0.75 (0.83)	0.95 (0.71)	0.99 (0.92)	0.99 (0.98)	0.98 (0.76)	0.99 (0.88)	0.99 (0.80)
CH1	0.46 (0.15)	0.43 (0.10)	0.65 (0.20)	0.97 (0.73)	0.99 (0.57)	0.98 (0.29)	0.98 (0.63)	0.99 (0.66)	0.98 (0.36)
CH2	0.49 (0.91)	0.46 (0.91)	0.69 (0.64)	0.96 (0.27)	0.99 (0.51)	0.99 (0.63)	0.98 (0.22)	0.99 (0.50)	0.99 (0.10)
CH3	0.52 (0.94)	0.51 (0.96)	0.81 (0.62)	0.84 (0.10)	0.91 (0.39)	0.95 (0.60)	0.91 (0.08)	0.92 (0.36)	0.95 (0.02)
CH4	0.45 (0.09)	0.42 (0.05)	0.65 (0.09)	0.93 (0.54)	0.98 (0.36)	0.98 (0.11)	0.96 (0.43)	0.98 (0.43)	0.99 (0.12)
DUST	0.90 (0.09)	0.90 (0.05)	0.45 (0.06)	0.14 (0.26)	0.10 (0.18)	0.13 (0.09)	0.25 (0.26)	0.13 (0.24)	0.11 (0.09)

Table A.9.5. (Continued).

Samples	RR3	RR5	RR7	2X3	2X5	2X7	4X3	4X5	4X7
RR3									
RR5	0.92 (0.98)								
RR7	0.87 (0.55)	0.99 (0.58)							
2X3	0.96 (0.82)	0.99 (0.82)	0.97 (0.92)						
2X5	0.89 (0.89)	0.99 (0.91)	0.99 (0.86)	0.98 (0.97)					
2X7	0.88 (0.65)	0.99 (0.69)	0.99 (0.97)	0.94 (0.94)	0.99 (0.91)				
4X3	0.96 (0.69)	0.99 (0.70)	0.97 (0.98)	0.99 (0.98)	0.98 (0.93)	0.97 (0.98)			
4X5	0.89 (0.91)	0.99 (0.93)	0.99 (0.81)	0.98 (0.96)	0.99 (0.99)	0.99 (0.87)	0.98 (0.89)		
4X7	0.87 (0.69)	0.99 (0.74)	0.99 (0.94)	0.97 (0.93)	0.99 (0.93)	0.99 (0.98)	0.97 (0.95)	0.99 (0.89)	
CH1	0.84 (0.73)	0.97 (0.68)	0.99 (0.24)	0.95 (0.54)	0.99 (0.58)	0.98 (0.31)	0.95 (0.42)	0.99 (0.65)	0.98 (0.30)
CH2	0.85 (0.25)	0.98 (0.23)	0.99 (0.79)	0.96 (0.70)	0.99 (0.55)	0.95 (0.71)	0.96 (0.78)	0.99 (0.54)	0.99 (0.62)
CH3	0.80 (0.11)	0.91 (0.08)	0.95 (0.78)	0.90 (0.61)	0.92 (0.44)	0.95 (0.68)	0.89 (0.74)	0.93 (0.40)	0.96 (0.59)
CH4	0.82 (0.53)	0.97 (0.42)	0.99 (0.11)	0.94 (0.40)	0.98 (0.35)	0.98 (0.14)	0.94 (0.29)	0.99 (0.43)	0.99 (0.13)
DUST	0.58 (0.40)	0.23 (0.27)	0.12 (0.10)	0.33 (0.28)	0.15 (0.21)	0.15 (0.10)	0.34 (0.22)	0.15 (0.22)	0.14 (0.11)

Samples	CH1	CH2	CH3	CH4	DUST
CH1					
CH2	0.99 (0.37)				
CH3	0.89 (0.10)	0.94 (0.94)			
CH4	0.98 (0.78)	0.99 (0.38)	0.94 (0.18)		
DUST	0.04 (0.24)	0.07 (0.11)	0.12 (0.19)	0.04 (0.54)	

Notes:
(1) CH1 denotes the roof and coal bench in the channel sample.
(2) CH2 denotes the bony coal bench in the channel sample.
(3) CH3 denotes the soft coal bench in the channel sample.
(4) CH4 denotes the bottom rock and coal bench in the channel sample.
(5) DUST denotes the rock dust sample.
(6) The values in parentheses are based only upon the trace elements.
(7) See Table A.9.1.

Table A.9.6. The Association Matrix of the Dust and Channel Samples at Section G (Mine Code 63-7-1).

Samples	ININ3	ININ5	ININ7	INOUT3	INOUT5	INOUT7	CI3	CI5	CI7
ININ3									
ININ5	0.99 (0.99)								
ININ7	0.92 (0.96)	0.87 (0.95)							
INOUT3	0.94 (0.98)	0.92 (0.99)	0.96 (0.97)						
INOUT5	0.98 (0.99)	0.98 (0.99)	0.92 (0.97)	0.98 (0.99)					
INOUT7	0.91 (0.77)	0.85 (0.77)	0.97 (0.79)	0.97 (0.79)	0.91 (0.78)				
CI3	0.89 (0.85)	0.88 (0.79)	0.95 (0.83)	0.99 (0.81)	0.95 (0.81)	0.93 (0.68)			
CI5	0.85 (0.99)	0.96 (0.97)	0.94 (0.98)	0.99 (0.98)	0.99 (0.98)	0.92 (0.81)	0.98 (0.90)		
CI7	0.99 (0.97)	0.86 (0.95)	0.99 (0.99)	0.95 (0.97)	0.91 (0.97)	0.97 (0.80)	0.94 (0.85)	0.94 (0.99)	
CR3	0.91 (0.66)	0.91 (0.72)	0.90 (0.74)	0.90 (0.74)	0.92 (0.74)	0.84 (0.61)	0.91 (0.26)	0.94 (0.65)	0.89 (0.72)
CR5	0.91 (0.94)	0.92 (0.95)	0.90 (0.98)	0.92 (0.97)	0.94 (0.97)	0.86 (0.81)	0.93 (0.74)	0.95 (0.95)	0.89 (0.98)
CR7	0.89 (0.96)	0.86 (0.94)	0.86 (0.99)	0.93 (0.97)	0.90 (0.96)	0.92 (0.80)	0.93 (0.88)	0.93 (0.99)	0.96 (0.99)
RR3	0.88 (0.93)	0.91 (0.94)	0.83 (0.97)	0.85 (0.96)	0.90 (0.96)	0.77 (0.79)	0.85 (0.74)	0.91 (0.94)	0.82 (0.97)
RR5	0.88 (0.92)	0.90 (0.90)	0.81 (0.91)	0.84 (0.90)	0.89 (0.91)	0.77 (0.77)	0.84 (0.91)	0.89 (0.94)	0.80 (0.92)
RR7	0.93 (0.95)	0.88 (0.92)	0.89 (0.91)	0.91 (0.92)	0.90 (0.92)	0.92 (0.74)	0.85 (0.96)	0.89 (0.96)	0.88 (0.93)
CH1	0.81 (0.26)	0.84 (0.24)	0.77 (0.19)	0.79 (0.24)	0.83 (0.23)	0.72 (0.40)	0.79 (0.24)	0.84 (0.25)	0.76 (0.20)
CH2	0.80 (0.27)	0.84 (0.26)	0.71 (0.19)	0.75 (0.25)	0.82 (0.24)	0.66 (0.41)	0.76 (0.24)	0.82 (0.26)	0.71 (0.21)
CH3	0.86 (0.46)	0.84 (0.54)	0.89 (0.55)	0.87 (0.26)	0.86 (0.55)	0.84 (0.46)	0.86 (0.01)	0.88 (0.44)	0.89 (0.53)
DUST	0.26 (0.11)	0.23 (0.08)	0.41 (0.08)	0.53 (0.10)	0.41 (0.10)	0.48 (0.11)	0.59 (0.11)	0.45 (0.11)	0.40 (0.08)

Table A.9.6. (Continued).

Samples	CR3	CR5	CR7	RR3	RR5	RR7	CH1	CH2	CH3
CR3									
CR5	0.99 (0.84)								
CR7	0.98 (0.69)	0.97 (0.96)							
RR3	0.99 (0.82)	0.98 (0.98)	0.92 (0.95)						
RR5	0.97 (0.51)	0.98 (0.86)	0.91 (0.92)	0.99 (0.91)					
RR7	0.89 (0.46)	0.90 (0.86)	0.91 (0.94)	0.88 (0.87)	0.90 (0.97)				
CH1	0.96 (0.11)	0.96 (0.23)	0.90 (0.18)	0.99 (0.25)	0.99 (0.35)	0.85 (0.30)			
CH2	0.94 (0.11)	0.94 (0.23)	0.85 (0.19)	0.98 (0.25)	0.98 (0.34)	0.80 (0.30)	0.99 (0.99)		
CH3	0.97 (0.97)	0.96 (0.68)	0.97 (0.48)	0.94 (0.65)	0.94 (0.30)	0.91 (0.23)	0.94 (0.06)	0.90 (0.06)	
DUST	0.24 (0.06)	0.30 (0.11)	0.31 (0.07)	0.16 (0.14)	0.15 (0.20)	0.24 (0.16)	0.10 (0.55)	0.06 (0.50)	0.18 (0.05)

Notes:
(1) CH1 denotes the top rock and bony coal bench in the channel sample.
(2) CH2 denotes the draw slate bench in the channel sample.
(3) CH3 denotes the coal bench in the channel sample.
(4) DUST denotes the rock dust sample.
(5) The values in parentheses are based only upon the trace elements.
(6) See Table A.9.1.

APPENDIX 10

ELEMENTAL COMPOSITIONS OF COAL MINE DUST AND CHANNEL SAMPLES

Note: All values are in % x 100 by weight.

Table A.10.1. Elemental Composition of the Samples from Section A (Mine Code 141-1-1).

Sampling	CI						RI					
Stage	3		5		7		3		5		7	
Sample	A	B	A	B	A	B	A	B	A	B	A	B
Elements												
Na	0.	0.	0.	0.	0.	0.	0.	0.	0.	0.	0.	0.
Mg	5.172	5.169	2.790	3.692	0.	2.775	2.543	4.466	2.887	2.937	3.085	4.675
Al	14.100	15.760	18.400	18.300	9.170	9.760	48.070	53.940	30.320	27.360	21.370	38.920
Si	21.440	22.520	33.520	31.110	13.530	13.640	94.610	102.110	51.310	44.590	28.700	46.850
P	3.700	2.737	2.233	2.805	2.928	3.361	0.938	1.860	1.320	0.954	1.015	1.060
S	13.579	13.395	10.446	8.301	2.166	8.862	23.220	27.503	9.934	9.391	5.495	4.192
Cl	2.099	1.375	1.162	1.561	0.844	0.930	1.309	1.505	0.658	0.472	0.182	0.238
K	1.918	2.128	3.895	3.364	1.327	1.699	13.071	13.457	7.056	6.018	4.028	6.710
Ca	22.858	25.837	11.973	11.042	6.911	5.107	16.096	20.442	3.540	3.2657	2.275	2.509
Sc	0.	0.	0.	0.	0.	0.	0.	0.	0.	0.	0.	0.
Ti	2.696	2.525	1.050	0.783	0.201	0.291	4.895	6.215	2.523	2.561	0.921	12.169
V	0.	0.	0.	0.	0.	0.029	0.231	0.223	0.084	0.101	0.016	0.018
Cr	0.419	0.	0.026	0.050	0.027	0.	0.092	0.138	0.056	0.047	0.040	0.068
Mn	0.474	0.774	0.064	0.036	0.018	0.033	0.364	0.355	0.178	0.201	0.086	0.080
Fe	82.020	102.250	6.540	5.590	1.330	1.790	49.700	72.680	21.010	20.120	0.070	8.540
Co	0.	0.	0.	0.	0.	0.	0.	0.	0.	0.	0.	0.
Ni	0.232	0.588	0.021	0.019	0.	0.011	0.066	0.047	0.014	0.036	0.013	0.016
Cu	1.891	1.415	0.228	0.218	0.089	0.088	0.097	0.039	0.059	0.054	0.025	0.062
Zn	15.664	13.072	0.672	0.795	0.855	0.743	1.049	0.934	0.481	0.439	0.267	0.332
Ga	0.	0.	0.	0.	0.	0.	0.	0.	0.	0.	0.	0.
Ge	0.	0.	0.	0.	0.	0.	0.	0.	0.	0.	0.	0.
As	0.	0.	0.020	0.028	0.	0.	0.027	0.054	0.021	0.015	0.010	0.007
Se	0.	0.	0.	0.	0.	0.	0.	0.	0.	0.	0.	0.
Br	0.537	0.263	0.038	0.033	0.	0.017	0.066	0.068	0.020	0.010	0.004	0.
Kr	0.	0.	0.	0.	0.	0.	0.	0.	0.	0.	0.	0.
Rb	0.	0.520	0.	0.017	0.	0.022	0.298	0.321	0.110	0.093	0.044	0.056
Sr	1.226	0.746	0.038	0.028	0.032	0.030	0.252	0.243	0.062	0.102	0.025	0.031
Y	0.	0.	0.	0.	0.	0.	0.	0.	0.	0.	0.	0.
Zr	0.	0.776	0.030	0.027	0.	0.	0.212	0.049	0.100	0.058	0.039	0.037
Mo	0.	0.702	0.	0.	0.	0.	0.	0.	0.100	0.076	0.023	0.
Cd	0.	0.	0.	0.	0.	0.	0.	0.	0.	0.	0.	0.
Pb	0.708	0.669	0.	0.	0.026	0.020	0.250	0.205	0.136	0.111	0.024	0.059

Table A.10.1. (Continued).

Sampling Locations	RR						2X					
Stage	3		5		7		3		5		7	
Sample	A	B	A	B	A	B	A	B	A	B	A	B
Elements												
Na	0.	0.	0.	0.	0.	0.	0.	0.	0.	0.	0.	0.
Mg	5.522	4.621	3.555	2.715	2.367	1.879	2.413	3.889	2.597	1.871	2.138	0.
Al	57.840	49.400	34.430	29.670	29.050	34.850	41.630	30.350	30.470	33.250	11.150	13.210
Si	99.720	83.970	54.740	48.630	35.930	44.470	64.420	44.030	50.270	51.530	16.720	17.780
P	1.694	1.116	1.270	1.231	1.047	0.849	1.714	2.463	2.560	2.566	3.169	2.692
S	26.529	23.984	10.279	9.688	4.188	5.335	40.257	27.715	18.371	16.709	9.458	3.764
Cl	1.471	1.486	0.509	0.545	0.077	0.390	2.449	2.824	1.788	1.815	1.158	0.493
K	12.092	10.444	7.169	6.530	5.237	6.088	7.868	5.058	6.914	7.177	2.082	1.731
Ca	13.833	10.762	4.010	3.488	2.046	2.285	14.551	11.880	7.927	9.037	5.578	6.128
Sc	0.	0.	0.	0.	0.	0.	0.	0.	0.	0.	0.	0.
Ti	4.443	3.413	2.437	2.223	1.068	1.161	12.627	7.991	3.965	3.882	0.385	0.378
V	0.114	0.166	0.128	0.087	0.037	0.023	2.053	1.383	15.382	0.223	0.	0.
Cr	0.110	0.108	0.034	0.046	0.025	0.139	4.983	1.530	0.088	0.156	0.035	0.043
Mn	0.302	0.222	0.185	0.155	0.072	0.086	7.418	1.424	0.170	0.176	0.036	0.037
Fe	45.350	37.640	20.910	18.610	7.560	9.260	1059.56	304.510	27.260	30.650	2.810	2.140
Co	0.	0.	0.	0.	0.	0.	0.	0.	0.	0.	0.	0.
Ni	0.029	0.043	0.008	0.021	0.007	0.047	2.412	1.116	0.047	0.043	0.023	0.
Cu	0.039	0.115	0.026	0.036	0.023	0.037	1.569	1.935	0.508	0.531	0.101	0.061
Zn	0.528	0.420	0.408	0.345	0.272	0.267	12.199	13.445	1.307	2.724	0.780	0.696
Ga	0.	0.	0.	0.	0.003	0.	0.	0.	0.014	0.	0.	0.
Ge	0.	0.	0.	0.	0.	0.	0.	0.	0.	0.	0.	0.
As	0.019	0.	0.038	0.013	0.006	0.016	0.	0.420	0.041	0.	0.	0.
Se	0.009	0.	0.	0.	0.	0.	0.	0.	0.	0.	0.	0.001
Br	0.066	0.067	0.023	0.022	0.015	0.008	1.275	0.490	0.067	0.081	0.012	0.011
Kr	0.	0.	0.	0.	0.	0.	0.	0.	0.	0.	0.	0.
Rb	0.342	0.268	0.125	0.086	0.060	0.070	4.261	1.110	0.118	0.113	0.019	0.037
Sr	0.177	0.217	0.090	0.074	0.036	0.042	3.001	1.182	0.145	0.143	0.021	0.043
Y	0.	0.	0.	0.	0.	0.	0.	0.	0.	0.	0.	0.
Zr	0.102	0.098	0.054	0.056	0.044	0.034	2.067	1.417	0.129	0.284	0.040	0.
Mo	0.063	0.064	0.	0.042	0.025	0.039	0.	0.	0.	0.097	0.	0.046
Cd	0.	0.	0.	0.	0.	0.	0.	0.	0.	0.	0.	0.
Pb	0.266	0.302	0.058	0.114	0.051	0.032	3.507	1.056	0.144	0.177	0.041	0.047

Table A.10.1. (Continued).

Sampling Locations	4X						
Stage	3		5		7		DUST
Sample	A	B	A	B	A	B	
Elements							
Na	0.	0.	0.	0.	0.	0.	0.
Mg	1.902	2.346	2.270	2.460	1.758	1.594	95.347
Al	26.470	27.300	29.540	33.440	8.240	9.680	0.
Si	45.350	42.090	46.250	49.970	10.050	13.260	146.330
P	2.282	2.457	1.555	1.616	1.614	1.609	2.751
S	22.977	22.777	13.293	14.146	4.849	4.469	0.
Cl	2.162	1.825	1.122	1.196	0.446	0.447	0.
K	5.246	4.540	6.348	6.470	1.350	1.846	61.585
Ca	10.684	9.546	6.156	6.675	2.231	2.864	3449.09
Sc	0.	0.	0.	0.	0.	0.	0.
Ti	2.576	2.512	2.874	3.503	0.553	0.678	2.016
V	0.	0.	0.094	0.115	0.	0.	0.
Cr	0.078	0.087	0.068	0.080	0.036	0.021	0.187
Mn	0.139	0.134	0.167	0.138	0.033	0.039	0.669
Fe	26.390	24.390	22.940	22.340	4.410	5.340	20.790
Co	0.	0.	0.	0.	0.	0.	0.
Ni	0.027	0.037	0.028	0.033	0.015	0.008	0.103
Cu	0.102	0.088	0.160	0.141	0.090	0.060	0.098
Zn	6.308	3.116	1.356	1.761	0.658	0.640	0.505
Ga	0.	0.	0.009	0.	0.010	0.	0.
Ge	0.	0.	0.	0.	0.	0.	0.
As	0.043	0.049	0.	0.	0.018	0.013	0.
Se	0.	0.	0.	0.	0.	0.	0.
Br	0.071	0.045	0.074	0.086	0.	0.017	0.
Kr	0.	0.	0.	0.	0.	0.	0.
Rb	0.061	0.033	0.080	0.127	0.	0.036	0.153
Sr	0.063	0.138	0.058	0.141	0.037	0.028	6.624
Y	0.	0.	0.	0.	0.	0.	0.
Zr	0.087	0.058	0.073	0.114	0.028	0.040	0.300
Mo	0.144	0.	0.	0.	0.	0.	0.067
Cd	0.	0.	0.	0.	0.	0.	0.
Pb	0.338	0.319	0.223	0.943	0.	0.	0.

Note: DUST denotes the rock dust sample.

Table A.10.2. Elemental Composition of the Samples from Section B (Mine Code 142-1-1).

Sampling Locations	CI						RI					
Stage	3		5		7		3		5		7	
Sample	A	B	A	B	A	B	A	B	A	B	A	B
Elements												
Na	0.	0.	0.	0.	0.	0.	0.	0.	0.	0.	0.	0.
Mg	6.888	3.529	7.454	11.247	1.053	0.	6.385	8.911	12.908	10.821	0.518	0.949
Al	22.030	23.930	56.360	118.167	9.640	9.664	111.162	110.156	164.332	141.689	13.295	13.278
Si	44.220	44.940	114.930	222.160	15.760	16.420	251.114	239.592	321.534	274.548	19.160	19.327
P	1.303	2.085	4.075	2.972	1.652	1.374	2.129	3.460	1.371	1.415	1.055	0.385
S	15.060	15.690	22.470	29.828	2.029	6.931	49.704	44.233	24.138	22.286	1.864	1.824
Cl	0.644	0.839	0.905	2.144	1.038	0.909	1.462	1.497	0.891	0.978	0.069	0.352
K	7.198	5.966	19.988	33.704	2.351	2.849	38.765	35.480	51.169	45.463	3.306	3.898
Ca	312.874	83.304	154.098	106.423	7.637	7.489	71.841	62.145	59.074	49.166	3.284	3.162
Sc	0.	0.	0.	0.	0.	0.	0.	0.	0.	0.	0.	0.
Ti	2.087	2.074	3.355	6.516	0.353	0.423	6.292	4.936	19.088	14.795	0.753	0.881
V	0.	0.	0.	0.	0.	0.	0.042	0.119	1.312	0.528	0.	0.
Cr	0.	0.047	0.	0.129	0.	0.	0.122	0.103	0.181	0.240	0.	0.
Mn	0.198	0.261	0.291	0.654	0.012	0.021	0.471	0.529	1.763	1.845	0.062	0.072
Fe	17.820	24.011	26.108	56.970	1.950	2.270	57.910	47.640	185.920	147.380	6.840	7.140
Co	0.	0.	0.	0.	0.	0.	0.	0.	0.	0.	0.	0.
Ni	0.050	0.062	0.040	0.098	0.022	0.005	0.039	0.063	0.159	0.165	0.013	0.013
Cu	0.401	0.596	0.697	1.731	0.107	0.096	0.128	0.660	0.548	1.617	0.047	0.063
Zn	1.731	2.011	2.659	2.829	0.926	0.896	1.381	2.573	2.163	4.495	0.673	0.622
Ga	0.083	0.157	0.081	0.294	0.013	0.010	0.016	0.142	0.109	0.386	0.006	0.101
Ge	0.	0.012	0.	0.	0.004	0.003	0.	0.	0.	0.	0.	0.
As	0.042	0.053	0.	0.019	0.009	0.016	0.	0.042	0.	0.	0.	0.
Se	0.019	0.	0.	0.	0.004	0.007	0.	0.	0.	0.	0.	0.
Br	0.042	0.014	0.058	0.029	0.021	0.034	0.	0.	0.106	0.165	0.022	0.017
Kr	0.	0.	0.	0.	0.	0.	0.	0.	0.	0.	0.	0.
Rb	0.	0.083	0.113	0.105	0.015	0.019	0.298	0.130	1.304	0.811	0.064	0.035
Sr	0.842	0.247	0.332	0.405	0.015	0.012	0.156	0.228	0.825	0.608	0.045	0.047
Y	0.	0.	0.	0.	0.	0.	0.	0.	0.	0.	0.	0.
Zr	0.141	0.141	0.070	0.080	0.027	0.	0.185	0.	0.706	0.370	0.026	0.071
Mo	0.179	0.140	0.097	0.125	0.	0.047	0.591	0.158	0.322	0.	0.	0.
Cd	1.687	0.	0.	0.	0.	0.	0.684	0.	0.	0.591	0.	0.
Pb	0.068	0.097	0.229	0.360	0.037	0.	0.298	0.067	0.886	0.709	0.060	0.042

Table A.10.2. (Continued).

Sampling Locations	RR						2X					
Stage	3		5		7		3		5		7	
Sample	A	B	A	B	A	B	A	B	A	B	A	B
Elements												
Na	0.	0.	0.	0.	0.	0.	0.	0.	0.	0.	0.	0.
Mg	9.611	6.990	3.430	3.523	1.036	0.667	0.	1.984	2.240	2.872	0.	0.801
Al	118.887	90.652	53.670	59.150	19.700	15.240	33.180	34.020	62.360	73.230	10.750	11.340
Si	248.302	186.449	102.810	108.180	28.440	24.210	54.510	55.350	107.140	121.000	16.610	17.920
P	1.776	1.203	0.791	1.122	1.208	1.882	0.371	1.092	0.626	0.973	1.933	1.193
S	28.745	21.623	8.170	8.525	2.051	6.138	35.414	34.335	44.296	47.944	9.502	8.893
Cl	0.600	0.396	0.197	0.588	0.	0.281	1.885	1.791	2.260	2.549	0.480	0.327
K	37.496	27.550	16.222	16.282	4.985	4.767	7.125	7.196	16.220	17.908	2.557	3.122
Ca	62.712	50.956	18.262	18.168	6.250	4.715	24.045	27.884	26.299	26.437	4.829	6.703
Sc	0.	0.	0.	0.	0.	0.	0.	0.	0.	0.	0.	0.
Ti	9.341	6.205	4.435	4.164	1.356	1.392	3.390	3.366	10.149	10.607	1.135	1.236
V	0.387	0.333	0.187	0.057	0.	0.	0.	0.030	0.279	0.513	0.	0.
Cr	0.091	0.021	0.091	0.037	0.	0.	0.023	0.063	0.054	0.	0.	0.
Mn	0.872	0.747	0.414	0.371	0.096	0.085	0.087	0.291	0.415	0.737	0.043	0.048
Fe	104.780	63.140	40.750	37.320	9.740	10.590	40.220	42.730	97.840	120.950	12.840	13.480
Co	0.	0.	0.	0.	0.	0.	0.	0.	0.	0.	0.	0.
Ni	0.049	0.057	0.038	0.023	0.	0.	0.017	0.078	0.032	0.067	0.027	0.021
Cu	0.165	0.571	0.074	0.111	0.068	0.033	0.123	0.675	0.741	1.528	0.159	0.182
Zn	1.084	1.945	0.980	1.066	1.389	1.096	1.037	2.296	1.375	2.461	1.283	1.416
Ga	0.028	0.187	0.013	0.	0.014	0.008	0.062	0.197	0.011	0.217	0.006	0.
Ge	0.	0.	0.	0.	0.006	0.	0.	0.	0.	0.012	0.008	0.
As	0.	0.	0.	0.	0.029	0.013	0.103	0.069	0.155	0.145	0.090	0.069
Se	0.	0.	0.	0.	0.	0.011	0.033	0.	0.	0.	0.017	0.
Br	0.015	0.017	0.	0.037	0.037	0.010	0.106	0.111	0.144	0.247	0.029	0.013
Kr	0.	0.	0.	0.	0.	0.	0.	0.	0.	0.	0.	0.
Rb	0.679	0.388	0.275	0.248	0.060	0.025	0.121	0.119	0.540	0.602	0.057	0.028
Sr	0.460	0.311	0.121	0.176	0.033	0.058	0.407	0.255	0.333	0.474	0.023	0.011
Y	0.	0.	0.	0.	0.	0.	0.	0.	0.	0.	0.	0.
Zr	0.234	0.360	0.143	0.363	0.042	0.021	0.	0.089	0.336	0.632	0.049	0.023
Mo	0.	0.	0.161	0.	0.	0.043	0.153	0.	0.	0.	0.	0.
Cd	0.830	0.701	0.120	0.	0.	0.	0.	0.	0.	0.	0.	0.
Pb	0.318	0.299	0.177	0.164	0.060	0.	0.101	0.195	0.336	0.759	0.	0.

Table A.10.2. (Continued).

Sampling Locations										
Stage	CH1		CH2		CH3		CH4		CH5	
Sample	A	B	A	B	A	B	A	B	A	B
Elements										
Na	0.	0.	0.	0.	0.	0.	50.637	52.499	0.	0.
Mg	0.	0.	0.	0.	0.	0.	93.121	86.111	54.265	54.463
Al	100.790	98.290	186.320	176.970	171.940	173.580	1095.56	1084.40	1159.71	1140.41
Si	105.620	103.170	155.880	147.410	159.380	163.000	2099.36	2063.38	1927.31	1913.99
P	2.797	2.918	0.	0.	2.445	2.617	0.	0.	0.	0.
S	205.755	207.242	214.626	210.283	192.964	191.452	9.379	7.038	85.997	87.569
Cl	15.352	15.172	16.329	16.376	14.347	14.031	2.365	0.	3.630	0.
K	7.572	6.836	8.935	8.256	10.376	10.721	303.311	301.330	296.283	291.497
Ca	26.344	26.654	35.030	32.705	18.127	16.987	9.974	9.964	12.479	14.751
Sc	0.	0.	0.	0.	0.	0.	0.	0.	0.	0.
Ti	4.741	4.880	8.056	7.957	9.821	9.765	67.355	68.354	71.692	69.487
V	0.152	0.142	0.077	0.175	0.276	0.277	3.236	3.410	3.757	3.924
Cr	0.202	0.210	0.333	0.251	0.306	0.292	1.145	1.233	1.646	1.603
Mn	0.223	0.230	0.139	0.166	0.261	0.271	2.454	2.349	1.268	1.348
Fe	151.985	153.007	62.171	16.234	145.649	145.952	258.500	260.151	237.564	223.956
Co	0.	0.	0.	0.	0.	0.	0.	0.	0.	0.
Ni	0.048	0.054	0.111	0.116	0.191	0.207	0.610	0.603	0.625	0.595
Cu	0.110	0.096	0.142	0.134	0.155	0.179	0.625	0.689	0.978	1.065
Zn	0.068	0.060	0.081	0.075	0.079	0.092	1.480	1.619	0.693	0.696
Ga	0.	0.009	0.024	0.034	0.061	0.047	0.178	0.188	0.173	0.204
Ge	0.	0.	0.	0.	0.	0.	0.	0.	0.	0.
As	0.019	0.019	0.	0.	0.	0.	0.	0.	0.	0.
Se	0.031	0.039	0.043	0.036	0.022	0.020	0.	0.	0.	0.
Br	0.458	0.443	0.520	0.618	0.491	0.547	0.	0.	0.023	0.
Kr	0.	0.	0.	0.	0.	0.	0.	0.	0.	0.
Rb	0.342	0.301	0.311	0.294	0.411	0.354	1.818	2.087	1.968	2.098
Sr	0.772	0.741	0.697	0.638	0.710	0.666	1.116	1.002	2.195	2.188
Y	0.	0.	0.	0.	0.	0.	0.	0.	0.	0.
Zr	0.064	0.097	0.252	0.246	0.227	0.194	1.792	1.621	2.206	2.088
Mo	0.077	0.076	0.023	0.	0.039	0.067	0.224	0.074	0.234	0.197
Cd	0.	0.	0.	0.	0.	0.	0.	0.	0.	0.
Pb	0.188	0.185	0.235	0.275	0.154	0.164	0.175	0.110	0.344	0.470

Notes: (1) CH1 denotes the channel sample from the second coal bench.
(2) CH2 denotes the channel sample from the bony coal and floor bench.
(3) CH3 denotes the channel sample from the first coal bench.
(4) CH4 denotes the channel sample from the first roof bench.
(5) CH5 denotes the channel sample from the second roof bench.
(6) Elemental data for the CR samples are included in Tables A.8.1. through A.8.3.

Table A.10.3. Elemental Composition of the Samples from Section C (Mine Code 03-3-1).

Sampling Locations	CI/RI						CH					
Stage	3		5		7		3		5		7	
Sample	A	B	A	B	A	B	A	B	A	B	A	B
Elements												
Na	0.	0.	0.	0.	0.	0.	0.	0.	0.	0.	0.	0.
Mg	2.492	2.236	0.958	0.790	0.	0.	1.123	0.754	0.	1.325	0.	0.
Al	44.230	47.040	14.120	12.860	3.850	2.790	42.560	39.720	36.640	37.040	5.180	4.400
Si	79.000	86.700	22.370	20.810	5.730	4.580	74.620	68.600	63.940	63.620	8.130	7.760
P	2.340	2.206	1.684	1.582	1.896	1.491	1.480	2.037	2.101	2.498	2.649	2.544
S	32.596	37.604	10.939	9.426	10.099	8.324	41.753	36.252	36.284	35.421	15.678	15.241
Cl	5.521	6.414	1.778	1.802	0.750	0.588	4.790	4.157	5.564	4.922	1.048	1.178
K	8.791	9.940	2.202	2.082	0.350	0.337	9.793	8.119	7.953	8.127	0.441	0.609
Ca	77.098	87.162	14.784	14.417	4.014	4.640	60.945	54.124	34.000	53.500	5.339	6.143
Sc	0.	0.	0.	0.	0.	0.	0.	0.	0.	0.	0.	0.
Ti	4.399	4.884	1.148	1.057	0.259	0.221	4.165	3.706	4.797	4.607	0.250	0.357
V	0.115	0.138	0.	0.	0.	0.	0.224	0.126	0.045	0.307	0.	0.
Cr	0.314	0.343	0.112	0.060	0.030	0.029	0.079	0.111	0.277	0.173	0.	0.
Mn	0.508	0.708	0.088	0.082	0.030	0.017	0.345	0.372	0.373	0.707	0.005	0.003
Fe	55.494	63.830	13.068	12.224	3.123	3.074	51.377	44.880	68.447	73.501	1.654	1.764
Co	0.	0.	0.	0.	0.	0.	0.	0.	0.	0.	0.	0.
Ni	0.166	0.163	0.032	0.030	0.019	0.016	0.055	0.042	0.081	0.218	0.011	0.006
Cu	0.157	0.547	0.024	0.028	0.025	0.043	0.215	0.559	0.288	1.101	0.033	0.018
Zn	1.750	2.346	0.909	0.971	0.905	1.064	1.022	2.053	2.339	4.100	0.736	0.737
Ga	0.038	0.164	0.009	0.002	0.013	0.018	0.030	0.111	0.032	0.314	0.013	0.007
Ge	0.	0.	0.	0.	0.	0.	0.010	0.	0.	0.	0.	0.
As	0.	0.	0.	0.	0.	0.018	0.	0.	0.	0.	0.	0.
Se	0.	0.	0.	0.	0.	0.	0.	0.	0.	0.	0.	0.
Br	0.172	0.243	0.024	0.037	0.029	0.029	0.162	0.111	0.126	0.148	0.011	0.016
Kr	0.	0.	0.	0.	0.	0.	0.	0.	0.	0.	0.	0.
Rb	0.167	0.211	0.046	0.025	0.	0.	0.154	0.189	0.332	0.211	0.029	0.
Sr	0.631	0.460	0.128	0.105	0.018	0.021	0.641	0.499	0.598	0.530	0.015	0.
Y	0.	0.	0.	0.	0.	0.	0.	0.	0.	0.	0.	0.
Zr	0.200	0.624	0.	0.	0.	0.	0.147	0.205	0.126	0.279	0.040	0.
Mo	0.104	0.	0.	0.	0.	0.	0.337	0.135	0.	0.	0.023	0.
Cd	0.	1.045	0.	0.	0.	0.	0.	0.	0.	0.	0.	0.
Pb	0.275	0.397	0.040	0.060	0.071	0.	0.188	0.284	0.125	0.248	0.050	0.035

Table A.10.3. (Continued).

Sampling	IN						RR					
Stage	3		5		7		3		5		7	
Sample	A	B	A	B	A	B	A	B	A	B	A	B
Elements												
Na	0.	0.	0.	0.	0.	0.	0.	0.	0.	0.	0.	0.
Mg	0.	0.	0.	0.	0.	0.	2.282	2.908	1.639	3.339	0.	0.938
Al	172.010	158.440	170.890	178.580	3.330	2.830	52.630	67.220	39.170	49.450	7.550	10.370
Si	336.330	254.050	285.950	318.150	5.600	5.070	103.710	133.190	68.970	82.610	12.650	16.380
P	104.946	105.629	62.006	59.371	2.725	1.956	1.817	1.298	1.468	1.157	1.581	3.102
S	384.440	426.735	334.627	396.790	12.668	11.176	20.699	27.828	15.298	14.605	14.098	17.463
Cl	49.697	42.379	34.255	38.328	0.845	0.545	1.993	2.799	1.743	2.110	0.639	1.146
K	5.215	0.	13.549	23.170	0.	0.	12.776	17.755	8.668	10.315	1.718	1.898
Ca	272.939	252.520	174.569	236.526	10.201	6.952	70.310	88.268	44.331	56.039	9.730	7.406
Sc	0.	0.	0.	0.	0.	0.	0.	0.	0.	0.	0.	0.
Ti	8.208	7.512	9.231	10.219	0.146	0.140	4.107	5.669	3.746	4.928	0.390	0.334
V	0.	0.	0.	0.	0.	0.	0.	0.179	0.	0.105	0.	0.
Cr	1.874	0.	0.	0.	0.	0.	0.143	0.253	0.170	0.174	0.	0.012
Mn	1.552	1.038	2.008	2.247	0.	0.027	0.491	0.710	0.452	0.743	0.037	0.021
Fe	113.500	92.930	195.186	218.377	2.398	1.372	36.635	56.183	40.428	53.744	2.443	2.601
Co	0.	0.	0.	0.	0.	0.	0.	0.	0.	0.	0.	0.
Ni	1.009	0.561	0.	0.958	0.018	0.016	0.023	0.110	0.081	0.131	0.010	0.009
Cu	0.935	0.	2.337	1.407	0.033	0.011	0.171	0.410	0.217	0.527	0.020	0.023
Zn	51.761	48.502	1.869	43.152	1.487	1.143	1.478	1.622	1.403	1.839	0.719	0.559
Ga	0.	0.	40.105	0.	0.022	0.007	0.070	0.112	0.091	0.163	0.014	0.007
Ge	0.	0.	0.464	0.	0.004	0.009	0.	0.	0.	0.	0.003	0.007
As	0.	0.	0.	0.	0.032	0.019	0.	0.	0.	0.	0.	0.006
Se	0.	0.	0.	0.	0.	0.	0.	0.	0.	0.	0.	0.
Br	0.694	0.513	0.	0.692	0.	0.	0.069	0.118	0.086	0.108	0.018	0.020
Kr	0.	0.	1.076	0.	0.	0.	0.	0.	0.	0.	0.	0.
Rb	0.	0.	0.	0.	0.	0.	0.	0.297	0.116	0.213	0.007	0.017
Sr	0.	0.	0.	2.011	0.	0.	0.151	0.499	0.243	0.345	0.	0.039
Y	0.	0.	0.	0.	0.	0.	0.	0.	0.	0.	0.	0.
Zr	0.	0.	1.020	1.931	0.	0.	0.	0.188	0.275	0.319	0.	0.010
Mo	2.942	0.	0.	3.114	0.	0.032	0.	0.104	0.157	0.055	0.	0.034
Cd	0.	0.	0.	0.	0.	0.	0.	0.	0.	0.	0.	0.
Pb	0.	2.336	0.	2.042	0.	0.	0.152	0.216	0.223	0.171	0.029	0.

Table A.10.3. (Continued).

Sampling Locations	2XCN						2XRR					
Stage	3		5		7		3		5		7	
Sample	A	B	A	B	A	B	A	B	A	B	A	B
Elements												
Na	0.	0.	0.	0.	0.	0.	0.	0.	0.	0.	0.	0.
Mg	2.065	1.647	0.590	0.	0.	0.	2.957	1.776	1.017	0.804	0.	0.
Al	56.000	53.790	11.710	12.710	4.180	4.390	69.020	45.840	26.490	21.340	5.630	6.310
Si	94.120	92.150	20.590	22.130	6.600	6.840	125.980	85.690	46.170	35.880	9.700	10.900
P	1.734	1.374	1.044	0.842	0.977	1.343	3.660	3.221	1.266	1.367	1.708	2.221
S	37.770	39.426	10.878	10.824	5.620	6.343	44.732	30.408	17.121	15.692	15.005	11.963
Cl	4.893	4.762	1.656	1.644	0.560	0.521	6.040	3.399	2.670	2.033	0.579	0.804
K	11.131	11.422	2.609	3.057	0.888	0.919	15.262	9.593	5.488	4.246	1.360	1.230
Ca	44.487	49.624	7.516	7.987	4.817	4.522	104.421	78.078	23.221	18.100	6.285	7.936
Sc	0.	0.	0.	0.	0.	0.	0.	0.	0.	0.	0.	0.
Ti	6.183	5.912	1.023	1.088	0.391	0.420	4.675	2.949	2.826	1.920	0.379	0.465
V	0.248	0.	0.	0.	0.	0.	0.	0.	0.056	0.084	0.	0.
Cr	0.207	0.167	0.	0.046	0.	0.	0.146	0.146	0.178	0.068	0.	0.032
Mn	0.381	0.499	0.057	0.049	0.024	0.004	0.439	0.554	0.210	0.389	0.	0.
Fe	60.900	60.440	10.860	11.368	4.237	3.767	42.789	33.745	31.141	24.387	3.041	3.024
Co	0.	0.	0.	0.	0.	0.	0.	0.	0.	0.	0.	0.
Ni	0.101	0.144	0.014	0.019	0.019	0.005	0.068	0.132	0.068	0.095	0.013	0.016
Cu	0.288	0.928	0.040	0.035	0.036	0.036	0.255	0.853	0.108	0.791	0.030	0.021
Zn	1.166	1.942	0.890	0.883	1.206	1.050	1.897	2.922	1.662	2.869	1.193	1.230
Ga	0.034	0.082	0.012	0.016	0.013	0.005	0.043	0.350	0.013	0.295	0.019	0.011
Ge	0.	0.	0.020	0.	0.015	0.	0.	0.	0.	0.027	0.004	0.
As	0.	0.	0.028	0.026	0.023	0.023	0.	0.067	0.	0.	0.022	0.016
Se	0.	0.016	0.004	0.007	0.	0.004	0.	0.	0.018	0.023	0.013	0.
Br	0.135	0.187	0.020	0.049	0.011	0.007	0.015	0.102	0.095	0.086	0.028	0.023
Kr	0.	0.	0.	0.	0.	0.	0.	0.	0.	0.	0.	0.
Rb	0.227	0.238	0.	0.063	0.	0.	0.110	0.126	0.162	0.087	0.030	0.
Sr	0.535	0.679	0.107	0.106	0.045	0.018	0.430	0.203	0.316	0.216	0.	0.
Y	0.	0.	0.	0.	0.	0.	0.	0.	0.	0.	0.	0.
Zr	0.173	0.189	0.038	0.121	0.	0.041	0.340	0.184	0.311	0.110	0.	0.
Mo	0.	0.209	0.	0.031	0.068	0.075	0.	0.210	0.223	0.	0.055	0.
Cd	1.206	0.680	0.	0.	0.	0.	0.	0.	0.	0.	0.	0.
Pb	0.222	0.317	0.031	0.	0.026	0.033	0.158	0.091	0.117	0.232	0.	0.

Table A.10.3. (Continued).

Sampling Locations	4XCR						4XRR					
Stage	3		5		7		3		5		7	
Sample	A	B	A	B	A	B	A	B	A	B	A	B
Elements												
Na	0.	0.	0.	0.	0.	0.	0.	0.	0.	0.	0.	0.
Mg	0.	1.858	1.682	0.	0.	0.	4.395	4.619	0.	1.063	0.	0.
Al	22.540	32.810	30.180	26.080	6.620	5.990	19.290	15.700	36.860	30.550	4.390	4.490
Si	38.890	55.640	51.620	46.040	9.640	10.640	33.910	27.520	66.840	56.200	7.020	7.920
P	1.293	2.042	2.074	0.809	2.643	2.129	2.512	1.979	2.601	1.772	1.536	2.194
S	26.129	27.406	23.150	24.583	8.996	11.566	20.130	18.628	28.076	26.800	9.051	10.837
Cl	2.363	2.747	3.288	3.280	1.003	0.850	1.907	1.437	5.220	4.018	0.971	1.037
K	4.917	7.285	6.181	5.870	0.865	1.202	3.561	2.520	8.410	7.220	1.140	0.978
Ca	32.186	100.685	17.588	17.562	5.236	6.617	41.835	34.507	41.451	32.983	6.695	7.323
Sc	0.	0.	0.	0.	0.	0.	0.	0.	0.	0.	0.	0.
Ti	1.568	2.486	3.688	3.314	0.258	0.307	3.505	3.280	2.749	2.263	0.261	0.218
V	0.	0.	0.	0.163	0.	0.	0.	0.	0.025	0.	0.	0.
Cr	0.016	0.051	0.150	0.024	0.	0.	0.	0.	0.121	0.123	0.017	0.012
Mn	0.121	0.451	0.317	0.287	0.	0.016	1.145	1.224	0.391	0.285	0.005	0.025
Fe	16.602	34.123	47.283	43.623	1.881	2.248	160.523	126.011	30.233	24.905	1.840	1.578
Co	0.	0.	0.	0.	0.	0.	0.	0.	0.	0.	0.	0.
Ni	0.035	0.111	0.041	0.096	0.007	0.040	0.238	0.355	0.094	0.099	0.009	0.006
Cu	0.061	0.451	0.131	0.435	0.043	0.077	1.047	0.443	0.596	0.354	0.025	0.025
Zn	1.064	1.530	1.472	1.758	0.721	0.736	21.063	20.191	2.333	1.587	0.793	0.815
Ga	0.011	0.015	0.	0.106	0.009	0.011	0.	0.402	0.246	0.122	0.009	0.004
Ge	0.008	0.	0.	0.016	0.	0.	0.	0.117	0.	0.	0.	0.009
As	0.034	0.	0.	0.	0.015	0.006	0.	0.	0.	0.046	0.012	0.024
Se	0.047	0.	0.	0.	0.006	0.005	0.	0.134	0.	0.	0.	0.
Br	0.081	0.104	0.125	0.130	0.	0.	0.423	1.198	0.127	0.077	0.015	0.003
Kr	0.	0.	0.	0.	0.	0.	0.	0.	0.	0.	0.	0.
Rb	0.	0.087	0.232	0.178	0.	0.	1.072	0.300	0.084	0.	0.008	0.011
Sr	0.294	0.442	0.286	0.361	0.	0.	0.956	0.622	0.197	0.106	0.013	0.019
Y	0.	0.	0.	0.	0.	0.	0.	0.	0.	0.	0.	0.
Zr	0.117	0.	0.173	0.204	0.	0.	0.958	1.282	0.151	0.298	0.042	0.
Mo	0.084	0.118	0.174	0.079	0.	0.	0.	0.	0.	0.095	0.	0.
Cd	0.	0.	0.	1.146	0.	0.	0.	0.	0.	0.	0.	0.
Pb	0.044	0.171	0.243	0.241	0.	0.034	0.503	0.558	0.087	0.	0.034	0.

Table A.10.3. (Continued).

Sampling Locations				
Stage	CH1		CH2	
Sample	A	B	A	B
Elements				
Na	0.	0.	0.	0.
Mg	0.	0.	0.	0.
Al	139.810	138.810	147.800	157.200
Si	170.040	169.820	182.070	196.410
P	3.603	3.581	2.900	2.588
S	138.127	139.315	139.805	123.568
Cl	18.258	18.225	18.816	17.921
K	17.375	17.946	19.113	21.552
Ca	15.050	14.820	11.190	15.230
Sc	0.	0.	0.	0.
Ti	6.551	6.627	7.178	7.334
V	0.495	0.434	0.491	0.587
Cr	0.196	0.234	0.216	0.261
Mn	0.231	0.242	0.233	0.260
Fe	92.989	97.004	91.665	79.895
Co	0.	0.	0.	0.
Ni	0.064	0.069	0.081	0.122
Cu	0.287	0.320	0.257	0.437
Zn	0.277	0.154	0.178	0.430
Ga	0.013	0.010	0.009	0.018
Ge	0.	0.	0.	0.
As	0.	0.	0.	0.
Se	0.	0.	0.	0.007
Br	0.289	0.322	0.280	0.278
Kr	0.	0.	0.	0.
Rb	0.267	0.334	0.283	0.283
Sr	0.706	0.756	0.784	0.745
Y	0.067	0.065	0.010	0.033
Zr	0.193	0.208	0.202	0.269
Mo	0.	0.137	0.040	0.040
Cd	0.	0.	0.	0.
Pb	0.097	0.121	0.132	0.107

Notes: (1) CH1 denotes the channel sample from the second coal bench.
(2) CH2 denotes the channel sample from the first coal bench.

Table A.10.4. Elemental Composition of the Samples from Section D (Mine Code 30-7-1).

Sampling Locations	CR1						CR2					
Stage	3		5		7		3		5		7	
	A	B	A	B	A	B	A	B	A	B	A	B
Elements												
Na	0.	0.	0.	0.	0.	0.	0.	0.	0.	0.	0.	0.
Mg	0.	0.	0.	0.	0.	0.	0.	0.	0.	0.	0.	0.
Al	118.890	108.380	45.750	67.740	10.990	6.200	89.570	89.280	40.380	37.470	7.000	9.350
Si	213.830	201.130	66.230	93.770	13.780	8.140	170.200	167.480	63.440	59.220	8.690	10.500
P	0.	0.	0.388	0.	1.349	1.038	0.	0.	0.515	0.	0.813	1.089
S	9.670	9.798	5.549	5.722	6.577	4.616	10.088	9.092	4.332	4.413	3.472	3.292
Cl	0.	0.	0.	0.	0.	0.	2.020	2.048	0.847	0.461	0.	0.
K	15.731	14.895	5.846	7.985	1.270	0.822	13.203	13.309	5.734	5.384	0.801	0.860
Ca	4.342	3.509	2.682	3.297	0.995	1.574	122.228	121.143	57.539	55.428	2.313	2.741
Sc	0.	0.	0.	0.	0.	0.	0.	0.	0.	0.	0.	0.
Ti	8.141	7.640	3.093	4.293	0.753	0.506	7.355	7.255	3.166	3.005	0.426	0.505
V	0.257	0.256	0.091	0.118	0.	0.	0.173	0.156	0.130	0.178	0.	0.041
Cr	0.167	0.144	0.071	0.105	0.	0.	0.157	0.129	0.	0.	0.	0.
Mn	0.100	0.089	0.054	0.044	0.	0.	0.093	0.101	0.064	0.057	0.015	0.016
Fe	20.030	18.040	9.081	12.533	3.118	2.119	17.101	17.277	8.820	8.220	1.295	1.559
Co	0.	0.	0.	0.	0.	0.	0.	0.	0.	0.	0.	0.
Ni	0.051	0.041	0.019	0.032	0.	0.	0.043	0.036	0.031	0.031	0.007	0.011
Cu	0.060	0.042	0.016	0.024	0.034	0.021	0.044	0.061	0.035	0.218	0.012	0.013
Zn	0.274	0.218	0.268	0.311	0.349	0.359	0.792	0.606	0.469	0.446	0.279	0.313
Ga	0.024	0.025	0.011	0.016	0.	0.	0.024	0.014	0.026	0.011	0.	0.
Ge	0.	0.	0.	0.	0.	0.	0.	0.	0.	0.	0.	0.
As	0.	0.	0.	0.	0.	0.	0.	0.021	0.	0.	0.	0.
Se	0.	0.	0.	0.	0.	0.	0.	0.	0.	0.	0.	0.
Br	0.014	0.011	0.009	0.	0.038	0.018	0.056	0.060	0.035	0.013	0.016	0.023
Kr	0.	0.	0.	0.	0.	0.	0.	0.	0.	0.	0.	0.
Rb	0.147	0.135	0.054	0.080	0.	0.	0.123	0.106	0.077	0.046	0.011	0.011
Sr	0.299	0.280	0.111	0.181	0.059	0.	0.277	0.328	0.174	0.134	0.031	0.020
Y	0.	0.	0.	0.	0.	0.	0.	0.	0.	0.	0.	0.
Zr	0.211	0.188	0.070	0.101	0.	0.034	0.201	0.159	0.100	0.109	0.018	0.017
Mo	0.	0.	0.	0.	0.	0.	0.051	0.	0.	0.029	0.	0.
Cd	0.	0.	0.	0.	0.	0.	0.	0.	0.	0.	0.	0.
Pb	0.056	0.066	0.023	0.040	0.033	0.	0.070	0.	0.035	0.032	0.	0.011

Table A.10.4. (Continued).

Sampling Locations								
Stage	CH1		CH2		CH3		CH4	
Sample	A	B	A	B	A	B	A	B
Elements								
Na	0.	0.	0.	0.	0.	0.	0.	0.
Mg	0.	0.	0.	0.	0.	0.	0.	64.575
Al	235.230	175.170	331.290	345.660	240.780	242.760	885.010	1348.48
Si	283.150	217.470	388.590	398.120	319.990	331.250	1495.93	2612.47
P	0.	0.	0.	0.	0.	0.	0.	5.845
S	136.346	143.963	135.703	135.997	78.032	81.591	247.866	0.
Cl	9.902	9.938	10.144	8.222	19.169	19.007	0.	0.
K	26.660	22.963	43.648	41.421	24.852	25.102	129.965	218.978
Ca	31.581	35.403	37.942	38.374	125.381	123.803	13.704	15.424
Sc	0.	0.	0.	0.	0.	0.	0.	0.
Ti	7.998	6.266	11.496	12.065	9.446	9.171	48.095	78.121
V	0.124	0.161	0.300	0.310	0.175	0.249	0.865	1.947
Cr	0.330	0.284	0.414	0.490	0.253	0.251	1.316	1.382
Mn	0.204	0.214	0.293	0.239	0.329	0.329	0.549	0.691
Fe	121.100	124.360	133.460	134.230	55.740	55.170	375.300	128.750
Co	0.	0.	0.	0.	0.	0.	0.	0.
Ni	0.130	0.144	0.202	0.216	0.068	0.067	0.487	0.281
Cu	0.137	0.106	0.217	0.230	0.150	0.172	0.680	0.647
Zn	0.206	0.196	0.293	0.302	0.081	0.085	0.796	0.553
Ga	0.048	0.053	0.844	0.076	0.028	0.025	0.145	0.278
Ge	0.	0.	0.	0.	0.	0.	0.	0.
As	0.	0.	0.	0.	0.	0.	0.	0.
Se	0.	0.	0.	0.	0.005	0.004	0.038	0.010
Br	0.110	0.158	0.144	0.181	0.175	0.160	0.068	0.
Kr	0.	0.	0.	0.	0.	0.	0.	0.
Rb	0.373	0.359	0.456	0.344	0.180	0.220	1.054	1.212
Sr	0.499	0.537	0.569	0.601	0.722	0.792	0.917	1.141
Y	0.	0.013	0.073	0.107	0.025	0.032	0.	0.426
Zr	0.249	0.220	0.317	0.290	0.397	0.274	1.463	1.977
Mo	0.089	0.	0.	0.046	0.	0.	0.153	0.061
Cd	0.	0.	0.	0.	0.	0.	0.	0.
Pb	0.110	0.093	0.107	0.136	0.065	0.053	0.528	0.204

Notes: (1) CH1 denotes the channel sample from the first coal bench.
(2) CH2 denotes the channel sample from the second coal bench.
(3) CH3 denotes the channel sample from the second slate bench.
(4) CH4 denotes the channel sample from the first slate bench.

Table A.10.5. Elemental Composition of the Samples from Section E (Mine Code 200-2-1).

Sampling Locations	CR1									
Stage	1		3		5		6		7	
Sample	A	B	A	B	A	B	A	B	A	B
Elements										
Na	0.	0.	0.	0.	0.	0.	0.	0.	0.	0.
Mg	18.312	15.062	2.538	1.821	0.	0.	1.698	1.664	0.	0.
Al	53.850	51.070	47.640	51.380	28.610	26.300	28.480	38.260	12.720	13.560
Si	76.860	73.520	72.380	77.130	45.890	45.270	35.360	49.500	16.760	16.930
P	4.890	5.358	1.016	1.292	0.666	0.	0.396	0.383	1.283	1.476
S	18.070	20.792	13.049	13.743	4.241	4.207	2.154	3.102	1.858	1.686
Cl	5.117	4.904	4.029	4.057	1.565	1.845	0.977	1.289	0.257	0.265
K	6.804	6.458	7.889	7.691	5.598	5.923	5.246	7.088	2.351	2.374
Ca	49.280	37.070	25.220	28.120	18.810	23.060	12.330	27.470	6.280	5.520
Sc	0.	0.	0.	0.	0.	0.	0.	0.	0.	0.
Ti	14.629	14.942	4.712	4.821	2.253	2.059	1.454	1.817	0.720	0.735
V	2.721	0.	0.081	0.199	0.	0.039	0.051	0.023	0.	0.
Cr	0.	0.	0.086	0.064	0.072	0.081	0.040	0.079	0.	0.
Mn	0.672	0.	0.068	0.212	0.071	0.086	0.045	0.041	0.029	0.028
Fe	391.270	368.750	19.860	24.440	11.130	11.120	7.710	9.720	3.130	3.150
Co	0.	0.	0.	0.	0.	0.	0.	0.	0.	0.
Ni	0.740	0.672	0.035	0.065	0.052	0.063	0.022	0.035	0.	0.
Cu	1.385	0.	0.094	0.440	0.045	0.072	0.059	0.059	0.013	0.014
Zn	46.219	43.178	0.905	1.594	0.547	0.484	0.253	0.349	0.461	0.457
Ga	0.722	0.	0.056	0.214	0.010	0.	0.015	0.013	0.	0.
Ge	0.	0.	0.	0.	0.	0.	0.	0.	0.	0.
As	0.	1.090	0.033	0.	0.	0.	0.	0.	0.	0.
Se	1.093	0.	0.	0.022	0.	0.	0.	0.006	0.	0.
Br	2.150	2.657	0.124	0.091	0.030	0.021	0.010	0.130	0.011	0.007
Kr	0.	0.	0.	0.	0.	0.	0.	0.	0.	0.
Rb	2.496	2.865	0.124	0.153	0.046	0.053	0.061	0.043	0.030	0.019
Sr	3.768	4.552	0.317	0.268	0.105	0.090	0.121	0.103	0.027	0.034
Y	0.	0.	0.	0.	0.	0.	0.	0.	0.	0.
Zr	7.375	4.216	0.144	0.114	0.076	0.046	0.012	0.031	0.018	0.026
Mo	6.629	0.	0.	0.221	0.	0.023	0.	0.	0.	0.
Cd	0.	0.	0.	0.	0.	0.	0.133	0.	0.	0.
Pb	1.472	0.	0.059	0.133	0.062	0.065	0.023	0.045	0.018	0.010

Table A.10.5. (Continued).

Sampling Locations	CR2									
Stage	1		3		5		6		7	
Sample	A	B	A	B	A	B	A	B	A	B
Elements										
Na	0.	0.	0.	0.	0.	0.	0.	0.	0.	0.
Mg	13.759	13.070	4.931	4.986	0.	0.	1.487	1.352	0.	0.
Al	121.430	94.620	77.150	95.430	26.480	25.660	35.500	25.700	8.640	8.910
Si	178.420	144.670	115.480	123.580	39.700	37.610	46.480	32.720	12.090	11.520
P	2.971	4.198	1.334	0.848	0.996	0.704	0.335	0.376	0.691	1.105
S	48.874	39.229	22.467	30.397	4.457	4.109	4.325	2.127	1.708	2.010
Cl	13.725	10.042	6.407	8.867	1.742	1.770	1.226	0.780	0.147	0.351
K	17.998	14.298	11.324	12.677	5.345	5.013	5.974	4.351	1.952	1.536
Ca	55.820	43.790	55.980	52.890	34.790	30.500	11.710	12.650	9.020	8.800
Sc	0.	0.	0.	0.	0.	0.	0.	0.	0.	0.
Ti	68.585	44.134	8.902	9.793	1.921	1.761	1.864	1.350	0.493	0.463
V	13.498	8.925	0.258	0.288	0.103	0.056	0.035	0.032	0.	0.
Cr	3.045	5.426	0.114	0.146	0.	0.	0.023	0.033	0.	0.
Mn	2.732	3.004	0.120	0.194	0.078	0.069	0.045	0.034	0.026	0.023
Fe	1064.170	990.260	35.660	39.950	10.010	9.000	8.030	7.090	2.460	2.330
Co	0.	0.	0.	0.	0.	0.	0.	0.	0.	0.
Ni	4.424	6.827	0.061	0.120	0.017	0.022	0.010	0.011	0.	0.
Cu	2.921	5.481	0.144	0.430	0.025	0.036	0.038	0.050	0.020	0.015
Zn	33.828	33.906	0.110	1.185	0.501	0.510	0.420	0.275	0.430	0.374
Ga	0.939	0.454	0.070	0.133	0.009	0.009	0.010	0.002	0.008	0.005
Ge	0.	0.288	0.	0.	0.	0.	0.003	0.	0.	0.
As	0.	0.	0.	0.	0.	0.	0.	0.	0.	0.
Se	0.	0.679	0.	0.014	0.	0.	0.	0.	0.	0.
Br	4.531	3.263	0.212	0.186	0.032	0.028	0.030	0.023	0.006	0.005
Kr	0.	0.	0.	0.	0.	0.	0.	0.	0.	0.
Rb	4.804	3.232	0.136	0.256	0.053	0.052	0.047	0.043	0.017	0.017
Sr	11.171	6.615	0.610	0.623	0.097	0.103	0.084	0.067	0.031	0.028
Y	0.	0.	0.	0.	0.	0.	0.	0.	0.	0.
Zr	4.467	4.841	0.212	0.256	0.047	0.044	0.057	0.070	0.	0.
Mo	2.413	3.198	0.	0.034	0.018	0.	0.023	0.	0.025	0.
Cd	0.	0.	0.	0.	0.	0.	0.	0.	0.	0.
Pb	4.103	2.769	0.103	0.130	0.027	0.030	0.028	0.053	0.012	0.011

Table A.10.5. (Continued).

Sampling Locations	CI/RI									
Stage	1		3		5		6		7	
Sample	A	B	A	B	A	B	A	B	A	B
Elements										
Na	0.	0.	0.	0.	0.	0.	0.	0.	0.	0.
Mg	0.	0.	0.	1.119	0.	0.	0.211	0.	0.	0.
Al	141.270	250.990	8.470	9.860	36.460	31.450	6.150	17.530	10.000	9.890
Si	282.430	430.910	14.090	14.070	64.380	59.060	10.100	28.480	15.250	14.940
P	110.377	89.698	2.456	2.484	3.417	2.240	0.264	0.832	5.728	4.763
S	214.410	241.054	7.064	9.581	13.018	14.362	1.561	6.960	12.648	13.044
Cl	41.317	52.348	2.646	2.773	7.173	9.133	1.176	3.691	2.277	1.742
K	10.562	62.076	1.183	1.438	8.881	8.897	1.661	4.192	1.270	0.976
Ca	342.940	589.870	10.840	11.850	20.250	19.450	4.760	14.670	12.000	11.730
Sc	0.	0.	0.	0.	0.	0.	0.	0.	0.	0.
Ti	10.560	33.096	0.484	0.876	1.329	1.574	0.566	1.855	0.232	0.294
V	0.	0.	0.	0.	0.	0.	0.012	0.	0.	0.
Cr	0.	0.	0.	0.	0.	0.	0.	0.	0.	0.255
Mn	1.094	1.695	0.010	0.238	0.093	0.092	0.051	0.105	0.	0.034
Fe	69.592	211.684	3.746	11.722	13.801	14.611	7.715	22.284	2.529	3.361
Co	0.	0.	0.	0.	0.	0.	0.	0.	0.	0.
Ni	0.	0.948	0.012	0.038	0.	0.	0.	0.	0.	0.105
Cu	1.557	1.716	0.066	1.241	0.023	0.066	0.029	0.054	0.034	0.025
Zn	53.836	49.630	1.823	2.818	0.766	0.734	0.358	1.299	0.775	0.744
Ga	0.455	0.686	0.037	0.251	0.	0.	0.	0.	0.	0.
Ge	0.	0.	0.	0.	0.	0.	0.003	0.023	0.	0.
As	0.	0.	0.	0.	0.	0.	0.	0.	0.	0.
Se	0.	0.	0.	0.031	0.	0.	0.	0.027	0.	0.
Br	0.	0.638	0.	0.	0.013	0.015	0.019	0.094	0.	0.
Kr	0.	0.	0.	0.	0.	0.	0.	0.	0.	0.
Rb	0.	1.594	0.038	0.037	0.032	0.056	0.031	0.040	0.023	0.
Sr	0.	1.820	0.020	0.028	0.059	0.046	0.041	0.136	0.020	0.
Y	0.	0.	0.	0.	0.	0.	0.	0.	0.	0.
Zr	1.298	1.977	0.273	0.	0.022	0.023	0.	0.045	0.027	0.
Mo	0.	0.	0.	0.	0.	0.	0.	0.	0.	0.
Cd	0.	0.	0.	0.	0.	0.	0.	0.	0.	0.
Pb	9.023	2.625	0.	0.104	0.023	0.041	0.029	0.144	0.014	0.030

Table A.10.5. (Continued).

Sampling Locations	RR											
Stage	1		3		5		6		7		CH	
Sample	A	B	A	B	A	B	A	B	A	B	A	B
Elements												
Na	0.	0.	0.	0.	0.	0.	0.	0.	0.	0.	0.	0.
Mg	0.	0.	2.131	1.295	0.	0.	0.484	0.623	0.	0.	0.	0.
Al	294.960	326.670	21.970	48.400	29.910	28.040	13.330	15.370	10.100	10.450	260.630	261.700
Si	645.290	754.190	39.480	27.120	55.990	51.380	20.980	23.420	18.360	20.380	326.220	324.620
P	83.886	62.082	2.421	4.908	1.214	1.657	0.725	0.532	3.865	2.796	0.	0.
S	239.661	251.891	8.351	22.561	6.178	6.317	3.029	3.329	5.975	6.309	120.669	119.330
Cl	61.445	84.158	3.900	5.957	5.836	6.393	1.767	2.117	1.010	0.990	19.418	18.498
K	66.037	125.239	4.248	3.433	8.098	7.851	3.140	3.612	1.932	3.289	33.922	34.514
Ca	664.190	2072.35	18.450	14.550	23.100	22.180	9.180	10.860	10.460	11.440	41.880	34.830
Sc	0.	0.	0.	0.	0.	0.	0.	0.	0.	0.	0.	0.
Ti	74.794	325.150	1.588	1.118	1.323	1.416	1.155	1.201	0.443	0.538	16.151	15.613
V	0.	5.976	0.	0.137	0.	0.	0.	0.	0.	0.	0.746	0.691
Cr	12.514	0.	0.	0.	0.	0.	0.	0.018	0.103	0.154	0.401	0.428
Mn	3.742	4.576	0.065	0.352	0.101	0.098	0.077	0.079	0.052	0.091	0.287	0.247
Fe	440.632	393.236	16.174	16.042	15.152	14.657	13.055	14.775	4.410	6.833	119.330	116.120
Co	0.	0.	0.	0.	0.	0.	0.	0.	0.	0.	0.	0.
Ni	6.010	2.721	0.	0.072	0.	0.	0.016	0.022	0.075	0.148	0.153	0.168
Cu	6.113	4.430	0.140	1.065	0.047	0.017	0.177	0.184	0.131	0.131	0.325	0.332
Zn	68.088	62.655	1.760	3.746	0.884	0.800	1.204	0.944	0.899	0.888	0.192	0.144
Ga	0.	0.	0.044	0.200	0.013	0.	0.080	0.011	0.	0.	0.051	0.034
Ge	0.	0.	0.	0.	0.	0.	0.	0.	0.	0.	0.	0.
As	0.	0.	0.	0.060	0.	0.	0.	0.	0.	0.	0.	0.
Se	0.	0.	0.	0.	0.	0.	0.008	0.	0.	0.	0.	0.
Br	1.508	1.112	0.025	0.055	0.022	0.016	0.011	0.	0.016	0.	0.301	0.292
Kr	0.	0.	0.	0.	0.	0.	0.	0.	0.	0.	0.	0.
Rb	0.828	1.584	0.098	0.	0.059	0.066	0.038	0.056	0.008	0.	0.398	0.481
Sr	2.820	4.639	0.153	0.	0.068	0.072	0.091	0.028	0.026	0.	1.198	1.207
Y	0.	0.	0.	0.	0.	0.	0.	0.	0.	0.	0.094	0.035
Zr	1.969	3.144	0.	0.	0.041	0.049	0.077	1.270	0.037	0.	0.514	0.449
Mo	0.	0.	0.	0.	0.025	0.	0.074	0.067	0.038	0.	0.054	0.152
Cd	0.	0.	0.	0.	0.	0.	0.	0.	0.	0.	0.	0.
Pb	3.641	6.501	0.185	0.060	0.032	0.027	0.032	0.050	0.029	0.052	0.159	0.186

Notes: (1) CH denotes the whole-seam channel sample.
(2) A and B under the stage number denote the two masses on each stage subjected to elemental analysis.
(3) Duplicated channel samples from an identical bench of the coal seam are designated as A and B.

Table A.10.6. Elemental Composition of the Samples from Section F (Mine Code 11-2-1).

Sampling Locations	CI						CR					
Stage	3		5		7		3		5		7	
Sample	A	B	A	B	A	B	A	B	A	B	A	B
Elements												
Na	0.	0.	0.	0.	0.	0.	0.	0.	0.	0.	0.	0.
Mg	0.	0.	0.	0.	0.	0.	0.	0.	0.	0.	0.	0.
Al	24.690	25.230	16.460	14.710	3.000	3.230	66.650	68.830	45.760	42.190	14.150	10.850
Si	41.860	42.030	27.910	25.390	4.200	4.080	106.190	108.650	72.240	70.920	18.160	14.330
P	1.927	1.678	2.945	2.584	1.761	1.794	0.	0.	0.	1.162	1.071	1.028
S	12.763	13.632	10.047	11.732	4.142	4.427	5.178	6.284	4.258	4.734	1.905	2.708
Cl	2.383	2.342	3.094	3.542	0.734	0.826	0.	0.	0.	0.573	0.	0.688
K	4.763	4.767	2.662	2.580	0.	0.	16.300	16.928	12.499	12.442	2.616	3.040
Ca	96.662	99.121	68.740	65.946	3.652	3.713	11.189	11.650	5.724	6.009	2.174	2.110
Sc	0.	0.	0.	0.	0.	0.	0.	0.	0.	0.	0.	0.
Ti	1.705	1.893	0.924	0.736	0.108	0.165	4.865	5.509	4.101	3.830	0.534	0.626
V	0.085	0.084	0.	0.	0.	0.	0.209	0.246	0.196	0.216	0.	0.
Cr	0.	0.105	0.107	0.109	0.	0.035	0.103	0.129	0.135	0.096	0.	0.055
Mn	0.104	0.099	0.098	0.091	0.045	0.037	0.142	0.164	0.155	0.131	0.	0.037
Fe	9.186	8.798	9.396	9.226	3.353	2.976	15.179	17.417	14.616	13.921	2.652	3.301
Co	0.	0.	0.	0.	0.	0.	0.	0.	0.	0.	0.	0.
Ni	0.025	0.034	0.	0.	0.	0.	0.032	0.064	0.037	0.034	0.	0.023
Cu	0.090	0.130	0.260	0.249	0.098	0.078	0.050	0.068	0.085	0.045	0.	0.052
Zn	0.801	0.784	0.838	0.766	0.722	0.685	0.588	0.484	0.736	0.683	0.441	0.455
Ga	0.	0.	0.	0.	0.	0.	0.017	0.026	0.023	0.	0.	0.
Ge	0.	0.	0.	0.	0.	0.	0.	0.	0.	0.	0.	0.
As	0.	0.	0.	0.034	0.	0.	0.	0.	0.	0.	0.	0.
Se	0.	0.	0.	0.	0.	0.	0.	0.	0.	0.	0.	0.
Br	0.040	0.020	0.021	0.021	0.	0.011	0.034	0.039	0.025	0.043	0.	0.
Kr	0.	0.	0.	0.	0.	0.	0.	0.	0.	0.	0.	0.
Rb	0.014	0.057	0.	0.022	0.	0.	0.108	0.151	0.124	0.096	0.168	0.024
Sr	0.131	0.157	0.073	0.094	0.	0.020	0.087	0.112	0.051	0.087	0.	0.019
Y	0.	0.	0.	0.	0.	0.	0.	0.	0.	0.	0.	0.
Zr	0.056	0.	0.067	0.	0.037	0.030	0.154	0.142	0.081	0.068	0.	0.060
Mo	0.	0.	0.	0.	0.	0.	0.	0.	0.	0.	0.	0.
Cd	0.	0.	0.	0.	0.	0.	0.	0.	0.	0.	0.	0.
Pb	0.117	0.112	0.210	0.138	1.313	0.084	0.060	0.058	0.058	0.077	0.	0.

Table A.10.6. (Continued).

Sampling Locations	RI						RR					
Stage	3		5		7		3		5		7	
Sample	A	B	A	B	A	B	A	B	A	B	A	B
Elements												
Na	0.	0.	0.	0.	0.	0.	0.	0.	0.	0.	0.	0.
Mg	0.	0.	0.	0.	0.	0.	0.	0.	0.	0.	0.	0.
Al	61.940	67.140	50.430	48.320	16.320	13.110	57.380	59.180	49.420	48.440	10.580	18.390
Si	102.800	112.180	73.860	73.520	18.900	16.070	102.310	103.090	74.210	72.950	13.810	24.120
P	0.	0.	0.	0.	1.128	0.835	0.	0.	0.	0.	0.905	0.841
S	5.650	6.593	2.456	1.876	1.586	1.761	6.866	6.378	2.290	2.606	2.527	1.868
Cl	0.	0.	0.361	0.	0.	0.	0.	0.	0.	0.	0.313	0.416
K	16.193	17.872	12.204	11.824	3.029	2.633	15.019	15.738	11.215	10.709	2.398	3.842
Ca	25.943	29.474	8.731	8.593	1.877	1.673	80.299	79.149	17.175	18.563	1.813	2.397
Sc	0.	0.	0.	0.	0.	0.	0.	0.	0.	0.	0.	0.
Ti	5.049	5.673	3.312	3.368	0.474	0.463	4.361	4.760	2.873	2.743	0.464	0.727
V	0.281	0.228	0.135	0.122	0.	0.019	0.251	0.204	0.151	0.086	0.	0.
Cr	0.130	0.151	0.108	0.093	0.	0.025	0.	0.126	0.061	0.068	0.021	0.031
Mn	0.156	0.193	0.176	0.169	0.029	0.026	0.271	0.280	0.182	0.170	0.023	0.053
Fe	17.206	19.331	15.175	14.159	2.371	2.207	21.006	21.438	13.407	13.050	2.249	3.386
Co	0.	0.	0.	0.	0.	0.	0.	0.	0.	0.	0.	0.
Ni	0.042	0.043	0.32	0.028	0.	0.	0.046	0.043	0.020	0.018	0.011	0.010
Cu	0.070	0.076	0.096	0.106	0.020	0.016	0.071	0.074	0.079	0.071	0.018	0.023
Zn	0.693	0.997	0.509	0.463	0.325	0.302	0.614	0.607	0.436	0.436	0.275	0.275
Ga	0.019	0.023	0.015	0.	0.	0.	0.	0.028	0.	0.007	0.004	0.006
Ge	0.	0.	0.	0.	0.	0.	0.	0.	0.	0.	0.004	0.
As	0.	0.	0.	0.	0.004	0.	0.019	0.	0.	0.	0.	0.
Se	0.	0.	0.	0.	0.	0.004	0.	0.	0.	0.	0.	0.006
Br	0.038	0.044	0.023	0.015	0.	0.	0.059	0.063	0.015	0.020	0.018	0.013
Kr	0.	0.	0.	0.	0.	0.	0.	0.	0.	0.	0.	0.
Rb	0.123	0.190	0.106	0.110	0.024	0.024	0.141	0.146	0.099	0.073	0.021	0.021
Sr	0.161	0.143	0.099	0.067	0.	0.	0.242	0.222	0.075	0.086	0.010	0.029
Y	0.	0.	0.	0.	0.	0.	0.	0.	0.	0.	0.	0.
Zr	0.105	0.110	0.077	0.105	0.024	0.030	0.159	0.066	0.063	0.059	0.022	0.018
Mo	0.	0.	0.	0.047	0.	0.	0.065	0.044	0.066	0.035	0.	0.
Cd	0.	0.	0.	0.	0.	0.	0.	0.	0.	0.	0.	0.
Pb	0.116	0.091	0.079	0.078	0.	0.	0.099	0.180	0.052	0.070	0.	0.166

Table A.10.6. (Continued).

Sampling Locations	2X						4X					
Stage	3		5		7		3		5		7	
Sample	A	B	A	B	A	B	A	B	A	B	A	B
Elements												
Na	0.	0.	0.	0.	0.	0.	0.	0.	0.	0.	0.	0.
Mg	0.	0.	0.	0.	0.	0.	0.	0.	0.	0.	0.	0.
Al	51.590	51.550	42.680	45.760	13.890	12.260	56.390	55.220	46.610	51.370	12.250	13.470
Si	96.330	89.290	64.300	67.940	17.780	17.220	95.100	97.460	67.060	73.750	15.250	16.650
P	0.	0.	0.	0.	0.955	0.545	0.633	0.	0.342	0.	1.072	0.762
S	5.499	6.638	2.883	2.421	2.700	2.700	7.144	7.172	3.387	3.211	2.672	2.576
Cl	0.296	0.577	0.433	0.	0.275	0.276	0.797	0.887	0.311	0.	0.238	0.211
K	14.451	13.812	9.734	9.865	2.825	2.734	14.332	15.587	9.918	11.264	2.313	2.671
Ca	37.137	31.978	9.636	9.632	2.966	2.059	34.111	37.640	9.426	10.617	2.026	2.499
Sc	0.	0.	0.	0.	0.	0.	0.	0.	0.	0.	0.	0.
Ti	4.934	4.232	2.685	2.843	0.635	0.574	4.760	5.185	2.669	2.801	0.473	0.530
V	0.132	0.160	0.083	0.096	0.031	0.029	0.133	0.167	0.093	0.113	0.	0.020
Cr	0.131	0.093	0.077	0.073	0.029	0.	0.130	0.118	0.100	0.080	0.024	0.
Mn	0.173	0.148	0.118	0.146	0.040	0.038	0.152	0.172	0.110	0.138	0.027	0.031
Fe	16.833	14.566	11.184	12.009	3.213	2.829	16.169	17.823	10.535	11.754	2.127	2.561
Co	0.	0.	0.	0.	0.	0.	0.	0.	0.	0.	0.	0.
Ni	0.034	0.037	0.023	0.018	0.012	0.009	0.026	0.040	0.027	0.027	0.	0.
Cu	0.077	0.077	0.065	0.072	0.025	0.022	0.066	0.080	0.077	0.071	0.015	0.119
Zn	0.616	0.492	0.441	0.446	0.301	0.289	0.792	0.749	0.370	0.346	0.295	0.316
Ga	0.021	0.013	0.011	0.008	0.007	0.006	0.017	0.	0.010	0.010	0.	0.
Ge	0.	0.	0.	0.	0.	0.	0.	0.	0.	0.	0.	0.
As	0.	0.	0.	0.	0.	0.007	0.025	0.	0.	0.	0.	0.
Se	0.	0.	0.	0.	0.	0.	0.	0.	0.	0.	0.	0.
Br	0.049	0.036	0.021	0.013	0.025	0.017	0.036	0.043	0.023	0.009	0.	0.007
Kr	0.	0.	0.	0.	0.	0.	0.	0.	0.	0.	0.	0.
Rb	0.129	0.079	0.098	0.091	0.014	0.021	0.105	0.148	0.067	0.102	0.019	0.009
Sr	0.207	0.097	0.061	0.058	0.026	0.	0.174	0.191	0.050	0.056	0.	0.027
Y	0.	0.	0.	0.	0.	0.	0.	0.	0.	0.	0.	0.
Zr	0.101	0.125	0.063	0.064	0.	0.020	0.123	0.090	0.073	0.043	0.015	0.017
Mo	0.038	0.054	0.	0.	0.	0.	0.	0.045	0.023	0.	0.	0.
Cd	0.	0.	0.	0.	0.	0.	0.	0.	0.	0.	0.	0.
Pb	0.160	0.163	0.105	0.083	0.027	0.020	0.193	0.158	0.077	0.086	0.017	0.012

Table A.10.6. (Continued).

Sampling Locations								
Stage	CH1		CH2		CH3		CH4	
Sample	A	B	A	B	A	B	A	B
Elements								
Na	59.341	59.237	0.	0.	0.	0.	0.	0.
Mg	86.264	84.035	13.250	17.390	31.106	29.956	0.	0.
Al	1175.67	1140.32	464.340	491.290	1208.90	1207.80	150.270	158.700
Si	1976.51	1906.27	642.860	673.750	1463.76	1471.42	131.760	139.040
P	0.	0.	0.	0.	0.	0.	3.059	3.874
S	29.458	27.995	63.973	62.750	67.042	68.216	70.293	73.978
Cl	0.	0.	4.679	3.890	0.	0.	6.936	7.141
K	325.014	308.972	74.948	79.256	109.790	107.953	6.390	7.283
Ca	14.620	13.821	27.867	28.976	7.025	6.987	19.478	20.472
Sc	0.	0.	0.	0.	0.	0.	0.	0.
Ti	63.013	61.746	30.187	30.228	83.618	81.479	8.143	8.597
V	4.093	3.887	1.213	1.511	4.191	4.096	0.436	0.468
Cr	1.413	1.324	0.583	0.539	1.615	1.698	0.193	0.205
Mn	3.133	3.333	0.339	0.339	0.381	0.338	0.073	0.075
Fe	289.728	288.293	81.139	80.425	141.557	138.508	29.577	35.116
Co	0.	0.	0.	0.	0.	0.	0.	0.
Ni	0.659	0.654	0.177	0.197	0.932	0.839	0.120	0.102
Cu	0.744	0.894	0.487	0.521	1.485	1.581	0.226	0.213
Zn	1.417	1.504	0.236	0.251	0.162	0.192	0.100	0.088
Ga	0.214	0.203	0.087	0.087	0.241	0.221	0.032	0.031
Ge	0.	0.	0.	0.	0.	0.	0.	0.
As	0.	0.	0.	0.	0.	0.	0.085	0.085
Se	0.	0.	0.048	0.043	0.057	0.069	0.015	0.008
Br	0.	0.027	0.225	0.189	0.021	0.052	0.362	0.339
Kr	0.	0.	0.	0.	0.	0.	0.	0.
Rb	2.189	2.080	0.515	0.570	1.131	1.115	0.080	0.117
Sr	0.890	0.871	0.411	0.356	3.355	3.061	1.413	1.405
Y	0.270	0.392	0.135	0.139	0.409	0.287	0.057	0.048
Zr	1.482	1.369	0.795	0.738	2.464	2.377	0.291	0.301
Mo	0.156	0.219	0.025	0.046	0.176	0.107	0.	0.
Cd	0.	0.	0.	0.	0.	0.	0.	0.
Pb	0.455	0.393	0.308	0.309	0.424	0.473	0.068	0.073

Notes: (1) CH1 denotes the channel sample from the roof and coal bench.
(2) CH2 denotes the channel sample from the bony coal bench.
(3) CH3 denotes the channel sample from the soft coal bench.
(4) CH4 denotes the channel sample from the bottom rock and coal bench.

Table A.10.7. Elemental Composition of the Samples from Section G (Mine Code 63-7-1).

Sampling Locations	CI						CR					
Stage	3		5		7		3		5		7	
Sample	A	B	A	B	A	B	A	B	A	B	A	B
Elements												
Na	0.	0.	0.	0.	0.	0.	0.	0.	0.	0.	0.	0.
Mg	0.	0.	0.	0.	0.	0.	0.	0.	0.	0.	0.	0.
Al	5.710	6.930	7.090	7.500	4.090	3.760	33.650	30.670	21.730	19.890	7.760	8.010
Si	16.900	15.570	30.130	29.020	8.650	8.540	64.610	60.270	40.750	38.020	10.860	11.170
P	1.893	2.136	3.472	3.803	3.468	3.424	2.670	2.581	2.901	2.790	2.706	2.482
S	6.392	7.770	10.523	9.172	7.003	7.040	20.180	20.949	10.210	9.695	5.948	6.184
Cl	0.	0.	0.385	0.290	0.562	0.281	1.957	2.889	0.539	0.779	0.685	0.384
K	0.806	0.450	0.257	0.268	0.	0.	5.598	4.537	3.024	2.661	0.557	0.557
Ca	13.032	13.328	14.705	1.000	4.971	5.199	15.825	14.758	12.842	12.671	4.754	4.358
Sc	0.	0.	0.	5.599	0.	0.	0.	0.	0.	0.	0.	0.
Ti	0.310	0.171	0.097	0.	0.	0.	1.894	1.892	1.357	1.314	0.252	0.432
V	0.	0.	0.	0.184	0.	0.	0.054	0.070	0.	0.	0.	0.
Cr	0.033	0.	0.	0.	0.	0.	0.	0.069	0.083	0.	0.	0.
Mn	0.040	0.028	0.067	0.050	0.032	0.043	0.043	0.055	0.047	0.040	0.	0.053
Fe	3.398	3.015	6.990	0.054	2.718	2.667	6.643	6.888	6.003	5.593	2.209	2.516
Co	0.	0.	0.	6.670	0.	0.	0.	0.	0.	0.	0.	0.
Ni	0.	0.	0.	0.	0.	0.	0.	0.034	0.016	0.	0.	0.025
Cu	0.038	0.062	0.131	0.	0.044	0.049	0.038	0.058	0.098	0.079	0.033	0.076
Zn	0.645	0.614	0.708	0.129	0.713	0.673	0.658	0.652	0.734	0.702	1.034	0.952
Ga	0.	0.	0.020	0.684	0.	0.	0.	0.015	0.021	0.	0.	0.
Ge	0.	0.	0.	0.	0.	0.	0.	0.	0.	0.	0.	0.
As	0.	0.009	0.	0.	0.	0.	0.	0.	0.028	0.021	0.	0.
Se	0.	0.009	0.	0.	0.	0.	0.	0.	0.018	0.	0.	0.
Br	0.015	0.010	0.031	0.	0.016	0.015	0.063	0.072	0.043	0.020	0.	0.021
Kr	0.	0.	0.	0.019	0.	0.	0.	0.	0.	0.	0.	0.
Rb	0.	0.	0.017	0.	0.	0.	0.039	0.029	0.017	0.016	0.	0.
Sr	0.019	0.014	0.020	0.	0.	0.020	0.135	0.075	0.061	0.036	0.	0.
Y	0.	0.	0.	0.	0.	0.	0.	0.	0.	0.	0.	0.
Zr	0.	0.	0.038	0.022	0.040	0.	0.	0.061	0.	0.083	0.	0.
Mo	0.	0.	0.071	0.	0.	0.083	0.	0.	0.060	0.	0.	0.
Cd	0.	0.	0.	0.	0.	0.	0.	0.	0.	0.	0.	0.
Pb	0.033	0.	0.024	0.	0.029	0.037	0.074	0.038	0.	0.	0.	0.

Table A.10.7. (Continued).

Sampling Locations	ININ						INOUT					
Stage	3		5		7		3		5		7	
Sample	A	B	A	B	A	B	A	B	A	B	A	B
Elements												
Na	0.	0.	0.	0.	0.	0.	0.	0.	0.	0.	0.	0.
Mg	0.	0.	0.	0.	0.	0.	0.	0.	0.	0.	0.	0.
Al	5.910	5.285	6.961	6.967	3.423	3.492	3.088	3.714	3.224	5.374	4.591	4.841
Si	18.742	16.540	40.084	42.090	7.151	7.173	24.368	21.876	50.552	44.888	9.386	12.225
P	2.696	2.778	3.761	4.225	2.900	2.962	2.634	2.843	2.124	4.543	3.800	4.429
S	8.610	7.259	12.116	10.646	5.463	4.755	9.467	8.745	10.554	11.642	7.883	8.924
Cl	0.609	0.311	0.500	0.424	0.640	0.338	0.382	0.236	0.	0.908	0.425	0.504
K	0.149	0.	0.317	0.398	0.	0.	0.	0.	0.	0.	0.	0.
Ca	13.524	11.370	18.484	18.482	4.179	7.320	6.611	5.711	10.725	9.955	6.438	6.273
Sc	0.	0.	0.	0.	0.	0.	0.	0.	0.	0.	0.	0.
Ti	0.131	0.110	0.199	0.178	0.063	0.	0.054	0.	0.	0.112	0.	0.150
V	0.	0.	0.	0.	0.	0.	0.	0.	0.	0.	0.	0.
Cr	0.	0.	0.	0.	0.	1.267	0.	0.	0.	0.	0.	0.
Mn	0.059	0.057	0.113	0.129	0.028	0.175	0.094	0.081	0.133	0.128	0.	0.053
Fe	7.707	6.031	12.604	13.648	2.544	7.378	11.479	8.993	16.535	13.655	2.400	4.528
Co	0.	0.	0.	0.	0.	0.	0.	0.	0.	0.	0.	0.
Ni	0.	0.015	0.	0.	0.	0.423	0.	0.	0.	0.	0.	0.
Cu	0.242	0.199	0.213	0.206	0.048	0.074	0.190	0.204	0.299	0.268	0.031	0.065
Zn	0.657	0.655	0.655	0.679	0.735	0.743	0.590	0.558	0.668	0.633	0.699	0.724
Ga	0.	0.	0.	0.	0.016	0.	0.	0.	0.	0.	0.	0.
Ge	0.	0.	0.	0.	0.	0.	0.	0.	0.	0.	0.	0.
As	0.	0.	0.	0.	0.	0.	0.	0.	0.	0.	0.	0.
Se	0.	0.014	0.	0.	0.	0.	0.	0.	0.	0.	0.	0.
Br	0.016	0.022	0.023	0.	0.020	0.032	0.021	0.032	0.012	0.022	0.048	0.023
Kr	0.	0.	0.	0.	0.	0.	0.	0.	0.	0.	0.	0.
Rb	0.034	0.013	0.	0.	0.025	0.025	0.	0.014	0.043	0.	0.	0.
Sr	0.019	0.025	0.041	0.	0.	0.071	0.	0.037	0.	0.	0.026	0.
Y	0.	0.	0.	0.	0.	0.	0.	0.	0.	0.	0.	0.
Zr	0.029	0.	0.	0.	0.063	0.	0.030	0.	0.029	0.	0.	0.
Mo	0.	0.	0.114	0.071	0.	0.	0.096	0.079	0.049	0.	0.064	0.102
Cd	0.	0.	0.	0.	0.	0.	0.	0.	0.	0.	0.	0.
Pb	0.051	0.050	0.056	0.	0.	0.036	0.029	0.023	0.	0.	0.064	0.030

Table A.10.7. (Continued).

Sampling Locations	RH											
Stage	3		5		7		CH1		CH2		CH3	
Sample	A	B	A	B	A	B	A	B	A	B	A	B
Elements												
Na	0.	0.	0.	0.	0.	0.	0.	0.	0.	0.	0.	0.
Mg	0.	0.	0.	0.	0.	0.	0.	0.	64.275	65.900	0.	0.
Al	59.976	59.687	43.074	37.257	9.125	6.814	160.680	155.210	1323.01	1335.42	571.230	606.460
Si	120.660	117.116	76.432	68.814	14.361	11.766	199.170	193.930	2316.96	2390.99	808.810	873.660
P	3.791	5.296	0.946	1.495	1.978	1.152	0.	0.	0.	0.	0.	0.
S	17.759	18.326	7.470	7.476	5.286	5.558	105.753	107.209	0.	0.	88.892	81.672
Cl	0.	1.266	0.	0.415	0.313	0.139	9.933	9.977	0.	0.	0.	0.
K	11.842	11.477	9.280	7.101	1.891	1.835	12.312	12.423	216.088	226.351	82.164	88.285
Ca	16.620	16.837	9.106	9.859	4.375	4.152	42.966	42.770	50.358	51.778	66.882	72.328
Sc	0.	0.	0.	0.	0.	0.	0.	0.	0.	0.	0.	0.
Ti	1.814	1.678	1.857	1.481	0.850	0.859	5.825	5.869	71.572	70.239	26.231	27.626
V	0.	0.	0.	0.	0.	0.	0.148	0.187	1.814	2.048	0.930	0.818
Cr	0.	0.	0.066	0.	0.	0.	0.209	0.179	1.488	1.360	0.579	0.602
Mn	0.227	0.186	0.278	0.228	0.190	0.207	0.164	0.147	0.785	0.741	0.370	0.403
Fe	12.423	11.910	17.078	13.200	10.066	10.537	45.917	43.754	129.828	127.699	100.631	101.027
Co	0.	0.	0.	0.	0.	0.	0.	0.	0.	0.	0.	0.
Ni	0.	0.	0.	0.	0.	0.	0.082	0.080	0.276	0.290	0.281	0.276
Cu	0.063	0.	0.055	0.057	0.027	0.356	0.096	0.107	0.713	0.714	0.238	0.256
Zn	0.734	0.712	0.681	0.645	1.073	0.957	0.093	0.084	0.830	0.776	0.336	0.355
Ga	0.015	0.	0.	0.	0.	0.	0.011	0.021	0.236	0.202	0.108	0.098
Ge	0.	0.	0.	0.	0.	0.	0.010	0.013	0.	0.	0.	0.
As	0.	0.	0.	0.021	0.	0.	0.	0.005	0.	0.	0.	0.
Se	0.	0.	0.	0.	0.	0.	0.006	0.006	0.	0.	0.	0.
Br	0.015	0.022	0.022	0.045	0.053	0.038	0.177	0.132	0.053	0.035	0.140	0.139
Kr	0.	0.	0.	0.	0.	0.	0.	0.	0.	0.	0.	0.
Rb	0.036	0.019	0.040	0.037	0.031	0.	0.123	0.118	1.390	1.450	0.663	0.663
Sr	0.064	0.060	0.094	0.057	0.090	0.064	0.407	0.425	1.736	1.772	0.926	0.834
Y	0.	0.	0.	0.	0.	0.	0.	0.	0.	0.	0.	0.
Zr	0.043	0.062	0.	0.033	0.	0.061	0.220	0.252	1.946	1.926	0.682	0.771
Mo	0.	0.	0.114	0.071	0.	0.	0.041	0.	0.099	0.055	0.077	0.092
Cd	0.	0.	0.	0.	0.	0.	0.	0.	0.	0.	0.	0.
Pb	0.032	0.	0.100	0.	0.040	0.	0.081	0.062	0.272	0.274	0.178	0.164

Notes: (1) CH1 denotes the channel sample from the coal bench.
(2) CH2 denotes the channel sample from the draw slate bench.
(3) CH3 denotes the channel sample from the top rock and bony coal bench.